



UNIVERSIDADE ESTADUAL DE CAMPINAS
Faculdade de Engenharia Mecânica

RENATO PICELLI SANCHES

***Evolutionary Topology Optimization
of Fluid-structure Interaction Problems***

***Otimização Topológica Evolucionária
de Problemas com Interação Fluido-estrutura***

CAMPINAS
2015

RENATO PICELLI SANCHES

*Evolutionary Topology Optimization
of Fluid-structure Interaction Problems*

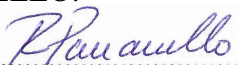
*Otimização Topológica Evolucionária
de Problemas com Interação Fluido-estrutura*

Thesis presented to the School of Mechanical Engineering of the University of Campinas in partial fulfillment of the requirements for the degree of Doctor in Mechanical Engineering in the area of Solid Mechanics and Mechanical Design.

Tese de Doutorado apresentada à Faculdade de Engenharia Mecânica da Universidade Estadual de Campinas como parte dos requisitos exigidos para obtenção do título de Doutor em Engenharia Mecânica na área de Mecânica dos Sólidos e Projeto Mecânico.

Orientador: Prof. Dr. Renato Pavanello

ESTE EXEMPLAR CORRESPONDE À VERSÃO FINAL DA TESE DEFENDIDA PELO ALUNO RENATO PICELLI SANCHES E ORIENTADA PELO PROF. DR. RENATO PAVANELLO.


.....
ASSINATURA DO ORIENTADOR

CAMPINAS
2015

Agência(s) de fomento e nº(s) de processo(s): FAPESP, 2011/09730-6

Ficha catalográfica
Universidade Estadual de Campinas
Biblioteca da Área de Engenharia e Arquitetura
Luciana Pietrosanto Milla - CRB 8/8129

Sanches, Renato Picelli, 1987-
Sa55e Evolutionary topology optimization of fluid-structure interaction problems /
Renato Picelli Sanches. – Campinas, SP : [s.n.], 2015.

Orientador: Renato Pavanello.
Tese (doutorado) – Universidade Estadual de Campinas, Faculdade de
Engenharia Mecânica.

1. Otimização estrutural. 2. Interação fluido-estrutura. 3. Método dos
elementos finitos. I. Pavanello, Renato, 1959-. II. Universidade Estadual de
Campinas. Faculdade de Engenharia Mecânica. III. Título.

Informações para Biblioteca Digital

Título em outro idioma: Otimização topológica evolucionária de problemas com interação
fluido-estrutura

Palavras-chave em inglês:

Structural optimization

Fluid-structure interaction

Finite element method

Área de concentração: Mecânica dos Sólidos e Projeto Mecânico

Titulação: Doutor em Engenharia Mecânica

Banca examinadora:

Renato Pavanello [Orientador]

José Roberto de França Arruda

Marco Lúcio Bittencourt

Emílio Carlos Nelli Silva

Eduardo Alberto Fancello

Data de defesa: 19-10-2015

Programa de Pós-Graduação: Engenharia Mecânica

COMISSÃO DE PÓS-GRADUAÇÃO EM ENGENHARIA MECÂNICA
DEPARTAMENTO DE MECÂNICA COMPUTACIONAL

TESE DE DOUTORADO

***Evolutionary Topology Optimization
of Fluid-structure Interaction Problems***

***Otimização Topológica Evolucionária
de Problemas com Interação Fluido-estrutura***

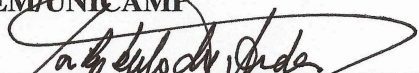
Autor: Renato Picelli Sanches

Orientador: Prof. Dr. Renato Pavanello

A Banca Examinadora composta pelos membros abaixo aprovou esta Tese:



Prof. Dr. Renato Pavanello
DMC/FEM/UNICAMP



Prof. Dr. José Roberto de França Arruda
DMC/FEM/UNICAMP



Prof. Dr. Marco Lúcio Bittencourt
DSI/FEM/UNICAMP



Prof. Dr. Emílio Carlos Nelli Silva
POLI/USP



Prof. Dr. Eduardo Alberto Fancello
GRANTE/EMC/UFSC

Campinas, 19 de Outubro de 2015.

Dedicatória

Aos meus amados pais, Ludimeri e José.

Agradecimentos

À minha família, Ludimeri, José, Emília, Luiz, Patrícia, Paschoina e Manoel, sem a qual eu seria absolutamente nada.

À minha querida namorada, Ana, e sua família, Fernando, Eliana, Izzolet, Valéria, Guilherme e Sandra por fazerem a vida em Barão Geraldo valer a pena.

Ao professor Renato Pavanello, pela valiosíssima oportunidade de estudar na Unicamp. Por sua amizade, dedicação, conhecimento, humildade e confiança, que nos proporcionaram todas as condições para executar este trabalho. Um exemplo pessoal e profissional que terei para o resto da minha vida.

Aos professores Matthijs Langelaar e Fred van Keulen, pelo apoio, amizade e oportunidade de passar um grande ano em Delft.

Ao professor Mike Xie, pelo exemplo de pessoa, apoio e valiosa parceria acadêmica.

Ao professor Gil Ho Yoon, pelo trabalho inspirador e pelas discussões nos congressos.

Aos professores da graduação, Cleber Santiago Alves, pela amizade e pelo meu início na carreira acadêmica, e Fábio Lúcio Santos, pelo grande incentivo na escolha do meu caminho profissional.

Ao amigo William M. Vicente, pelos ótimos momentos de amizade dentro e fora da universidade e pela parceria acadêmica neste trabalho.

Aos amigos da universidade, Renan Caetano, José Geraldo, Luciano Evangelista, Jacob Torrejón, Carlos Souza, Rafael Bispo, Renan Ozelo, René Quispe, Sergio Quispe, André Gomes, Edgar Andres, Andrea Peña, Tainan Khalil, Jaime Carbajal, Claudia Madrid, Zulma Anaya, Felipe Azevedo, Luis Filipe, Andrés Felipe, Kevin Nakabashi, Mohammad Shaterzadeh, Diogo Moraes, Richard Ortiz, Walter Ramirez e Alan Tavares, pela amizade diária e convivência acadêmica essencial.

Aos amigos Thomas Benson, Filipe Tereso, Daniel Pires, Marcelo Arnellas, Thiago Brandão, Paulo Button, Mariana Ceriani, Sarah Adani, Daniel Baldin, Braian Makoto, Victor Sebinelli, Kleber Oliveira, Maria Lucia, Alice Gauto, Maria Padilha, Mariana Lucena, Monize Terra, Juliana Garcia, Kamiel Vreugdenhil, Guérios Mansur, Flávio Imazu, Silvio Neves, Fernanda Moutinho, Cinthia Silva, Halisson Júnior, Daniel Orsini, Flávio Pedro, Guilherme Telles, Daniel Malgarin, Fernando Izelli, Fábio Lima, Luiz Maehana e todos os outros pelos grandes momentos.

Aos amigos de Delft, Alex Verbart, Floris van Kempen, Michael Kirschneck, Rob Eling, Evert Hoojikamp, Banafshe Sajadi, Stijn Kerst, Marteen van der Seijs, Sasan Keyvani e Wang Qi pelo grande ano na Holanda.

À Faculdade de Engenharia Mecânica da UNICAMP pela oportunidade de realizar este trabalho e à FAPESP pelo suporte financeiro.

Acknowledgements

To my family, Ludimeri, José, Emília, Luiz, Patrícia, Paschoina and Manoel, without which I would be absolutely nothing.

To my dearest girlfriend, Ana, and her family, Fernando, Eliana, Izzolet, Valéria, Guilherme and Sandra by making life worth in Barão Geraldo.

To Renato Pavanello, for the invaluable opportunity to study at Unicamp. For his friendship, dedication, knowledge, humility and confidence, which provided us all the conditions to carry out this work. A role model, personal and professional, that I will follow for the rest of my life.

To Matthijs Langelaar and Fred van Keulen, for the support, friendship and the opportunity to spend a great year in Delft.

To Mike Xie, for being a great person and for the support and academic collaboration.

To Gil Ho Yoon, for the inspirational work and for the discussions in the conferences.

To my graduation supervisors Cleber Santiago Alves, for the friendship and my beginning in the academic career, and to Fábio Lúcio Santos, for the great encouragement in the choice of my profession.

To my friend William M. Vicente, for the great moments of friendship inside and outside the university and for the academic collaboration in this work.

To my friends from the university, Renan Caetano, José Geraldo, Luciano Evangelista, Jacob Torrejón, Carlos Souza, Rafael Bispo, Renan Ozelo, René Quispe, Sergio Quispe, André Gomes, Edgar Andres, Andrea Peña, Tainan Khalil, Jaime Carbajal, Claudia Madrid, Zulma Anaya, Felipe Azevedo, Luis Filipe, Andrés Felipe, Kevin Nakabashi, Mohammad Shaterzadeh, Diogo Moraes, Richard Ortiz, Walter Ramirez and Alan Tavares, for the friendship and essential academic experience.

To my friends Thomas Benson, Filipe Tereso, Daniel Pires, Marcelo Arnellas, Thiago Brandão, Paulo Button, Mariana Ceriani, Sarah Adani, Daniel Baldin, Braian Makoto, Victor Sebinelli, Kleber Oliveira, Maria Lucia, Alice Gauto, Maria Padilha, Mariana Lucena, Monize Terra, Juliana Garcia, Kamiel Vreugdenhil, Guérios Mansur, Flávio Imazu, Silvio Neves, Fernanda Moutinho, Cinthia Silva, Halisson Júnior, Daniel Orsini, Flávio Pedro, Guilherme Telles, Daniel Malgarin, Fernando Izelli, Fábio Lima, Luiz Maehana and all the others for the great moments.

To my friends from Delft, Alex Verbart, Floris van Kempen, Michael Kirschneck, Rob Eling, Evert Hoojikamp, Banafshe Sajadi, Stijn Kerst, Marteen van der Seijs, Sasan Keyvani and Wang Qi for the great year in The Netherlands.

To the Faculty of Mechanical Engineering at Unicamp for the opportunity to carry out this work and to FAPESP for the financial support.

“Whenever you feel like criticizing any one,” he told me, “just remember that all the people in this world haven’t had the advantages that you’ve had.”

F. Scott Fitzgerald, in *The Great Gatsby*

Resumo

PICELLI, Renato. Otimização Topológica Evolucionária de Problemas com Interação Fluido-estrutura. 2015. 189p. Tese (Doutorado). Faculdade de Engenharia Mecânica, Universidade Estadual de Campinas, Campinas, Brasil.

O objetivo desta tese é o desenvolvimento de uma ferramenta computacional para projeto de estruturas considerando interação fluido-estrutura usando otimização topológica. Uma metodologia de otimização estrutural topológica é proposta associada à formulações de elementos finitos em problemas fluido-estrutura acoplados. Nesses tipos de problemas a estrutura sofre carregamentos advindos do meio fluido, ou seja, pressão e/ou forças viscosas. As dificuldades em se projetar estruturas sob carregamentos de fluidos surgem devido à variação da localização, direção e magnitude dos carregamentos quando a forma e topologia da estrutura são alteradas durante a otimização. Isso se torna o principal desafio para os métodos tradicionais baseados na interpolação da densidade do material. Nesses métodos, as superfícies em contato com o fluido não são definidas explicitamente devido à existência de elementos estruturais de densidade intermediária. Neste trabalho é proposta uma metodologia alternativa para esse tipo de carregamento dependente da topologia. Com a extensão do método de *otimização estrutural evolucionária bidirecional* (BESO) associada à formulações fluido-estrutura acopladas, pressões e forças viscosas podem ser modeladas diretamente para qualquer topologia estrutural devido à natureza discreta dos métodos evolucionários. Assim, o problema é resolvido sem a necessidade de parametrização das superfícies de carregamentos de pressão. A metodologia BESO é estendida considerando os procedimentos de alteração entre elementos fluido-estrutura-vazios, novas análises de sensibilidade e restrições. Problemas em estado estacionário são considerados, incluindo elasticidade linear para a análise estrutural e as equações de Laplace, Helmholtz e escoamento incompressível de Navier-Stokes para a análise do fluido. Carregamentos constantes e não constantes são modelados. Diversos exemplos e aplicações são explorados com a metodologia proposta.

Palavras-chave: Otimização Topológica; Otimização Estrutural Evolucionária; Método BESO; Carregamentos dependentes do desenho; Interação fluido-estrutura

Abstract

PICELLI, Renato. Evolutionary Topology Optimization of Fluid-structure Interaction Problems. 2015. 189p. Thesis (PhD). School of Mechanical Engineering, University of Campinas, Campinas, Brazil.

The aim of this thesis is the development of a computational tool for the design of structures considering fluid-structure interaction using topology optimization. A methodology of structural topology optimization is proposed in association with finite element formulations of fluid-structure coupled problems. In this type of problems, the structure undergoes fluid loading, i.e., pressure and/or viscous loads. The difficulties in designing fluid loaded structures arise due to the variation of location, direction and magnitude of the loads when the structural shape and topology change along the optimization procedure. This turns out to be an additional difficulty for the traditional density-based topology optimization methods. In density-based methods, the pressure loaded surfaces are not explicitly defined due to the existence of intermediate density elements. In this thesis, it is suggested an alternative methodology to handle this type of design-dependent loads. With an extended *bi-directional evolutionary structural optimization* (BESO) method associated with different fluid-structure formulations, pressures and viscous loads can be modelled straightforwardly for any structural topology due to the discrete nature of the method. Thus, the problem is solved without any need for pressure load surfaces parametrization. The BESO methodology is extended considering the procedures of switching fluid-structure-void elements, new sensitivity analyses and constraints. Steady state problems are considered, including linear elasticity for the structural analysis and Laplace, Helmholtz and incompressible Navier-stokes flow equations for the fluid analysis. Constant and non constant loads are modelled. Several examples and applications are explored with the proposed methodology.

Keywords: Topology Optimization; Evolutionary Structural Optimization; BESO Method; Design-dependent loads; Fluid-structure Interaction

List of Figures

1.1	Archimedes' lever representation.	25
1.2	(a) Abstraction of a cantilever problem by Galilei (1933) and (b) representation of its solution by Lee (2007).	26
1.3	Santos Dumont's first ultra-light monoplane named 14-bis (image extracted from Portal São Francisco website at the url http://www.portalsaofrancisco.com.br/alfa/historia-do-aviao/historia-do-aviao.php , in 14th July, 2015).	28
1.4	Representation of the (a) structural design problem; and three different types of structural optimization: (b) sizing, (c) shape and (d) topology optimization (van Dijk, 2012).	29
1.5	Example of structural design problem and solution with topology optimization.	30
1.6	Solutions for (a) a structural design problem; by the (b) SIMP-model (Sigmund, 2001a) and (c) BESO approaches.	32
1.7	Example of (a) structural topology design problem of a cantilever beam, (b) solution by the standard BESO method and (c) evolutionary history of the optimization problem.	36
1.8	Example of Michell-structure.	37
1.9	Results of the search on "topology optimization" keyword in the Web of Science data in March/2015.	41
1.10	Illustration presented by Chen and Kikuchi (2001) of (a) structural topology design problem and possible solutions obtained with (b) fixed load cases and (c) design-dependent loads.	42
1.11	Example of topology design problem with (a) design-dependent pressure loads; (b) 2D design with non-uniform and discontinuous density distributions; (c) points of equal densities, (d) Bézier curves and (e) parametrized pressure surface. Method for pressure surfaces parametrization proposed by Hammer and Olhoff (2000).	43
1.12	Literature review flowchart of design-dependent pressure loading problems illustrating the scientific spot where the extended BESO method of this thesis is inserted on.	44
1.13	Elastic solids immersed on different types of fluids: (a) nonviscous hydrostatic fluids, (b) acoustic fluids and (c) viscous fluid flows.	45
1.14	Optimization step: fluid region update as a new operation in each iteration step of the BESO method procedure.	47
1.15	Structure of this thesis.	49

2.1	The solid (Ω_s) and fluid (Ω_f) domains and boundary conditions. Pressure P_0 is imposed on the portion S_p of the fluid boundary. Fluid pressure loads act on the structure through the fluid-structure interface S_{fs}	54
2.2	Coupling forces configuration before and after a structural element removal. The derivative $\partial \mathbf{L}_{fs} / \partial x_i$ can be approximated by the change of the coupling matrices $(\Delta \mathbf{L}_{fs})^i = (\mathbf{L}_{fs}^* - \mathbf{L}_{fs})^i$ after the i th element removal. The arrows indicate the pressure loads $\mathbf{L}_{fs} \mathbf{P}_f$ from the fluid elements acting on the structure.	58
2.3	Fluid-structure model: An underwater structure subject to hydrostatic pressure.	64
2.4	Example of elemental sensitivity numbers distribution evaluated by the Equation 2.25 for the the left side of the initial design domain.	64
2.5	BESO's topology solution for the arch-like example.	65
2.6	Convergence history of the arch-like structure's mean compliance.	65
2.7	BESO's topology snapshot with and without pressure loading sensitivities.	66
2.8	BESO's topology evolution for the arch-like example with initial guess design.	67
2.9	Convergence history of the arch-like structure's mean compliance starting with an initial guess design.	68
2.10	Fluid-structure model: piston head structure under pressure loading.	68
2.11	BESO's topology solution for the piston head example with iteration number n and structural volume V_n	69
2.12	Convergence history of the piston head mean compliance.	70
2.13	Sensitivities for the solid elements along the fluid-structure interface in the initial full design for the piston head finite element model.	70
2.14	Fluid-structure model: A pressurized fluid inside a channel between the structural design domains.	71
2.15	Pressure chamber design by the BESO method with: (a) 60×38 (2280 elements), (b) 120×76 (9120 elements), (c) 300×190 (57000 elements) and (d) 1200×260 (912000 elements).	72
2.16	Pressure chamber design by the BESO method with inlet pressure $(P_0)^i = 15$ Pa and outlet pressure $(P_0)^o = 10$ Pa. The pressure field is shown for the fluid domain.	73
2.17	Convergence history of the chamber's mean compliance with different inlet and outlet pressure.	74
2.18	Final solutions for the pressure chamber design problem by the BESO method with inlet pressure $(P_0)^i = 15$ Pa and different outlet pressures $(P_0)^o$	74
3.1	Examples of geometric configurations of subsea oil pipelines supported by buoyancy modules, represented as bullets in the illustrations. Buoyancy modules provide upward forces which counteracts the pipeline weight, holding the pipelines in the desired configurations.	77

3.2	The solid (Ω_s), fluid (Ω_f) and void (Ω_v) domains and boundary conditions. Pressure P_0 is imposed on the portion S_p of the fluid boundary. Fluid pressure loads act on the structure through the fluid-structure interface S_{fs}	80
3.3	Coupling forces configuration before and after an element removal. The derivative $\partial \mathbf{L}_{fs} / \partial x_i$ can be approximated by the change in the coupling matrices $(\Delta \mathbf{L}_{fs})^i = (\mathbf{L}_{fs}^* - \mathbf{L}_{fs})^i$ after removal of the i th element. The arrows indicate the pressure loads $\Delta \mathbf{L}_{fs} \mathbf{P}_f$ exerted by the fluid elements on the structure. . . .	86
3.4	Change in B due to a solid element removal at (a) the fluid-structure interface and (b) an interior element.	87
3.5	Design problem: complete fluid-structure model and the design domain used (a quarter of the model) including boundary conditions.	92
3.6	(a) Displacement field and (b) sensitivities distribution for the buoyant structure model.	93
3.7	Snapshots of the test case solution.	93
3.8	Evolutionary history of the buoyancy area B of the buoyant structure.	94
3.9	Evolutionary history of the global mean compliance of the buoyant structure. . .	94
3.10	Geometric properties of the hollow cylinder associated with the solutions for the test case.	95
3.11	Example of subsea buoy module for oil pipeline support (image extracted from Flotation Technologies [®] website at the url http://www.flotec.com/products/buckle-migration-buoyancy-modules , in 18th September, 2013).	97
3.12	Structural optimization design problem: (a) complete fluid-structure model and (b) design domain using half of the model showing the boundary conditions for the structure.	97
3.13	Buoy module designs with topology optimization: (a) Case 1 - full design domain and final topology; (b) Case 2 - initial semicircle solution and final topology (design-dependent loads); (c) Case 3 - initial semicircle solution and final topology with fixed fluid-structure interfaces (fixed loads).	98
3.14	Snapshots of the Case 2 solution after different iterations.	99
3.15	Evolutionary history of the buoyancy area for Case 2.	100
3.16	Evolutionary history of the mean compliance of the buoy in Case 2.	100
3.17	Different solutions with different evolutionary ratios.	101
3.18	Different solutions with different maximum admission ratios.	101
3.19	Different solutions with different penalty factors p	101
3.20	Normalized strain energy distribution for the buoyancy module designed with the proposed methodology using $p = 1 \cdot 10^5$ and variable and fixed boundaries. .	102
4.1	The coupled acoustic-structure system: the acoustic fluid domain Ω_f and the structural domain Ω_s coupled by integrals on the acoustic-structure interface S_{fs} . .	107

4.2	A clamped beam between two fluid domains under free vibration.	115
4.3	Clamped beam solutions obtained with the BESO method with initial structure starting from the: (a) full design domain; (b) initial guess design with 50% of the design domain.	115
4.4	Snapshots of the BESO solution starting from an initial guess design.	116
4.5	Evolutionary history of the objective function for the clamped beam example. .	116
4.6	Tunable device with open and closed acoustic fluid cavities.	117
4.7	First three natural frequencies and vibration modes for the (a) open and the (b) closed device configuration.	118
4.8	Topology solutions considering maximization of the first natural frequency, ω_1 , for the (a) open and the (b) closed fluid cavity configurations.	118
4.9	Evolutionary history of the objective function for both (a) open and (b) closed device configuration.	119
4.10	Water tank model.	119
4.11	Topology and evolutionary history for the solutions of the water tank design problem considering (a) ω_1 maximization and (b) multiple $\omega_1 + \omega_2$ maximization.	120
4.12	Pressure distribution according to the acoustic vibration modes Φ_1 and Φ_2 for (a) the initial guess design, (b) after ω_1 maximization and (c) after $\omega_1 + \omega_2$ maximization.	121
4.13	Water tower model.	122
4.14	Water tower model example: (a) structural topology solution for ω_1 maximization and (b) evolutionary history of the objective function.	123
4.15	Water tower model example: (a) structural topology solution for $\omega_1 + \omega_2$ maximization and (b) evolutionary history of the objective function.	123
4.16	Coupled vibration modes for (a) initial full design and for the structures obtained with (b) ω_1 maximization and with (c) $\omega_1 + \omega_2$ maximization.	124
5.1	Representation of “dry” and “wet” topology optimization approaches in FSI problems, as classified by Jenkins and Maute (2015).	127
5.2	The viscous fluid domain Ω_f and boundary conditions. A velocity profile $\mathbf{v}_f = \mathbf{v}_0$ is given at inlet boundary S_{in} , outlet pressure is set as $P_f = 0$ in S_{out} and the no-slip conditions (zero velocities $\mathbf{v}_f = 0$) are imposed at the fluid flow walls S_w .	130
5.3	The solid (Ω_s), fluid (Ω_f) and void (Ω_v) domains and boundary conditions. With steady-state fluid velocities and pressures profiles, fluid flow reaction forces can be calculated on the fluid-structure interfaces S_{fs} and imposed as loads in the structural analysis.	132
5.4	Mixed finite element Q2rP1.	134
5.5	Benchmark examples for fluid flow pressure drop minimization: (a) pipe bend and (b) double pipe models.	143

5.6	Fluid flow paths for (a) pipe bend and (b) double pipe models obtained with the BESO method and Darcy-Stokes equations.	144
5.7	Topology evolution of the pipe bend example obtained with BESO method for pressure drop minimization.	144
5.8	Fluid flow with obstacle example for pressure drop minimization.	145
5.9	Fluid flow with obstacle: (a) final fluid path obtained with BESO method, (b) fluid velocity and (c) pressure fields.	145
5.10	Fluid flow in a channel: example for aerodynamic profile.	146
5.11	Aerodynamic example: (a) solution obtained with BESO method and (b) fluid flow streamlines.	147
5.12	Fluid-structure model for “dry” structural topology optimization.	147
5.13	Solution for “dry” structural topology optimization of the aerodynamic profile considering: (a) Stokes fluid flow loads and (b) full Navier-Stokes fluid flow loads.	148
5.14	Fluid flow responses in the aerodynamic profile example: (a) velocity field and (b) pressure field considering incompressible Stokes flow equations and (c) velocity field and (d) pressure field considering incompressible Navier-Stokes flow equations.	149
5.15	Structural design problem for a fluid flow channel.	150
5.16	Topology solutions obtained with BESO method for the structural barrier example with inlet velocities: (a) $v_0 = 0.0001$ m/s, (b) $v_0 = 0.1$ m/s and (c) $v_0 = 1$ m/s. The fluid flow in Case 1 is governed by incompressible Stokes flow equations and for Cases 2 and 3 the fluid flows are governed by incompressible Navier-Stokes equations.	150
5.17	Velocity and pressure fields for the fluid flow in Cases 1, 2 and 3.	151
5.18	Topology evolution of the structural barrier obtained with BESO method in “wet” FSI topology optimization for Case 1.	152
5.19	Topology and velocity field evolution of the structural barrier example in “wet” FSI topology optimization for Case 3.	152
5.20	Topology and velocity field evolution of the structural barrier example in “wet” FSI topology optimization for: (a) Case 1 and (b) Case 3.	153
5.21	Structural design problem for a fluid flow chamber.	154
5.22	Structural topology solution for the flow chamber example.	154
5.23	Snapshots of the structural topology solution and its velocity fields for the n th iterations.	155
5.24	Structural topologies and pressure fields obtained considering loads from: (a) viscous fluid flow and (b) nonviscous pressurized fluid.	155
A.1	Computational tasks distribution for the presented methodology.	182
A.2	BESO fluid region update scheme illustration.	187

List of Tables

3.1	Dimensions of the hollow cylinders identified as the stiffest buoyant structures using the BESO method with different values of B_{lim} in the buoyancy inequality constraint. Values of the thickness t_s are shown for the geometrical measurements of the topology solutions and the numerical results of Equation 3.41 in the column <i>BESO</i> and <i>Theory</i> , respectively, as well as the absolute difference between them (column <i>Diff.</i>).	96
3.2	Objective function data for the cases shown in Fig. 3.13.	99

Notations

Latin Letters

A_c	- Area of a circle
A_i	- Area of an element
A_s	- Quarter of the cross-sectional area of a hollow cylinder
AR	- Volume addition ratio
AR_{max}	- Maximum volume addition ratio
B	- Buoyancy volume
B^*	- Buoyancy volume after an element removal
\mathbf{B}	- Matrix with derivatives of the finite element shape functions
B_{lim}	- Minimum required buoyancy volume
c_f	- Speed of sound in acoustic domain
C	- Structural mean compliance
C_n	- Structural mean compliance at iteration n
D	- Fluid potential power function
E	- Young's modulus
ER	- Evolutionary ratio
\mathbf{f}	- General body forces
\mathbf{f}_{fs}	- Global vector of interface fluid to structure forces
\mathbf{f}_{sf}	- Global vector of interface structure to fluid forces
\mathbf{f}_{fsi}	- Vector with viscous fluid flow forces
\mathbf{F}	- General vector of nodal loads
\mathbf{F}_B	- Buoyancy force acting on the structure
\mathbf{F}_s	- Global vector of nodal structural forces
$f(\mathbf{x})$	- Objective function
g_a	- Value of the gravitational acceleration
\mathbf{g}_a	- Vector of gravitational acceleration
$g(\mathbf{x})$	- Inequality constraint
$h(\mathbf{x})$	- Equality constraint
\mathbf{K}	- General global stiffness matrix
\mathbf{K}_f	- Global fluid stiffness matrix
\mathbf{K}_{fs}	- Global fluid-structure stiffness matrix
\mathbf{K}_g	- Global stiffness matrix in the extended BESO method

\mathbf{K}_s^i	- Elemental structural stiffness matrix
\mathbf{K}_n	- Global stiffness matrix in the extended BESO method at iteration n
\mathbf{K}_s	- Global structural stiffness matrix
\mathbf{K}_T	- Tangent stiffness matrix in viscous flows
\mathbf{K}_α	- Finite element matrix for Brinkman equations
l_i	- Length of the i th element's edge
\mathbf{L}_c^i	- Matrix which represents the coupling configuration change
\mathbf{L}_{fs}	- Spatial fluid-structure coupling matrix
\mathbf{L}_{fs}^*	- Spatial fluid-structure coupling matrix after an element removal
m_s	- Structural mass
\mathbf{M}_f	- Global fluid mass matrix
\mathbf{M}_{fs}	- Global fluid-structure mass matrix
\mathbf{M}_g	- Global mass matrix in the extended BESO method
\mathbf{M}_s^i	- Elemental structural mass matrix
\mathbf{M}_n	- Global mass matrix in the extended BESO method at iteration n
\mathbf{M}_s	- Global structural mass matrix
n	- Iteration number
\mathbf{n}	- Normal vector
\mathbf{n}_f	- Normal vector to the fluid
\mathbf{n}_s	- Normal vector to the solid
nel	- Number of elements
N	- Convergence parameter
\mathbf{N}	- Vector of finite element shape functions
\mathbf{N}_f	- Finite element shape functions for the fluid
\mathbf{N}_s	- Finite element shape functions for the structure
p	- Penalty factor
P_0	- Imposed nodal fluid pressure
P_f	- Fluid pressures field
\mathbf{P}_i	- Elemental vector of nodal fluid pressures
\mathbf{P}_f	- Global vector of nodal fluid pressures
q	- Penalty parameter in Brinkman equations
\mathbf{Q}	- Global fluid incompressibility matrix
\mathbf{Q}^i	- Element fluid incompressibility matrix
r_c	- Radius of a circle
r_{ij}	- Distance between a node j and an element i
r_{min}	- Filter radius
Re	- Reynolds number
S_{in}	- Fluid boundary for inflow
S_f	- Fluid boundary for hard-wall condition

S_{fs}	- Fluid-structure interface
S_{out}	- Fluid boundary for outflow
S_p	- Fluid boundary for imposed pressures
S_u	- Structure boundary for imposed displacements
S_w	- Fluid flow walls
t	- Time
t_s	- Thickness
\mathbf{u}	- Structural displacements field
\mathbf{u}_i	- Elemental vector of nodal structural displacements
\mathbf{u}_{fs}	- Global vector of nodal fluid-structural responses
\mathbf{u}_s	- Global vector of nodal structural displacements
\mathbf{U}	- General vector of nodal structural displacements
\mathbf{v}_0	- Imposed nodal fluid velocities
\mathbf{v}_i	- Element vector of nodal fluid velocities
\mathbf{v}_f	- Global vector of nodal fluid velocities
V_0	- Volume of the design domain
V_{n+1}	- Volume fraction at iteration $n + 1$
V_n	- Volume fraction at iteration n
V_f	- Prescribed final fluid volume fraction
V_s	- Prescribed final structural volume fraction
V_{NS}^k	- Approximation of the solution in Newton-Raphson solver
$V(x_i)$	- Volume of existent material
w	- Weight factor for numerical filter
\mathbf{W}_s	- Vector of structural weight
\mathbf{x}	- Set of design variables
x_i	- Design variable
x_{min}	- Lower bound design variable

Greek Letters

α	- Fluid inverse permeability
α_B	- Analytical derivative of the buoyancy volume
α_{Bi}	- Element sensitivity number with respect to buoyancy volume
α_C	- Analytical derivative of the structural mean compliance
α_{Bi}	- Element sensitivity number with respect to structural mean compliance
α_i	- Sensitivity number of the i th element
α_{fi}	- Global and analytical derivative of the objective function
α_j	- Sensitivity number of the j th node
α_{th}	- Sensitivity threshold

α_L	-	Lower limit of the fluid inverse permeability
α_U	-	Upper limit of the fluid inverse permeability
μ	-	Fluid dynamic viscosity
ν	-	Poisson's ratio
ρ_f	-	Fluid mass density
ρ_s	-	Structural mass density
ρ_e	-	Element density
ρ_{min}	-	Lower bound density
$\rho(\mathbf{x})$	-	Set of design variables as densities

Initials

b.c.	-	Boundary conditions
BESO	-	Bi-directional Evolutionary Structural Optimization
DOF	-	Degree of freedom
ESO	-	Evolutionary Structural Optimization
FEM	-	Finite Element Method
FSI	-	Fluid-structure Interaction
F-S	-	Fluid-structure
GPU	-	Graphics Processing Units
HPC	-	High Performance Computing
ISSMO	-	International Society for Structural and Multidisciplinary Optimization
LBB	-	<i>Ladyzenskaja-Babuska-Brezzi</i>
LSM	-	Level-set Method
MMA	-	Method of Moving Asymptotes
PhD	-	Doctor of Philosophy
RAMP	-	Rational Approximation of Material Properties
SIMP	-	Solid Isotropic Material With Penalization
SPH	-	Smooth Particle Hydrodynamics
WCSMO	-	World Congress of Structural and Multidisciplinary Optimization

Other Notations

\mathbf{A}^T	-	Transpose of a matrix \mathbf{A}
2D	-	Two-dimensional space
3D	-	Three-dimensional space

Table of Contents

List of Figures	11
List of Tables	16
Notations	17
Table of Contents	21
1 INTRODUCTION	24
1.1 Engineering design: handling forces	24
1.2 Structural design: science and engineering	26
1.3 Background	28
1.3.1 Structural optimization	28
1.3.2 Topology optimization of continuum structures	30
1.3.3 Evolutionary topology optimization methods	33
1.3.3.1 BESO algorithm for structural compliance minimization	35
1.4 Scientific literature review	37
1.4.1 The design-dependent problem	41
1.5 Fluid-structure interaction models	43
1.6 Extended BESO update scheme	46
1.7 Objectives and contributions	47
1.8 Layout of the thesis	48
2 STRUCTURAL TOPOLOGY OPTIMIZATION FOR DESIGN-DEPENDENT FLUID PRESSURE LOADS	50
Context	50
2.1 Introduction	50
2.2 Fluid-structure model: Governing equations and finite element discretization . .	52
2.2.1 Fluid domain	53
2.2.2 Structural domain	53
2.2.3 The coupled fluid-structure system	54
2.3 Problem formulation and sensitivity analysis	56
2.3.1 Topology optimization problem	56
2.3.2 Sensitivity analysis	56
2.4 Numerical implementation	60
2.4.1 The extended fluid-structure BESO method	62

2.5	Numerical results	63
2.5.1	Arch-like structure	63
2.5.2	Piston head model	67
2.5.3	Pressure chamber design	71
2.6	Conclusions	73
3	TOPOLOGY OPTIMIZATION OF SUBMERGED BUOYANT STRUCTURES	76
	Context	76
3.1	Introduction	76
3.2	Fluid-structure model: governing equations and finite element discretization . .	79
3.2.1	Fluid domain	79
3.2.2	Structural domain	80
3.2.3	The coupled fluid-structure system	81
3.3	Problem formulation	82
3.3.1	Topology optimization problem	82
3.3.2	Sensitivity analysis	83
3.4	Optimization procedure	88
3.4.1	Implementation issues for a BESO-based method	88
3.4.2	The extended fluid-structure BESO method	90
3.5	Numerical results	91
3.5.1	Test case	91
3.5.2	Subsea buoy design case	95
3.6	Conclusions	102
4	NATURAL FREQUENCY MAXIMIZATION OF ACOUSTIC-STRUCTURE INTERACTION SYSTEMS	104
	Context	104
4.1	Introduction	104
4.2	Acoustic-structure interaction: governing equations and finite element model . .	106
4.2.1	Acoustic domain	106
4.2.2	Structural domain	107
4.2.3	Discretized coupled acoustic-structure system	107
4.3	Evolutionary topology optimization for free vibration problems including acoustic-structure interaction	109
4.3.1	Problem statement	110
4.3.2	Sensitivity analysis	110
4.3.3	Summary of the evolutionary procedure	112
4.4	Numerical results	114
4.4.1	Beam example	114
4.4.2	Open and closed acoustic cavity	117

4.4.3	Water tank example	118
4.4.4	Water tower example	121
4.5	Conclusions	123
5	STRUCTURAL TOPOLOGY OPTIMIZATION CONSIDERING STATION- ARY VISCOUS FLUID FLOW LOADS	126
	Context	126
5.1	Introduction	126
5.2	Fluid-structure models: governing equations and finite element discretizations .	128
5.2.1	Viscous fluids	129
5.2.2	Solid domain	131
5.2.3	Fluid-structure interaction model	132
5.3	Topology optimization problems	136
5.3.1	Pressure drop minimization	137
5.3.2	Sensitivity analysis: Pressure drop minimization	137
5.3.3	Structural compliance minimization under FSI loads	138
5.3.4	Sensitivity analysis: Structural compliance minimization	139
5.4	Optimization procedures	141
5.4.1	The extended BESO method for fluid-structure interaction problems . .	141
5.5	Numerical results	142
5.5.1	Pressure drop minimization	143
5.5.2	Structural compliance minimization: “dry” optimization	146
5.5.3	Structural compliance minimization: “wet” optimization	148
5.6	Conclusions	154
6	CONCLUDING REMARKS	157
6.1	Summary and discussions	157
6.2	Suggestions for further research	159
	References	160
	Appendix	182
A	IMPLEMENTATION DETAILS	182
A.1	Preprocessing	182
A.2	Processing	183
A.3	Postprocessing	189

1 INTRODUCTION

The modelling of complex systems involving the interaction between two or more physical phenomena that occur in different time and space scale is one of the main current paradigms in computational mechanics. The knowledge resulted from the many researchers in this field can be used to grasp the behavior of our complex multiphysics surroundings. An adequate model can be obtained by using a finite number of discrete subcomponents of the system. Between the available discretization methods, the Finite Element Method (FEM) is a computational technique widely used to solve multiphysics engineering problems (Zienkiewicz and Taylor, 2005).

In complex geometries or multiphysics systems, the FEM provides for engineers the informations they could not obtain intuitively nor analytically. The method is then a powerful tool that can be used to improve engineering analysis and to better design complex systems, such as those found in coupled multiphysics problems. Furthermore, the FEM can be associated with optimization techniques, e.g., structural topology optimization, leading to non-intuitive optimal designs.

This thesis proposes and investigates a new approach to improve engineering design by performing structural topology optimization in different fluid-structure interaction (FSI) problems. We start with a brief historical introduction of structural design from the Western point of view.

1.1 Engineering design: handling forces

Throughout history, mankind has been striving to design all kinds of tools to different purposes. Let us consider *design* as the act to build hand tools, buildings, machineries, pieces of art and include *engineering* on it as any intellectual attempt to turn ideas into reality using different tools.

Engineering design involves the handling of different types of forces to move things or to achieve a final product. The concept of force was mathematically and intuitively, although not fully correctly, understood and used in the beginning years of science. A proof of that is the acclaimed quotation by Archimedes:

“Give me a place to stand on, and I can move the earth.”

– Archimedes, (Heath, 2002)

In his quotation, Archimedes referred to the possibility of small forces moving great weights with the help of a lever system. Archimedes' Law of the Lever states that a weight equivalent to a force F_E can be moved with the aid of a lever and a fulcrum when a force F_A applied at the opposite side of the lever is large enough such that

$$F_A d_a = F_E d_e \quad (1.1)$$

where d_a and d_e are the distance from the fulcrum of F_A and F_E , respectively, as illustrated in Figure 1.1. The greater the distance d_a , smaller is the magnitude of the force needed to move the weight. This leads to the important idea of the center of mass of a mass configuration, as well as the concept of *moment* used in classical mechanics.

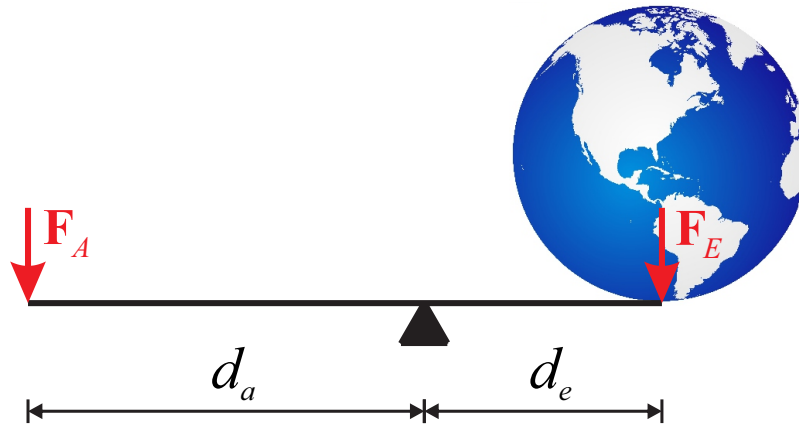
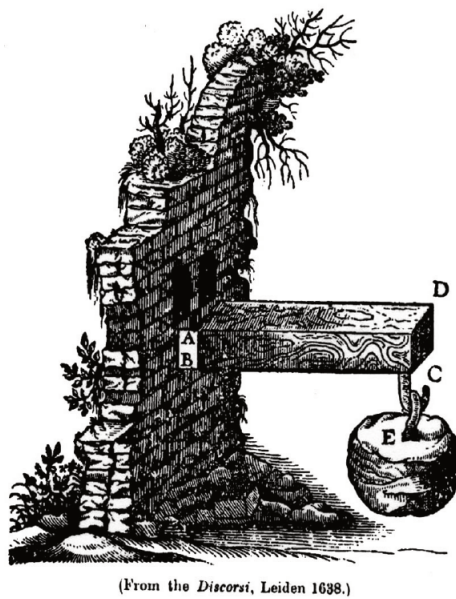


Figure 1.1: Archimedes' lever representation.

A problem can be formulated and solved to find the minimum force needed to move a large weight with an available lever and a fulcrum. Would that lead us to a first idea of an optimization problem?

Galileo Galilei also aimed to build better with less. In 1638, Galileo presented a logical abstraction of the shape of a cantilever beam for uniform strength (Lee, 2007), as given in Figure 1.2. The famous Italian scientist was a polymath. He investigated different types of forces, apart from a structural design scope. For instance, he carried out experiments culminating in the law of falling bodies.

Some years later, Sir Isaac Newton lapidated Galileo's conclusions, introduced new ideas and took the concept of force to a reliable mathematical level by formulating his famous three equations of motion with the aid of calculus (Newton, 1999). His groundbreaking work opened a wide range of possibilities to modern science and engineering.



(a)



(b)

Figure 1.2: (a) Abstraction of a cantilever problem by Galilei (1633) and (b) representation of its solution by Hooke (1665).

1.2 Structural design: science and engineering

Although the human being was capable of designing breathtaking buildings and bridges from ancient until medieval times, the essential shape of structural engineering was molded in a very short space of time by a few individuals in the later Renaissance (Wells, 2010).

While Galileo attempted to investigate the behavior of solid structures, he gave us insights of strength of materials. However, he failed in estimating correct stresses by not knowing elasticity (Timoshenko, 1953). Very few decades later, Robert Hooke published a paper discussing the linear elastic properties of materials for the first time and, subsequently, Edme Mariotte carried out tensile and bending experiments.

During the eighteenth century, structural design development was driven basically by the European society activities, such as colonial experience, military engineering and the industrial revolution. At that time, although few people were actually interested in the mechanics of elastic bodies, the new challenges in military and structural engineering required not only experience and practical knowledge, but also the ability to analyze new problems rationally and the scientific results of the preceding hundred years were gradually introduced in various fields of engineering (Timoshenko, 1953).

In the early nineteenth century, attempts were made to give the mechanics of elastic bod-

ies a more fundamental basis, culminating in the beginning of the mathematical theory of elasticity. Throughout the first half of the century, French engineers such as Claude Navier, Augustin Cauchy, Siméon-Denis Poisson, Barré de Saint-Venant and others, were occupied with the mathematical theory of elasticity. In England, engineers studied strength of materials experimentally in order to solve the numerous engineering problems during the intense industrial development, after the work of James Watt in machinery industry (Timoshenko, 1953). The introduction of iron and steel into structural and mechanical engineering made the experimental study of the mechanical properties of those materials essential.

New developments in industrial, military and civil societies initiated a rush in structural engineering in the Western world. First, in North America, commercial conditions implied the need of different machinery and infrastructure to transportation and mercantilism. Later on, the American reconstruction post-civil war represented a special stage in human society development, leading to new types of engineering for economic recovering concentrated on system development (Wells, 2010). At the end of that time, in Europe, theory of elasticity had received significant contributions by famous scientists such as, between many others, George Gabriel Stokes, comparing solids and viscous fluids, and James Clerk Maxwell, who developed the technique of photoelastic stress analysis.

The highly stressed conditions met by the components used in modern structural design called for a new and challenging set of load environments in structural problems. New materials were developed by metallurgy under the investigation of fatigue phenomena. This would be critical later in airship design.

Between the turn of the twentieth century, the brazilian young student Alberto Santos Dumont envisioned flight as a personal means of transportation, fostering an approach to lightweight structures. In 1906, Santos Dumont created the first ‘ultra-light’ monoplane, as illustrated in Figure 1.3.

Unfortunately, the world suffered two World Wars in the following years, which stopped the structural attenuation of aeroplane structures at that time and demanded different, stockier structures to support the inertial forces generated by the high speeds and tight turns of aerial combat (Wells, 2010). Again, military efforts guided the development of technologies, as well as structural engineering.

Until the mid-1900’s, extensive contributions were made to structural design in science and engineering. Fracture mechanics was investigated, three dimensional solutions were derived in elasticity and theories of vibration and impact were deepened (Timoshenko, 1953). Post-world war times increased the need for different structural applications, such as aerospace en-

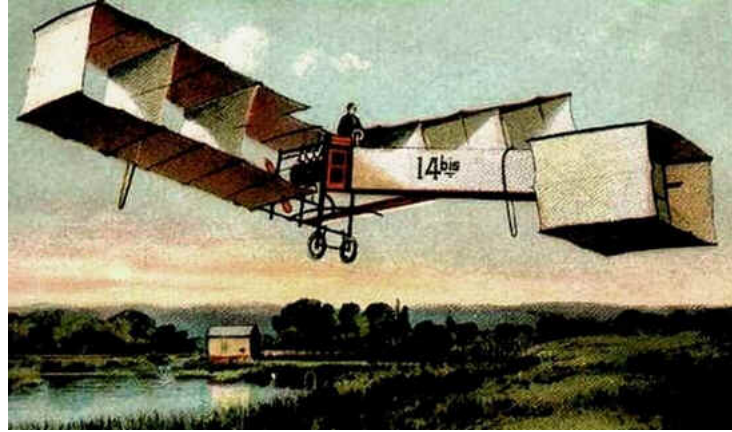


Figure 1.3: Santos Dumont's first ultra-light monoplane named 14-bis (image extracted from Portal São Francisco website at the url <http://www.portalsaofrancisco.com.br/alfa/historia-do-aviao/historia-do-aviao.php>, in 14th July, 2015).

gineering. Numerical methods were developed, e.g., the FEM (Zienkiewicz and Taylor, 2005). Architectural approaches were also incorporated to engineering design.

History showed that science and engineering were devoted to develop structural designs with many different ambitions. Although structural engineering was used to whatever human society demanded, e.g., economic growth or military efforts, engineers always attempted to improve performance considering the available resources. By attempting to improve performance and to reach better (or best) solutions, engineers carried out optimization.

1.3 Background

In structural design, many different types of engineering problems can be approached with optimization. This thesis is focused on topology optimization of structures interacting with multiphysics surroundings. Herein, specific fluid-structure interaction problems are considered. The following sections aim to describe the background and the state of the art of structural topology optimization. At last, the methodology is briefly described and the objectives and contributions are bounded.

1.3.1 Structural optimization

Structural optimization can be interpreted as the attempt to find the best structure to support specific load cases respecting some possible constraints. Mathematically, a general engi-

neering optimization problem consists in finding the design variables x_1, x_2, \dots, x_n , that

$$\begin{aligned} & \text{minimize:} && f(\mathbf{x}) \\ & \mathbf{x} \\ & \text{subject to:} && g(\mathbf{x}) \leq 0 \\ & && h(\mathbf{x}) = 0 \end{aligned} \quad (1.2)$$

where $\mathbf{x} = [x_1, x_2, \dots, x_n]^T$, the scalar function $f(\mathbf{x})$ is the objective function and $g(\mathbf{x}) = [g_1(\mathbf{x}), g_2(\mathbf{x}), \dots, g_m(\mathbf{x})]^T$ and $h(\mathbf{x}) = [h_1(\mathbf{x}), h_2(\mathbf{x}), \dots, h_p(\mathbf{x})]^T$ are functions that represent inequality and equality constraints, respectively, of the optimization problem (Herskovits *et al.*, 2007).

In the scope of structural optimization, the objective function $f(\mathbf{x})$ can be used to classify the structure, indicating the global structural performance. Usual objective functions are defined in terms of volume, local displacements, overall stresses, structural mean compliance, vibration responses and others. The constraints $g(\mathbf{x})$ and $h(\mathbf{x})$ usually indicate any design requirements or restrictions, e.g., structural mass, equilibrium conditions, maximum displacements, etc. The vector \mathbf{x} describes the structural configuration and can change during the optimization process. Each design variable x_n is defined depending on the type of optimization.

One can identify three main types of numerical structural optimization, namely *sizing*, *shape* and *topology optimization* (Papalambros and Wilde, 2000). They are distinguished between the changes they can cause to structural geometries, defined by the type of design parametrization, i.e., the set of design variables \mathbf{x} . Figure 1.4 illustrates the different structural optimization categories.

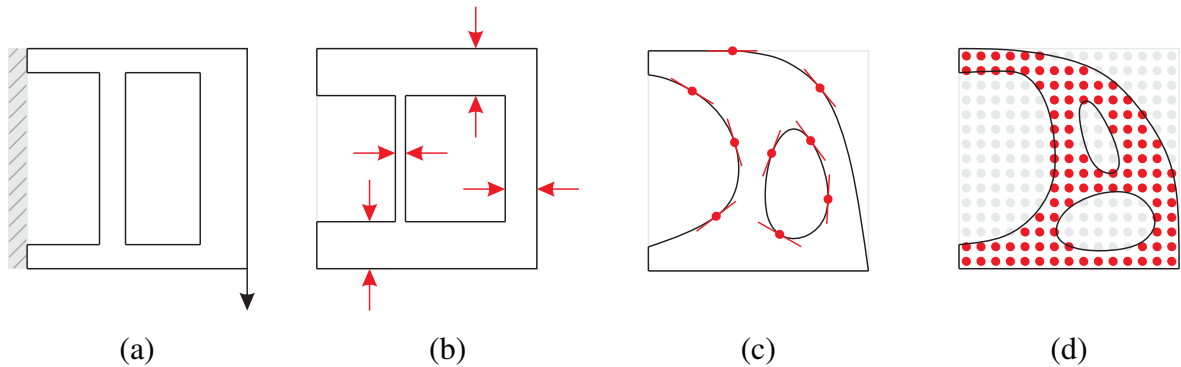


Figure 1.4: Representation of the (a) structural design problem; and three different types of structural optimization: (b) sizing, (c) shape and (d) topology optimization (van Dijk, 2012).

In *sizing optimization* geometric parameters such as thickness, diameters and lengths are set as design variables (Rozvany *et al.*, 1995). Consequently, the structural shape and topology are kept fixed in this type of optimization and the final result resembles that of the initial design,

as seen in Figure 1.4(b). The optimization method is able then to define the optimal dimensional values of the design variables according with the objective function.

Shape optimization is able to modify the position and geometry of the structural boundaries by parameterizing the shape of the design (Bendsoe, 1989). In Figure 1.4(c), the red dots and lines indicate the control points and tangents that can be used as design variables \mathbf{x} in this type of optimization (van Dijk, 2012). This approach is more complex than sizing optimization but not as flexible as the third optimization category.

A more general class of structural optimization relies on finding the optimal distribution of material inside a structural design domain and it is called *topology optimization* (Bendsoe and Sigmund, 2003). This type of optimization allows the creation of new cavities and structural members by altering not only sizes and shapes but also the layout of the structure. Points in the structural domain are set as design variables and can represent the existence or the absence of solid material, as illustrated in Figure 1.4(d).

1.3.2 Topology optimization of continuum structures

The idea of structural topology optimization is to design optimal structures by distributing solid material inside a design domain. In this case the geometry of the structure is defined by a set of design variables $x_i(\mathbf{x})$ in a “0-1” configuration. This leads to an indicator function

$$x_i(\mathbf{x}) = \begin{cases} 1 & \text{for } \Omega_s, \\ 0 & \text{for } \Omega_v, \end{cases} \quad (1.3)$$

where Ω_s and Ω_v are the solid and void domains, respectively (Maute *et al.*, 1999). The function x_i is defined by the design variables along the structural design domain and represents the material ($x_i = 1$) and the no material ($x_i = 0$) domains. Figure 1.5 illustrates a structural design problem and a possible solution using topology optimization.

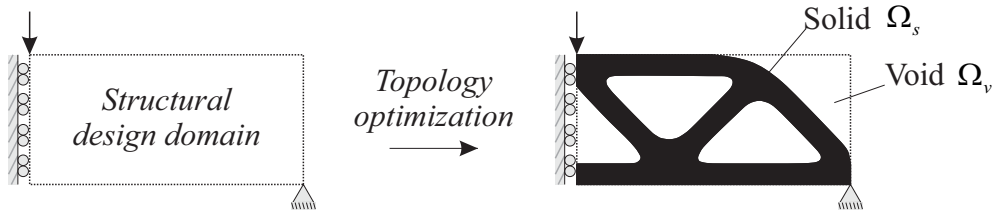


Figure 1.5: Example of structural design problem and solution with topology optimization.

The design variables in topology optimization are usually associated with a discretized

model using the Finite Element Method (FEM). The function x_i can indicate the material properties of the i th element in the finite element mesh or even its existence or absence. The manner that the elemental material properties are defined may be called as material model. The material model and the design variables update scheme (optimizer) can be used to classify the types of topology optimization methods. Currently, the most established methods are:

1. Density-based methods, including the homogenization and the Solid Isotropic Material with Penalization (SIMP) models.
2. Discrete methods, which include the Bi-directional Evolutionary Structural Optimization (BESO) method used in this thesis.
3. Boundary variation methods, such as the Level-set Method (LSM) and topological derivative-based methods.

Density-based topology optimization methods are the most widely used and describe the design variables in terms of a material density distribution $\rho_{min} \leq \rho(\mathbf{x}) \leq 1$, indicating the amount of solid material existent in each point \mathbf{x} of the design domain (Bendsoe and Sigmund, 2003; van Dijk, 2012). In the FEM discretization, an element density ρ_e is employed for each finite element. A critical aspect of these methods is the selection of interpolation functions to express the element densities as a function of continuous design variables. The whole set of design variables (interpolated densities) forms \mathbf{x} . The element densities are restricted to a lower bound ρ_{min} to avoid singular structural problems (Bendsoe and Sigmund, 2003) and intermediate densities $\rho_{min} < \rho_e < 1$ represent a specific volume fraction of the completely solid material. This leads to a gray-scale representation, as illustrated in Figure 1.6(b). This interpretation of continuous variables as material densities identifies a means to avoid numerical issues with purely 0-1 problems and iteratively steer the solution towards a discrete solid/void solution (Deaton and Grandhi, 2014). An optimizer such as the *Method of Moving Asymptotes* (MMA) by Svanberg (1987) can be used to solve the optimization problem and find the optimal densities configuration $\rho(\mathbf{x})$. A general density-based topology optimization on linearly static finite element analysis can be formulated as:

$$\begin{aligned}
 &\text{minimize:} && f(\rho(\mathbf{x}), \mathbf{U}) \\
 &\rho(\mathbf{x}) \\
 &\text{subject to:} && \mathbf{K}(\rho(\mathbf{x})) \mathbf{U} = \mathbf{F}(\rho(\mathbf{x})) \\
 &&& g_i(\rho(\mathbf{x}), \mathbf{U}) \leq 0 \\
 &&& h_i(\rho(\mathbf{x}), \mathbf{U}) = 0 \\
 &&& \rho_{min} \leq \rho(\mathbf{x}) \leq 1
 \end{aligned} \tag{1.4}$$

where f is the objective function, depending on the vector of design variables $\rho(\mathbf{x})$ and the vector of structural displacements \mathbf{U} , \mathbf{K} is the global stiffness matrix, \mathbf{F} is the force vector and g and h are the inequality and equality constraints, respectively.

The evolutionary methods apply a discrete design update scheme (optimizer) to iteratively guide the solution to the optimum. This implies crisply defined structural boundaries that are free of gray-scale intermediate densities, as seen in Figure 1.6(c). In these methods the design variables are described in a discrete manner as $x_i \in [0, 1]$, which defines the existence ($x_i = 1$) or the absence ($x_i = 0$) of solid material in each finite element (Xie and Huang, 2010). One may state that both density-based and evolutionary methods are quite similar in the light of the fact that both are gradient-based methods and present similar procedures and final solutions while having different design update schemes. In the evolutionary methods, a lower bound $x_i = x_{min}$ can also be employed to avoid singular structural problems and interpolation functions can also be used to develop the sensitivity analysis, which approximates even more these methods to the density-based ones (Huang and Xie, 2009). However, the main drawbacks of the evolutionary methods concern the handling of different constraints. The discrete update scheme is based on a target volume, which defines the amount of solid material in each iteration. Thus, an equality volume constraint is always present and different constraints should be able to coexist with this volume-based update scheme. This scheme also leads to criticisms on its absence of mathematical optimization theories. A standard evolutionary optimization problem can be formulated as:

$$\begin{aligned}
 &\underset{x_i}{\text{minimize:}} && f(x_i, \mathbf{U}) \\
 &\text{subject to:} && \mathbf{K}(x_i) \mathbf{U} = \mathbf{F}(x_i) \\
 & && h = V(x_i) / V_0 = V_s \\
 & && x_i \in [0, 1]
 \end{aligned} \tag{1.5}$$

where $V(x_i)$ is the volume of the existent material, V_0 is the volume of the structural design domain and V_s the prescribed final structural volume fraction.

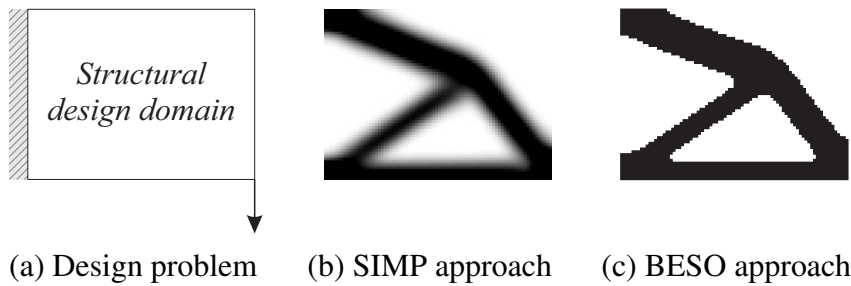


Figure 1.6: Solutions for (a) a structural design problem; by the (b) SIMP-model (Sigmund, 2001a) and (c) BESO approaches.

On the other hand, in the category of boundary variation methods, a level set function Φ

can be employed to describe a material domain inside the structural design domain as

$$x_i(\mathbf{x}) = \begin{cases} \Phi(\mathbf{x}) > c & \text{for } \mathbf{x} \in \text{material domain} \\ \Phi(\mathbf{x}) = c & \text{for } \mathbf{x} \in \text{interface} \\ \Phi(\mathbf{x}) < c & \text{for } \mathbf{x} \in \text{void} \end{cases} \quad (1.6)$$

where c is a constant, usually taken as 0 (van Dijk *et al.*, 2012). The Level-set Method (LSM) relies on finite elements and a Heaviside function can be used to map the geometries of the material domain. These methods are also closely related to density-based approaches (van Dijk *et al.*, 2012) and MMA can be used to solve LSM topology optimization problems. The shape of the geometric boundary is modified by controlling the motion of the level set (e.g., Heaviside) function according to the physical problem and optimization conditions (Deaton and Grandhi, 2014). Holes can merge, leading to new and different structural members. Other types of functions can also be used, such as a shape functional and its topological derivative, which measures the sensitivity of the function with respect to an infinitesimal singular domain perturbation, e.g., the insertion of holes (Norato *et al.*, 2007; Novotny and Sokolowskixie, 2003).

1.3.3 Evolutionary topology optimization methods

The topology optimization problems considered in this thesis are solved adopting the discrete update scheme of the evolutionary methods. In this subsection, general remarks are outlined and the standard BESO method is depicted in the manner it was developed by Huang and Xie (2007).

Originally, the evolutionary methods were based on the evolution of structures in nature, in which material is placed near regions subjected to high stresses. The so called Evolutionary Structural Optimization (ESO) method was performed with a gradual elimination of inefficient material from a structural domain discretized by the FEM, leading the structure to evolve towards better shapes and topologies (Xie and Steven, 1993). The idea is to use the gradient (derivative) information of the objective function as an indicator of the efficiency of each element in the structural performance, similarly as the carried out by density-based methods.

Attempts to extend the ESO algorithm to a bi-directional approach were carried out by ranking elements for removal and for addition separately (Yang *et al.*, 1999a; Querin and Steven, 1998; Querin *et al.*, 2000). Such treatment showed to be illogical and could lead to non optimal solutions (Xie and Huang, 2010). Following research on the evolutionary methods conducted by Huang and Xie (2007) proposed a new algorithm using a bi-directional approach, the so called *Bi-directional Evolutionary Structural Optimization* (BESO) method. The BESO method

in the manner it was developed by Huang and Xie (2007) addresses the known issues related to topology optimization of continuum structures, such as proper statement of the optimization problem, checkerboard pattern, mesh-dependency and convergence of solution (Xie and Huang, 2010).

Starting from a full design domain or initial guess design, the BESO method can simultaneously remove and add elements in each iteration step. The elements in the structural design domain are listed and ranked according to their efficiency relatively to the objective function. This efficiency is evaluated by a sensitivity analysis. The sensitivity of the objective function is defined by its derivative:

$$\alpha_{fi} = \frac{\partial f(x_i, \mathbf{U})}{\partial x_i} \quad (1.7)$$

where α_{fi} is the derivative of the objective function f with respect to the design variables x_i . The derivative is evaluated locally at the element level, generating a so called sensitivity number α_i for each element. The sensitivity numbers represent the contribution of each design variable x_i to the structural performance. The elements with the lowest sensitivities can be removed from the design domain with a minimum change in the objective function. To address numerical problems such as checkerboard and mesh-dependency, a spatial filter technique similar to the one proposed by Sigmund and Peterson (1998) is applied on the sensitivities. Huang and Xie (2007) have shown that the filtered sensitivity numbers should be averaged with their previous iteration values to help in the stabilization of the optimization.

The discrete update scheme of the BESO method is based on a target volume V_{n+1} which specifies the structural volume fraction of the following iteration, $n + 1$. The target volume is defined as

$$V_{n+1} = V_n(1 \pm ER), \quad (1.8)$$

where ER is the *evolutionary ratio* and sets the percentage of structural volume which increases or decreases V_n towards the prescribed final volume fraction V_s .

The rank list of elemental sensitivities is then used to set a new distribution of solid ($x_i = 1$) and void ($x_i = 0$) elements, based on a sensitivity threshold α_{th} , for which

$$\begin{cases} \alpha_i \leq \alpha_{th} & \text{is set as} & x_i = 0, \\ \alpha_i > \alpha_{th} & \text{is set as} & x_i = 1, \end{cases} \quad (1.9)$$

where α_{th} is the sensitivity of the i th element at the rank list position equivalent to the target volume fraction. A maximum volume addition ratio AR_{max} is introduced to limit the maximum number of added elements. For further details of the BESO method and the discrete design update scheme the reader is referred to the original article by Huang and Xie (2007) or the

reference book by Xie and Huang (2010). The previous procedures are repeated until a final structural volume fraction V_s is achieved and a convergence criterion is satisfied.

1.3.3.1 BESO algorithm for structural compliance minimization

The most common problem of structural topology optimization is the structural compliance minimization. For this case, the evolutionary topology optimization problem can be formulated as:

$$\begin{aligned} \min_{x_i} \quad & C(x_i) = \frac{1}{2} \mathbf{u}_s^T \mathbf{K}_s \mathbf{u}_s \\ \text{subject to:} \quad & \mathbf{K}_s \mathbf{u}_s = \mathbf{F}_s \\ & h = V(x_i) / V_0 = V_s \\ & x_i = [0, 1] \end{aligned} \quad (1.10)$$

where C is the structural mean compliance and \mathbf{K}_s and \mathbf{u}_s are the global stiffness matrix and the vector of structural displacements, respectively, and \mathbf{F}_s the vector of forces. The equality constraint h defines the prescribed final structural volume as a fraction of the initial full design domain volume. The mechanical equilibrium $\mathbf{K}_s \mathbf{u}_s = \mathbf{F}_s$ is another equality constraint and it is usually satisfied in advance with the finite element analysis. For such optimization problem, the basic following BESO algorithm is the current and standard evolutionary approach (Xie and Huang, 2010):

1. Discretize the design domain using a finite element mesh and assign initial property values (0 or 1) for the elements to construct an initial design.
2. Perform finite element analysis to obtain the structural responses by solving the equilibrium equation:

$$\mathbf{K}_s \mathbf{u}_s = \mathbf{F}_s. \quad (1.11)$$

3. Calculate the elemental sensitivity numbers. In structural compliance minimization, the sensitivity numbers are equivalent to the elemental strain energy as follows:

$$\alpha_i = \frac{1}{2} \mathbf{u}_i^T \mathbf{K}_s^i \mathbf{u}_i. \quad (1.12)$$

where \mathbf{K}_i and \mathbf{u}_i are the elemental stiffness matrix and nodal displacements, respectively.

4. Apply a numerical filter scheme to smooth the sensitivities.
5. Average the sensitivity numbers with their history information.
6. Determine the target volume V_{n+1} .

7. Set a new solid-void distribution by using the update BESO scheme given by Equation 1.9.
8. Repeat steps 2-8 until the constrained volume V_s is achieved and a convergence criterion is satisfied.

The evolutionary history of a compliance minimization problem using the BESO procedures is shown in Figure 1.7.

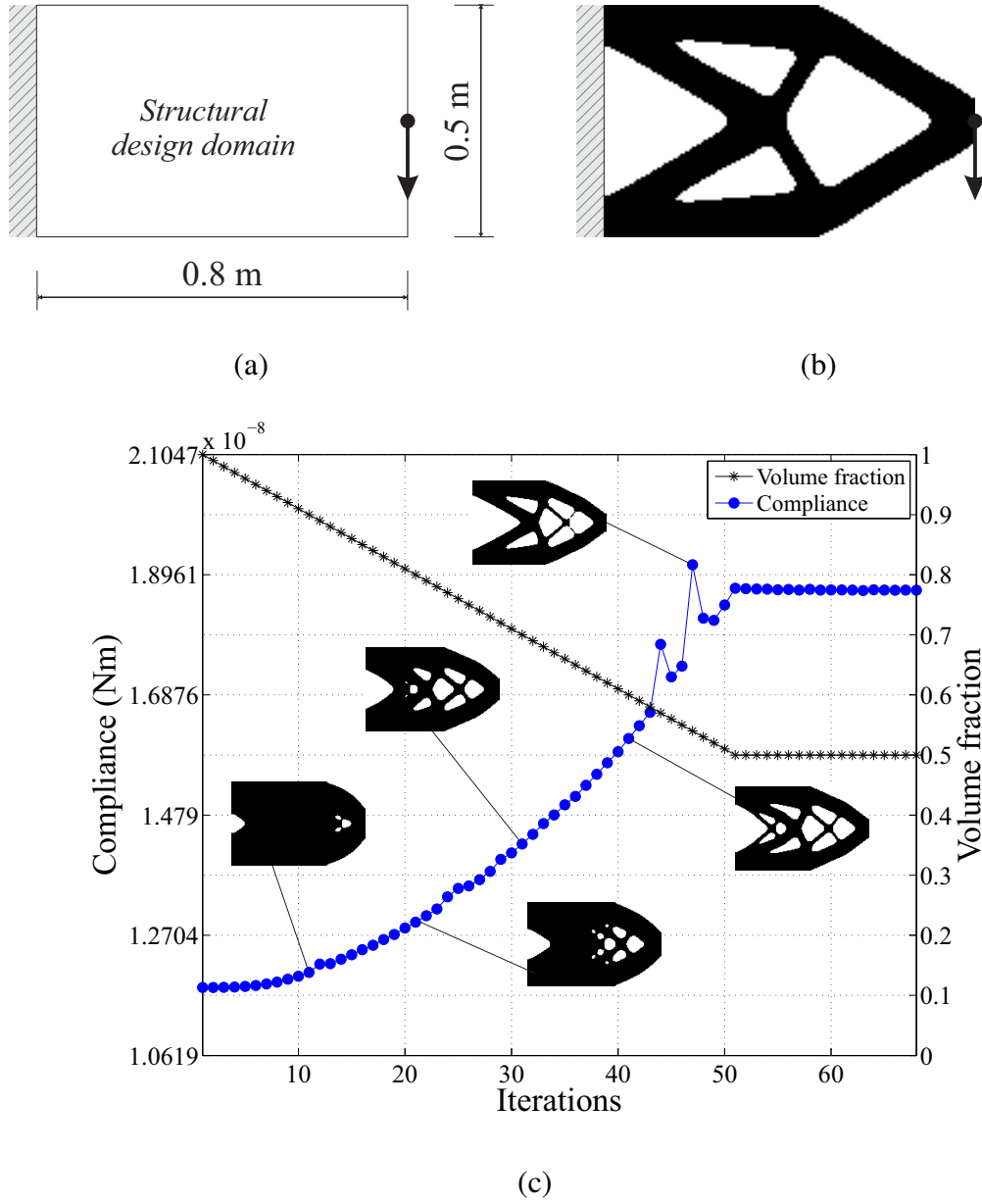


Figure 1.7: Example of (a) structural topology design problem of a cantilever beam, (b) solution by the standard BESO method and (c) evolutionary history of the optimization problem.

1.4 Scientific literature review

The first approach of topology optimization dates back to 1864 when James Clark Maxwell published “On reciprocal figures and diagrams of forces” (Maxwell, 1864), where he discussed fundamental principles for the layout of truss structures of minimum weight and prescribed maximum stresses. Forty years later, the Australian mechanical engineer Anthony G. M. Michell extended Maxwell’s principles to quasi-continuum truss structures (Michell, 1904). For one load cases, Michell presented orthogonal curved trusses with no shear stresses and maximum stiffness for given structural mass, see Figure 1.8.

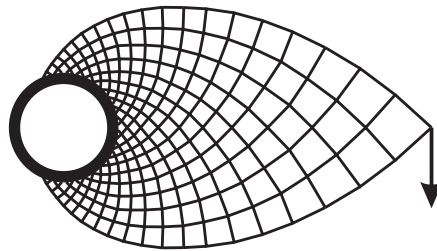


Figure 1.8: Example of Michell-structure.

In the 70’s, Hemp (1973) and Prager and Rozvany (1977) extended Michell’s approach to more complex optimization problems with multiple constraints and load cases applying analytical methods (Maute *et al.*, 1999). With the advance of the computers, the topology optimization methods for truss and beam structures have been developed into a design tool (Kirsch, 1989). These approaches were based on the so-called ground-structure approach (Dorn *et al.*, 1964). Topology optimization of grounded-structures became an important topic in structural optimization (Rozvany *et al.*, 1995; Lewinski and Rozvany, 2008) and it is still a special research field (Lyu and Saitou, 2005; Sokól and Rozvany, 2013; Zegard and Paulino, 2014; Sokól and Rozvany, 2015; Tangaramwong and Tin-Loi, 2015; Zhong *et al.*, 2015).

Research on optimal topologies in continuum structures began with Rossow and Taylor (1973) with the idea of finding optimal designs with variable thickness using the FEM. In a very pioneering work from 1988, Martin P. Bendsoe and Noboru Kikuchi suggested a homogenization method to relate solid and void elements with their microstructure density in a topology optimization problem (Bendsoe and Kikuchi, 1988). Their method was expanded to multiple load cases (Diaz and Bendsoe, 1992) and eigenproblems (Diaz and Kikuchi, 1992). Further work emphasized the mathematical aspects of the homogenization method (Hassani and Hinton, 1999) and the wide use in topology optimization by Bendsoe (1995). The material interpolation technique named SIMP (*Solid Isotropic Material with Penalization*) was first introduced in the paper by Rozvany *et al.* (1992) for shape optimization and further used in

topology optimization by Rozvany *et al.* (1994) and Yang and Chuang (1994).

Some authors were devoted then to address the many issues of topology optimization using the density-based approach, such as checkerboard patterns (Bendsoe *et al.*, 1993; Diaz and Sigmund, 1995; Sigmund and Peterson, 1998) and the development of optimality criteria (Rozvany *et al.*, 1994) as well as convergence analysis (Svanberg, 1994; Cheng and Pedersen, 1997). The SIMP technique rapidly became a popular material interpolation scheme for topology optimization with the work by Ole Sigmund (Sigmund, 1994, 1995) and his role in the dissemination of the method, publishing later the famous 99 line topology optimization code (Sigmund, 2001b).

The density-based methods of topology optimization have undergone a rapid development and were incremented with many different techniques. Efforts were carried out to integrate boundary design optimization and topology design (Olhoff *et al.*, 1993; Maute and Ramm, 1997). Restriction methods were implemented first by Haber *et al.* (1996) who considered perimeter constraints. Gradient and slope constrained methods were also developed (Peterson and Sigmund, 1998; Borrvall and Peterson, 2001), while Poulsen (2001) introduced minimum length scale controls in topology optimization. Stolpe and Svanberg (2001) proposed an alternative interpolation scheme for topology optimization, namely *Rational Approximation of Material Properties* (RAMP). Topology optimization was extended to a wide range of structural design problems, such as vibration problems (Ma *et al.*, 1995; Krog and Olhoff, 1999; Pedersen, 2000), stability (Min and Kikuchi, 1997; Neves *et al.*, 2002), stress constraints (Duysinx and Bendsoe, 1998; Duysinx and Sigmund, 1998), geometric non-linearities (Jog, 1996; Buhl *et al.*, 2000; Bruns and Tortorelli, 2001), synthesis of compliant mechanisms (Sigmund, 1997; Chen and Kikuchi, 2001) and materials design for different types of applications (Sigmund and Torquato, 1996; Terada and Kikuchi, 1996; Silva *et al.*, 1997; Yi *et al.*, 2000). All these developments and extensions were compiled in a reference book of structural topology optimization by Bendsoe and Sigmund (2003), establishing the density-based methods as new techniques of structural design.

Still in the 90's, different topology optimization methods were developed. The so called *Evolutionary Structural Optimization* (ESO) was proposed by Yi Min Xie and Grant P. Steven as a topology optimization method based on successive material elimination (Xie and Steven, 1993). The ESO method became well known, however not as popular as the density-based topology optimization, receiving severe criticism years later (Zhou and Rozvany, 2001) on its heuristic inspiration and lack of mathematical formulation. Attempts were made to extend the ESO methods to different structural design problems (Chu *et al.*, 1996; Xie and Steven, 1996; Chu *et al.*, 1997; Li *et al.*, 1999) and a first book was published (Xie and Steven, 1997). Steven *et al.* (2000) used ESO for the first time for general physical field uncoupled problems, including

a fluid domain design case. Nevertheless, the method still presented some limitations because of its complete elimination of material. Further improvements to the ESO method proposed a bi-directional algorithm (Querin and Steven, 1998) and the *Sequential Element Rejections and Admissions* (SERA) method (Rozvany and Querin, 2002) to allow void (or very low density) elements to return to the solid condition. At that time other types of topology optimization developed from the combination of different techniques, such as *Genetic Algorithms* (GA) (Chapman *et al.*, 1994) and later on the early 2000 the *Level-set Method* (LSM) (Sethian, 1999; Wang *et al.*, 2003). A topological derivative concept was formalized by Sokolowski and Zochowski (1999) in shape optimization and used in topology optimization by C  a *et al.* (2000); Novotny (2003).

Post years 2000 the research field of topology optimization has virtually exploded and has been extended to many different design problems. New procedures were proposed and discussed in terms of convergence analysis (Martinez, 2005; Sigmund, 2007) as well as regularization techniques, such as numerical filtering in mesh-independence and checkerboard control (Poulsen, 2002, 2003; Jang *et al.*, 2003; Lazarov and Sigmund, 2011; Sigmund and Maute, 2012) and projection methods (Guest *et al.*, 2004, 2011; Wang *et al.*, 2011). Other extensions were developed for density-based methods in structural topology optimization such as considering nonlinear responses (Yoon and Kim, 2005; Jung and Gea, 2004; Yoon and Kim, 2007), heat transfer and thermoelasticity (Gersborg-Hansen *et al.*, 2006; Gao *et al.*, 2008; Gao and Zhang, 2010) and design-dependent loads, pressure (Hammer and Olhoff, 2000; Sigmund and Clausen, 2007; Lee and Martins, 2012) and self-weight (Bruyneel and Duysinx, 2005). Stress constraints (Pereira *et al.*, 2004; Duysinx *et al.*, 2008; Qiu and Li, 2010) and dynamic systems (Du and Olhoff, 2007b; Yoon *et al.*, 2007) also followed to be important and challenging topics in topology optimization.

A variety of engineering disciplines rather than structural design began to be handled with topology optimization. The density-based approach was applied to design fluid flow paths (Borrvall and Petersson, 2003; Gersborg-Hansen *et al.*, 2005; Evgrafov, 2006) as well as acoustic and wave propagation systems (Wadbro and Berggren, 2006; Du and Olhoff, 2007a; Duhring *et al.*, 2008). Relatively new applications of density-based topology optimization emerged in the last decade such as aerolasticity (Maute and Allen, 2004; Leon *et al.*, 2012) and biomedical design (Sutradhar *et al.*, 2010).

On the other hand, the years 2000 were important to the development of the ESO-based methods. Attempts were made to improve the efficiency of the evolutionary methods (Kim *et al.*, 2003) and to extend them to different problems (Li *et al.*, 2004; Yang *et al.*, 2005; Ansola *et al.*, 2006). In 2007, Xiaodong Huang and Yi Min Xie proposed a new and efficient bi-directional update scheme for the evolutionary methods, calling it *Bi-directional Evolutionary Structural*

Optimization (BESO) method (Huang and Xie, 2007). The BESO method from Huang and Xie (2007) is the standard and currently used version of the evolutionary methods and addresses the many known issues of the topology optimization methods, such as checkerboard patterns, mesh-dependency and convergence. One year later, Huang and Xie (2008a) published a work showing that the new BESO algorithm circumvent the many problems pointed years earlier by Zhou and Rozvany (2001). The BESO method could then efficiently solve different topology optimization problems such as for nonlinear structures (Huang and Xie, 2008b), multiple materials design (Huang and Xie, 2009), natural frequencies maximization (Huang *et al.*, 2010), self-weight loads (Huang and Xie, 2011) and others. A further review of ESO type methods for topology optimization was published (Huang and Xie, 2010) as well as a reference book by Xie and Huang (2010). Therewith, the evolutionary methods reached maturity and are currently applied to different problems with similar results as the density-based ones. Some problems concerning the handling of different constraints are still an issue for the BESO method.

Very recent works confirm the intense area of topology optimization for both density-based (Yoon, 2013; Alexandersen *et al.*, 2014; Evgrafov, 2015; Jenkins and Maute, 2015) and evolutionary (Zuo and Xie, 2014; Xia and Breitkopf, 2014; Vicente *et al.*, 2015; Huang *et al.*, 2015) methods. The level-set methods experienced also a rapid development in the last years and are currently established as one of the main topology optimization tools (Allaire *et al.*, 2004; Pingen *et al.*, 2010; van Dijk *et al.*, 2010; Shu *et al.*, 2011; Kreissl and Maute, 2012; van Dijk *et al.*, 2012). A complete review of the LSM is presented by van Dijk *et al.* (2013). Some researchers took use of level-set functions to improve the geometry update scheme of the topological derivative-based methods (Norato *et al.*, 2007; Amstutz *et al.*, 2012; Lopes *et al.*, 2015). Other types of topology optimization such as genetic algorithms still exist but are less used. Figure 1.9 presents the amount of publications concerning the keyword “topology optimization” in the Web of Science data post years 2000, an evidence of the recent growth and activity of this scientific area.

Deaton and Grandhi (2014) surveyed the current state of the topology optimization methods considering developments after the year 2000. The authors detailed all the procedures of the existent topology optimization methods and their research stages. They also present a list of recommendations and perspectives related to the field of structural and multidisciplinary optimization. The list outlines the needs for the near future research in the area. The list of future perspectives is composed by: design-dependent physics; stress-based topology optimization; multidisciplinary and multiphysics applications; biomedical design and medical applications; robust and reliability-based topology; topology to shape and size transition; advanced manufacturing capabilities and high performance computing (HPC) and graphics processing unit (GPU) implementations.

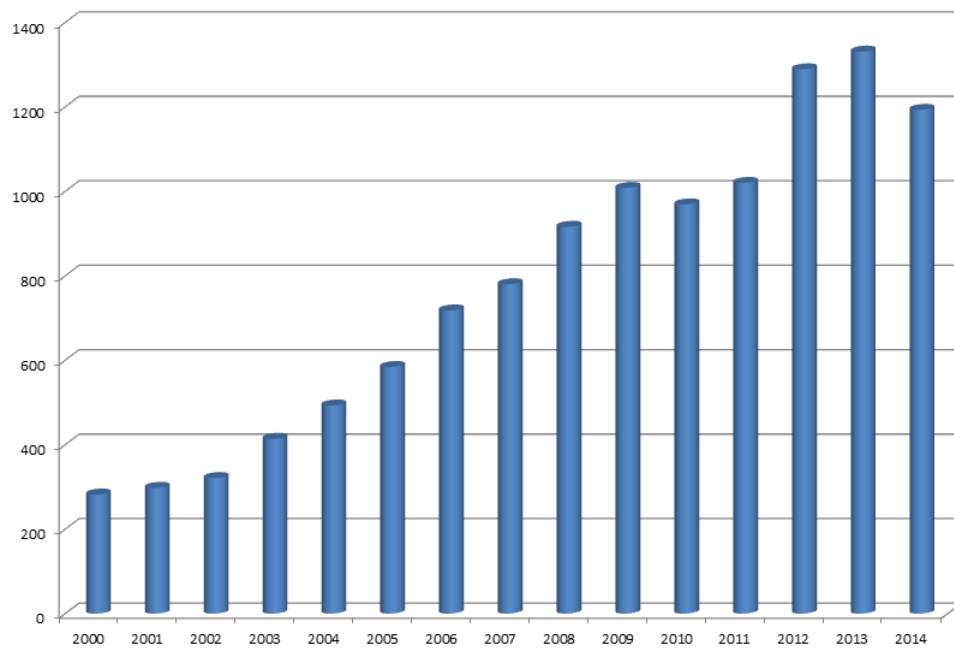


Figure 1.9: Results of the search on “topology optimization” keyword in the Web of Science data in March/2015.

The open research topics summarized in this list (Deaton and Grandhi, 2014) also reflects the class of sections and works presented at the *11th World Congress of Structural and Multidisciplinary Optimization (WCSMO-11)*, which took place in 2015 at Sydney, Australia, organized by the *International Society for Structural and Multidisciplinary Optimization (ISSMO)*. Between them one can cite the works by Picelli *et al.* (2015c) on design-dependent fluid flow loads, de Leon *et al.* (2015) on stress constraints, Norgaard *et al.* (2015) on unsteady fluid flow patterns, Chang (2015) on biomedical applications, Hu *et al.* (2015) on reliability-based design optimization, Lian and Sigmund (2015) on combination of topology and shape optimization, Smith *et al.* (2015) on additive manufacturing and Andreassen *et al.* (2015) on HPC.

1.4.1 The design-dependent problem

Much has been done to extend the methods of topology optimization to a multitude of design problems. However, relatively few authors have been devoted to model design-dependent physics, which is the focus of this thesis. In this type of problems, two or more physical fields governed by different differential equations interact between each other and their responses depend on the configuration of the interface they share.

The idea of this thesis is to develop methodologies for design-dependent problems using specific fluid-structure interaction models. In this case, design-dependency is characterized by

allowing the fluid-structure interfaces to change their location during optimization. Usually, the structures in these problems are loaded by fluid pressure loads.

In pressure loaded structural design problems, the position of the loads depends on the shape and topology of the structure. Such problems are encountered in hydrostatics and dynamics of wind, water loaded mechanical and civil structures such as ships, submerged structures, airplanes, pumps, etc. (Sigmund and Clausen, 2007). Figure 1.10 illustrates the design-dependency of this type of problems. While the structural topology changes by the optimization procedures, the location, direction and even the magnitude of the pressure loads can also change.

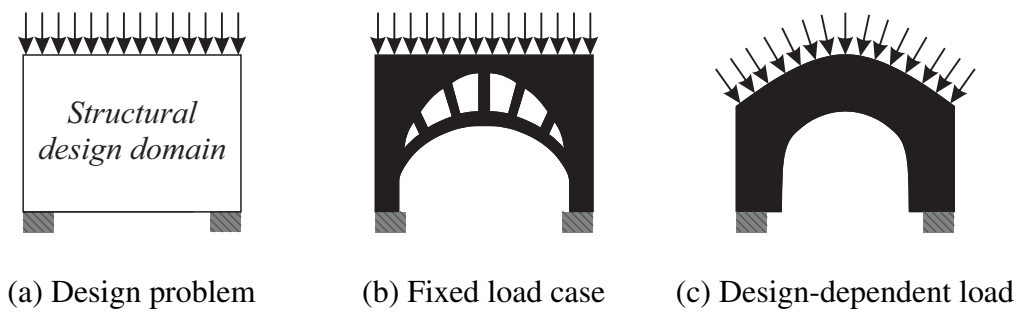


Figure 1.10: Illustration presented by Chen and Kikuchi (2001) of (a) structural topology design problem and possible solutions obtained with (b) fixed load cases and (c) design-dependent loads.

The density-based methods were created considering fixed load cases such as shown in Figure 1.10(b). In these methods, moving load surfaces is an issue related to boundary data (Sigmund and Clausen, 2007). The identification of the surfaces where design-dependent loads will act is not straightforwardly determined because of the presence of intermediate density elements. The interface between lower and higher densities is usually smooth during the optimization procedures and the load boundaries are unknown. Hammer and Olhoff (2000) pointed out the problem first in topology optimization. The authors proposed the identification of equal density points and the use of Bézier curves to model load surfaces in pressure problems, as illustrated in Figure 1.11. A complete literature review of design-dependent pressure loading problems is given in Chapter 2.

In most of the works attempting to address this class of loads, the pressure field is considered constant and directly applied as tractions in the structural analysis after a pressure surface parametrization. Some others can describe non constant pressure fields, however with mixed multiphysics models and overlapping domains. This thesis proposes the modelling of classic fluid governing equations and the discrete BESO design update scheme as a basis to topology optimization of different types of fluid-structure interaction problems. The structural and fluid domains are modelled separately and interact through their interfaces. The configuration

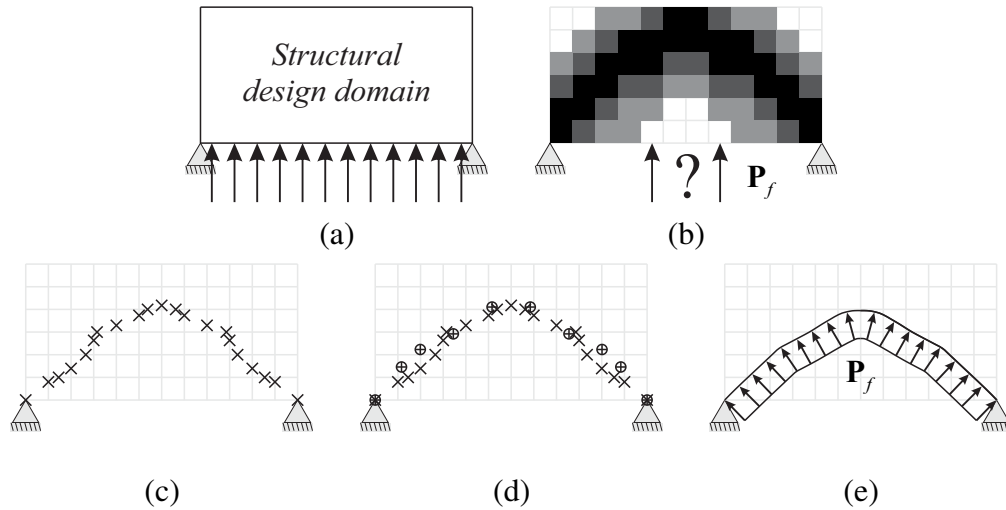


Figure 1.11: Example of topology design problem with (a) design-dependent pressure loads; (b) 2D design with non-uniform and discontinuous density distributions; (c) points of equal densities, (d) Bézier curves and (e) parametrized pressure surface. Method for pressure surfaces parametrization proposed by Hammer and Olhoff (2000).

and position of the fluid-structure interfaces are allowed to change during the optimization procedures. The idea is that the methodologies developed here can be extended to different multi-physics applications in the near future. Figure 1.12 presents a flowchart illustrating the scientific slot of the methodology of this thesis (first published with the paper by Picelli *et al.* (2015b)) on design-dependent pressure loads literature. The flowchart links the publications which are chronologically or thematically related, according to the type of technique it is used to solve the design-dependent problem.

1.5 Fluid-structure interaction models

This work is devoted to designing improved structures using as performance information the structural responses induced by fluid pressure loads. Herein, one shall consider three different types of fluids interacting with linear elastic structures, see Figure 1.13, sorted here as:

- *Fluid 1*: Nonviscous incompressible and irrotational fluids, describing a hydrostatic analysis.
- *Fluid 2*: Acoustic fluids, describing a vibroacoustic analysis.
- *Fluid 3*: Viscous fluid flows, describing viscous and pressure loads from a stationary fluid flow.

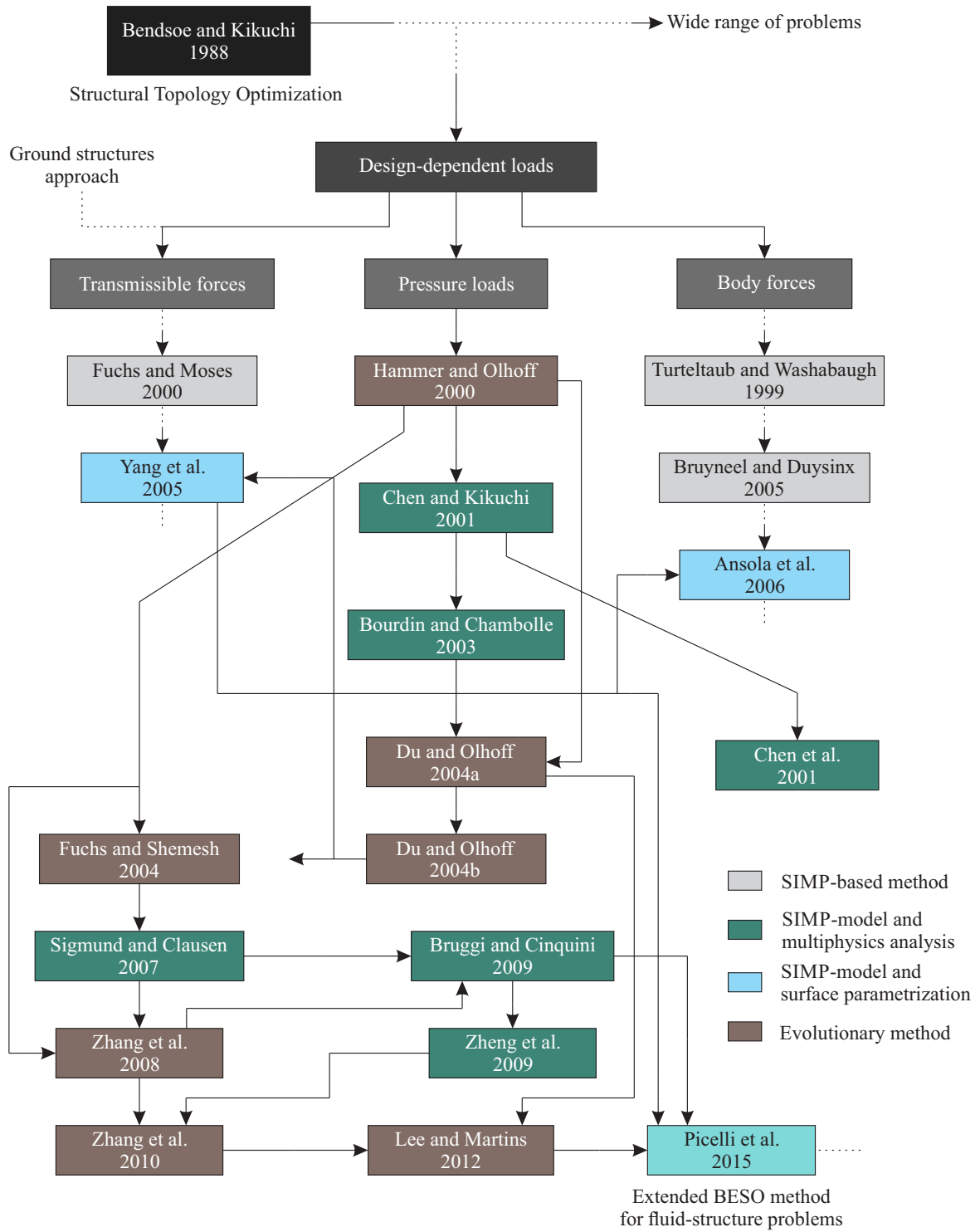


Figure 1.12: Literature review flowchart of design-dependent pressure loading problems illustrating the scientific spot where the extended BESO method of this thesis is inserted on.

In hydrostatic analysis (*Fluid I*), the equilibrium of the solid can be considered as a function of the static fluid pressure field P_f , which loads the structure at the wetted walls S_{fs} , as illustrated in Figure 1.13(a). It is of interest to notice that this static problem is not coupled, because P_f is the solution of a hydrostatic problem which can be solved independently from

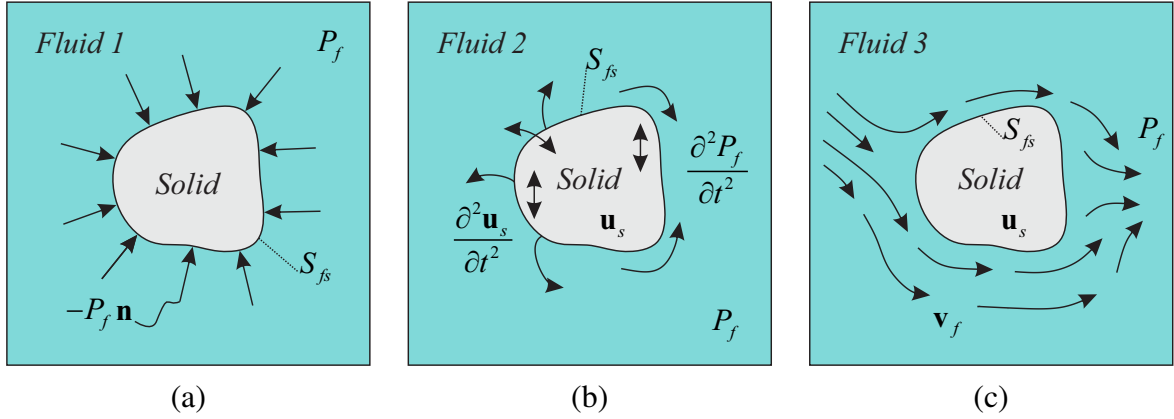


Figure 1.13: Elastic solids immersed on different types of fluids: (a) nonviscous hydrostatic fluids, (b) acoustic fluids and (c) viscous fluid flows.

the equilibrium of the solid. In contrast with the static case, the dynamical problem (*Fluid 2*) is found to be coupled. The motion of the structure induces some motion within the fluid, while the motion of the fluid generates a fluctuating pressure field which loads the structure, see Figure 1.13(b). As a consequence, the motion of the solid is modified (Axisa and Antunes, 2007).

For viscous fluid flows (*Fluid 3*), the equilibrium of the structure depends on viscous and pressures forces on the wetted wall S_{fs} of a fluid flowing with certain velocity \mathbf{v}_f , see Figure 1.13(c). If the structural displacement field \mathbf{u}_s is large enough, the fluid flow path changes along time. Consequently, the fluid responses also change (Bazilevs *et al.*, 2013).

In general, coupling conditions in a fluid-structure model can be given by ensuring the continuity of the velocity and the equilibrium between both domains on the wetted wall S_{fs} , assuming the fluid adheres to the walls and a fluid-structural stress balance on S_{fs} . The structures are considered here to be linearly elastic for all interacting fluids, which brings three different fluid-structure interaction models explored in this thesis.

Although the interaction between a structure and the three different types of fluids described here can be classified as *fluid-structure interaction* (Axisa and Antunes, 2007; Bazilevs *et al.*, 2013), in the field of topology optimization fluid-structure interaction is referred to the group of problems involving a structure and a viscous fluid flow in the manner described by Bazilevs *et al.* (2013), while acoustic-structure interaction is referred to problems such as the ones described by Morand and Ohayon (1995) and Axisa and Antunes (2007). Examples of that are the references papers by Yoon (2010), for fluid-structure interaction, and Yoon *et al.* (2007), for acoustic-structure interaction.

All types of motion for Newtonian fluids can be derived by using the momentum and continuity equations, which when combined build the Navier-Stokes equations. The following chapters describe the specific fluid cases considered and the equations which describe the different fluid-structure interaction models used in this work. Herein, both physical fields are formulated within the framework of continuum mechanics. However, the fluid formulations are derived by using the Eulerian viewpoint while a Lagrangian viewpoint is used to derive the structure formulation. The variables of the fluid and the solid domains are shared between all types of models.

The three fluid-structure models described here are used in four different topology optimization problems. Chapters 2 and 3 apply the case of *Fluid 1* in design-dependent fluid pressure loading problems and subsea buoyancy modules design, respectively. Chapter 4 uses *Fluid 2* as a fluid model in natural frequency maximization of acoustic-structure interaction systems, while Chapter 5 uses viscous fluid flows (*Fluid 3*) in fluid-structure interaction optimization problems. All these fluid-structure systems are designed with the proposed BESO method extension.

1.6 Extended BESO update scheme

The proposed methodology used in this thesis is a BESO-based approach. The main contribution to the BESO method is the handling of different types of incompressible fluid models in the optimization problems. This allows fluid-structure interaction to be formulated in evolutionary structural optimization problems. Basically, incompressible fluid domains are placed alongside structural design domains.

In the finite element discretized form, the discrete BESO update scheme sets a new design variables distribution (solid/void) for the structural design domain in each optimization step. The void elements which appear in the design domain and are next to the initial fluid domain can be substituted by incompressible fluid elements. Thus, the initial fluid region is updated and the fluid-structure interface S_{fs} is allowed to move, i.e., to change its position in each iteration of the optimization procedure, as illustrated in Figure 1.14.

With the *moving interface* procedure, the fluid region tracks the fluid-structure interface changes. Then, coupling stress balances can be carried out straightforwardly for any discrete design configuration and design-dependent loads can be easily handled in the optimization problem. This is the main feature of the extended BESO method proposed in this thesis.

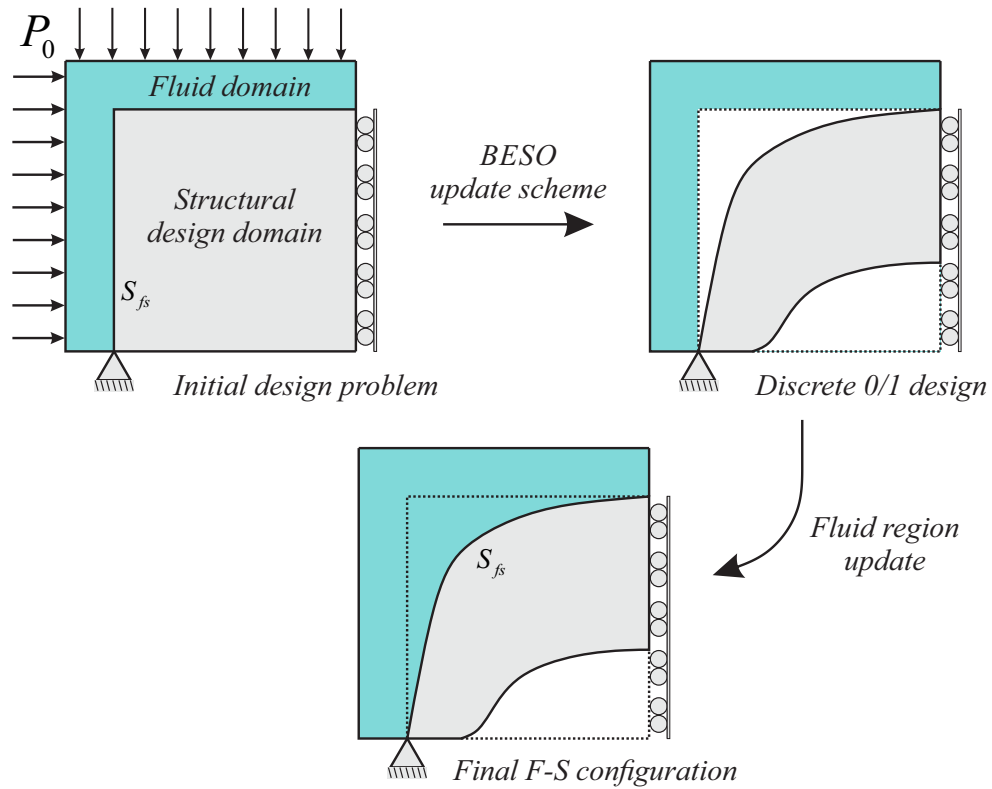


Figure 1.14: Optimization step: fluid region update as a new operation in each iteration step of the BESO method procedure.

1.7 Objectives and contributions

The main objective of this work is to contribute to the methods of *Structural Topology Optimization* in problems with design-dependent physics by using fluid-structure interaction (FSI) models. An extension of the evolutionary optimization methods is developed in this work and applied in four different optimization problems, namely:

- *Structural topology optimization for design-dependent fluid pressure loads.*
- *Topology optimization of submerged buoyant structures.*
- *Natural frequency maximization of acoustic-structure interaction systems.*
- *Structural topology optimization considering stationary viscous fluid flow loads.*

As specific objectives, this thesis intends to:

- implement a numerical code to solve different fluid-structure interaction equations with the finite element method.

- develop a technique to allow the switch of different types of finite elements such as fluids and solids with the BESO method procedures.
- solve topology optimization problems with design-dependent FSI loads using the proposed fluid-structure BESO method.
- introduce an inequality constraint in the standard evolutionary topology optimization problem.

The following conference papers have been derived from this PhD research:

- *Evolutionary Topology Optimization for Fluid-structure Interaction Problems and Natural Frequency Maximization* (Picelli et al., 2012).
- *Topology Optimization Considering Design-dependent Loads*, abstract only (Picelli et al., 2013).
- *Topology Optimization Including Buoyancy Inequality Constraints* (Picelli et al., 2014).
- *Topology Optimization Considering Design-dependent Stokes Flow Loads* (Picelli et al., 2015c).

The following journal papers have been derived from this PhD research:

- *Bi-directional Evolutionary Structural Optimization for Design-dependent Fluid Pressure Loading Problems* (Picelli et al., 2015b).
- *Evolutionary Topology Optimization for Natural Frequency Maximization Problems Considering Acoustic-structure Interaction* (Picelli et al., 2015d).
- *Topology Optimization for Submerged Buoyant Structures*, submitted on August 2015 (Picelli et al., 2015a).

1.8 Layout of the thesis

This thesis is composed by seven chapters to divide the main contributions of the research, as shown schematically in Figure 1.15. This introductory chapter described the state of the art in *Structural Topology Optimization* and the “scientific spot” this doctoral research is inserted

on. A brief description of the fluid-structure interaction models and the extended BESO update scheme were also presented in this introduction.

The four different optimization problems previously mentioned are introduced, formulated, solved and discussed with numerical results in Chapters 2, 3, 4 and 5. These chapters are self-contained and may be read independently, since they are mainly composed by texts from conference and journal papers. In each chapter, specific introductions, literature reviews and problem formulations are presented.

Chapter 6 brings final conclusions and suggestions for further research and Appendix A presents the implementation details of the developed methodologies.

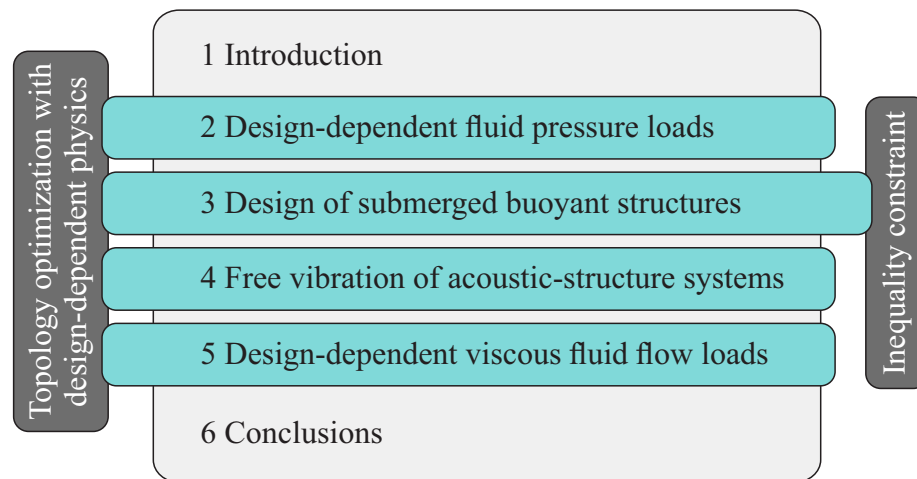


Figure 1.15: Structure of this thesis.

2 STRUCTURAL TOPOLOGY OPTIMIZATION FOR DESIGN-DEPENDENT FLUID PRESSURE LOADS

Context

To minimize structural compliance in problems with design-dependent pressure loads, a hydrostatic fluid (*Fluid 1* mentioned in Chapter 1) has been employed to model pressure fields in an evolutionary topology optimization approach. The discrete procedures of the evolutionary methods allow the modelling of separate fluid and structural domains. Thus, constant and non constant fluid pressure fields can be solved using classic governing equations and finite element discretizations. A new sensitivity term has been derived from the design-dependent loads. This work has been the first attempt to solve the design-dependent pressure loading problem with evolutionary topology optimization and multiphysics analysis. This contribution has first been published in the conference proceedings of the 5th International Conference on Coupled Problems in Science and Engineering (Picelli *et al.*, 2013) and later in *Engineering Optimization* (Picelli *et al.*, 2015b).

2.1 Introduction

Topology optimization of continuum structures (Bendsoe and Sigmund, 2003) has been used to solve many structural and multiphysics problems in engineering. The idea is to find optimal topologies inside predefined design domains concerning objective functions and constraints. Since its introduction (Bendsoe and Kikuchi, 1988), the methods of topology optimization have been extended to different applications (Chen and Kikuchi, 2001; Sigmund, 2001b; Duhring *et al.*, 2008; Silva and Pavanello, 2010). Although some of these procedures have reached a satisfactory level, many topics are still open to research, such as design-dependent pressure loading problems.

The difficulties to optimize structures subjected to pressure loads arise due to the variation of location, direction and magnitude of the loads during the optimization procedure. This turns to be an additional difficulty for the traditional density based topology optimization methods, like in the SIMP (Bendsoe and Sigmund, 2003) and homogenization approaches (Bendsoe and Kikuchi, 1988). In these methods, the pressure loaded surfaces are not explicitly defined due to the existence of intermediate density elements (Hammer and Olhoff, 2000).

Some of the main efforts to solve the topology optimization problem considering design-

dependent pressure loads have been in the creation of the surface where the pressure will act. Initially, Hammer and Olhoff (2000) proposed the identification of iso-density nodal points and the usage of Bézier spline functions to obtain the boundary where the pressure will act. Their method was further improved by Du and Olhoff (2004a,b), in which the authors modify the technique of finding the density isolines. More recently, other methods to identify the pressure surfaces were proposed. Zhang *et al.* (2008) proposed an alternative boundary search scheme by using a density threshold to classify all the elements in load-carrying and nonloading-carrying elements. The same method was extended further for 3D cases (Zhang *et al.*, 2010). Zheng *et al.* (2009) used a potential function based on an electric potential to model the pressure surface. Lee and Martins (2012) improved the method of Du and Olhoff (2004a), eliminating the need of isoline endpoints predefinition.

Also for the density based methods, other schemes have been proposed to handle design-dependent pressure loads, being some of them heuristic techniques or even treating artificial multiphysics problems. To simulate the pressure loading, Chen and Kikuchi (2001) considered a fictitious thermal problem. The hydrostatic pressure was simulated by thermal loads between a solid and a fluid domain due to the mismatch of their thermal expansion coefficients. Similarly, Bourdin and Chambolle (2003) used a fictitious liquid in a fluid-solid-void topology optimization. Perimeter penalization was applied in order to avoid homogenization of the phases. Sigmund and Clausen (2007) suggested the use of a mixed equivalent formulation to model an incompressible fluid-structure region. Later, Bruggi and Cinquini (2009) proposed a mixed model using another element approximation in order to avoid some numerical difficulties due to the incompressible model assumptions. Also, Andreasen and Sigmund (2013) extended the same idea for applying topology optimization to fluid-structure interaction problems in saturated poroelastic media.

The techniques mentioned above present volumes with intermediate density materials and not well defined pressure surfaces. As an alternative scheme, Yang *et al.* (2005) explored cases including structural downward surface loads with the evolutionary methods. Very recently, Xia *et al.* (2015) used a level set method to solve pressure load problems. In this work, the extended BESO method for applications in fluid loaded structural problems is explored.

In the evolutionary methods the design variables are restricted to discrete values 1 and 0, which corresponds to complete solid and void elements, respectively. Then, no intermediate density elements are allowed during the optimization procedures. Herein, the extended BESO method substitutes some of the void elements by incompressible fluid ones capable to model the pressure field. The fluid/void elements are easily controlled by expanding both fluid and void regions considering their neighboring elements. For instance, new fluid elements should appear only besides fluid neighbor elements. With no intermediate densities, both solid-void

and fluid regions as well as the pressure surfaces are explicitly defined. In this context the traditional displacement-pressure (\mathbf{u}/P) formulation (Zienkiewicz and Bettess, 1978) can be used for the fluid-structure model. In the static analysis, the solid and fluid fields are governed by the elasticity equation and Laplace's equation, respectively. The two separate fields are partially coupled by surface-coupling integrals, which guarantees equilibrium conditions on the fluid-structure interfaces.

Herein, it is considered static equilibrium and the compliance minimization of structures in contact with pressurized fluids. This methodology can be applied to different engineering fields, such as the automotive, aeronautical and metallurgic industry or also offshore structures, where there are different types of fluid-structure interaction. With the proposed method, design-dependent pressure loads can be easily handled with the classical and simple finite element formulations. Furthermore, the pressure surface changes are tracked straightforwardly.

This chapter is outlined as follows: Section 2.2 presents the governing equations and the finite element model for the fluid-structure system. In Section 2.3, the topology optimization problem and the sensitivity analysis are described. Section 2.4 discusses the implementation matters and the steps of the extended fluid-structure BESO method. Section 2.5 shows the numerical results achieved with the proposed methodology for three benchmark examples. Section 2.6 concludes the chapter.

2.2 Fluid-structure model: Governing equations and finite element discretization

It is considered the static analysis of flexible structures in contact with incompressible pressurized fluids. The fluid-structure system is modelled assuming small strain and displacements for a linearly elastic continuum solid domain and an inviscid and irrotational fluid domain. All the details about this formulation can be found in the reference article of Zienkiewicz and Bettess (1978) or in reference books (Morand and Ohayon, 1995; Axisa and Antunes, 2007). Following, the governing equations for the fluid and structural domains as well as the coupling boundary conditions are briefly outlined.

2.2.1 Fluid domain

In the static analysis, the governing equation for the homogeneous, inviscid and irrotational fluid domain Ω_f can be described by Laplace's equation

$$\nabla^2 P_f = 0 \quad \text{in } \Omega_f, \quad (2.1)$$

where P_f is the fluid pressure and ∇^2 is the Laplacian differential operator.

Proper boundary conditions must be imposed. In this work, the following boundary conditions are considered (see Figure 2.1):

$$P_f = P_0 \quad \text{on } S_p, \quad (2.2)$$

$$\nabla P_f \cdot \mathbf{n} = 0 \quad \text{on } S_f, \quad (2.3)$$

representing the pressure boundary condition (Equation 2.2) and the hard wall condition (Equation 2.3) on the fluid boundaries S_p and S_f , respectively. The term P_0 is the constrained pressure, \mathbf{n} is the outward unit normal vector to the fluid and ∇ is the gradient vector operator.

2.2.2 Structural domain

Neglecting body forces, the linear structural static analysis is governed by

$$\nabla \cdot \boldsymbol{\sigma}_s(\mathbf{u}) = \mathbf{0} \quad \text{in } \Omega_s, \quad (2.4)$$

where $\nabla \cdot \boldsymbol{\sigma}_s$ is the divergence of the Cauchy stress tensor and \mathbf{u} is the displacement field on the solid domain Ω_s . In this work, only Dirichlet boundary conditions are applied to the solid domain:

$$\mathbf{u} = \mathbf{u}_0 \quad \text{on } S_u, \quad (2.5)$$

representing the displacement boundary conditions for all points on the solid boundaries S_u , as seen in Figure 2.1. The term \mathbf{u}_0 is the vector of prescribed displacements on S_u and \mathbf{u}_s is the vector of displacements.

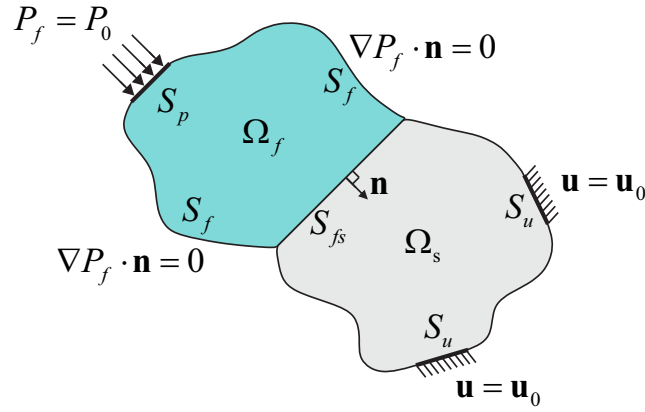


Figure 2.1: The solid (Ω_s) and fluid (Ω_f) domains and boundary conditions. Pressure P_0 is imposed on the portion S_p of the fluid boundary. Fluid pressure loads act on the structure through the fluid-structure interface S_{fs} .

2.2.3 The coupled fluid-structure system

At the interface S_{fs} between the structural and fluid domains, the fluid and the structure move together in the normal direction of the boundary. The normal vector \mathbf{n} (see Figure 2.1) can be used in order to obtain the continuity in pressure on the interface S_{fs} as follows:

$$\boldsymbol{\sigma}_s \mathbf{n} = -P_f \mathbf{n} \quad \text{on } S_{fs}. \quad (2.6)$$

This equation ensures the continuity in pressure on the the interface S_{fs} , which indicates the pressure forces $\mathbf{f}_{fs} = P_f \mathbf{n}$ exerted by the fluid on the structure.

Using an approximation based on the finite element method (FEM), the force acting on the structure provided by the fluid pressure can be calculated as

$$\mathbf{f}_{fs} = \int_{S_{fs}} \mathbf{N}_s^T \mathbf{n} \mathbf{N}_f dS_{fs} \mathbf{P}_f, \quad (2.7)$$

where \mathbf{P}_f is the vector of nodal pressures, \mathbf{n} is the normal vector inwards the structural domain and \mathbf{N}_s and \mathbf{N}_f contains the finite element shape functions for the interface. This formulation is equivalent to the static part of the dynamic acoustic-structure interaction model described in terms of structural displacements and fluid pressures (\mathbf{u}/P_f) by Zienkiewicz and Bettess (1978); Morand and Ohayon (1995); Axisa and Antunes (2007). The integral in Equation 2.7 defines an interface finite element placed on the line shared by neighboring fluid and structural elements and connects pressures and displacements degrees of freedom. In the present thesis, both fluid and structural elements are modelled with linear shape functions. Thus, the interface element is a two-node element with linear shape functions and $\mathbf{N}_s = \mathbf{N}_f$. Writing the surface coupling

integral as

$$\mathbf{L}_{fs} = \int_{S_{fs}} \mathbf{N}_s^T \mathbf{n} \mathbf{N}_f dS_{fs}, \quad (2.8)$$

the coupling forces \mathbf{f}_{fs} can be written in a discretized form as

$$\mathbf{f}_{fs} = \mathbf{L}_{fs} \mathbf{P}_f. \quad (2.9)$$

Thus, in the context of the finite element approximation, and assuming no external loads are applied, the hydroelastic equilibrium problem can be described by a nonsymmetric system of equations

$$\begin{bmatrix} \mathbf{K}_s & -\mathbf{L}_{fs} \\ \mathbf{0} & \mathbf{K}_f \end{bmatrix} \begin{Bmatrix} \mathbf{u}_s \\ \mathbf{P}_f \end{Bmatrix} = \begin{Bmatrix} \mathbf{0} \\ \mathbf{0} \end{Bmatrix}, \quad (2.10)$$

where \mathbf{u}_s is the vector of nodal structural displacements and \mathbf{K}_s and \mathbf{K}_f are the stiffness matrices of the structural and fluid domains, respectively, expressed in an element domain Ω_e as

$$\mathbf{K}_s = \int_{\Omega_e} (\nabla \mathbf{N}_s)^T \mathbf{D}_s \nabla \mathbf{N}_s d\Omega_e, \quad (2.11)$$

$$\mathbf{K}_f = \int_{\Omega_e} (\nabla \mathbf{N}_f)^T \nabla \mathbf{N}_f d\Omega_e, \quad (2.12)$$

where \mathbf{D}_s is the elasticity matrix. The matrix \mathbf{L}_{fs} is the global coupling matrix (Morand and Ohayon, 1995).

In this one-way coupled multiphysics model, the fluid analysis provides pressure loads to the structural analysis through the application of the coupling matrices. In this case, the fluid pressure field can actually be solved separately. However, for the sake of generality, by imposing the boundary conditions from Equations 2.2, 2.3, 2.5 and 2.6 and solving Equation 2.10, both fluid and structure responses can be obtained simultaneously for any discretized fluid-structure configuration. This turns to be handy for the iterative procedures of topology optimization. The equilibrium equation for the structure alone can be expressed as

$$\mathbf{K}_s \mathbf{u}_s = \mathbf{L}_{fs} \mathbf{P}_f, \quad (2.13)$$

extracted from Equation 2.10.

2.3 Problem formulation and sensitivity analysis

2.3.1 Topology optimization problem

The examples considered in this work concern compliance minimization with volume constraint of structures under fluid pressure loading. The objective is to find the distribution of a given amount of solid material to obtain a structure with maximum stiffness, which is equivalent to a minimum compliance $C(x_i)$ (external work), a physical quantity that can be understood as the flexibility of the structure. The evolutionary topology optimization problem for this case can be formulated as:

$$\begin{aligned}
 \min_{x_i} \quad & C(x_i) = \frac{1}{2} \mathbf{u}_s^T \mathbf{K}_s \mathbf{u}_s, \\
 \text{subject to:} \quad & \begin{bmatrix} \mathbf{K}_s & -\mathbf{L}_{fs} \\ \mathbf{0} & \mathbf{K}_f \end{bmatrix} \begin{Bmatrix} \mathbf{u}_s \\ \mathbf{P}_f \end{Bmatrix} = \begin{Bmatrix} \mathbf{0} \\ \mathbf{0} \end{Bmatrix} \text{ and b.c.,} \\
 & h = V(x_i) / V_0 = V_s, \\
 & x_i = [0,1],
 \end{aligned} \tag{2.14}$$

where V_0 is the volume of the full design domain, V_s is the prescribed final structural volume fraction, nel is the number of elements inside the design domain and x_i represents the discrete design variables, in which 1 is a solid element and 0 is void or fluid. The extended BESO method substitutes some of the void elements by incompressible fluid ones capable of modelling the pressure field. First, the standard BESO update scheme is used to set a 0/1 design. Then, the fluid region is updated considering their neighboring elements. For instance, new fluid elements should be placed only besides fluid neighbor elements, as illustrated in Figure 1.14. Fluid elements which appear inside the design domain are considered equivalent to a void design variable ($x_i = 0$) in the optimization procedure, i.e., in the sensitivity analysis and in the 0/1 update scheme. However, they are fluid elements in the finite element analysis.

2.3.2 Sensitivity analysis

The sensitivity of the structural compliance due to an element removal can be obtained by its direct derivative:

$$\frac{\partial C}{\partial x_i} = \mathbf{u}_s^T \mathbf{K}_s \frac{\partial \mathbf{u}_s}{\partial x_i} + \frac{1}{2} \mathbf{u}_s^T \frac{\partial \mathbf{K}_s}{\partial x_i} \mathbf{u}_s. \tag{2.15}$$

The equilibrium equation of the structural system (Equation 2.13) can be derived in order

to find the unknown $\partial \mathbf{u}_s / \partial x_i$:

$$\frac{\partial (\mathbf{K}_s \mathbf{u}_s)}{\partial x_i} = \frac{\partial (\mathbf{L}_{fs} \mathbf{P}_f)}{\partial x_i}. \quad (2.16)$$

Applying the chain rule on both sides of the previous equation, one has

$$\frac{\partial \mathbf{K}_s}{\partial x_i} \mathbf{u}_s + \mathbf{K}_s \frac{\partial \mathbf{u}_s}{\partial x_i} = \frac{\partial \mathbf{L}_{fs}}{\partial x_i} \mathbf{P}_f + \mathbf{L}_{fs} \frac{\partial \mathbf{P}_f}{\partial x_i}. \quad (2.17)$$

The passive pressure change due to a solid element removal is considered in this work to be small enough and the derivative $\partial \mathbf{P}_f / \partial x_i$ is neglected. Then, isolating the derivative of the displacement vector:

$$\frac{\partial \mathbf{u}_s}{\partial x_i} = \mathbf{K}_s^{-1} \left(\frac{\partial \mathbf{L}_{fs}}{\partial x_i} \mathbf{P}_f - \frac{\partial \mathbf{K}_s}{\partial x_i} \mathbf{u}_s \right). \quad (2.18)$$

With the substitution of Equation 2.18 in Equation 2.15, one can rewrite the compliance derivative as

$$\frac{\partial C}{\partial x_i} = \mathbf{u}_s^T \mathbf{K}_s \mathbf{K}_s^{-1} \left(\frac{\partial \mathbf{L}_{fs}}{\partial x_i} \mathbf{P}_f - \frac{\partial \mathbf{K}_s}{\partial x_i} \mathbf{u}_s \right) + \frac{1}{2} \mathbf{u}_s^T \frac{\partial \mathbf{K}_s}{\partial x_i} \mathbf{u}_s. \quad (2.19)$$

Then, the sensitivity of the objective function is expressed as

$$\frac{\partial C}{\partial x_i} = \mathbf{u}_s^T \frac{\partial \mathbf{L}_{fs}}{\partial x_i} \mathbf{P}_f - \frac{1}{2} \mathbf{u}_s^T \frac{\partial \mathbf{K}_s}{\partial x_i} \mathbf{u}_s. \quad (2.20)$$

The sensitivity must be evaluated for each element of the design domain in order to rank their contribution to the objective function. To evaluate the sensitivity from Equation (2.20) at the elemental level, the variation of the stiffness $\partial \mathbf{K}_s / \partial x_i$ due to the i th element removal must be found. The presented version of the BESO method is developed using a “hard-kill” technique, where the densities of the void elements are set as zero similarly as proposed by Huang and Xie (2007). A material interpolation scheme similar to the SIMP method can also be used in order to set a very small density for the void elements in a “soft-kill” evolutionary procedure (Huang and Xie, 2009). Both hard-kill and soft-kill approaches present similar results for structural design and can be used in a similar manner.

In the hard-kill approach, no material interpolation functions or design variables with very small values appear in the element modelling. The material is then the simple superposition (finite element assembly) of all solid element stiffness matrices \mathbf{K}_s^i . Thus, the definition of the sensitivities cannot be derived as a continuous function in the manner it is carried out by the SIMP approach. Therefore, an approximation based on a single step finite difference can

be carried out for the hard-kill sensitivities, considering the structural configuration before and after an element removal (Xie and Huang, 2010). The derivative of the global structural stiffness matrix with respect to the design variable of the i th element can be then expressed as

$$\frac{\partial \mathbf{K}_s}{\partial x_i} \approx \mathbf{K}_s^i. \quad (2.21)$$

The derivative of the coupling matrix $\partial \mathbf{L}_{fs} / \partial x_i$ also needs to be evaluated. It indicates the change in the coupling condition due to the i th element removal. This change can be predicted considering the difference in coupling between the system configuration after and before the element removal. Thus,

$$\frac{\partial \mathbf{L}_{fs}}{\partial x_i} \approx (\Delta \mathbf{L}_{fs})^i = (\mathbf{L}_{fs}^* - \mathbf{L}_{fs})^i, \quad (2.22)$$

where \mathbf{L}_{fs} is the coupling matrix before the element removal and \mathbf{L}_{fs}^* is the final coupling matrix after the element removal.

For a general solid element, one may verify the change in the coupling configuration by the interface coupling forces. Figure 2.2 presents a possible coupling forces configuration before and after an element removal. By knowing this configuration, the change $(\mathbf{L}_{fs}^* - \mathbf{L}_{fs})^i$ can be evaluated. The minus sign changes the direction of the coupling forces, as seen in Figure 2.2.

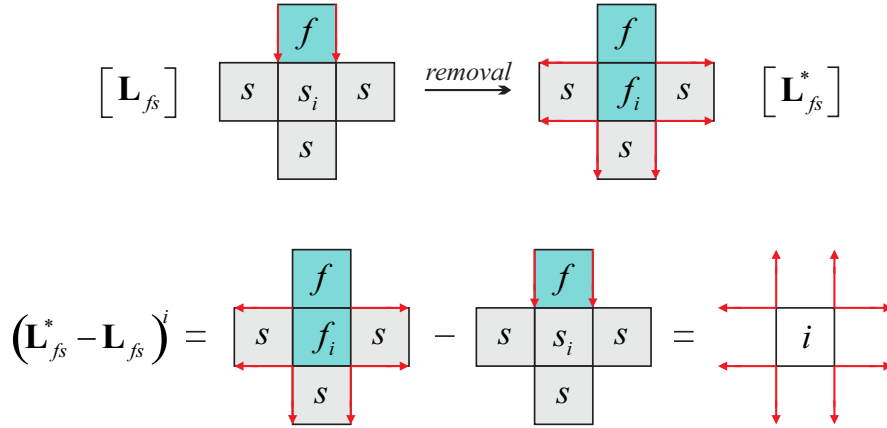


Figure 2.2: Coupling forces configuration before and after a structural element removal. The derivative $\partial \mathbf{L}_{fs} / \partial x_i$ can be approximated by the change of the coupling matrices $(\Delta \mathbf{L}_{fs})^i = (\mathbf{L}_{fs}^* - \mathbf{L}_{fs})^i$ after the i th element removal. The arrows indicate the pressure loads $\mathbf{L}_{fs} \mathbf{P}_f$ from the fluid elements acting on the structure.

It can be noticed that, no matter what the initial coupling configuration is, the change $(\mathbf{L}_{fs}^* - \mathbf{L}_{fs})^i$ always ends up as that showed in Figure 2.2. It represents the change in pressure

loads when a solid element is removed and a fluid element is placed in, transferring the interface pressure through the whole element. Therefore, for any solid element, a (8×4) matrix containing the coupling matrices through the element boundaries can represent the change in the coupling configuration, as following:

$$\frac{\partial \mathbf{L}_{fs}}{\partial x_i} \approx (\mathbf{L}_{fs}^* - \mathbf{L}_{fs})^i = \mathbf{L}_c^i, \quad (2.23)$$

where \mathbf{L}_c^i is the matrix assembled according to the coupling configuration change, showed in Figure 2.2. In a regular mesh with square elements, this matrix is evaluated considering the normal vector \mathbf{n} outwards the fluid element and it can be directly expressed as

$$\mathbf{L}_c^i = \frac{l_i}{6} \begin{bmatrix} 2 & 0 & 0 & 1 \\ 2 & 1 & 0 & 0 \\ 0 & -2 & -1 & 0 \\ 1 & 2 & 0 & 0 \\ 0 & -1 & -2 & 0 \\ 0 & 0 & -2 & -1 \\ 1 & 0 & 0 & 2 \\ 0 & 0 & -1 & -2 \end{bmatrix}, \quad (2.24)$$

where l_i is the length of the element's edge.

Finally, substituting the derivatives $\partial \mathbf{K}_s / \partial x_i$ and $\partial \mathbf{L}_{fs} / \partial x_i$ into Equation 2.20 and rearranging it, the sensitivity numbers for design-dependent fluid pressure loading problems in the evolutionary topology optimization are

$$\alpha_i = -\frac{\partial C}{\partial x_i} = \begin{cases} \frac{1}{2} \mathbf{u}_i^T \mathbf{K}_s^i \mathbf{u}_i - \mathbf{u}_i^T \mathbf{L}_c^i \mathbf{P}_i & x_i = 1 \\ 0 & x_i = 0 \end{cases}, \quad (2.25)$$

where \mathbf{u}_i and \mathbf{P}_i are the vectors with nodal displacements and pressures, respectively, at the i th element.

This analysis can be carried out for each element i in the design domain. For solid elements which are not at the fluid-structure interface, the pressure transferred by the occupying fluid is null and the term $\mathbf{u}_i^T \mathbf{L}_c^i \mathbf{P}_i$ in Equation 2.25 vanishes, leading to the traditional number $\frac{1}{2} \mathbf{u}_i^T \mathbf{K}_s^i \mathbf{u}_i$, the elemental strain energy. Thus, in practice, the complete sensitivity number is evaluated just for the solid elements at the fluid-structure interface. For solid elements with only three neighbors, the change presented in Figure 2.2 is not completely true. However, a very small amount of elements at the fluid-structure interface has only three neighbors and this situation may be disregarded. The new term $\mathbf{u}_i^T \mathbf{L}_c^i \mathbf{P}_i$ in the sensitivity analysis can be interpreted as the work done by the pressure loads at the elemental level, since $\mathbf{L}_c^i \mathbf{P}_i$ is a vector of cou-

pling forces at the solid element, which is multiplied by the elemental displacements in order to compute the sensitivities. The sensitivity number α_i ranks the contribution of the i th element to the objective function. The solid elements with the smallest sensitivity numbers are considered structurally inefficient or underutilized and they can be removed from the finite element model with a minimum change in the total compliance.

2.4 Numerical implementation

Originally, the Evolutionary Structural Optimization (ESO) was based on a successive elimination of material from the initial design domain (Xie and Steven, 1993). The ESO method was extended to different structural design problems (Xie and Steven, 1996; Li *et al.*, 1999). Steven *et al.* (2000) used the ESO method for the first time for general physical field uncoupled problems, including a fluid domain design case. One of the last most important developments in the ESO-based methods was the convergent and mesh-independent bi-directional version, the BESO method from Huang and Xie (2007). The BESO method allows material to be simultaneously removed and added in the domain until the volume constraint and a convergence criterion are satisfied. The method was initially addressed as a hard-kill technique and a further improvement introduced an interpolation scheme, exploring the method in a soft-kill approach (Huang and Xie, 2009).

In this work, the proposed methodology is a hard-kill BESO-based approach, in which some void elements are substituted by incompressible fluid ones and the loads are generated by imposed pressures in the coupled model. To rank all the elements according to their contribution to the objective function, the sensitivity number from Equation 2.25 is evaluated for each element. Boundary and interior elements are identified by checking their neighboring elements. A solid element is a boundary element if it has at least one fluid neighbor element and an interior element if it does not have any fluid neighbors. A mesh-independence filter is applied all over the mesh by averaging each elemental sensitivity number with its neighboring elements. The filter scheme is similar to that presented by Sigmund and Peterson (1998). To evaluate the filter weights, nodal sensitivity numbers α_j are calculated by averaging the elemental sensitivity numbers of the j th connected elements. These nodal sensitivity numbers must be converted back into elemental sensitivities by projecting a sub-domain Ψ_i with length scale r_{min} and centered in the i th element. All the nodes inside Ψ_i must have their nodal sensitivity numbers averaged to the i th elemental level as follows:

$$\alpha_i = \sum_{j=1}^{nod} w(r_{ij}) \alpha_j / \sum_{j=1}^{nod} w(r_{ij}), \quad (2.26)$$

where r_{ij} is the distance between the node j and the center of the element i , nod is the total number of nodes inside the design domain and $w(r_{ij})$ is a weight factor that is equal to $r_{min} - r_{ij}$ for nodes inside the sub-domain Ψ_i and 0 for nodes outside the sub-domain. The above filter scheme can effectively address mesh-dependency and checkerboard problems. However, the objective function and the corresponding topology may not be convergent. In order to avoid this problem, Huang and Xie (2007) showed that the above sensitivity numbers should be averaged with its previous iteration numbers, given as

$$\alpha_i = \frac{\alpha_i^n + \alpha_i^{n-1}}{2}, \quad (2.27)$$

where n is the current iteration number. Thus, the updated sensitivity number includes the history of the sensitivity information in the previous iterations (Huang and Xie, 2007).

For each iteration, a target volume V_{n+1} is defined as

$$V_{n+1} = V_n(1 \pm ER), \quad (2.28)$$

where ER is the evolutionary ratio and n the number of the iteration. ER is the percentage of the current structural volume and increases or decreases V_{n+1} towards a structural desired final volume fraction V_s . The target volume V_{n+1} sets the threshold α_{th} of the sensitivity numbers. Solid elements ($x_i = 1$) which

$$\alpha_i \leq \alpha_{th} \quad (2.29)$$

are switched to fluid/void condition ($x_i = 0$). Fluid elements ($x_i = 0$) are switched to solid condition ($x_i = 1$) when

$$\alpha_i > \alpha_{th}. \quad (2.30)$$

Meanwhile, the addition volume (AR) is restricted to a maximum addition ratio AR_{max} , which declares the maximum allowable solid volume fraction that can be added per iteration. Once $AR > AR_{max}$, only some of the elements with highest sensitivity numbers are added in order to set $AR = AR_{max}$. Then, some of the elements with the lowest sensitivity numbers are removed to satisfy the target volume V_{n+1} . Each target volume defines the amount of elements that the structure must have in the iteration $n + 1$. The capability of a fluid/void element to have a higher sensitivity number is played by the filter scheme. The projection scheme allows fluid/void elements near highly solicited solid regions to have nonzero sensitivity numbers and return to solid condition. It also controls the size of the members in the structure related to the r_{min} parameter, which indicates how intense is the smoothing of the sensitivity numbers through the design domain.

Once the prescribed final volume is achieved, the target volume remains constant as V_s . The algorithm evolves until a convergence criterion with a predefined tolerance τ is satisfied. This convergence is estimated as

$$\frac{|\sum_{k=1}^5 C_{n-k+1} - \sum_{k=1}^5 C_{n-5-k+1}|}{\sum_{i=1}^5 C_{n-k+1}} \leq \tau, \quad (2.31)$$

which means that the compliance variation is evaluated for the last 10 successive iterations of the algorithm. More details about these implementation issues (e.g. filter scheme, element removal/addition and convergence criterion) can be found in Huang and Xie (2007).

2.4.1 The extended fluid-structure BESO method

The evolutionary procedures of the presented BESO method for fluid pressure problems are given as follows:

1. Discretize the design domain using a finite element (FE) mesh for the given boundary conditions. Initially, a global fluid-structure stiffness matrix \mathbf{K}_g must be assembled uncoupled.
2. Couple and store a current global matrix \mathbf{K}_n with the coupling matrices according to the current design of the n th iteration and the appropriate boundary conditions. Thus, the current \mathbf{K}_n becomes equivalent to the fluid-structure stiffness matrix from Equation 2.10.
3. Perform FE analysis on the current design to obtain the displacement and pressure responses.
4. Calculate the sensitivity numbers according to Equation 2.25.
5. Apply the filter scheme. Project the nodal sensitivity numbers to the design domain and smooth the sensitivity numbers for all (fluid, void and solid) elements in the design domain.
6. Average the sensitivity numbers with their previous iteration ($n - 1$) numbers and then save the resulting sensitivity numbers for the next iteration.
7. Determine the target structural volume V_{n+1} for the next iteration.
8. Construct a new fluid-structure design by switching design variables x_i from 1 to 0 and from 0 to 1. In order to control the fluid and void regions, a decision should be taken when the elements must have their design variables stated as $x_i = 0$. If the element has at least

one fluid element as neighbor, it must be turned also into a fluid element. If the element does not have any fluid neighbors, the element must be turned into a void. This procedure is repeated until there are no more changes in the fluid-void regions. In this case, some layers of structural elements nearby the fluid-structure interface can be replaced by fluid elements and void holes appear only inside the structure.

9. Remove and/or add the elemental stiffness matrices from the original uncoupled global matrix \mathbf{K}_g according to the change of the current design.
10. Repeat steps 2-10 until the prescribed structural volume V_s is reached and the convergence criterion from Equation 2.31 is satisfied.

2.5 Numerical results

In this section, three benchmark examples from the literature are explored in order to expose the capabilities of the presented extended BESO method considering fluid pressure loads. The parameters and features of the method are discussed, as well as convergence analysis is shown.

2.5.1 Arch-like structure

In this example, the influence of the new sensitivity number from Equation 2.25 and the main features of the method are discussed. The 2D model is illustrated in Figure 2.3. An underwater structure subject to hydrostatic pressure from a fluid domain is considered for compliance minimization. The imposed pressure is $P_0 = 1$ Pa. In this case, when the pressure is constant all over the fluid domain, the dimensions of the fluid field are not relevant. Moreover, the imposed fluid pressure can be chosen arbitrarily resulting in the same structural topology solution because of the linear behavior of the structure. The design domain is equally divided into 200×100 four-node plane stress elements, totaling 20000 elements. The material is considered with Young's modulus $E = 70$ GPa and Poisson's ratio $\nu = 0.3$. Equation 2.10 is used to obtain the pressure and displacement responses.

An example of sensitivity number distribution is shown in Figure 2.4 considering the left half of the full initial design domain. The sensitivity numbers indicate the relative elemental efficiency with respect to the objective function. The elements with dark blue color have the lowest sensitivity numbers and those in red have the highest numbers. If one wants to maximize the stiffness, it is reasonable to remove the elements with the lowest sensitivities (lower strain energy).

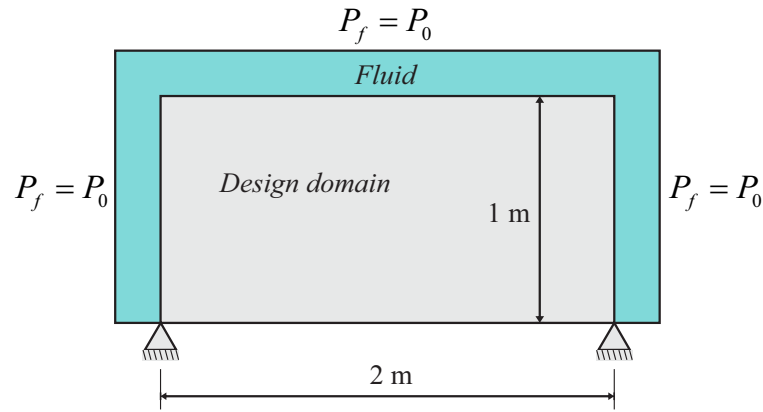


Figure 2.3: Fluid-structure model: An underwater structure subject to hydrostatic pressure.

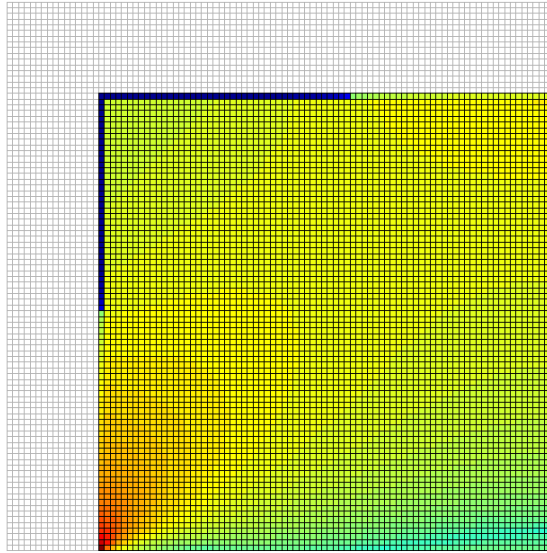


Figure 2.4: Example of elemental sensitivity numbers distribution evaluated by the Equation 2.25 for the the left side of the initial design domain.

Starting from the initial full design, BESO's evolutionary ratio is chosen to be $ER = 5\%$ for this example. The final prescribed volume is $V_s = 20\%$ and the filter radius used is $r_{min} = 0.1$ m. The other parameters are set as $AR_{max} = 5\%$ and $\tau = 0.01$. Figure 2.5 presents the BESO's topology solution with the iteration number n and structural volume V_n . Figure 2.6 shows the convergence history for this example. The final solution converged to a structure with an almost constant mean compliance of $0.213 \cdot 10^{-9}$ Nm.

Concerning the general purposes of the method, the design domain is gradually evolving to an arch-like structure with no gray scale patterns, such as those observed in the SIMP approach. During the evolution of the algorithm, solid elements are changed by fluid ones, activating and deactivating degrees of freedom. The fluid region evolves and occupies the structural

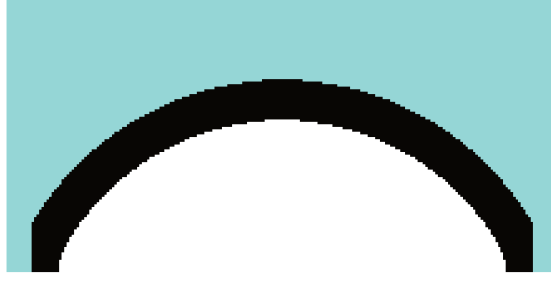


Figure 2.5: BESO's topology solution for the arch-like example.

design domain. Also, a void region is created when a hole is generated inside the structure and it is not in contact with the fluid domain. All intermediate topologies (see Figure 2.6) have their fluid-structure interfaces explicitly defined, which features the main advantage of the method. It turns the evolutionary algorithm into a simple tool to handle pressure loading problems. Furthermore, the arch-like structure obtained by the BESO method is consistent with the results published in reference articles (Chen and Kikuchi, 2001; Bourdin and Chambolle, 2003; Du and Olhoff, 2004a; Sigmund and Clausen, 2007; Zhang *et al.*, 2008; Bruggi and Cincinini, 2009; Zheng *et al.*, 2009) without the need of pressure surfaces parametrization.

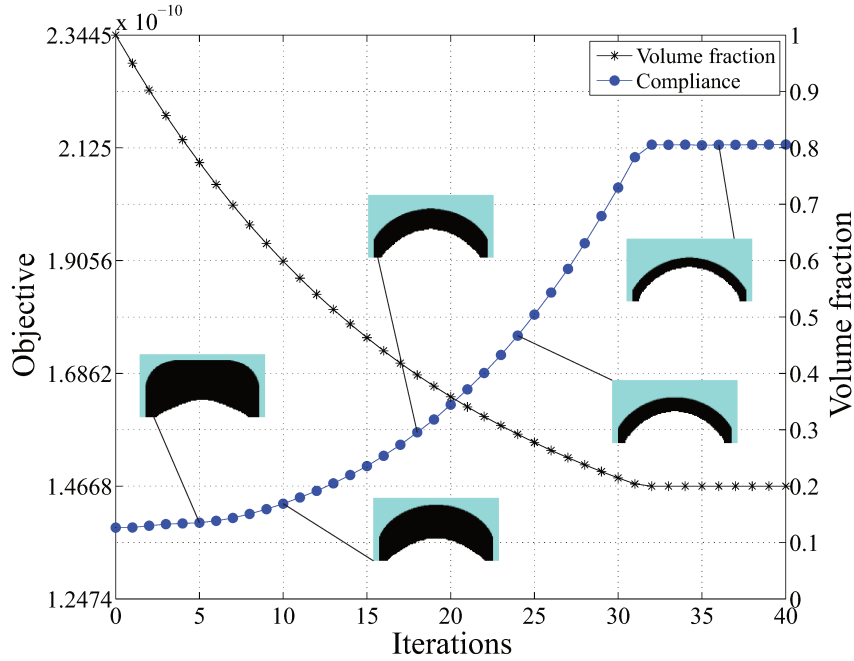


Figure 2.6: Convergence history of the arch-like structure's mean compliance.

The term $\mathbf{u}_i^T \mathbf{L}_c^i \mathbf{P}_i$ in the sensitivity introduces a slightly different and corrected value for the solid elements at the fluid-structure interface, specially reducing the sensitivities of regions with lower strain energy $\frac{1}{2} \mathbf{u}_i^T \mathbf{K}_s^i \mathbf{u}_i$. In comparison with the case previously shown, Figure 2.7 presents a topology snapshot when the sensitivities are evaluated without the pressure loading term $\mathbf{u}_i^T \mathbf{L}_c^i \mathbf{P}_i$. The topologies with the complete sensitivity numbers (including the sensitivities

at the interface) have smoother boundaries than those obtained disregarding the pressure loading derivatives, specially at earlier stages of the optimization. It may confirm that the introduction of the term $\mathbf{u}_i^T \mathbf{L}_c^i \mathbf{P}_i$ corrects the gradient information of the objective function for this problem. At latter stages, the topologies present less low strain energy regions, which minimizes the effect of the pressure sensitivity term.

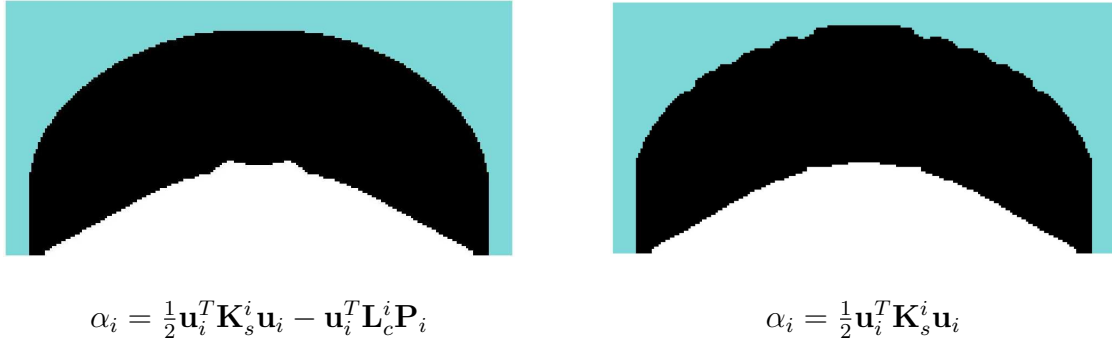


Figure 2.7: BESO's topology snapshot with and without pressure loading sensitivities.

As expressed in Equation 2.28, the discrete update scheme of the BESO method is based on a target volume V_{n+1} and is able to reduce or increase V_n towards V_s , as well as to keep volume constant when $V_n = V_s$. Therewith, an initial guess structural design can be set in the design domain before the optimization starts. For this same example, Figure 2.8 presents the evolution of the arch-like structure obtained with the extended BESO method with an initial guess design. The final result is the same arch presented in Fig. 2.5.

One advantage of starting with a smaller portion of structural elements is that computation time can be saved because of the reduced degrees of freedom when the hard-kill approach is used, specially for large models such as 3D cases. Figure 2.9 presents the convergence history for the arch-like structure with initial guess design. It can be noticed that the initial structure has already the prescribed final volume, i.e., $V_n = V_s$. Then, the structure evolves to an arch without changing its volume presenting the final compliance value $C = 0.211 \cdot 10^{-9}$ Nm, very close to the case with initial full design.

The initial guess design presents a compliance higher than the final arch-like structure and the convergence curve from Figure 2.9 evidences the minimization of the structural compliance. Starting with the full design domain, the minimization problem starts with a non feasible solution (volume constraint not active) and presents initial lower compliance because of the higher amount of solid material.

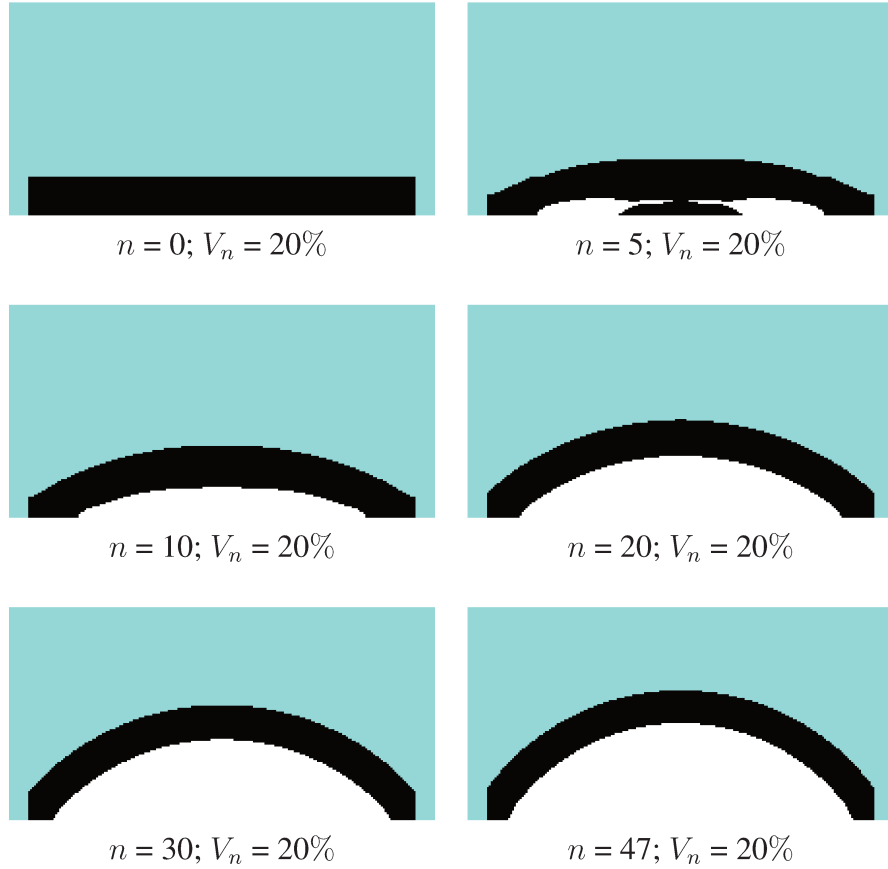


Figure 2.8: BESO's topology evolution for the arch-like example with initial guess design.

2.5.2 Piston head model

This example features a piston head model and it is similar to the piston problem explored by Lee and Martins (2012). Due to combustion explosion, the structure suffers a fluid pressure loading in its top edge. Figure 2.10 illustrates the right half of 2D approximation of a piston head model. The articles from Sigmund and Clausen (2007) and Bruggi and Cinquini (2009) also explore similar examples.

The structural design domain is equally divided into 300×200 four-node plane stress elements, totaling 60000 elements. The material is considered with Young's modulus $E = 32$ GPa and Poisson's ratio $\nu = 0.3$. A pressure $P_0 = 1$ MPa is imposed at the top edge of the fluid domain. BESO starts from the initial full design with an evolutionary ratio $ER = 2.5\%$ until a prescribed volume $V_s = 30\%$. The filter radius used is $r_{min} = 0.08$ m. The other parameters are chosen to be $AR_{max} = 2.5\%$ and $\tau = 0.001$. Figure 2.11 presents the snapshots of the topology evolution with the iteration number n and structural volume V_n until the convergence.

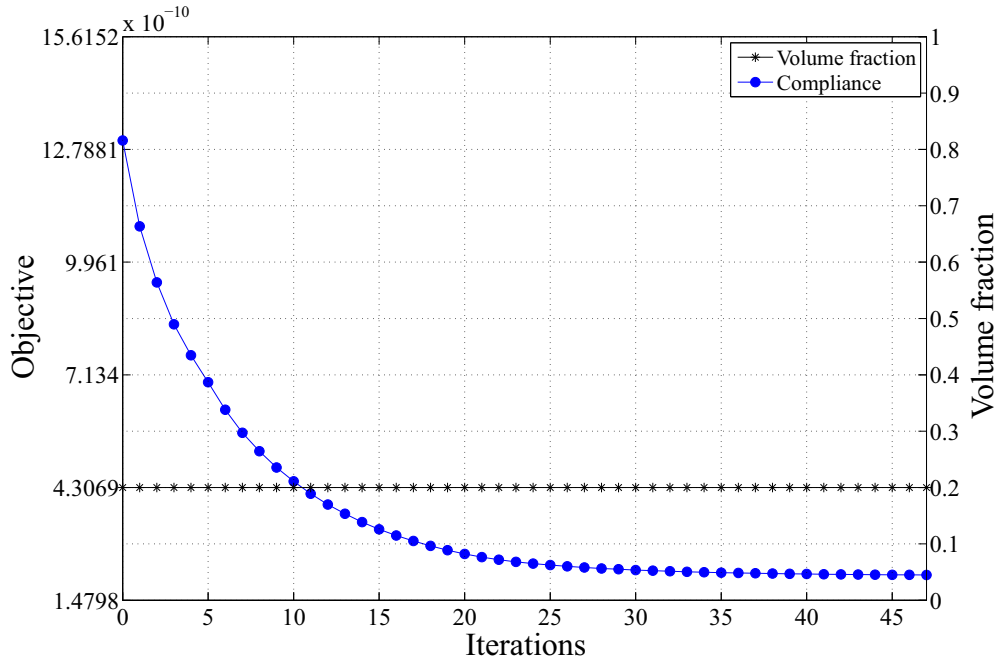


Figure 2.9: Convergence history of the arch-like structure's mean compliance starting with an initial guess design.

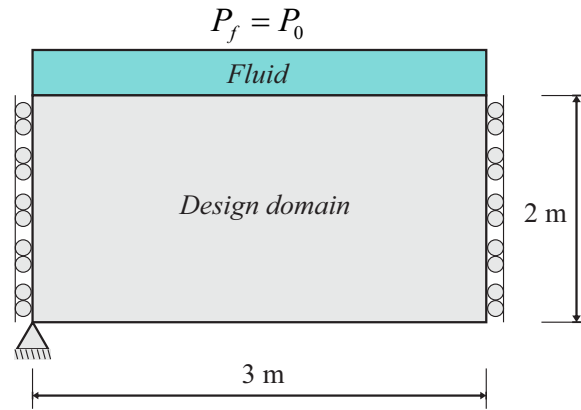


Figure 2.10: Fluid-structure model: piston head structure under pressure loading.

Even though the design update schemes from both BESO and SIMP methods are different, the topology evolution obtained by the BESO method showed some similarities with the intermediate solutions presented by Lee and Martins (2012). The obtained final solution is also in agreement with the topology obtained by Lee and Martins (2012). However, herein there is no need for additional material boundary parametrization schemes such as the ones proposed by Lee and Martins (2012) and other authors.

The mixed finite element models from Sigmund and Clausen (2007) and Bruggi and Cinqini (2009) turn the problem slightly different and the fluid volume should be constrained

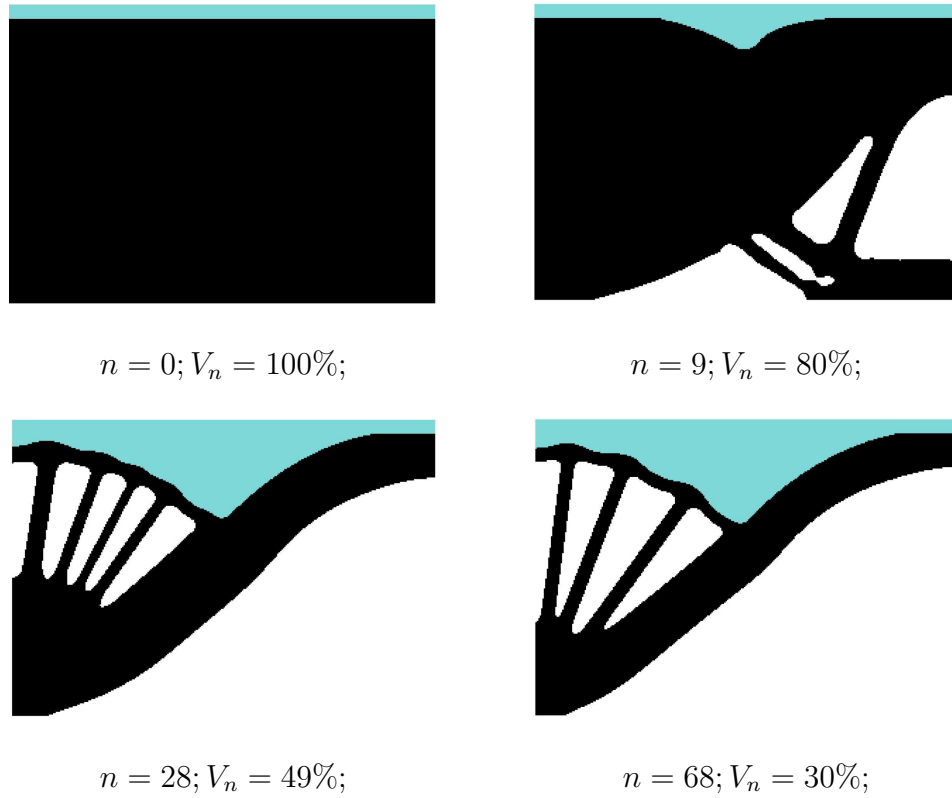


Figure 2.11: BESO's topology solution for the piston head example with iteration number n and structural volume V_n .

in order to avoid fluid cavities formation. It implies in different topologies depending on the constrained fluid volume. Nevertheless, the results are somewhat similar with the presented method. Figure 2.12 presents the convergence history of the piston head's mean compliance with the BESO method. The final mean compliance obtained is $C = 1964.9$ Nm.

In order to compare both strain energy and pressure loading sensitivities from Equation 2.25, Figure 2.13 presents the sensitivity values for the solid elements along the fluid-structure interface in the initial full design. The elements are sorted from the left to the right side, according to their centroids in the horizontal axis. It is showed that the pressure loading sensitivities $\mathbf{u}_i^T \mathbf{L}_c^i \mathbf{P}_i$ can be either positive or negative, smaller or higher than $\frac{1}{2} \mathbf{u}_i^T \mathbf{K}_s^i \mathbf{u}_i$, although generally smaller. This value corrects the gradient information due to the fluid-structure boundary changes. When solid elements are removed, the sensitivity term $\frac{1}{2} \mathbf{u}_i^T \mathbf{K}_s^i \mathbf{u}_i$ globally increases more than $\mathbf{u}_i^T \mathbf{L}_c^i \mathbf{P}_i$, which makes the strain energy term more representative while the algorithm evolves.

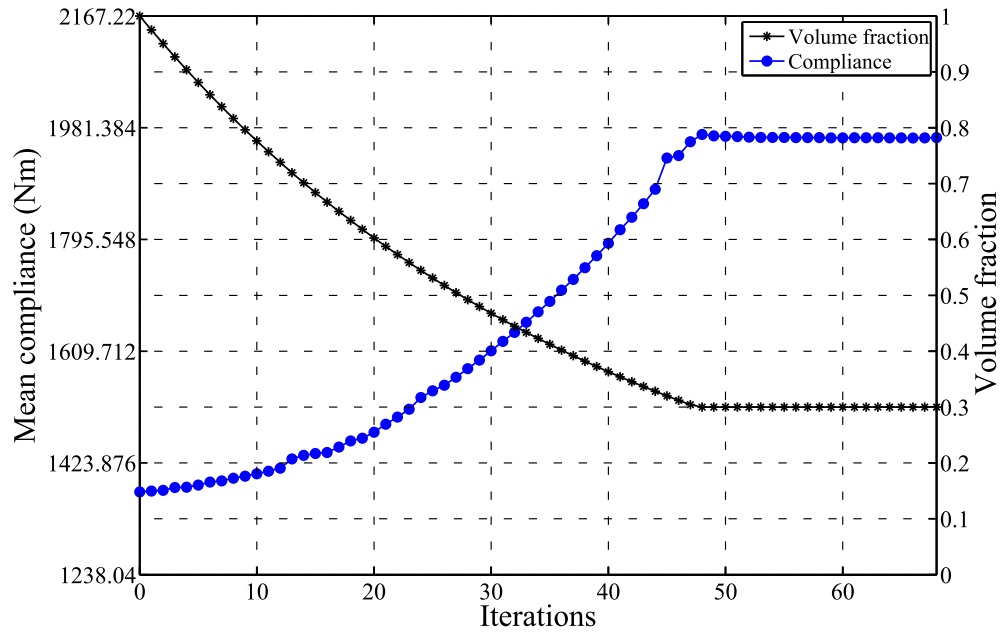


Figure 2.12: Convergence history of the piston head mean compliance.

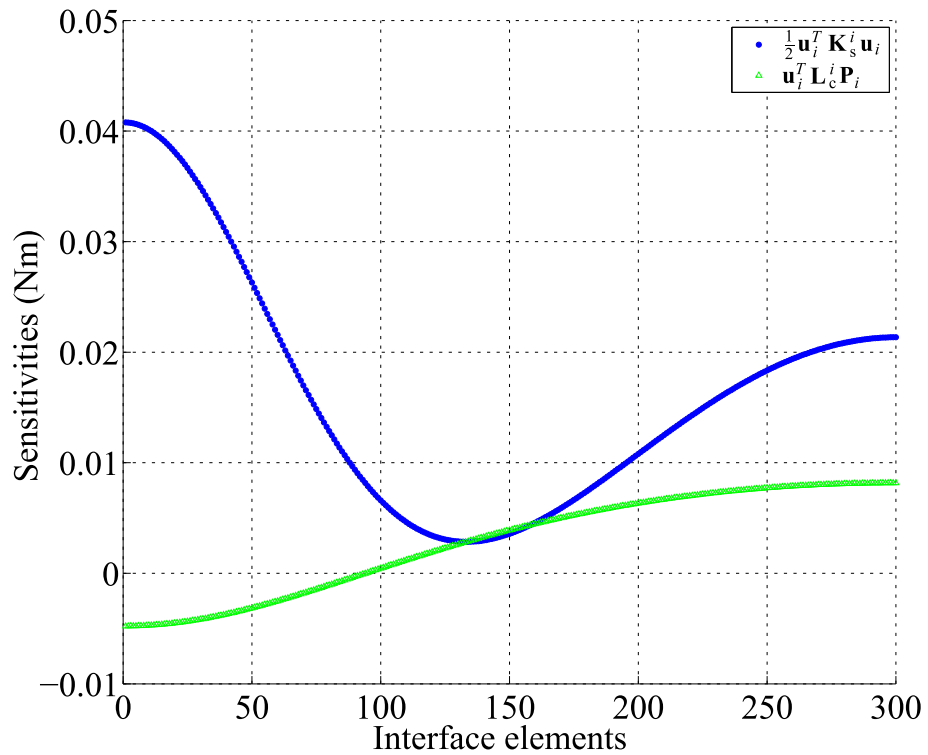


Figure 2.13: Sensitivities for the solid elements along the fluid-structure interface in the initial full design for the piston head finite element model.

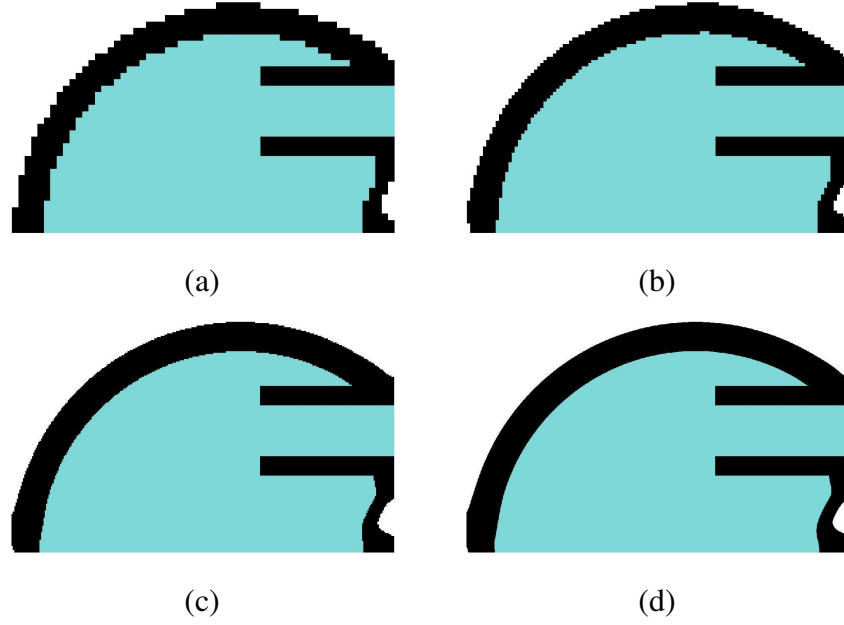


Figure 2.15: Pressure chamber design by the BESO method with: (a) 60×38 (2280 elements), (b) 120×76 (9120 elements), (c) 300×190 (57000 elements) and (d) 1200×260 (912000 elements).

The presented extended fluid-structure BESO method is capable to model non constant pressure fields. In order to explore this feature and show the new possibilities of the method, the inlet pressure of the model from Figure 2.14 is set as $(P_0)^i = 15$ Pa while the outlet pressure is $(P_0)^o = 10$ Pa. Figure 2.16 presents the snapshots of the topology evolution (including the pressure field contours) for the chamber design using different inlet and outlet pressure and using the same BESO parameters of the previous case. It is possible to observe, specially at earlier stages, the variation of pressure contours while the solid topology is evolving. Figure 2.17 presents the convergence history of this chamber optimization problem. The final mean compliance obtained is $C = 2.24 \cdot 10^{-7}$ Nm. In this case, the pressure loads change their location, direction and magnitude during the optimization procedure, in which the algorithm uses the fluid-structure system of Equation 2.10 to solve the pressure fields of each iteration.

Different pressure fields imply in different final topologies, as shown in Figure 2.18 for different values of $(P_0)^o$. Pressure surfaces parametrization schemes usually are not able to model non constant pressure fields, since they interpolate only a constant pressure boundary on a structural model, such as those presented by reference articles (Hammer and Olhoff, 2000; Du and Olhoff, 2004a,b; Zhang *et al.*, 2008; Zheng *et al.*, 2009; Lee and Martins, 2012; Yang *et al.*, 2005). The mixed models from Sigmund and Clausen (2007) and Bruggi and Cinquini (2009) are capable to model any linear pressure field, however with overlapping fluid and structural domains and the final results presenting some intermediate density materials. The presented BESO solution is able to model any linear pressure field in the optimization process with separate

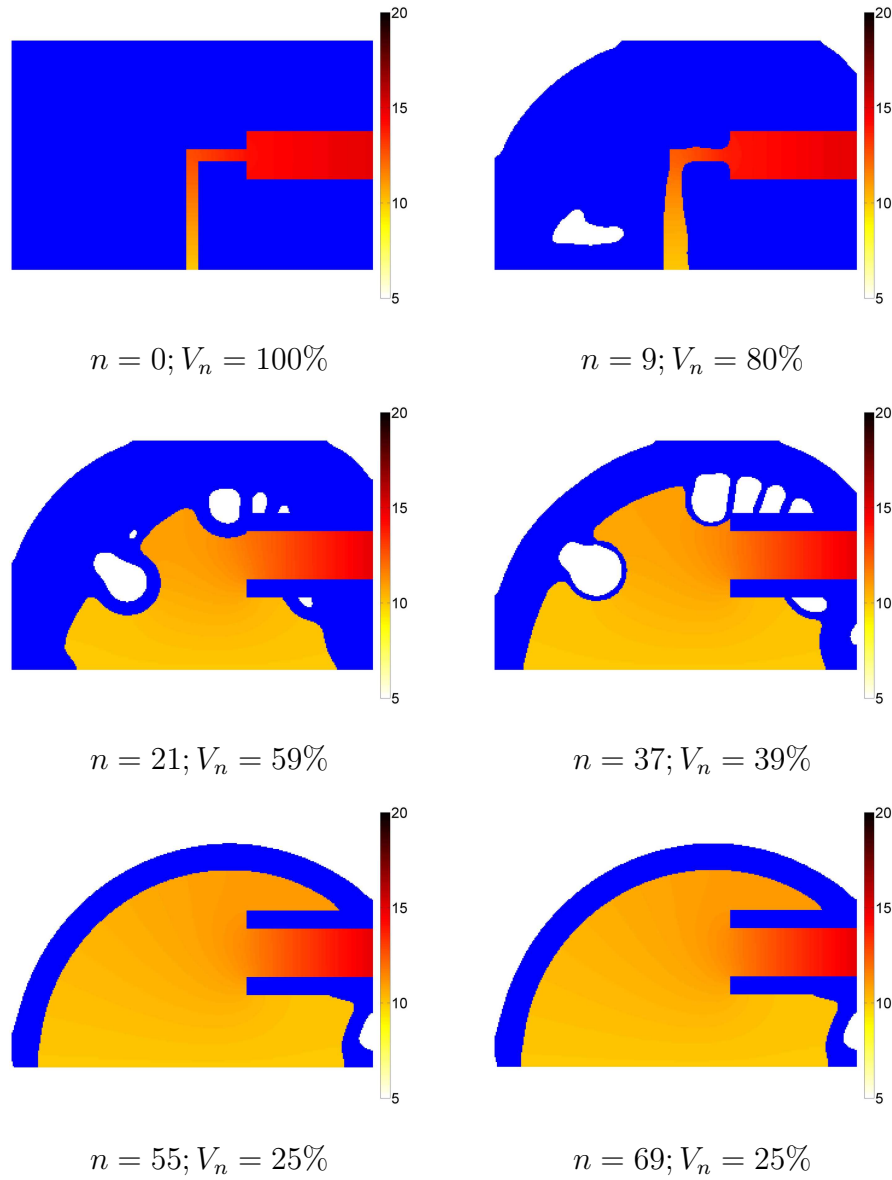


Figure 2.16: Pressure chamber design by the BESO method with inlet pressure $(P_0)^i = 15$ Pa and outlet pressure $(P_0)^o = 10$ Pa. The pressure field is shown for the fluid domain.

domains and classical finite element formulations. Furthermore, no boundary parametrization schemes are needed or intermediate density elements are obtained with the BESO method.

2.6 Conclusions

In this work the extended version of the BESO method for structures subjected to fluid pressure loads has been investigated. The approach is based on the substitution of void elements by incompressible fluid ones capable to transfer pressure through the fluid region. The pressure loading is automatically obtained by the use of coupling matrices integrated over the

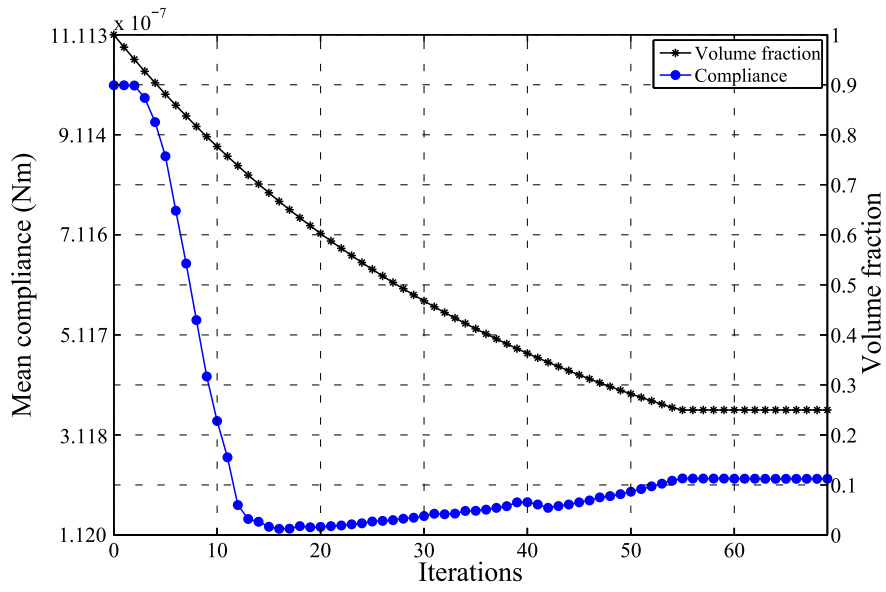


Figure 2.17: Convergence history of the chamber's mean compliance with different inlet and outlet pressure.

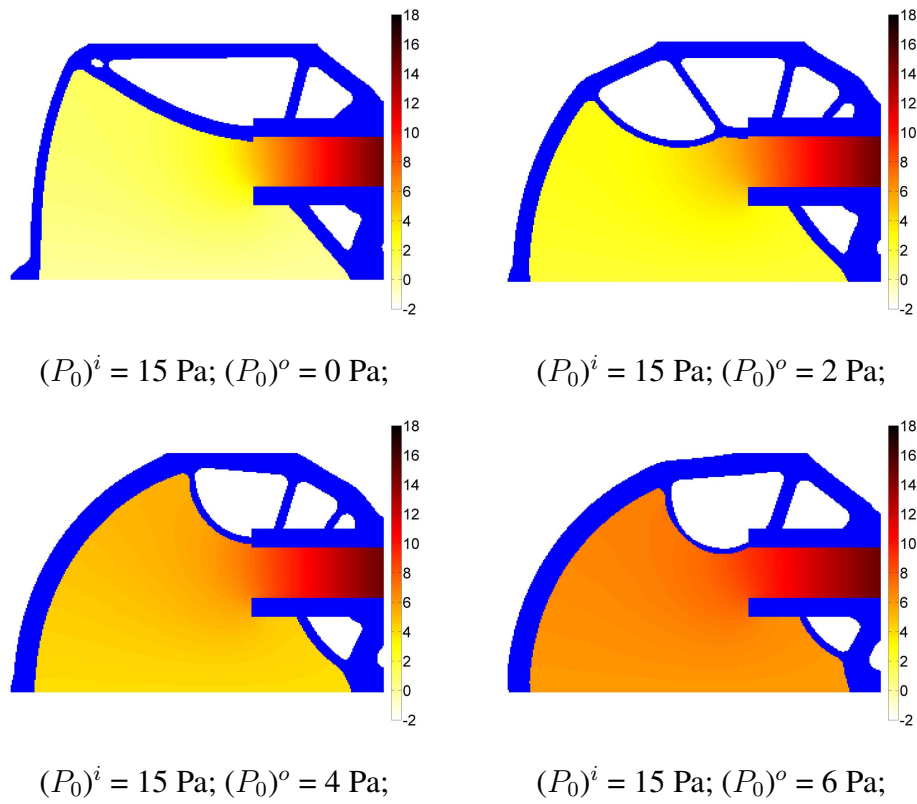


Figure 2.18: Final solutions for the pressure chamber design problem by the BESO method with inlet pressure $(P_0)^i = 15 \text{ Pa}$ and different outlet pressures $(P_0)^o$.

fluid-structure interfaces. It is shown that this technique presents solutions in which the pressure loading surfaces are explicitly defined. Results presented convergence (tolerance $\tau = 0.001$) in less than 70 iterations for all examples and the final topologies showed to be quite similar with the current scientific literature. With the presented methodology separate fields are used to model both structural and fluid domains, which makes the finite element model easy to implement and computationally cheaper than with the mixed models. The method is also capable to model any linear pressure field, differently from most of the reference articles. This gives potential to the evolutionary methods to explore different fluid-structure systems.

In general, the BESO method is proposed as a simple algorithm to treat pressure loading problems using a partially coupled formulation. This work may provide an insight to the multiphysics optimization by showing that a fluid-structural optimization with moving multiphysics interfaces can be easily handled with the BESO method and the classic mathematical formulations.

3 TOPOLOGY OPTIMIZATION OF SUBMERGED BUOYANT STRUCTURES

Context

To design submerged buoyant structures, an inequality constraint has been introduced in the evolutionary topology optimization problem. The inequality constraint prescribes a minimum volume of solid material plus interior voids in order to guarantee the structure to be buoyant. This constraint is shifted to the objective function with the aid of a penalty factor in order to use the volume-based BESO update approach. The same fluid model (*Fluid 1*) from the previous chapter is used to model the underwater pressure field. This contribution has first been published in the conference proceedings of the 11th World Congress on Computational Mechanics (Picelli *et al.*, 2014) and later submitted to *Engineering Optimization* (Picelli *et al.*, 2015a).

3.1 Introduction

Structural topology optimization (Bendsoe and Sigmund, 2003) has been used extensively in structural design problems, especially in the aerospace and automotive industries. Over the last decade considerable effort has been made to extend the methods used in topology optimization to different problems, such as those involving different objective functions and constraints or even multiphysics problems (Chen and Kikuchi, 2001; Sigmund, 2001b; Yoon *et al.*, 2007; Duhring *et al.*, 2008; Silva and Pavanetto, 2010; Andreasen and Sigmund, 2013). Here, it is proposed the use of topology optimization in offshore structural engineering, specifically in the design of completely submerged (subsea) buoyancy modules to support oil pipelines. Subsea buoyancy modules provide buoyancy forces for offshore pipelines (flexible risers, cables and umbilicals) to hold them in specific geometric configurations other than the natural self-weight catenary riser shape, as seen in Figure 3.1. Buoyancy also reduces the overall weight of the pipeline, shifting up buckling loads. Deepwater buoyancy modules of this type are usually made from polymers and may be used at water depths of up to 2000 m.

To design subsea polymer buoys with topology optimization, buoyancy effects and design-dependent underwater pressure loads must be considered. Topology optimization considering interior voids has already been explored, as in the paper by Clausen *et al.* (2014), but buoyancy has not been considered. To the best of the authors' knowledge, this work is the first to take buoyancy effects into account in topology optimization. Design-dependent pressure loads

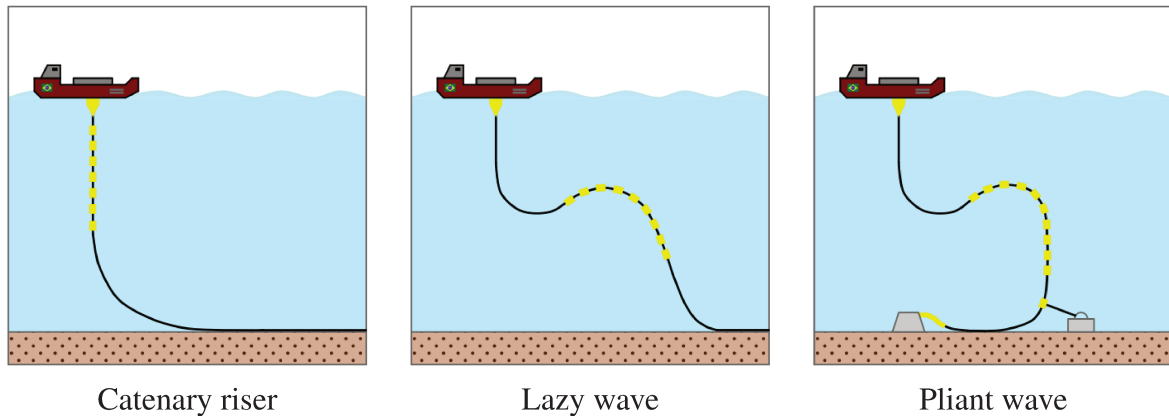


Figure 3.1: Examples of geometric configurations of subsea oil pipelines supported by buoyancy modules, represented as bullets in the illustrations. Buoyancy modules provide upward forces which counteracts the pipeline weight, holding the pipelines in the desired configurations.

have proved to be a challenging topic for topology optimization (Sigmund and Clausen, 2007) and are still a subject under research (Deaton and Grandhi, 2014).

The difficulties in optimizing structures subjected to pressure loads arise because of the variation in the location, direction and magnitude of the loads during the optimization procedure. This variation requires additional modelling techniques when the traditional density-based topology optimization methods are applied in such problems. For instance, in the SIMP model (Bendsoe and Sigmund, 2003), the pressure-loaded surfaces are not explicitly defined because of the existence of intermediate density (gray scale) elements (Hammer and Olhoff, 2000). The main efforts to solve pressure-load problems in topology optimization have used pressure surface parametrization schemes (Hammer and Olhoff, 2000; Du and Olhoff, 2004a; Lee and Martins, 2012; Zhang *et al.*, 2008; Zheng *et al.*, 2009; Zhang *et al.*, 2010) and multiphysics approaches (Chen and Kikuchi, 2001; Bourdin and Chambolle, 2003; Sigmund and Clausen, 2007; Bruggi and Cini, 2009). These works showed that pressure loading problems can be efficiently solved with density-based topology optimization by using different pressure boundaries modelling techniques. The idea of using mixed element formulations by Sigmund and Clausen (2007) could be further applied in a range of different multiphysics problems (Yoon *et al.*, 2007; Yoon and Sigmund, 2008; Yoon, 2010; Andreasen and Sigmund, 2013).

On the other hand, Picelli *et al.* (2015b) proposed an extended BESO method for use in hydrostatic fluid-loaded structural design problems using a partially coupled fluid-structure formulation. Because of the discrete nature of the BESO method, no intermediate density elements are allowed during the optimization and the problem is solved without any need for pressure load surface parametrization schemes. In comparison with the SIMP model, the BESO scheme can be used with staggered analysis and separate domains, which can be handy for its

association with commercial finite element codes and the use of classical formulations. However, the evolutionary methods still lack of procedures in handling multiple linear and nonlinear constraints, while this is simpler to be considered with the density-based methods.

The idea by Picelli *et al.* (2015b) was extended to acoustic-structure interaction problems, as shown by Vicente *et al.* (2015) and Picelli *et al.* (2015d). This evidences the recent uses of the BESO method on multiphysics problems (Picelli *et al.*, 2015c). The discrete nature of these methods are also recently explored in multiscale problems (Xie *et al.*, 2012; Zuo *et al.*, 2013; Xia and Breitkopf, 2014; Huang *et al.*, 2015; Xia and Breitkopf, 2015). Similar approaches can also be adopted by other topology optimization methods with explicit boundaries definition, such as level set based methods (Luo *et al.*, 2012; Shu *et al.*, 2014; Xia *et al.*, 2015).

To handle pressure loads, the fluid-structure BESO method described by Picelli *et al.* (2015b) is used. This approach substitutes some of the void elements with hydrostatic fluid ones that can model the pressure field. Laplace's equation is used to model the fluid domain, allowing the existence of constant and non-constant pressure fields at wet fluid-structure interfaces. The use of surface coupling matrices turns out the problem handy for the discrete topology optimization scheme by transferring pressure loads automatically to the structural analysis whatever is the structural topology. Herein, buoyancy requirements are introduced as an inequality constraint in the optimization problem. According to Archimedes' principle, the buoyancy force is equivalent to the weight of the fluid displaced by the submerged structure and can be expressed as:

$$\mathbf{F}_B = -\rho_f V_f \mathbf{g}_a, \quad (3.1)$$

where \mathbf{F}_B is the buoyancy force acting on the structure, ρ_f is the mass density of the fluid, V_f the volume of the displaced fluid and \mathbf{g}_a the vector of the gravitational acceleration. The force \mathbf{F}_B is balanced by the weight \mathbf{W}_s of the structure, expressed as:

$$\mathbf{W}_s = m_s \mathbf{g}_a, \quad (3.2)$$

where m_s is the mass of the structure, implying in a resulting force

$$\mathbf{F}_{resulting} = \mathbf{F}_B + \mathbf{W}_s. \quad (3.3)$$

As the mass of the structure is a constraint in the proposed optimization method, \mathbf{W}_s is constant and the only variable in the force diagram is \mathbf{F}_B , which depends exclusively on V_f , since ρ_f and \mathbf{g}_a are also constant. The volume V_f of the displaced fluid is equivalent to the sum of the volumes of the structural material and the buoy's interior voids. Thus, in order to guarantee higher buoyancy, the entire buoy volume (including structure and interior voids) must be as

big as possible, implying in a positive $F_{resulting}$. In this work it is assumed that the buoyancy modules must withstand the underwater surrounding pressure and exhibit minimal deformation so that they maintain the correct displaced volume. Hence, the final goal of the optimization problem is to design a structure as stiff as possible that can handle design-dependent underwater pressure loads and has high buoyancy (displaced fluid volume).

This chapter is organized as follows: Section 3.2 introduces the governing equations and the finite element model for the fluid-structure system. In Section 3.3, the topology optimization problem and sensitivity analysis are described. Section 3.4 discusses implementation issues and the steps in the fluid-structure BESO method. Section 3.5 presents the discussion and the numerical results obtained using the proposed methodology. Section 3.6 presents final conclusions.

3.2 Fluid-structure model: governing equations and finite element discretization

We consider the static analysis of completely submerged flexible structures floating in an incompressible fluid domain. The use of subsea buoyancy modules in deepwater conditions implies high pressures in the fluid domain. Because of the depth at which the modules are operating, these pressures can be considered constant in this case.

The fluid-structure system is modelled assuming a linearly elastic continuum solid domain and hydrostatic fluids. All the details of this formulation can be found in the article by Zienkiewicz and Bettess (1978) or in reference books (Morand and Ohayon, 1995; Axisa and Antunes, 2007). The following sections briefly outline the governing equations for the fluid and structural domains, the coupling boundary conditions and the finite element discretization.

3.2.1 Fluid domain

In the static analysis, the governing equation considering a homogeneous, inviscid, irrotational fluid domain Ω_f can be described by Laplace's equation

$$\nabla^2 P_f = 0 \quad \text{in } \Omega_f, \quad (3.4)$$

where P_f is the fluid pressure (Morand and Ohayon, 1995).

The following boundary conditions are imposed:

$$P_f = P_0 \quad \text{on } S_p, \quad (3.5)$$

$$\nabla P_f \cdot \mathbf{n} = 0 \quad \text{on } S_f, \quad (3.6)$$

representing the pressure boundary condition (Equation 3.5) and the hard wall condition (Equation 3.6) on the fluid boundaries S_p and S_f , respectively, as illustrated in Figure 3.2. The term P_0 is the imposed deepwater pressure value and must be different than zero.

3.2.2 Structural domain

Neglecting body forces, the linear structural static analysis is governed by

$$\nabla \cdot \boldsymbol{\sigma}_s(\mathbf{u}) = 0 \quad \text{in } \Omega_s, \quad (3.7)$$

where $\nabla \cdot \boldsymbol{\sigma}_s(\mathbf{u})$ is the divergence of the Cauchy stress tensor and \mathbf{u} is the displacement field on the solid domain Ω_s . Dirichlet boundary conditions are applied to the solid domain as:

$$\mathbf{u} = \mathbf{u}_0 \quad \text{on } S_u. \quad (3.8)$$

This represents the constrained displacements for all points on the solid boundaries S_u , as shown in Figure 3.2. A void domain Ω_v can also exist inside the solid domain.

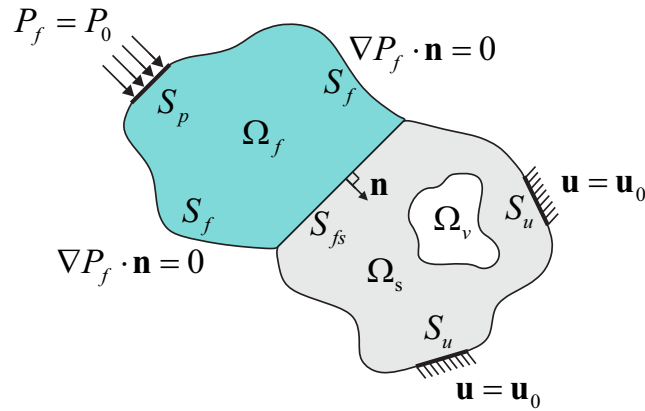


Figure 3.2: The solid (Ω_s), fluid (Ω_f) and void (Ω_v) domains and boundary conditions. Pressure P_0 is imposed on the portion S_p of the fluid boundary. Fluid pressure loads act on the structure through the fluid-structure interface S_{fs} .

3.2.3 The coupled fluid-structure system

The normal vector \mathbf{n} (see Figure 3.2) can be used in order to guarantee the equilibrium condition between fluid pressures and structural tractions on the interface S_{fs} as follows:

$$\boldsymbol{\sigma}_s \mathbf{n} = -P_f \mathbf{n} \quad \text{on } S_{fs}. \quad (3.9)$$

With the aid of relations derived from the governing equations and the coupling condition from Equation 3.9, the interface loads can be obtained (Morand and Ohayon, 1995; Axisa and Antunes, 2007). An approximation based on the finite element method (FEM) can be used to model a spatial coupling matrix

$$\mathbf{L}_{fs} = \int_{S_{fs}} \mathbf{N}_s^T \mathbf{n} \mathbf{N}_f dS_{fs} \quad (3.10)$$

and to write the coupling forces \mathbf{f}_{fs} in a discretized form as

$$\mathbf{f}_{fs} = \mathbf{L}_{fs} \mathbf{P}_f, \quad (3.11)$$

where \mathbf{P}_f is the vector of nodal pressures, \mathbf{n} is the normal vector inwards the structural domain and \mathbf{N}_s and \mathbf{N}_f contains the finite element shape functions for the interface.

Thus, in the context of the finite element approximation, and assuming no external loads are applied, the hydroelastic equilibrium problem can be described by a non-symmetric system of equations

$$\begin{bmatrix} \mathbf{K}_s & -\mathbf{L}_{fs} \\ \mathbf{0} & \mathbf{K}_f \end{bmatrix} \begin{Bmatrix} \mathbf{u}_s \\ \mathbf{P}_f \end{Bmatrix} = \begin{Bmatrix} \mathbf{0} \\ \mathbf{0} \end{Bmatrix}, \quad (3.12)$$

where \mathbf{u}_s is the vector of structural displacements and \mathbf{K}_s and \mathbf{K}_f are the stiffness matrices of the structural and fluid domains, respectively. The matrix \mathbf{L}_{fs} is the coupling matrix (Morand and Ohayon, 1995).

In this one-way coupled multiphysics model, the fluid analysis provides pressure loads to the structural analysis through the application of the coupling matrices. In this case, the fluid pressure field can actually be solved separately. However, for the sake of generality, by imposing the boundary conditions from Equations 3.5, 3.6, 3.8 and 3.9 and solving Equation 3.12, both fluid and structure responses can be obtained simultaneously for any discretized

fluid-structure configuration. This turns to be handy for the iterative procedures of topology optimization. Furthermore, this methodology can be extended to different design-dependent physics problems, where fully coupled equations might exist (Vicente *et al.*, 2015; Picelli *et al.*, 2015d).

3.3 Problem formulation

3.3.1 Topology optimization problem

The buoy design problems considered in this work involve minimizing the mean compliance of structures under design-dependent pressure loads while satisfying volume and buoyancy constraints. The objective is to find how a given amount of solid material should be distributed to ensure that the structure has maximum stiffness (or minimum compliance $C(x_i)$) and a prescribed buoyancy. The evolutionary topology optimization problem for this case can be formulated as:

$$\begin{aligned}
 \min_{x_i} \quad & C(x_i) = \frac{1}{2} \mathbf{u}_s^T \mathbf{K}_s \mathbf{u}_s, \\
 \text{subject to:} \quad & \begin{bmatrix} \mathbf{K}_s & -\mathbf{L}_{fs} \\ \mathbf{0} & \mathbf{K}_f \end{bmatrix} \begin{Bmatrix} \mathbf{u}_s \\ \mathbf{P}_f \end{Bmatrix} = \begin{Bmatrix} \mathbf{0} \\ \mathbf{0} \end{Bmatrix} \text{ and b.c.,} \\
 & g = 1 - \frac{B}{B_{lim}} \leq 0, \\
 & h = V(x_i)/V_0 = V_s, \\
 & x_i = [0,1],
 \end{aligned} \tag{3.13}$$

where $C(x_i)$ is the mean structural compliance, B_{lim} is the minimum required buoyancy volume (displaced fluid area for 2D cases), B is the buoyancy volume of the current structural design, V_0 is the full design domain volume, V_s is the prescribed final solid volume fraction, nel is the number of elements inside the design domain and x_i represents the discrete design variables, 1 being a solid element and 0 a fluid/void. The inequality constraint g sets a threshold for the required buoyancy volume and the equality constraint h sets the amount of solid material to be used with respect to the volume of the design domain. The constraint g is considered to be active when B , measured by the joint volume of structural and void elements, is equal as the prescribed buoyancy volume B_{lim} . The final solution do not need to present an active g , since $B > B_{lim}$ is also in the feasible solution region and it g is inactive in this case. The constraint h must be active in the final solution, ensuring the solution to present a final volume fraction equal to V_s .

To enable the procedures in the standard evolutionary method to be used, the previous problem statement is modified so that it can be solved in a penalty form (Luenberger and Ye,

2008). Thus, the topology optimization problem becomes:

$$\begin{aligned}
 \min_{x_i} \quad & f(x_i) = \frac{1}{2} \mathbf{u}_s^T \mathbf{K}_s \mathbf{u}_s + p \max(0, g), \\
 \text{subject to:} \quad & \begin{bmatrix} \mathbf{K}_s & -\mathbf{L}_{fs} \\ \mathbf{0} & \mathbf{K}_f \end{bmatrix} \begin{Bmatrix} \mathbf{u}_s \\ \mathbf{P}_f \end{Bmatrix} = \begin{Bmatrix} \mathbf{0} \\ \mathbf{0} \end{Bmatrix} \text{ and b.c.,} \\
 & h = V(x_i) / V_0 = V_s, \\
 & x_i = [0, 1],
 \end{aligned} \tag{3.14}$$

where p is an arbitrary penalty factor. When B is lower than B_{lim} , g is greater than 0 and is added to the objective function $f(x_i)$. This behavior is then discouraged by a high penalty factor.

3.3.2 Sensitivity analysis

Evolutionary methods are based on the evolution of structures in nature, in which material is placed near regions subjected to high stresses (Xie and Steven, 1993; Xie and Huang, 2010). Starting from a full design domain (or initial solution), the BESO method slowly removes elements and reduces the solid volume fraction towards V_s . Void elements near high-stressed regions can return to the solid. A sensitivity analysis is needed to determine the efficiency of each element in the structural performance and decide which element should be eliminated or returned to the solid. This is achieved by determining the derivative of the objective function with respect to the design variables, which represents the change in the objective function when element x_i is removed. The derivative of $f(x_i)$ with respect to x_i is:

$$\frac{\partial f(x_i)}{\partial x_i} = \alpha_{Ci} + p \alpha_{Bi}, \tag{3.15}$$

where α_C and α_B correspond to the derivatives of the compliance and buoyancy objective functions, respectively. The derivative of the compliance is

$$\alpha_{Ci} = \frac{\partial C}{\partial x_i} = \mathbf{u}_s^T \mathbf{K}_s \frac{\partial \mathbf{u}_s}{\partial x_i} + \frac{1}{2} \mathbf{u}_s^T \frac{\partial \mathbf{K}_s}{\partial x_i} \mathbf{u}_s. \tag{3.16}$$

The equilibrium equation of the structural system (first equation in the system of Equation 3.12) can be derived to find the unknown $\partial \mathbf{u}_s / \partial x_i$:

$$\frac{\partial (\mathbf{K}_s \mathbf{u}_s)}{\partial x_i} = \frac{\partial (\mathbf{L}_{fs} \mathbf{P}_f)}{\partial x_i}. \tag{3.17}$$

Applying the chain rule on both sides of the previous equation, we have

$$\frac{\partial \mathbf{K}_s}{\partial x_i} \mathbf{u}_s + \mathbf{K}_s \frac{\partial \mathbf{u}_s}{\partial x_i} = \frac{\partial \mathbf{L}_{fs}}{\partial x_i} \mathbf{P}_f + \mathbf{L}_{fs} \frac{\partial \mathbf{P}_f}{\partial x_i}. \quad (3.18)$$

Assuming that the values of the high depth pressure field \mathbf{P}_f are constant, the derivative $\partial \mathbf{P}_f / \partial x_i$ is zero. Then, isolating the derivative of the displacement vector

$$\frac{\partial \mathbf{u}_s}{\partial x_i} = \mathbf{K}_s^{-1} \left(\frac{\partial \mathbf{L}_{fs}}{\partial x_i} \mathbf{P}_f - \frac{\partial \mathbf{K}_s}{\partial x_i} \mathbf{u}_s \right), \quad (3.19)$$

and substituting Equation 3.19 in Equation 3.16, we can rewrite the derivative of the compliance as

$$\alpha_{Ci} = \mathbf{u}_s^T \mathbf{K}_s \mathbf{K}_s^{-1} \left(\frac{\partial \mathbf{L}_{fs}}{\partial x_i} \mathbf{P}_f - \frac{\partial \mathbf{K}_s}{\partial x_i} \mathbf{u}_s \right) + \frac{1}{2} \mathbf{u}_s^T \frac{\partial \mathbf{K}_s}{\partial x_i} \mathbf{u}_s. \quad (3.20)$$

After simplification, the derivative of the compliance is given by

$$\alpha_{Ci} = \mathbf{u}_s^T \frac{\partial \mathbf{L}_{fs}}{\partial x_i} \mathbf{P}_f - \frac{1}{2} \mathbf{u}_s^T \frac{\partial \mathbf{K}_s}{\partial x_i} \mathbf{u}_s. \quad (3.21)$$

The derivative of the buoyancy can be expressed as

$$\alpha_{Bi} = \frac{\partial g}{\partial x_i} = \frac{\partial (1 - \frac{B}{B_{lim}})}{\partial x_i} = -\frac{1}{B_{lim}} \frac{\partial B}{\partial x_i}. \quad (3.22)$$

The derivatives are then evaluated locally at the element level, generating a sensitivity number α_i for each element represented by both compliance (α_{Ci}) and buoyancy (α_{Bi}) element sensitivities

$$\alpha_i = -\frac{\partial f(x_i)}{\partial x_i} = -(\alpha_{Ci} + p\alpha_{Bi}). \quad (3.23)$$

The minus sign is introduced when minimization of the objective function is considered in the optimization problem.

The version of the BESO method described here is developed using a hard-kill technique, where the densities of the void elements are set to zero, as proposed by Huang and Xie (2007). A material interpolation scheme similar to the SIMP-model can also be used to set a very small density for the void elements in a soft-kill evolutionary procedure described by Huang and Xie (2009). When used with a mesh-independence filter, both hard-kill and soft-kill approaches present similar results for structural design and can be used in a similar manner, as shown by Huang and Xie (2010).

In the hard-kill approach, no material interpolation functions or design variables with very small values appear in the element modelling. The material is then the simple superposition

(finite element assembly) of all solid element stiffness matrices \mathbf{K}_s^i . Thus, the definition of the sensitivities cannot be derived as a continuous function in the manner it is carried out by the SIMP approach. Therefore, an approximation based on a single step finite difference can be carried out for the hard-kill sensitivities, considering the structural configuration before and after an element removal (Xie and Huang, 2010). The derivative of the global structural stiffness matrix with respect to the design variable of the i th element can be then expressed as

$$\frac{\partial \mathbf{K}_s}{\partial x_i} \approx \mathbf{K}_s^i. \quad (3.24)$$

The derivative of the global structural stiffness matrix with respect to the design variable of the i th element can be approximated by a finite difference step considering the element removal and can be expressed as

$$\frac{\partial \mathbf{K}_s}{\partial x_i} \approx \mathbf{K}_s^i. \quad (3.25)$$

The derivative of the coupling matrix $\partial \mathbf{L}_{fs} / \partial x_i$ indicates the change in the coupling condition when the i th element is removed. This change can be predicted by a finite difference with step equivalent as the system configuration before and after the element removal. Thus,

$$\frac{\partial \mathbf{L}_{fs}}{\partial x_i} \approx (\Delta \mathbf{L}_{fs})^i = (\mathbf{L}_{fs}^* - \mathbf{L}_{fs})^i, \quad (3.26)$$

where \mathbf{L}_{fs} is the coupling matrix before the element is removed and \mathbf{L}_{fs}^* is the final coupling matrix after the element is removed.

For a general solid element, we can determine the change in the coupling configuration from the interface coupling forces. Figure 3.3 shows a possible coupling configuration before and after removal of an element. Knowing this configuration, the change $(\mathbf{L}_{fs}^* - \mathbf{L}_{fs})^i$ can be evaluated. The minus sign changes the direction of the coupling force given by \mathbf{L}_{fs} , as shown in Figure 3.3.

It can be seen that, no matter what the initial coupling configuration, the change $(\mathbf{L}_{fs}^* - \mathbf{L}_{fs})^i$ is always as shown in Figure 3.3. This represents the change in the coupling forces when a solid element is removed and replaced with a fluid element, which transfers the interface pressure through the whole element. Therefore, for any solid element, a matrix containing the coupling terms through the element boundaries can represent the change in the coupling configuration, as follows:

$$\frac{\partial \mathbf{L}_{fs}}{\partial x_i} \approx (\mathbf{L}_{fs}^* - \mathbf{L}_{fs})^i = \mathbf{L}_c^i, \quad (3.27)$$

¹We use the term “buoyancy area” to refer to the cross sectional area of the buoy.

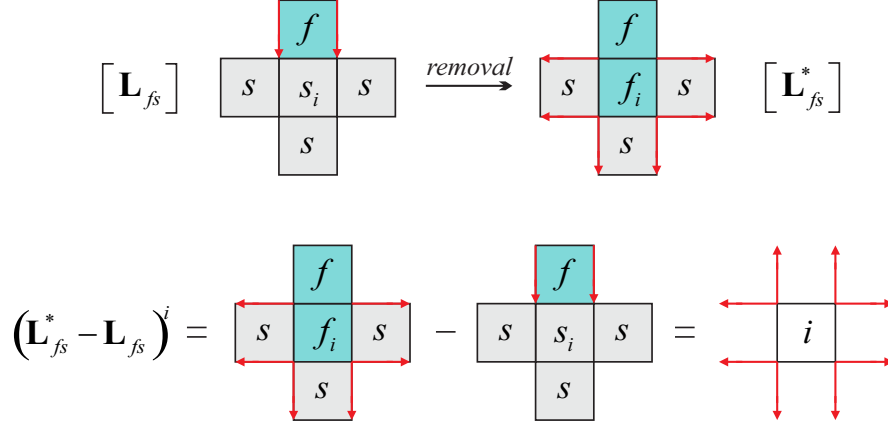


Figure 3.3: Coupling forces configuration before and after an element removal. The derivative $\partial \mathbf{L}_{fs} / \partial x_i$ can be approximated by the change in the coupling matrices $(\Delta \mathbf{L}_{fs})^i = (\mathbf{L}_{fs}^* - \mathbf{L}_{fs})^i$ after removal of the i th element. The arrows indicate the pressure loads $\Delta \mathbf{L}_{fs} \mathbf{P}_f$ exerted by the fluid elements on the structure.

where \mathbf{L}_c^i is the matrix assembled according to the change in the coupling configuration, shown in Figure 3.3. Thus, the term α_{Ci} can be expressed as

$$\alpha_{Ci} = \mathbf{u}_i^T \mathbf{L}_c^i \mathbf{P}_i - \frac{1}{2} \mathbf{u}_i^T \mathbf{K}_s^i \mathbf{u}_i. \quad (3.28)$$

To find α_{Bi} , the derivative $\partial B / \partial x_i$ must be calculated. This derivative represents the change in the total buoyancy volume B when element x_i is removed. The absolute change in B can be approximated as

$$\left(\frac{\partial B}{\partial x_i} \right)^i \approx |\Delta B(x_i)| = |(B^* - B)^i| = (A_i)^{fs}, \quad (3.29)$$

where B^* is the buoyancy volume after removal of the i th element, and the superscript fs indicates that the term is valid only for elements at the fluid-structure interface. Removal of elements in the interior of the structure does not cause any change in B . For 2D cases, solid elements at the fluid-structure boundaries cause a change equivalent to the area A_i of the element, as seen in Figure 3.4. In these cases, the derivative of the buoyancy objective function is a constant valid only for solid elements at the fluid-structure interface. For all other elements, the sensitivity value is 0. Thus, returning to Equation 3.22, α_{Bi} can be expressed as:

$$\alpha_{Bi} = \frac{\partial g}{\partial x_i} \approx -\frac{1}{B_{lim}} (A_i)^{fs}. \quad (3.30)$$

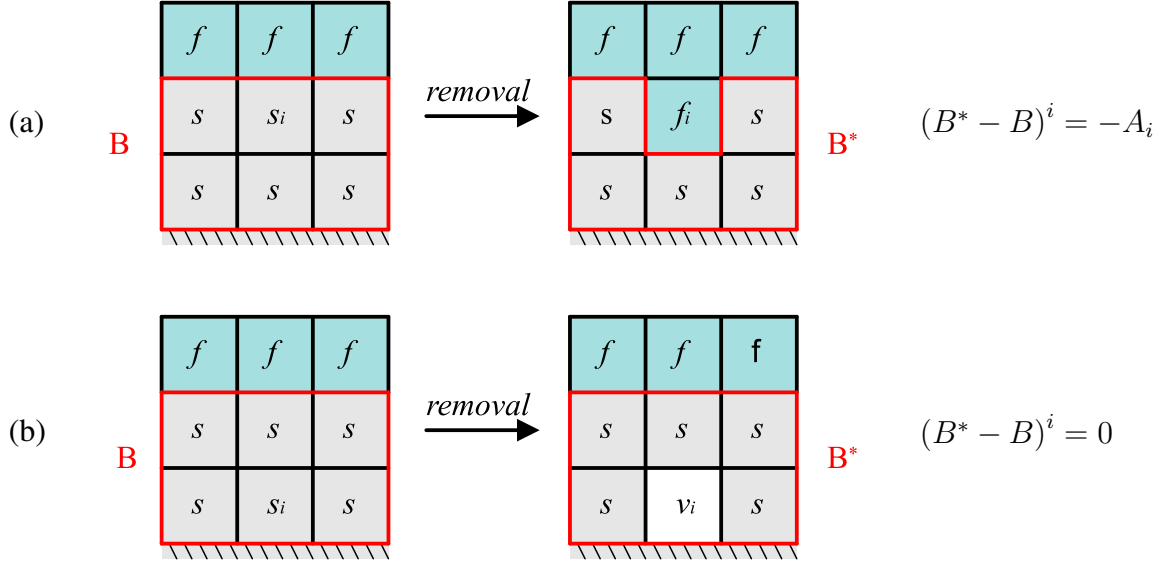


Figure 3.4: Change in B due to a solid element removal at (a) the fluid-structure interface and (b) an interior element.

Combining Equation 3.30 and 3.28 and rewriting Equation 3.23, the sensitivity numbers that should be used in the buoyancy-module design are

$$\alpha_i = -\frac{\partial f(x_i)}{\partial x_i} = \begin{cases} \frac{1}{2} \mathbf{u}_i^T \mathbf{K}_s^i \mathbf{u}_i - \mathbf{u}_i^T \mathbf{L}_c^i \mathbf{P}_i + \frac{p}{B_{lim}} (A_i)^{fs} & x_i = 1 \\ 0 & x_i = 0 \end{cases}. \quad (3.31)$$

This analysis is carried out for each element i in the design domain. For solid elements which are not at the fluid-structure boundary (interface), the pressure transferred by the occupying fluid is null and the term $\mathbf{u}_i^T \mathbf{L}_c^i \mathbf{P}_i$ vanishes. The term for buoyancy in the sensitivities are also only for boundary elements. Although the sensitivities for void elements are computed as zero, the application of a numerical filter scheme extrapolates the sensitivities on the finite element mesh and neighboring voids close to regions with high sensitivities can return to solid.

It is also important to note that the new term α_{Bi} is only valid when the inequality constraint g is active. The first term of α_i is the strain energy of element x_i . The second term is the derivative of the pressure loads at the element level. The elements with the lowest sensitivities can be removed from the domain with a minimum change in the objective function. When g is not active, the compliance derivatives will provide the gradient information for the optimization procedure. For buoyant structures, the minimum compliance would be obtained with the smallest possible structure without holes, i.e., a structure with a very small B . However, as B decreases, g will be active and the solid elements at the fluid-structure interfaces will have a

high sensitivity number because of the penalty factor p , causing elements to be added in the regions next to the fluid-structure interfaces so that the volume (and consequently B) of the structural design increases. At this point, only elements in the interior of the structure will be removed, since these elements have lower sensitivities.

3.4 Optimization procedure

Originally, evolutionary structural optimization (ESO) was based on successive elimination of material from the initial design domain (Xie and Steven, 1993). Subsequently, the method was extended to different structural design problems (Xie and Steven, 1996; Li *et al.*, 1999). Steven *et al.* (2000) used ESO for the first time for general physical field uncoupled problems, including a fluid domain design case. Further improvements to the ESO method were made using a bi-directional algorithm (Querin and Steven, 1998) and the sequential element rejections and admissions (SERA) method (Rozvany and Querin, 2002) to allow void (or very low density) elements to return to the solid condition.

One of the last major developments in ESO-based methods was the convergent and mesh-independent BESO method proposed by Huang and Xie (2007), which allows material to be simultaneously removed and added in the domain until a volume constraint and convergence criterion are satisfied. The method was initially used as a hard-kill technique, but a further improvement introduced an interpolation scheme that adopted a soft-kill approach (Huang and Xie, 2009). In general, these methods can be considered gradient-based methods that rely on design updates and result only in 0/1 solutions during the optimization process.

The proposed methodology described in this article is a hard-kill BESO approach, in which some void elements are substituted by incompressible fluid ones and the loads are generated by imposed pressures in the coupled model. Finite element analysis is carried out and Equation 3.12 is used to obtain the fluid-structure responses.

3.4.1 Implementation issues for a BESO-based method

In order to rank all the elements according to their contribution to the objective function, the sensitivity numbers from Equation 3.31 are evaluated for each element. A mesh-independence filter is applied over the whole mesh by averaging each elemental sensitivity number with its neighboring elements. The filter scheme is similar to that described by Sigmund and Peterson (1998). To evaluate the filter weights, nodal sensitivity numbers α_j are

calculated by averaging the elemental sensitivity numbers of the j th connected elements. These nodal sensitivity numbers must be converted back into elemental sensitivities by projecting a sub-domain Ψ_i with length scale r_{min} centered on the i th element. All the nodes inside Ψ_i must have their nodal sensitivity numbers averaged back to the i th elemental level as follows:

$$\alpha_i = \sum_{j=1}^{nod} w(r_{ij}) \alpha_j / \sum_{j=1}^{nod} w(r_{ij}), \quad (3.32)$$

where r_{ij} is the distance between the node j and the center of the element i , nod is the total number of nodes inside the design domain and $w(r_{ij})$ is a weight factor whose value is $r_{min} - r_{ij}$ for nodes inside the sub-domain Ψ_i and 0 for nodes outside the sub-domain. This filter scheme can effectively address mesh-dependency and checkerboard problems. However, the objective function and corresponding topology may not be convergent. To avoid this problem, Huang and Xie (2007) showed that the above sensitivity numbers should be averaged with their previous iteration numbers as follows

$$\alpha_i = \frac{\alpha_i^n + \alpha_i^{n-1}}{2}, \quad (3.33)$$

where n is the current iteration number. Thus, the updated sensitivity number includes the history of the sensitivity information in the previous iterations (Huang and Xie, 2007).

For each iteration, a target volume V_{n+1} is defined as

$$V_{n+1} = V_n(1 \pm ER), \quad (3.34)$$

where ER is the evolutionary ratio and n the number of the iteration. ER is the percentage change in the structural volume and causes V_{n+1} to increase or decrease toward the final desired structural volume fraction V_s . When $V_n = V_s$, the equality constraint h is active and the target volume V_{n+1} is kept equal to V_s until the convergence of the algorithm. The target volume V_{n+1} sets the threshold α_{th} of the sensitivity numbers. Solid elements ($x_i = 1$) for which $\alpha_i \leq \alpha_{th}$ are switched to the fluid/void condition ($x_i = 0$). Fluid/void elements ($x_i = 0$) are switched to the solid condition ($x_i = 1$) when $\alpha_i > \alpha_{th}$.

Meanwhile, the volume addition ratio (AR) is restricted to a maximum addition ratio AR_{max} , which specifies the maximum allowable solid volume fraction that can be added per iteration. It plays an important role when the inequality constraint g is violated and solid elements at the interfaces have highly penalized sensitivities. Because of filtering, exterior fluid/void elements close to the interfaces are also given high sensitivities and tend to return to solid condition. The amount of these new solid elements is controlled by the maximum admission ratio AR_{max} . This parameter is usually set with similar values to ER , e.g., between 1% and 5%. If $AR > AR_{max}$, only some of the elements with highest sensitivity numbers are added to set

$AR = AR_{max}$. Then, some of the elements with the lowest sensitivity numbers are removed to satisfy the target volume V_{n+1} . When the variables x_i for an element are equal to zero, a decision must be taken as the element can become a fluid element or a void. If the element has at least one fluid element as neighbor, it must be turned into a fluid element. If the element does not have any fluid neighbors, it must be turned into a void. This procedure is repeated until there are no more changes in the fluid-void regions. Thus, some layers of structural elements near the fluid-structure interface can be replaced by fluid elements, and void elements appear only inside the structural domain.

When the prescribed final volume V_s is reached, the target volume remains constant, i.e., $V_{n+1} = V_n$. The algorithm evolves until a stop criterion with a predefined tolerance τ is satisfied. Differently from the standard convergence criterion proposed by Huang and Xie (2007) for the BESO method and used by Picelli *et al.* (2015b) for pressure loads, here the following formula is used to evaluate the convergence of the solution:

$$\frac{|C_n - C_{n-1}| + |C_{n-1} - C_{n-2}|}{C_n - C_{n-1}} \leq \tau, \quad (3.35)$$

where C_n is the structural compliance value for the current iteration. This formula is a particular case of the standard one, using less iterations to determine the convergence of the solution. This is justified by the hydrostatic stress state in which the buoyant structures are found. For these structures every small change in their structural design leads to higher changes in compliance than for the structures presented in Picelli *et al.* (2015b) when no buoyancy is considered and bending stress is predominant. The following numerical results show that the proposed formula is satisfactory to determine the convergence of this optimization problem.

3.4.2 The extended fluid-structure BESO method

The evolutionary procedure for the BESO method presented here for buoyancy module design problems is as follows:

1. Define the design domain, loads and boundary conditions.
2. Define the BESO parameters.
3. Discretize the design domain using a finite element (FE) mesh for the given boundary conditions. Initially, a global fluid-structure stiffness matrix \mathbf{K}_g must be assembled uncoupled.

4. Couple and store a current global matrix \mathbf{K}_n with the coupling matrices according to the current design of the n th iteration and the appropriate boundary conditions. Thus, the current \mathbf{K}_n becomes equivalent to the stiffness matrix from Equation 3.12.
5. Perform FE analysis (using Equation 3.12) on the current design to obtain the displacement and pressure responses.
6. Calculate the sensitivity numbers according to Equation 3.31.
7. Apply the filter scheme. Project the nodal sensitivity numbers on the finite element mesh and smooth the sensitivity numbers for all (fluid, void and solid) elements in the design domain.
8. Average the sensitivity numbers with their values in the previous iteration ($n-1$) numbers and then save the resulting sensitivity numbers for the next iteration.
9. Determine the target structural volume V_{n+1} for the next iteration.
10. Construct a new fluid-structure design by switching design variables x_i from 1 to 0 and from 0 to 1, tracking the update of the fluid-void regions.
11. Remove and/or add the element stiffness matrices from the original uncoupled global matrix \mathbf{K}_g according to the change in the current design.
12. Repeat steps 2-12 until the stop criterion from Equation 3.35 is satisfied.

3.5 Numerical results

In this section two examples are explored to show the capabilities of the BESO method when used for buoyancy module design as described in this work. The parameters and features of the method are discussed. Convergence analysis is carried out for both examples.

3.5.1 Test case

To test the algorithm, a simple square-shaped, buoyant structure is chosen. Figure 3.5 shows the structure floating in a fluid domain. A quarter of the model is discretized with 11664 finite elements, of which 10000 are solid and 1664 fluid. The solid material used is a polymer with Young's modulus $E = 1.25$ KPa and Poisson's ratio $\nu = 0.37$. The pressure P_0 imposed on the fluid domain is an arbitrary value of 1 Pa. The fluid properties are not taken into account in the static analysis when body forces are neglected. Similarly to the previous chapter, when

the pressure is constant all over the fluid domain, the imposed fluid pressure can be chosen arbitrarily resulting in the same structural topology solution.

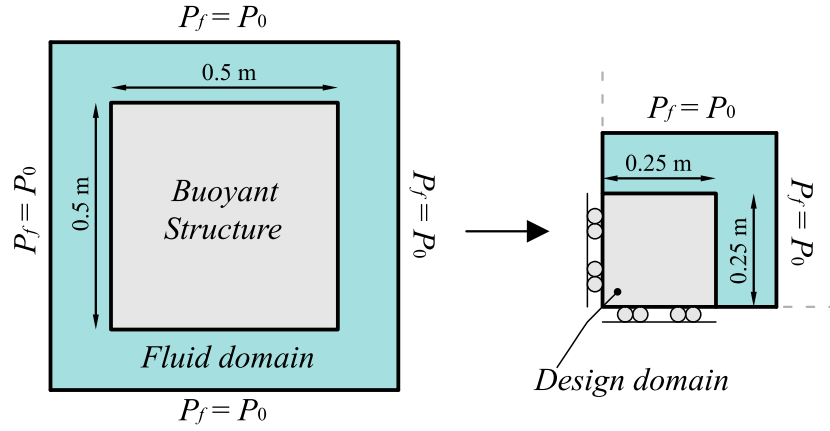


Figure 3.5: Design problem: complete fluid-structure model and the design domain used (a quarter of the model) including boundary conditions.

Because of the buoyant nature of the structure, this type of model behaves differently from those used previously in structural topology optimization (Bendsoe and Sigmund, 2003; Xie and Huang, 2010). A floating structure suffers equal compression in all directions, and if it is completely solid, is therefore in a hydrostatic pressure state with the same stress values all over the structural domain independently of the coordinate system. This also implies that the strain energy term $\frac{1}{2} \mathbf{u}_i^T \mathbf{K}_s^i \mathbf{u}_i$ on α_i is equal for all the elements in a structure with no holes inside. Then, starting from a full design domain, the evolutionary topology optimization method would not work without the derivatives $\mathbf{u}_i^T \mathbf{L}_c^i \mathbf{P}_i$ of the design-dependent pressure loads, otherwise all solid elements would have the same sensitivities. Furthermore, the following expression is also valid for this model of buoyant structures at the initial full solid design:

$$\mathbf{u}_i^T \mathbf{K}_s^i \mathbf{u}_i = \mathbf{u}_i^T \mathbf{L}_c^i \mathbf{P}_i. \quad (3.36)$$

The parameters of the BESO method for the test case design problem are set to $ER = 5\%$, $AR_{max} = 5\%$ and $V_s = 20\%$. The filter radius applied is $r_{min} = 0.015$ m, the penalty factor is chosen to be $p = 1 \cdot 10^4$ and the buoyancy lower limit B_{lim} is set to 0.0331 m^2 , which is equivalent to the area of 5300 elements from the design domain. Figure 3.7 shows snapshots of the evolutionary topology solution until final convergence. Initially, only solid elements at the fluid-structure interface are removed because of the influence of $\mathbf{u}_i^T \mathbf{L}_c^i \mathbf{P}_i$ on the sensitivities. When the buoyancy inequality constraint is active, the penalty factor p gives the elements at the interface a high sensitivity number. Then, holes are created in the structure and the algorithm evolves until convergence is reached. In Figure 3.8, it can be seen that the buoyancy area B decreases in the first iterations until the buoyancy inequality constraint is

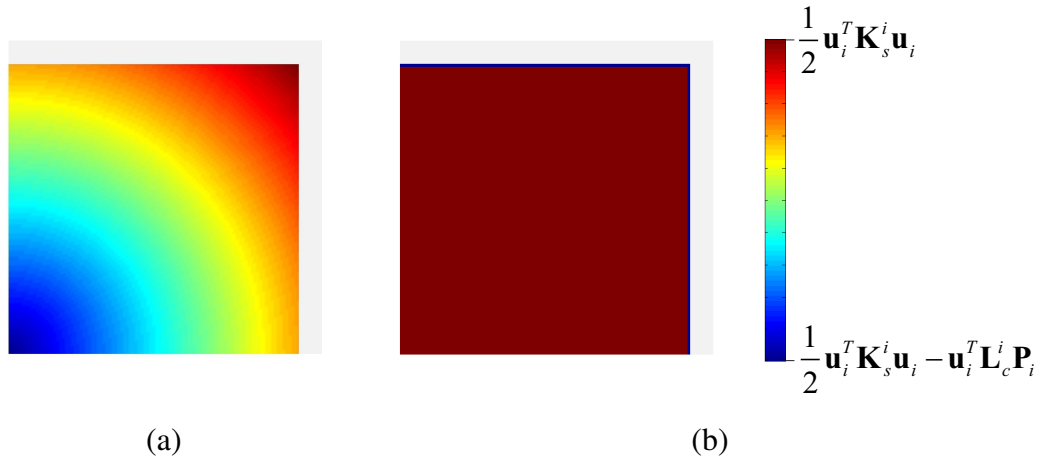


Figure 3.6: (a) Displacement field and (b) sensitivities distribution for the buoyant structure model.

active (iteration 10) and B increases. The same phenomena can be observed in iteration 39, when the inequality constraint is active again. Figure 3.9 shows the evolutionary history for the global mean compliance of the buoyant structure.

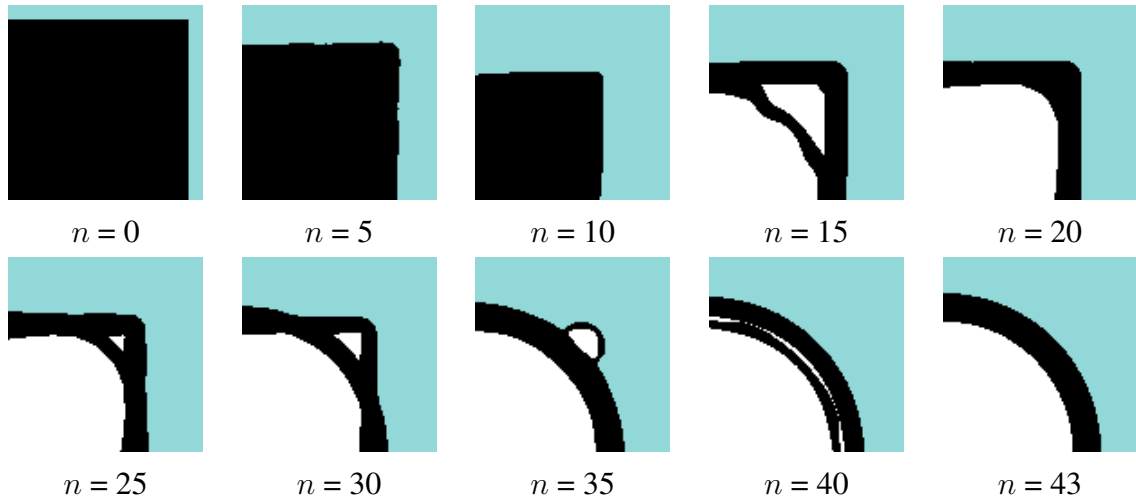


Figure 3.7: Snapshots of the test case solution.

For this simple 2D test case, the final solution obtained is a hollow cylinder. This result is intuitive and is already expected as the optimal buoyant structure with a volume constraint. If one takes the formula for the area A_c of a circle

$$A_c = 4B = \pi r_c^2, \quad (3.37)$$

where r_c is the radius of the circle and the number 4 appears because a quarter of the whole design model is used (see Figure 3.10), one can predict the radius of the optimal structure for

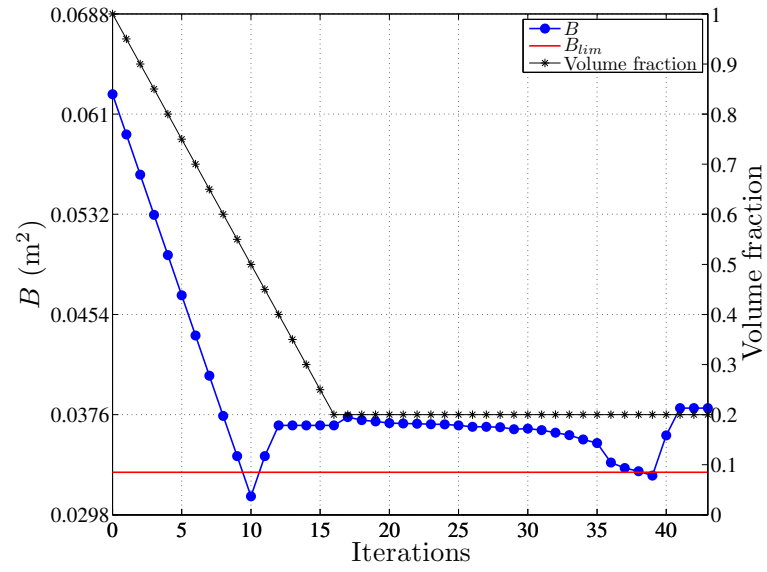


Figure 3.8: Evolutionary history of the buoyancy area B of the buoyant structure.

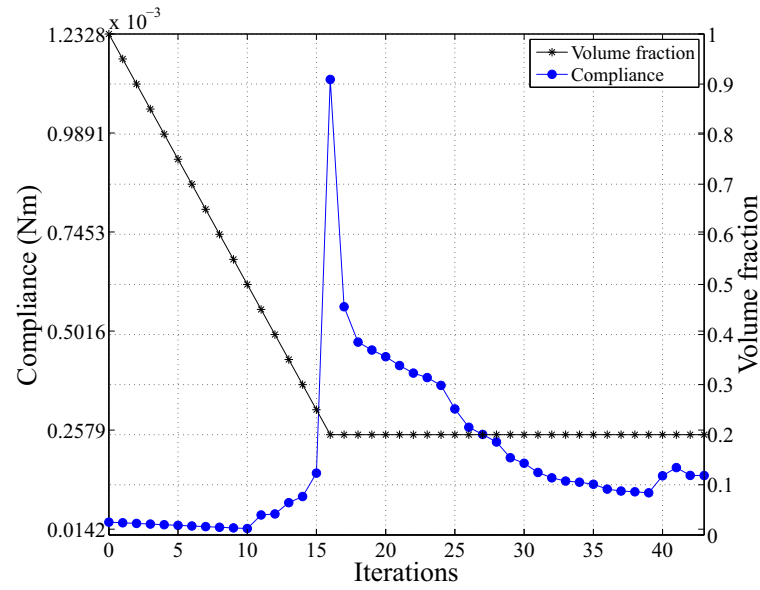


Figure 3.9: Evolutionary history of the global mean compliance of the buoyant structure.

this test case as function of B :

$$r_c = \sqrt{\frac{4B}{\pi}}. \quad (3.38)$$

The formula of a cross-sectional area A_s of a hollow cylinder with an external radius r_c and internal radius r_i can be given as

$$4A_s = \pi (r_c^2 - r_i^2). \quad (3.39)$$

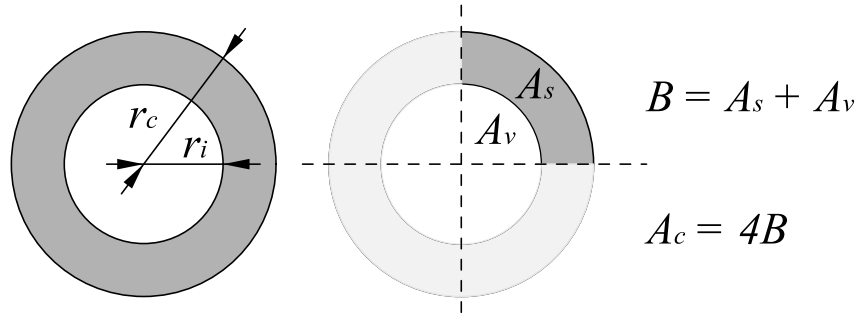


Figure 3.10: Geometric properties of the hollow cylinder associated with the solutions for the test case.

If r_c is substituted and r_i is isolated, one can predict the internal radius for the final optimal hollow cylinder as a function of A_s ,

$$r_i = \sqrt{\frac{4(B - A_s)}{\pi}}, \quad (3.40)$$

and, consequently, the thickness t_s of the hollow cylinder





$$t = r_c - r_i. \quad (3.41)$$

In conclusion, for this simple test case r_c depends on B and r_i is directly determined by V_s , since A_s depends on the final volume of solid material. The results of numerical analysis of the previous equations for different hollow cylinders obtained using the BESO method with different values of B_{lim} are shown in Table 3.1. The differences between the geometrical measurements of the BESO topology solutions and the analytical results of the previous equations are given by the thickness t_s in Table 3.1, which is always smaller than the element size (0.0025). Thus, the numerical BESO solutions agree with the analytical equations, validating the methodology. Problems with greater complexity (as in the next example) can be expected to result in more complex designs.

3.5.2 Subsea buoy design case

As a study case, a subsea buoy design problem is chosen. The buoy is built with two semicircles with an inner and outer radius, and the pipeline is attached to the buoy's inner edge, similarly as shown in Figure 3.11. At higher oil temperatures and deepwater pressures, a pipeline's natural tendency is to relieve its axial stress by buckling. The type of buoyancy

Table 3.1: Dimensions of the hollow cylinders identified as the stiffest buoyant structures using the BESO method with different values of B_{lim} in the buoyancy inequality constraint. Values of the thickness t_s are shown for the geometrical measurements of the topology solutions and the numerical results of Equation 3.41 in the column *BESO* and *Theory*, respectively, as well as the absolute difference between them (column *Diff.*).

Topology	B_{lim} (m ²)	B (m ²)	A_s (m ²)	r_c (m)	r_i (m)	$BESO$	t_s (m) <i>Theory</i>	% <i>Diff.</i>
	0.0288	0.0333	0.0125	0.2050	0.1625	0.0425	0.0431	0.0007
	0.0331	0.0381	0.0125	0.2200	0.1800	0.0400	0.0397	0.0003
	0.0375	0.0429	0.0125	0.2325	0.1975	0.0350	0.0370	0.0020
	0.0419	0.0477	0.0125	0.2450	0.2125	0.0325	0.0347	0.0022

module described here reduces the severity of buckle bending by using buoyancy to decrease the operational submerged weight of the pipeline, especially in long vertical pipelines such as the catenary riser. In some other applications, e.g., when pipelines are installed over subsea soil, the buoyancy module decreases lateral soil-structure friction using the same buoyancy principle.

For this buoyancy-module problem, only one of the two semicircles making up the design is considered. The extended design domain is shown in Figure 3.12. Figure 3.12(a) shows the buoyant structural model immersed in a pressurized fluid domain. Half of the model is discretized with finite elements. The boundary conditions for the finite element model used are shown in Figure 3.12(b); these include a symmetry condition and a blocked degree of freedom which makes the model non-singular. The inner edge (represented by a thick black line) is considered a non-design domain, i.e., it remains as solid material during the whole algorithm. The inner radius should remain fixed as a design requirement. The solid material adopted is a polymer with Young's modulus $E = 1.25$ kPa and Poisson's ratio $\nu = 0.37$. The pressure P_0 imposed on the fluid domain is an arbitrary value of 1 Pa. The fluid properties are not taken into



Figure 3.11: Example of subsea buoy module for oil pipeline support (image extracted from Flotation Technologies[®] website at the url <http://www.flotec.com/products/buckle-migration-buoyancy-modules>, in 18th September, 2013).

account in the static analysis when body forces are neglected.

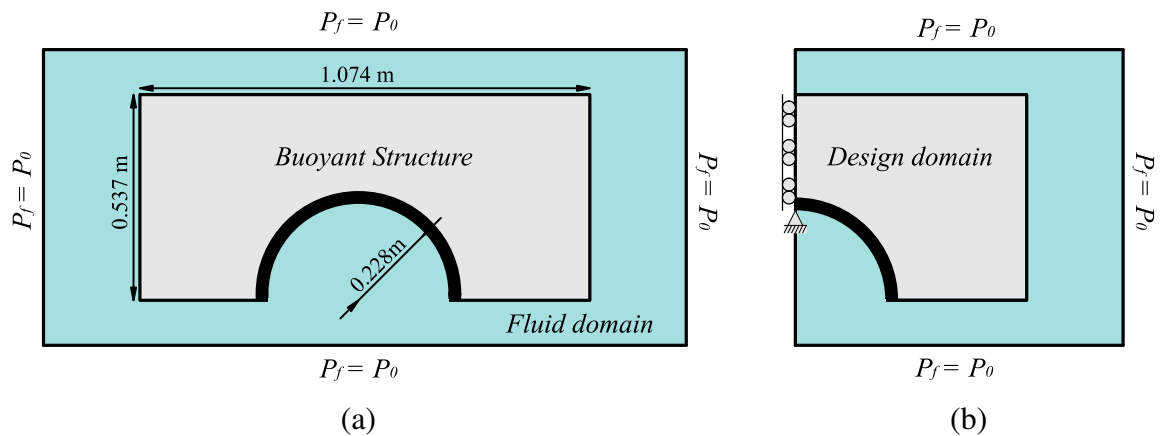


Figure 3.12: Structural optimization design problem: (a) complete fluid-structure model and (b) design domain using half of the model showing the boundary conditions for the structure.

For the design problem shown in Figure 3.12 two initial solutions are considered, one starting from the initial full design and another with an initial semicircle solution covering 75% of the design domain. The whole model is discretized with 51513 finite elements. The evolutionary ratio (ER) is chosen to be 1%, i.e., the volume of solid material decreases 1% in each iteration until it reaches V_s , which is chosen to be 30%. The other parameters of the BESO method are set as, $AR_{max} = 5\%$, $r_{min} = 0.0125$ m and $\tau = 0.001$. Figure 3.13 shows the initial solutions and final topologies for both cases, as well as a comparison case in which the fluid-structure interfaces are kept fixed. The buoyancy area limit B_{lim} is chosen as 0.1485 m², which is equivalent to 80% of the area of the initial semicircle solution in Figure 3.13(b). The penalty factor is chosen as $p = 1 \cdot 10^5$.

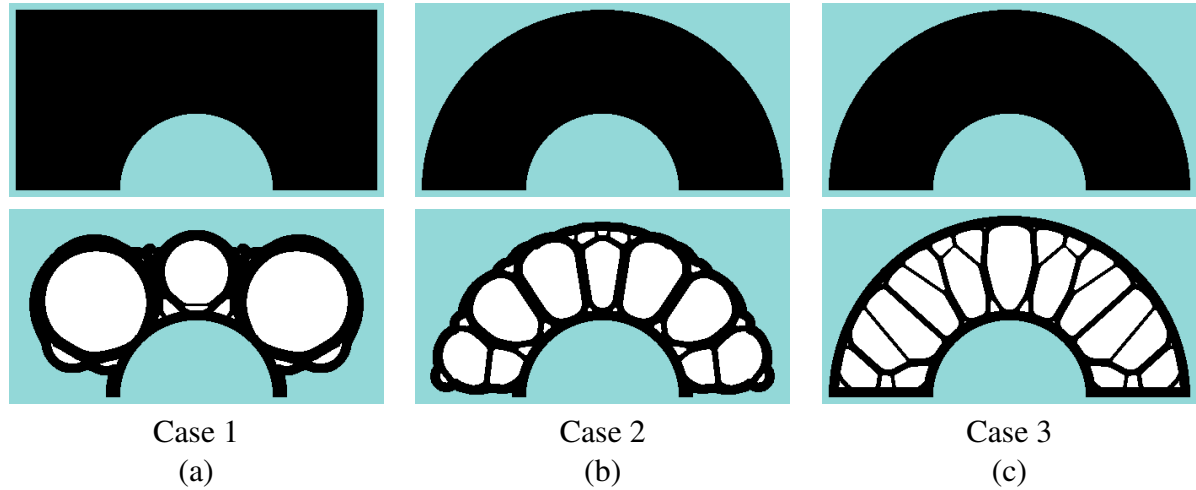


Figure 3.13: Buoy module designs with topology optimization: (a) Case 1 - full design domain and final topology; (b) Case 2 - initial semicircle solution and final topology (design-dependent loads); (c) Case 3 - initial semicircle solution and final topology with fixed fluid-structure interfaces (fixed loads).

It can be seen that the final topologies in Figures 3.13(a) and 3.13(b) mainly cover the areas in the initial guess solutions, indicating that the starting topology has a strong influence on the final solution and suggesting that the designer should choose the initial guess according to some desired final solution. This behavior is expected since the structure is floating. When pressure is applied all over a floating structure that can change its shape and topology, the structure starts to seek an equilibrium state, behaving like bubbles. Indeed, the final results in this work are bubble-like structures. This behavior can be observed in Figure 3.14, which shows snapshots of the solution for Case 2.

Table 3.2 shows some objective function data for all the cases in Figure 3.13. Although it uses the same amount of solid material, the structure in Case 2 is the stiffest and represents an increase in stiffness and reduction in buoyancy area compared with Case 3 of around 39% and less than 13%, respectively. The results for Case 1 were very similar to those for Case 2. Figure 3.15 and 3.16 show the evolutionary history of the buoyancy area and structural mean compliance, respectively, for Case 2. They correlate in each iteration the values of B and C . It can be seen that when the inequality constraint g is active (iterations 16 and 44), the buoyancy area B increases drastically because of the penalty parameter in the sensitivities from Equation 3.31. With sudden structural changes, the mean compliance value presents high oscillations. However, these values are minimized in the following iterations and converge to an almost constant value satisfying the proposed convergence criterion, as seen in Figure 3.16.

The following analyses show the different solutions obtained using different parameter settings and allow the details of the method to be explored. The reference parameters are the

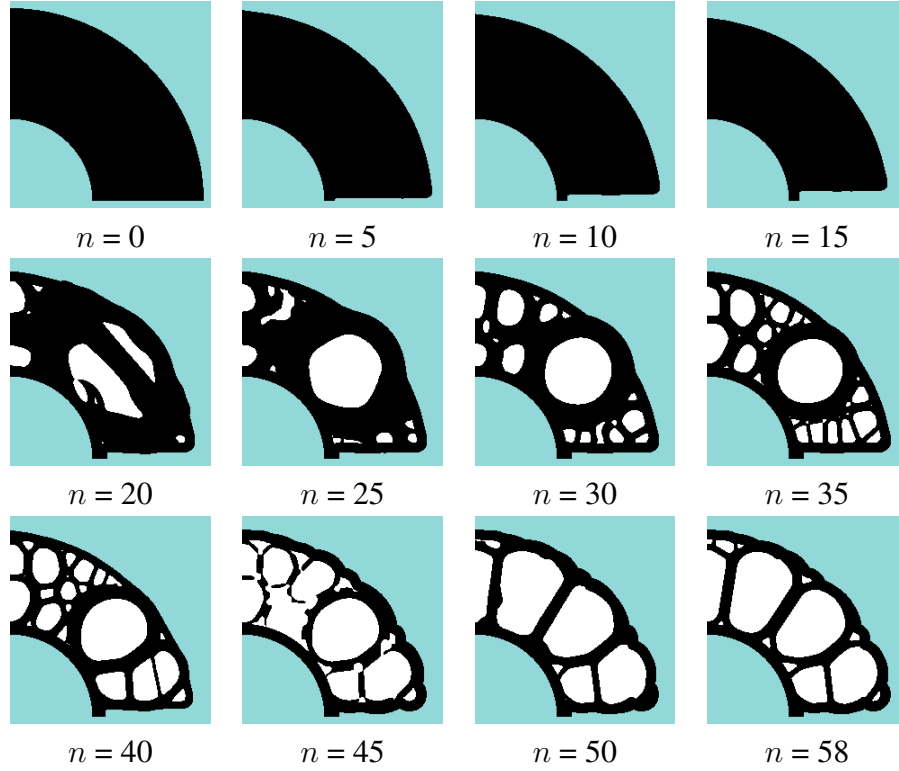


Figure 3.14: Snapshots of the Case 2 solution after different iterations.

Table 3.2: Objective function data for the cases shown in Fig. 3.13.

	Case 1	Case 2	Case 3
V_s	30%	30%	30%
B	0.1622 m ²	0.1628 m ²	0.1856 m ²
Compliance	$4.2429 \cdot 10^{-4}$ Nm	$4.2061 \cdot 10^{-4}$ Nm	$5.8800 \cdot 10^{-4}$ Nm

same from Case 2. Figure 3.17 shows the topologies produced when three different evolutionary ratios are used (1%, 3% and 5%). The numerical results did not vary significantly, and the final solutions differed only in some aspects of their topology, reflecting different local minima.

Another important parameter of the method is the maximum admission ratio AR_{max} , which can limit the amount of added solid elements per iteration. Figure 3.18 presents different solutions obtained with different AR_{max} 's. It was observed that smaller AR_{max} 's led to smaller changes in the fluid-structure boundaries because less solid elements are allowed to be added in these regions per iteration. Higher admission ratios allow more drastic changes in the interface shapes. However, the amount of solid elements is also limited by the filter radius, which extrapolates the highly penalized sensitivities in the interface regions. Thus, the AR_{max} parameter does not affect the solution with a high enough value. As seen in Figure 3.18, the final solution is the same for $AR_{max} = 5\%$ and $AR_{max} = 100\%$, this last being equivalent as not considering the rule of maximum addition ratio.

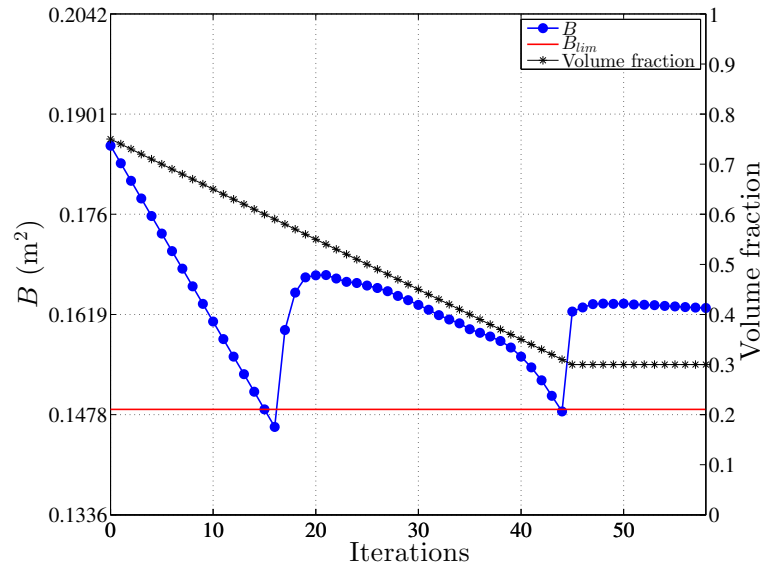


Figure 3.15: Evolutionary history of the buoyancy area for Case 2.

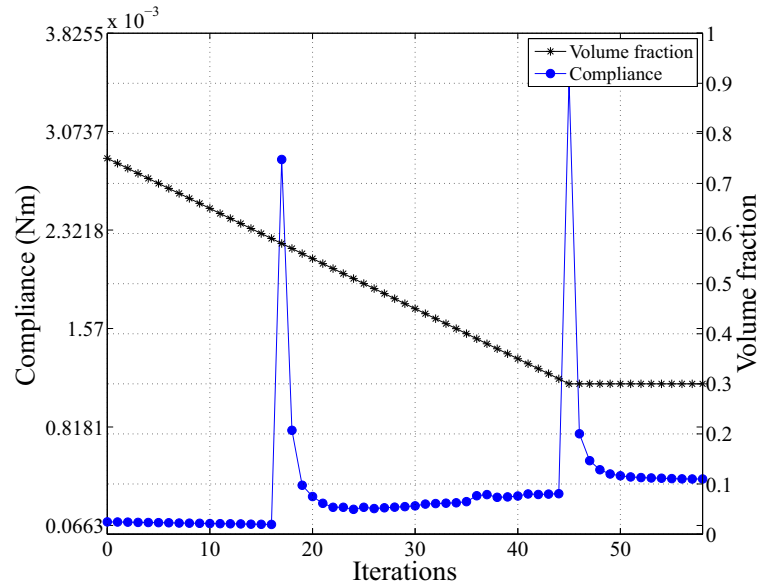


Figure 3.16: Evolutionary history of the mean compliance of the buoy in Case 2.

Figure 3.19 shows the different solutions when the penalty factor p was varied. It can be seen that this variable can exert a considerable influence on the solution. The penalty method seemed to be convergent with p between $1 \cdot 10^7$ and $1 \cdot 10^9$. Smaller penalty factors produced greater variations in the outer shape than higher penalty factors.

The strain energy distributions of the final structures for Case 2 (variable boundary) and Case 3 (fixed boundary) for $p = 1 \cdot 10^5$ are shown in Figure 3.20. Both strain energy distributions are normalized to the maximum strain energy in Case 3 so that the same scale can be used. It

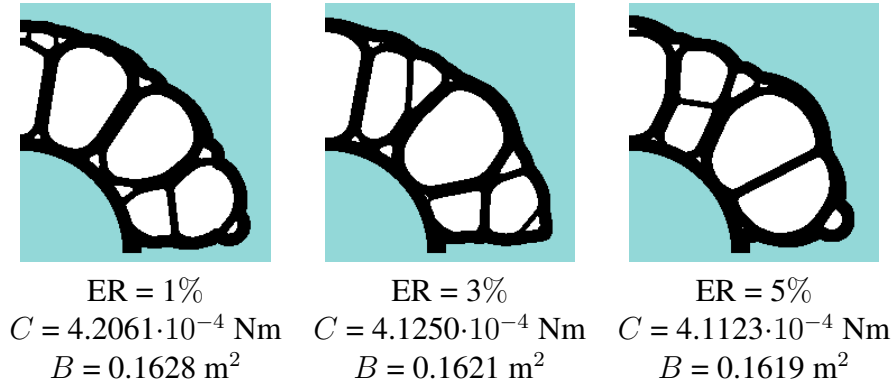


Figure 3.17: Different solutions with different evolutionary ratios.

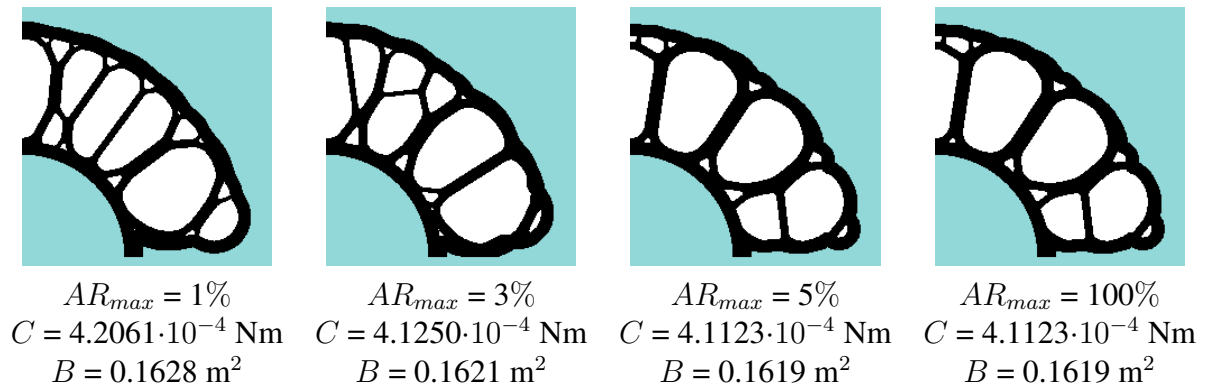
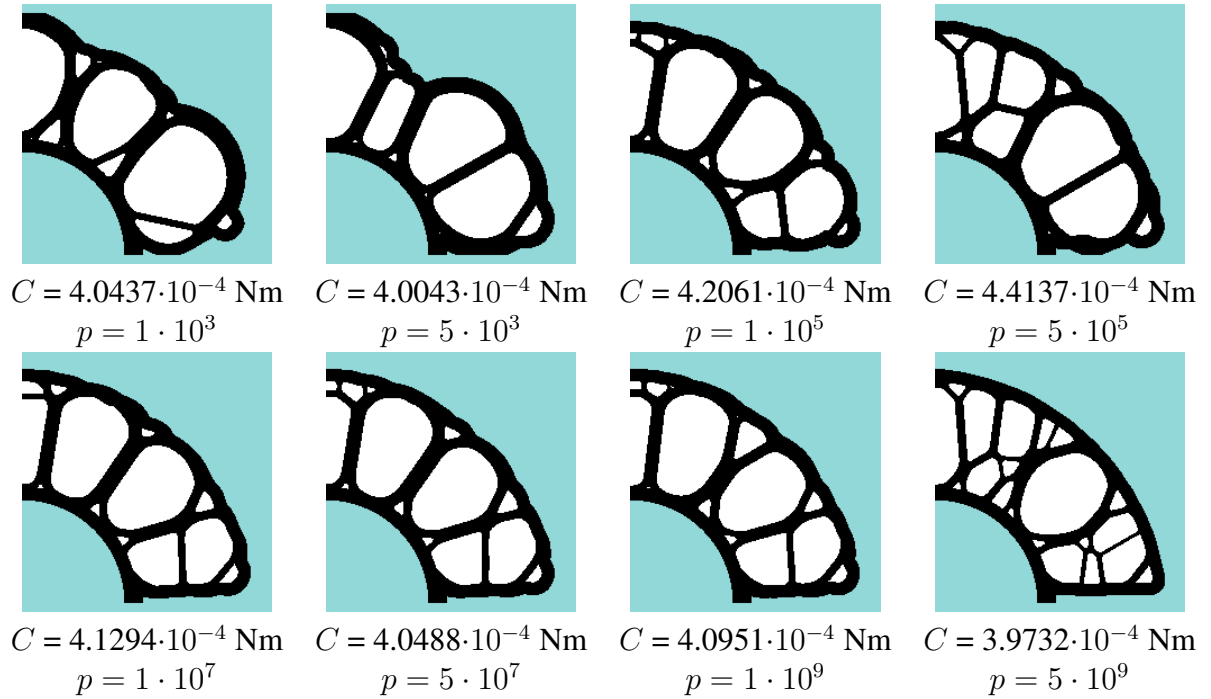


Figure 3.18: Different solutions with different maximum admission ratios.

Figure 3.19: Different solutions with different penalty factors p .

can be observed that for the bubble-like structure (Case 2) the strain energy distribution is much smoother than for Case 3, in which the predominant structural patterns are bars under compression. This result is reflected in the compliance value, which is around 39% smaller for the bubble-like design, as shown in Table 3.2. This justifies the use of the proposed methodology even though the final buoyancy area of the buoy with the variable boundary is smaller than the buoyancy area of the fixed-boundary buoy in this example. One important point worth noticing is that the proposed buoy module can be used in a region where drag forces are negligible, i.e., where the loads produced by subsea fluid flows are much smaller than the deepwater pressure loads. Because its external shape is similar to that of the buoy in Case 3, this solution may also be suitable for use in regions where drag forces are quite high. However, in cases where the solution looks like Case 1, i.e., the buoy has a significantly different shape, further analysis may be needed.

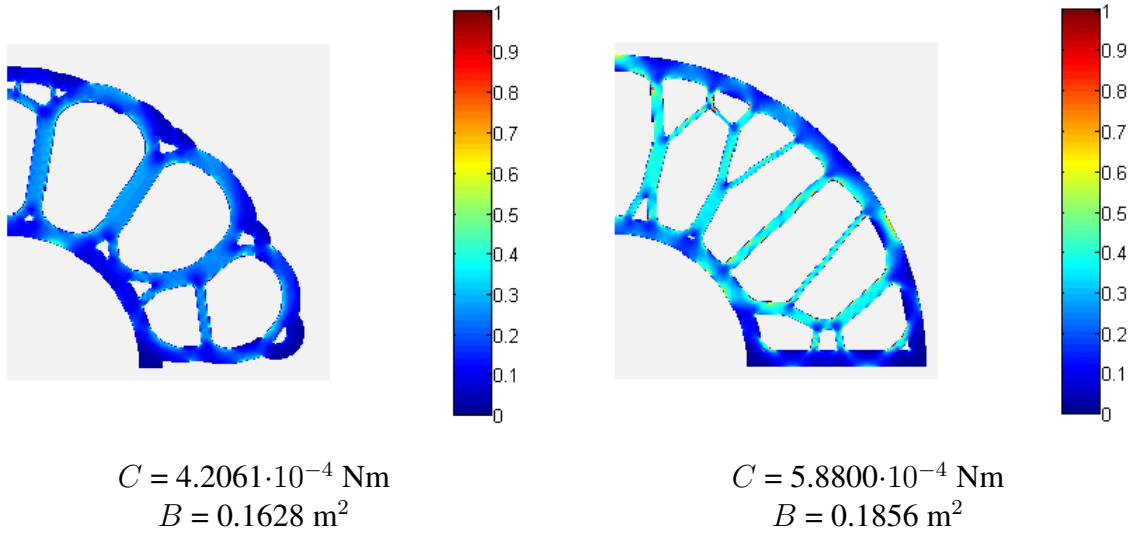


Figure 3.20: Normalized strain energy distribution for the buoyancy module designed with the proposed methodology using $p = 1 \cdot 10^5$ and variable and fixed boundaries.

3.6 Conclusions

This work proposes the use of topology optimization to identify alternative structural designs in offshore engineering. The specific case of fully submerged buoyancy modules under constant underwater pressure loads is considered. The extended BESO method proposed by Picelli *et al.* (2015b) is used to directly circumvent the known issues in topology optimization of design-dependent pressure loading problems. The discrete nature of the evolutionary procedures allows the switch between solids, fluids and voids with explicitly defined fluid-structure interfaces. Thus, no parametrization schemes are needed to model the pressure surfaces. A new inequality constraint is used to guarantee minimum required buoyancy effects, measured by

the volume of the displaced fluid. It was shown that with a penalty factor, the evolutionary optimization problem could handle a different constraint rather than only the standard volume one. The final topologies were bubble-like structures, results that confirm the effectiveness of the proposed methodology. The parameters of the method were discussed. Comparison of the results with a case in which the pressure loads are fixed showed that a stiffer structure could be designed by moving the fluid-structure interfaces and fulfilling the buoyancy requirements simultaneously. If other types of forces are negligible, e.g., viscous flow loads, the proposed solutions can be used as a starting point for the design of new deepwater buoyancy modules to support oil pipelines. Further improvements can be carried out, such as the consideration of non constant pressure fields or buckling constraints.

4 NATURAL FREQUENCY MAXIMIZATION OF ACOUSTIC-STRUCTURE INTERACTION SYSTEMS

Context

Attempts have been made to maximize natural frequencies of structures using topology optimization, however, generally with no multiphysics analysis. This work investigates the influence of acoustic fluids on the vibration modes of a coupled acoustic-structure interaction system and how the natural frequencies of the structures in these systems can be maximized. The dynamic acoustic-structure interaction model (using *Fluid 2* mentioned in Chapter 1) and the same extended BESO fluid-structure update scheme by Picelli *et al.* (2015b) have been applied in this work. This contribution has been published in *Finite Elements in Analysis and Design* (Picelli *et al.*, 2015d).

4.1 Introduction

Structural Topology Optimization method for continuum structures (Bendsoe and Sigmund, 2003; Xie and Huang, 2010) has gained in popularity and now is used daily as a design tool in industry and academy. The basic idea is to find an optimal distribution of material in a structural design domain considering an objective function and constraints. Commercial topology optimization tools have been developed based on special Finite Element Method (FEM) solvers or have been added in standard commercial packages, many of them concerning stiffness or natural frequencies maximization.

Although the optimization procedures have reached a satisfactory level of maturity, many topics are still open to research. An important group consists of multiphysics problems. Commercial FEM packages often contain solvers for multiphysics problems, however they do not enable optimization.

Through the last 10 years, the methods of topology optimization have been under a considerable scientific effort to be extended to different physical phenomena problems. One may cite aerolastic structures (Maute and Allen, 2004), acoustics design (Duhring *et al.*, 2008; Silva and Pavanello, 2010; Yoon, 2013), thermo-elastic stresses (Gao *et al.*, 2008), fluid flows (Aage *et al.*, 2008) and fluid-structure interaction (Kreissl *et al.*, 2010; Yoon, 2010; Andreasen and Sigmund, 2013), acoustic-structure responses (Yoon *et al.*, 2007; Shu *et al.*, 2014; Vicente *et al.*, 2015), multiscale analysis (Xie *et al.*, 2012; Xia and Breitkopf, 2014) and others.

The presented work aims to contribute in the design of multiphysics systems, more specifically in acoustic-structure interaction design problems. Yoon *et al.* (2007) proposed a mixed element formulation to model acoustic-structure responses. The method approximated both acoustic and solid domains in an overlapped mixed model, allowing the solid isotropic material with penalization (SIMP) technique to be applied. Vicente *et al.* (2015) developed a new sensitivity analysis for the bi-directional evolutionary structural optimization (BESO) method for frequency responses minimization of acoustic-structure systems. The authors considered the minimization of pressures and displacements under harmonic loads. Differently from Yoon *et al.* (2007) and Vicente *et al.* (2015), herein no loads are applied and free vibration of coupled acoustic-structure systems is considered for eigenvalues maximization. The fluid and solid fields considered here are modelled with the classic finite element formulation from Zienkiewicz and Bettess (1978), currently and widely used in commercial codes. In the coupled eigenproblem both acoustic and structural fields strongly influence the vibration modes of the system in all directions since no harmonic excitation is applied. This type of modal analysis has been explored in topology optimization for purely structural analysis (Pedersen, 2000; Jensen and Pedersen, 2006; Huang *et al.*, 2010; Du and Olhoff, 2007b), but not for free vibration of acoustic-structure problems using the classic formulation.

In order to allow the switch between solid, fluid and void elements, the BESO method is applied. The discrete update scheme of the evolutionary methods allow the use of separate and different governing equations during the optimization problems, such as proposed by Picelli *et al.* (2015b). This overcomes a well known challenge of the classic density based methods in dealing with moving multiphysics loads and interfaces (Sigmund and Clausen, 2007; Lee and Martins, 2012). Thus, in the context of multiphysics optimization, the BESO method presents some potential applications specially considering classic formulations, which can be advantageous for the combination of commercial FEM packages and the optimization codes.

The technique called Evolutionary Structural Optimization (ESO) was first introduced in the 90's by Xie and Steven (1993). The ESO method was initially proposed as a gradual removal of inefficient material from the design domain until the remaining structure converges to the optimum topology. Material elimination is done after a sensitivity analysis. A later development of this method was called Bi-directional ESO (BESO), in which elements are also added in void positions near to the elements with the highest sensitivity numbers (Querín and Steven, 1998). In the evolutionary optimization methods, the elemental sensitivity number is a local index and represents the sensitivity of the objective function when the element is added or removed. Papers considering the BESO method have presented convergent and mesh independent solutions (Huang and Xie, 2007), natural frequencies constraints (Huang *et al.*, 2010) and others. Recently, Sigmund and Maute (2013) and Deaton and Grandhi (2014) have cited the evolutionary methods as one class of the main structural topology optimization methods.

The chapter is organized as follows: Section 4.2 presents the governing equations and the finite element model for the acoustic-structure coupled system. In Section 4.3, the topology optimization problem for free vibration is formulated and the sensitivity analysis is carried out. Details of the method are also described. Section 4.4 shows the numerical results achieved with the proposed methodology. Finally, conclusions are drawn in Section 4.5.

4.2 Acoustic-structure interaction: governing equations and finite element model

Herein, the analyzed systems are limited to free vibration of flexible structures in contact with acoustic fluids. For this system, the structure can be described by the differential equation of motion for a continuum body assuming small deformations and the fluid by the acoustic wave equation. All the details of this formulation can be found in the article by Zienkiewicz and Bettess (1978) or in reference books (Morand and Ohayon, 1995; Axisa and Antunes, 2007). The governing equations for the fluid and structural domains as well as the coupling boundary conditions are defined as follows.

4.2.1 Acoustic domain

In this work, the fluid is considered inviscid, irrotational and only under small translation conditions. The governing equation for the pressure field in a homogeneous acoustic fluid medium can be described by the acoustic wave equation

$$\frac{1}{c_f^2} \frac{\partial^2 P_f}{\partial t^2} - \nabla^2 P_f = 0 \quad \text{in } \Omega_f, \quad (4.1)$$

where P_f is the acoustic pressure and c_f is the speed of sound in the acoustic domain Ω_f . The following boundary conditions are considered:

$$P_f = 0 \quad \text{on } S_p, \quad (4.2)$$

and,

$$\nabla P_f \cdot \mathbf{n}_f = 0 \quad \text{on } S_f. \quad (4.3)$$

Equation 4.2 represents the pressure Dirichlet boundary condition applied on the boundary S_p , where $P_f = 0$ in all the examples considered in this work. When $P_f = 0$, the boundary S_p is considered to be as a free open surface, while Equation 4.3 represents the hard wall natural

boundary condition applied on S_f , which can be considered as a closed surface (Zienkiewicz and Bettess, 1978). Figure 4.1 illustrates the acoustic-structure interaction system used in this work.

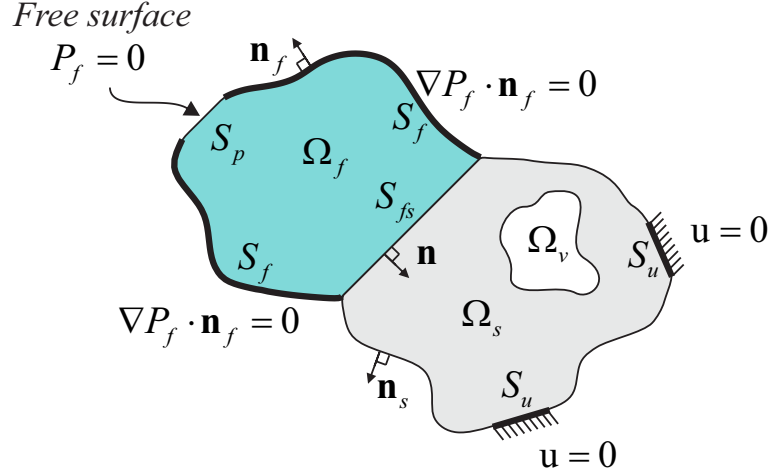


Figure 4.1: The coupled acoustic-structure system: the acoustic fluid domain Ω_f and the structural domain Ω_s coupled by integrals on the acoustic-structure interface S_{fs} .

4.2.2 Structural domain

It is considered the equilibrium of a linearly elastic structure in the domain Ω_s . The solid domain is governed by the equilibrium equation

$$\nabla \cdot \boldsymbol{\sigma}_s(\mathbf{u}) - \rho_s \frac{\partial^2 \mathbf{u}}{\partial t^2} = 0 \quad \text{in } \Omega_s, \quad (4.4)$$

where $\nabla \cdot \boldsymbol{\sigma}_s(\mathbf{u})$ is the divergence of the Cauchy stress tensor, ρ_s is the structural mass density and \mathbf{u} is the structural displacement vector field. Dirichlet boundary conditions are applied as follows:

$$\mathbf{u} = 0 \quad \text{on } S_u. \quad (4.5)$$

Body forces are not considered in this work.

4.2.3 Discretized coupled acoustic-structure system

At the interface S_{fs} between the structural and fluid domains, the fluid and the structure move together in the normal direction of the boundary. The normal vector $\mathbf{n} = \mathbf{n}_f = -\mathbf{n}_s$ (see

Figure 4.1) can be used in order to guarantee the equilibrium condition between fluid pressures and structural tractions on S_{fs}

$$\boldsymbol{\sigma}_s \mathbf{n}_s = P_f \mathbf{n}_f \quad \text{on } S_{fs}. \quad (4.6)$$

With relations derived from the governing equations and the previous coupling conditions, the interface forces may be obtained. Using a finite element discretization, the force acting on the structure provided by the acoustic fluid pressure is

$$\mathbf{f}_{fs} = \int_{S_{fs}} \mathbf{N}_s^T \mathbf{n} \mathbf{N}_f dS_{fs} \mathbf{P}_f, \quad (4.7)$$

and the excitation acting on the fluid domain can be expressed in terms of the structural acceleration

$$\mathbf{f}_{sf} = -\rho_f \int_{S_{fs}} \mathbf{N}_f^T \mathbf{n} \mathbf{N}_s dS_{fs} \ddot{\mathbf{u}}_s, \quad (4.8)$$

where \mathbf{P}_f is the vector of nodal pressure in the finite element model, ρ_f is the mass density of the fluid, \mathbf{u}_s is the vector of nodal structural displacements and \mathbf{N}_s and \mathbf{N}_f contain the finite element shape functions for structural and fluid elements.

The introduction of a spatial coupling matrix \mathbf{L}_{fs} , where

$$\mathbf{L}_{fs} = \int_{S_{fs}} \mathbf{N}_s^T \mathbf{n} \mathbf{N}_f dS_{fs}, \quad (4.9)$$

allows the coupling forces to be written as

$$\mathbf{f}_{fs} = \mathbf{L}_{fs} \mathbf{P}_f, \quad (4.10)$$

and

$$\mathbf{f}_{sf} = -\rho_f \mathbf{L}_{fs}^T \ddot{\mathbf{u}}_s, \quad (4.11)$$

where \mathbf{f}_{fs} and \mathbf{f}_{sf} are the nodal force vectors on the interfaces.

Thus, the acoustic-structure problem can be described by an unsymmetrical system of equations (Morand and Ohayon, 1995)

$$\begin{bmatrix} \mathbf{M}_s & \mathbf{0} \\ \rho_f \mathbf{L}_{fs}^T & \mathbf{M}_f \end{bmatrix} \begin{bmatrix} \ddot{\mathbf{u}}_s \\ \ddot{\mathbf{P}}_f \end{bmatrix} + \begin{bmatrix} \mathbf{K}_s & -\mathbf{L}_{fs} \\ \mathbf{0} & \mathbf{K}_f \end{bmatrix} \begin{bmatrix} \mathbf{u}_s \\ \mathbf{P}_f \end{bmatrix} = \begin{bmatrix} \mathbf{0} \\ \mathbf{0} \end{bmatrix}, \quad (4.12)$$

where \mathbf{M}_s and \mathbf{K}_s are the structural mass and stiffness matrices, respectively, and \mathbf{M}_f and \mathbf{K}_f

are the fluid mass and stiffness matrices, respectively, expressed as

$$\mathbf{K}_s = \int_{\Omega_e} (\nabla \mathbf{N}_s)^T \mathbf{D}_s \nabla \mathbf{N}_s d\Omega_e, \quad (4.13)$$

$$\mathbf{M}_s = \rho_s \int_{\Omega_e} \mathbf{N}_s^T \mathbf{N}_s d\Omega_e, \quad (4.14)$$

$$\mathbf{K}_f = \int_{\Omega_e} (\nabla \mathbf{N}_f)^T \nabla \mathbf{N}_f d\Omega_e, \quad (4.15)$$

$$\mathbf{M}_f = \frac{1}{c_f^2} \int_{\Omega_e} \mathbf{N}_f^T \mathbf{N}_f d\Omega_e, \quad (4.16)$$

where \mathbf{D}_s is the elasticity matrix. This formulation is equivalent to the dynamic acoustic-structure interaction model described in terms of structural displacements and fluid pressures (\mathbf{u}_s/P_f) by Zienkiewicz and Bettess (1978); Morand and Ohayon (1995); Axisa and Antunes (2007). Compactly,

$$[\mathbf{M}_{fs}] [\ddot{\mathbf{u}}_{fs}] + [\mathbf{K}_{fs}] [\mathbf{u}_{fs}] = [\mathbf{f}_{fs}], \quad (4.17)$$

where \mathbf{M}_{fs} and \mathbf{K}_{fs} are the acoustic-structure mass and stiffness matrix, respectively. These matrices comprise the structural and fluid matrices, represented by the subscript s for the structural field and f for the acoustic field.

4.3 Evolutionary topology optimization for free vibration problems including acoustic-structure interaction

In this section the optimization problem is formulated, the sensitivity analysis is derived and the evolutionary procedure is described.

In the evolutionary topology optimization methods for structural problems, the design variable, x_i , is restricted to discrete values 1 or 0 (0 for hard-kill or x_{min} for the soft-kill procedure), which corresponds to solid and void elements, respectively. Then, no intermediate density elements are allowed during the optimization procedures (Xie and Huang, 2010). Herein, the extended BESO method can substitute the solid elements by fluid or void ones (Picelli *et al.*, 2015b; Vicente *et al.*, 2015). With no intermediate densities, solid, void and fluid regions as well as the interface between the domains are explicitly defined.

4.3.1 Problem statement

In free vibration analysis the following eigenproblem is solved to describe the dynamic behavior of an acoustic-structural system:

$$(\mathbf{K}_{fs} - \omega_k^2 \mathbf{M}_{fs}) \Phi_k = 0, \quad (4.18)$$

where ω_k is the k th natural frequency and Φ_k is the corresponding coupled eigenmode.

Premultiplying Equation 4.18 with the transposed eigenvector, Φ_k^T , the eigenvalue ω_k^2 can be related with Φ_k by

$$\omega_k^2 = \frac{\Phi_k^T \mathbf{K}_{fs} \Phi_k}{\Phi_k^T \mathbf{M}_{fs} \Phi_k}, \quad (4.19)$$

which is called the Rayleigh quotient.

For natural frequencies maximization of the described acoustic-structure system, the discrete optimization problem can be defined as

$$\begin{aligned} \min: \quad & \omega_k^2, \\ & x_i \\ \text{subject to:} \quad & (\mathbf{K}_{fs} - \omega_k^2 \mathbf{M}_{fs}) \Phi_k = 0 \text{ and b.c.,} \\ & V(x_i) / V_0 = V_s, \\ & x_i = [x_{min}, 1], \end{aligned} \quad (4.20)$$

where V_0 is the full design domain volume, V_s is the prescribed final solid volume fraction and nel is the number of elements inside the design domain. The binary design variable x_i declares the presence of a completely solid element (1) or a void element with a small value of x_{min} (e.g. 10^{-4}). In dynamic cases, the soft-kill procedure is adopted for the evolutionary methods in order to avoid localized vibration modes, according to Huang *et al.* (2010). Herein, some of the voids elements are substituted by fluid ones, tracking the changes of the fluid-structure interfaces during the optimization. It is important to point out that all void elements in the design domain are set as $x_{min} = 10^{-4}$, even when a fluid is placed in the same position. Thus, a small region of the design domain presents overlapped fluid and void (soft) elements.

4.3.2 Sensitivity analysis

Considering that maximizing ω_k^2 is the same as maximizing ω_k , the sensitivity of the objective function due to a structure element removal can be obtained by deriving ω_k with

respect to the design variables,

$$\frac{\partial \omega_k}{\partial x_i} = \frac{1}{2\omega_k \Phi_k^T \mathbf{M}_{fs} \Phi_k} \left[2 \frac{\partial \Phi_k^T}{\partial x_i} (\mathbf{K}_{fs} - \omega_k^2 \mathbf{M}_{fs}) \Phi_k + \Phi_k^T \left(\frac{\partial \mathbf{K}_{fs}}{\partial x_i} - \omega_k^2 \frac{\partial \mathbf{M}_{fs}}{\partial x_i} \right) \Phi_k \right]. \quad (4.21)$$

With the aid of Equation 4.18, the derivative may be simplified as

$$\frac{\partial \omega_k}{\partial x_i} = \frac{1}{2\omega_k \Phi_k^T \mathbf{M}_{fs} \Phi_k} \left[\Phi_k^T \left(\frac{\partial \mathbf{K}_{fs}}{\partial x_i} - \omega_k^2 \frac{\partial \mathbf{M}_{fs}}{\partial x_i} \right) \Phi_k \right]. \quad (4.22)$$

In order to evaluate the derivatives of the acoustic-structure mass and stiffness matrices, a material model can be chosen. For the soft-kill BESO method developed by Huang and Xie (2009), to keep the ratio between mass and stiffness constant when $x_i = x_{min}$ it is required that

$$\begin{aligned} \rho(x_{min}) &= x_{min} \rho_s, \\ E(x_{min}) &= x_{min} E_s, \end{aligned} \quad (4.23)$$

where ρ_s and E_s are the density and Young's modulus of the solid material, respectively. To guarantee the previous condition the material interpolation scheme can be applied as follows

$$\begin{aligned} \rho(x_{min}) &= x_i \rho_s \\ E(x_i) &= \left[\frac{x_{min} - x_i^p}{1 - x_{min}^p} (1 - x_i^p) + x_i^p \right] E_s, \end{aligned} \quad (4.24)$$

where $(0 < x_{min} \leq x_i \leq 1)$ and p is a penalization factor.

Neglecting the alteration in \mathbf{M}_f , \mathbf{K}_f and \mathbf{L}_{fs} due to the i th solid element removal, the derivatives of the global acoustic-structure mass and stiffness matrices may be evaluated by

$$\frac{\partial \mathbf{M}_{fs}}{\partial x_i} = \mathbf{M}_i^s, \quad (4.25)$$

$$\frac{\partial \mathbf{K}_{fs}}{\partial x_i} = \frac{1 - x_{min}}{1 - x_{min}^p} p x_i^{p-1} \mathbf{K}_i^s, \quad (4.26)$$

where \mathbf{M}_i^s and \mathbf{K}_i^s are the mass and stiffness matrices of the i th solid element, respectively.

With the derivatives of \mathbf{K}_{fs} and \mathbf{M}_{fs} from Equations 4.25 and 4.26 and considering that the eigenvector is mass-normalized ($\Phi_k^T \mathbf{M}_{fs} \Phi_k = 1$), the sensitivity for the k th natural frequency is

$$\frac{\partial \omega_k}{\partial x_i} = \frac{1}{2\omega_k} \Phi_k^T \left(\frac{1 - x_{min}}{1 - x_{min}^p} p x_i^{p-1} \mathbf{K}_i^s - \omega_k^2 \mathbf{M}_i^s \right) \Phi_k. \quad (4.27)$$

For the solid-fluid-void design, the sensitivity numbers α_i for natural frequency maximization can be expressed as

$$\alpha_i = \begin{cases} \frac{1}{2\omega_k} \Phi_k^T \left(\frac{1-x_{\min}}{1-x_{\min}^p} \mathbf{K}_i^s - \frac{\omega_k^2}{p} \mathbf{M}_i^s \right) \Phi_k & x_i = 1 \\ \frac{1}{2\omega_k} \Phi_k^T \left(\frac{x_{\min}^{p-1}-x_{\min}^p}{1-x_{\min}^p} \mathbf{K}_i^s - \frac{\omega_k^2}{p} \mathbf{M}_i^s \right) \Phi_k & x_i = x_{\min} \end{cases}, \quad (4.28)$$

or when x_{\min} tends to 0

$$\alpha_i = \begin{cases} \frac{1}{2\omega_k} \Phi_k^T \left(\mathbf{K}_i^s - \frac{\omega_k^2}{p} \mathbf{M}_i^s \right) \Phi_k & x_i = 1 \\ -\frac{\omega_k}{2p} \Phi_k^T \mathbf{M}_i^s \Phi_k & x_i = x_{\min} \end{cases}. \quad (4.29)$$

Sometimes, cases with multiple frequencies optimization might be considered, e.g., both ω_k and ω_{k+1} maximization, where the objective function is the sum of ω_k and ω_{k+1} . For this case, we can mention that the sensitivity numbers are evaluated by the mean value of the sensitivities of both k and $k+1$ considered eigenmodes, as shown by Xie and Steven (1996) and Zuo *et al.* (2010).

4.3.3 Summary of the evolutionary procedure

The main steps of the extended fluid-structure BESO methodology are given as follows:

1. Discretize the design domain using a finite element (FE) mesh for the given boundary conditions. Initially, the global acoustic-structure mass, \mathbf{M}_{fs} , and stiffness, \mathbf{K}_{fs} , matrices must be assembled uncoupled assuming that all the degrees of freedom can alternate between displacement and pressure.
2. Couple and store current design matrices \mathbf{M}_n and \mathbf{K}_n with the coupling matrices according to the current design of the n th iteration and the appropriate boundary conditions. Thus, the current matrices become equivalent to the acoustic-structure matrices from Equation 4.12.
3. Perform FE analysis (solve Equation 4.18) on the current design to obtain the eigenvalues, ω_k^2 , and the coupled eigenmodes, Φ_k .
4. Evaluate the sensitivity numbers α_i according to Equation 4.28.
5. Apply a filter scheme. Evaluate nodal sensitivity numbers α_j by averaging the elemental sensitivity numbers of the j th connected elements. Project a sub-domain Ψ_i with length scale equal to the filter radius r_{\min} and centered in the i th element. All the nodes inside

Ψ_i must have their nodal sensitivity numbers averaged back to the i th elemental level as follows:

$$\alpha_i = \sum_{j=1}^{nod} w(r_{ij}) \alpha_j / \sum_{j=1}^{nod} w(r_{ij}), \quad (4.30)$$

where r_{ij} is the distance between the node j and the center of the element i , nod is the total number of nodes inside the design domain and $w(r_{ij})$ is a weight factor that values $r_{min} - r_{ij}$ for nodes inside the sub-domain Ψ_i and 0 for nodes outside the sub-domain.

6. Average the sensitivity numbers with their previous iteration $(n - 1)$ numbers as follows

$$\alpha_i = \frac{\alpha_i^n + \alpha_i^{n-1}}{2} \quad (4.31)$$

where n is the current iteration number. Huang and Xie (2007) have showed that this averaging helps in the stabilization of the optimization process. This procedure demonstrated to be an effective way to avoid convergence problems.

7. Determine the target structural volume V_{n+1} for the next iteration $n+1$. The target volume V_{n+1} is defined as

$$V_{n+1} = V_n(1 \pm ER) \quad (4.32)$$

where ER is the evolutionary ratio. ER is the percentage of V_0 and increases or decreases V_{n+1} towards the final prescribed structural volume fraction V_s .

8. Update the design variables. The target volume V_{n+1} sets the threshold α_{th} of the sensitivity numbers. Solid elements ($x_i = 1$) which

$$\alpha_i \leq \alpha_{th} \quad (4.33)$$

are switched to void condition ($x_i = x_{min}$). Void elements ($x_i = x_{min}$) are switched to solid condition ($x_i = 1$) when

$$\alpha_i > \alpha_{th} \quad (4.34)$$

Meanwhile, the volume addition ratio (AR) is restricted to a maximum addition ratio AR_{max} , which declares the maximum allowable addition volume per iteration. Once $AR > AR_{max}$, only some of the elements with highest sensitivity numbers are switched to $x_i = 1$ in order to set $AR = AR_{max}$. Then, some of the elements with the lowest sensitivity numbers are switched to $x_i = x_{min}$ to satisfy the target volume V_{n+1} . Each target volume defines the percentage of solid elements that the structure must have in the iteration $n + 1$.

9. Update the fluid region considering the elements with design variable $x_i = x_{min}$. If the void element has at least one fluid element as neighbor, it must be turned also into a fluid

element. If the element does not have any fluid neighbors, the element must be kept as void. This procedure is repeated until there are no more changes in the fluid-void regions. In this case, some layers of structural elements nearby the fluid-structure interface can be replaced by fluid elements and void holes appear only inside the structural domain.

10. Update the original uncoupled global matrices \mathbf{K}_{fs} and \mathbf{K}_{fs} according to the change of the current design.
11. Repeat steps 2-11 until the prescribed structural volume fraction is achieved and the convergence criterion with a predefined tolerance τ is satisfied. The variation in the objective function is calculated as

$$\frac{|\sum_{m=1}^3 C_{n-m+1} - \sum_{m=1}^3 C_{n-m-2}|}{\sum_{i=1}^3 C_{n-m+1}} \leq \tau \quad (4.35)$$

where n is the current iteration number and C is the value of the objective natural frequency ω_k or $\omega_k + \omega_{k+1}$ for multiple natural frequencies objectives. This equation estimates the change in the objective function during the last 6 iterations of the algorithm.

More details about implementation issues (e.g. filter scheme, element removal/addition and convergence criterion) can be found in Xie and Huang (2010); Huang and Xie (2007).

4.4 Numerical results

In this section, some optimization problems are solved with the extended BESO method. The first example considers a clamped beam vibrating between two acoustic fluid domains and it is used as a comparison to the literature. The second example proposes the optimization of a tunable resonant device, in which open and closed fluid cavities are used. The last example considers the maximization of the first two natural frequencies of a water dam model.

4.4.1 Beam example

The first example considers a clamped beam between two acoustic fluid domains. The unitary thickness coupled model (showed in Figure 4.2) is under free vibration and plane stress condition. This example is similar to the one presented by Yoon *et al.* (2007). Herein, the solid Young's modulus used is 70 GPa, the density is 2700 kg/m³ and the Poisson's ratio is 0.3. The fluid domain has density of 1000 kg/m³ and the speed of sound in the medium of 1450 m/s. An amount of 90000 finite elements is used to discretized the model.

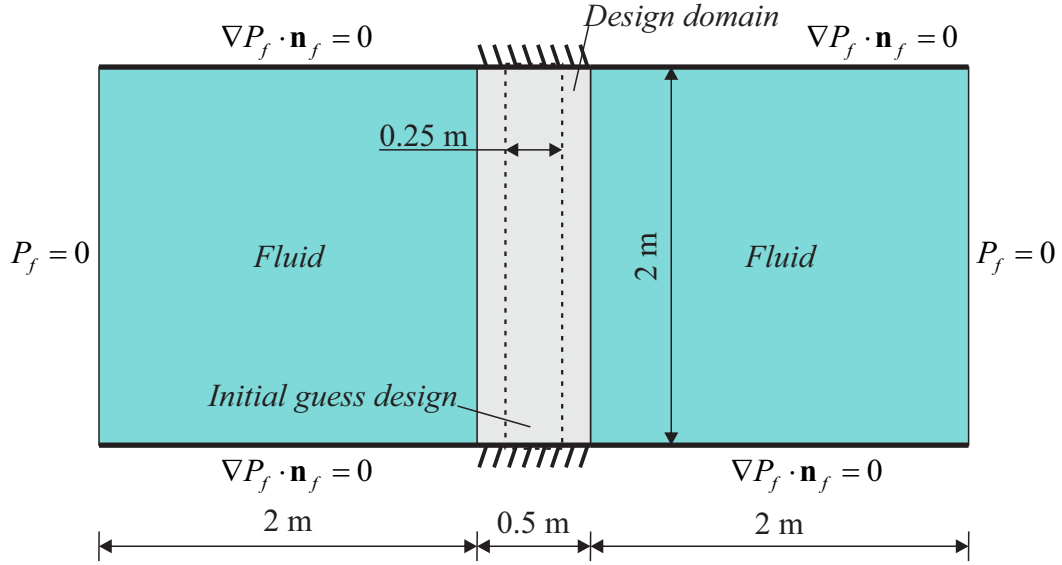


Figure 4.2: A clamped beam between two fluid domains under free vibration.

For this design problem BESO's evolutionary ratio is chosen to be as $ER = 2\%$ and the final prescribed volume $V_s = 50\%$. The filter radius used is $r_{min} = 60$ mm and the penalty factor is $p = 3$. The other parameters are set as $x_{min} = 0.001$, $AR_{max} = 5\%$ and $\tau = 0.001$. Figure 4.3 presents the solution obtained with the initial structure starting from the full design domain and from an initial guess design (thinner clamped beam) with initial volume fraction most nearly to $V(x_i) = 50\% = V_s$. This last allows the optimization to be carried out with constant volume during the whole algorithm. Both topologies showed to be similar between each other, with the final natural frequency $\omega_1 = 152.31$ Hz for the solution starting with the full design domain and $\omega_1 = 152.41$ Hz starting with the initial guess design. Both topologies are in accord with the one obtained by Yoon *et al.* (2007), which used the SIMP method and a mixed finite element formulation. Figure 4.4 presents some snapshots of the final solution for the case with initial guess design.



Figure 4.3: Clamped beam solutions obtained with the BESO method with initial structure starting from the: (a) full design domain; (b) initial guess design with 50% of the design domain.

No intermediate density elements are present in the final solution. This allows the fluid elements to be updated and placed inside the design domain, tracking the fluid-structure interfaces

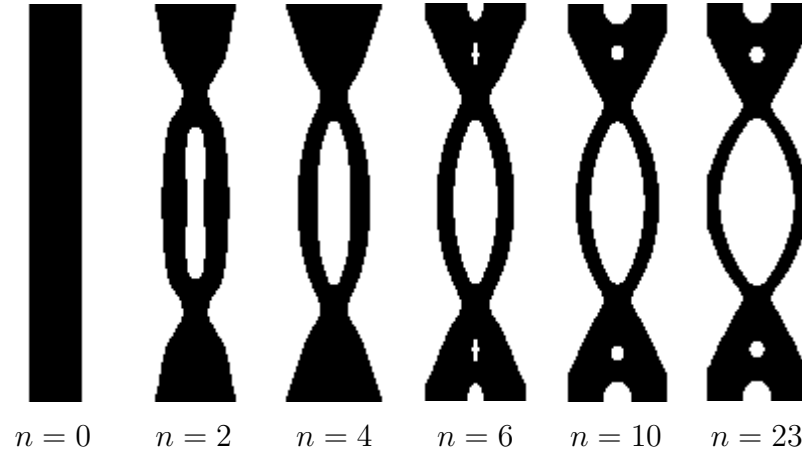


Figure 4.4: Snapshots of the BESO solution starting from an initial guess design.

and moving coupled loads. Thus, the coupling integrals can be evaluated straightforwardly in each step of the optimization using the classic formulation by Zienkiewicz and Bettess (1978). For the case with initial guess design, Figure 4.5 shows the evolution history of the objective function along the iterations. In this case, the objective function, ω_1 increased from 125.03 Hz to 152.41 Hz, an increase of almost 22%.

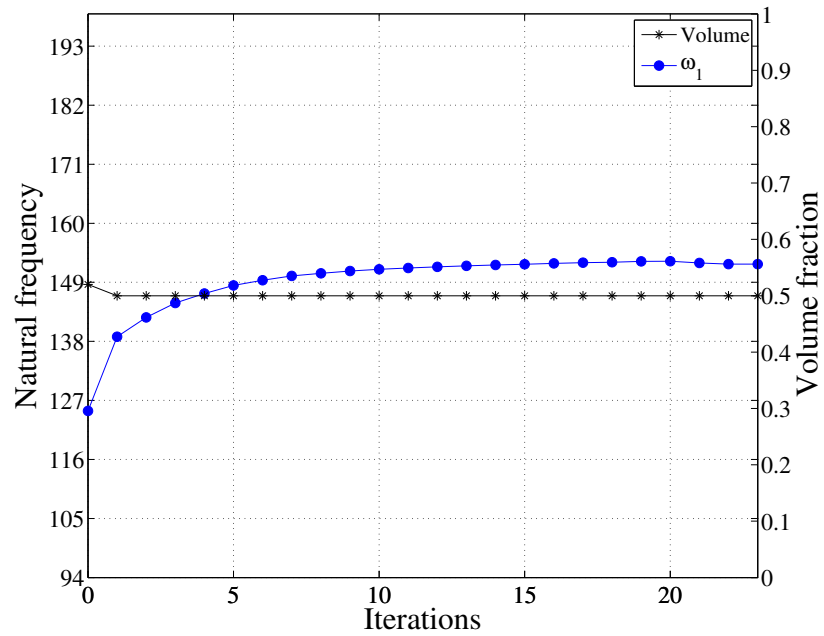


Figure 4.5: Evolutionary history of the objective function for the clamped beam example.

4.4.2 Open and closed acoustic cavity

This example aims to maximize the natural frequencies of a tunable device (showed in Figure 4.6), which can be set opening or closing its superior fluid domain edge. The closed cavity condition is represented by the hard wall boundary condition, $\nabla P_f \cdot \mathbf{n}_f = 0$ shown as thicker edge lines in Figure 4.6, and the open cavity is set defining the imposed pressure boundary condition, $P_f = 0$ (Zienkiewicz and Bettess, 1978). Both open and closed configurations present different natural frequencies. Numerically, closed cavities present a zero eigenvalue, which it is not of real practice interest and it is disregarded here. The system showed in Figure 4.6 is modelled with 99200 finite elements with thickness of 0.2 m and plane stress condition. The solid Young's modulus used is 70 GPa, density of 2700 kg/m³ and the Poisson's ratio is taken as 0.3. The fluid domain has density of 1000 kg/m³ and the speed of sound in the medium of 1450 m/s. The model is defined with an structural initial guess design as showed in Figure 4.6. Figure 4.7 presents the first three resonant frequencies of the model for both open and closed configuration.

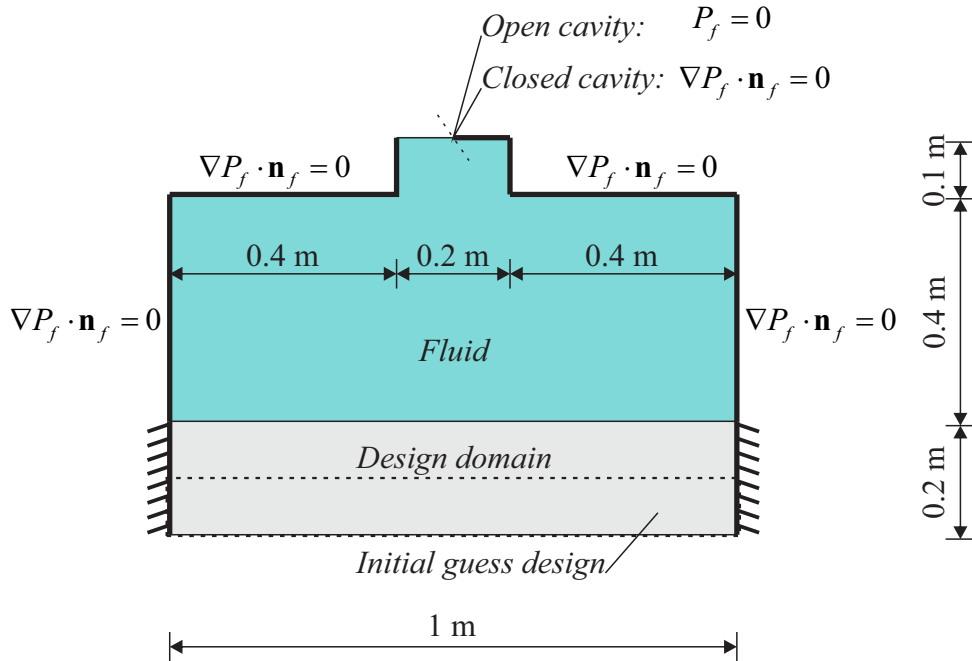


Figure 4.6: Tunable device with open and closed acoustic fluid cavities.

For the BESO method starting with the initial guess design, the evolutionary ratio is set as $ER = 1\%$ and the prescribed volume fraction $V_s = 50\%$. The other parameters are set as $r_{min} = 25$ mm, $AR_{max} = 1\%$, $x_{min} = 0.0001$, $\tau = 0.0001$ and, finally, the penalty factor $p = 3$. Figure 4.8 presents the structural topology solution considering maximization of the first natural frequency, ω_1 , for both open and closed fluid cavity configuration. The difference in the topology solutions is expected since the first vibration mode of the coupled system is altered

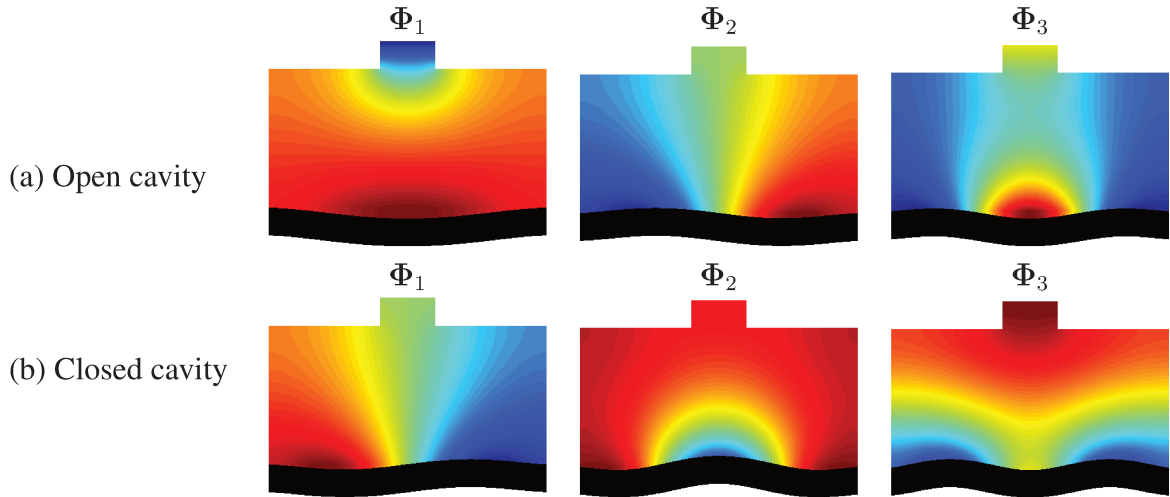


Figure 4.7: First three natural frequencies and vibration modes for the (a) open and the (b) closed device configuration.

while closing the fluid cavity. This might be related with shifting vibration modes by structural modification. Here, closed fluid cavities can change significantly the practical vibration modes of the coupled system and topology optimization can be used to design structures in order to avoid resonance modes as much as possible. Figure 4.9 presents the evolutionary history of the objective function, ω_1 , for the open and closed devices. In these cases, the increase ratios on ω_1 are 64% for the open configuration and 52% for the closed configuration.

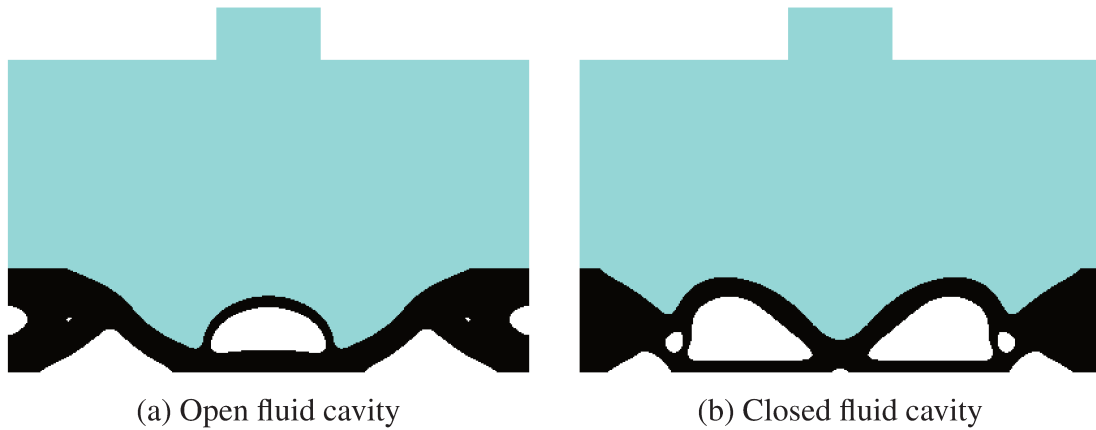


Figure 4.8: Topology solutions considering maximization of the first natural frequency, ω_1 , for the (a) open and the (b) closed fluid cavity configurations.

4.4.3 Water tank example

This example aims to verify the natural frequencies maximization of a water tank model, showed in Figure 4.10. A similar example is discussed in Figure 2 of the reference article

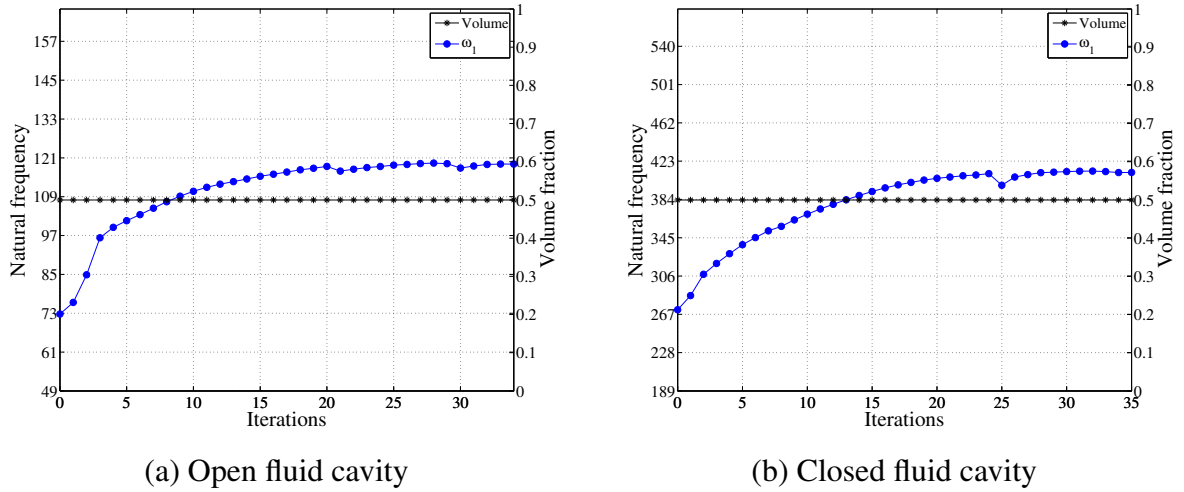


Figure 4.9: Evolutionary history of the objective function for both (a) open and (b) closed device configuration.

by Zienkiewicz and Bettess (1978). Disregarding surface waves, a free surface condition is imposed at the upper edge of the fluid domain as $P_f = 0$ and the hard-wall condition, $\nabla P_f \cdot \mathbf{n}_f = 0$, at the inferior and the right edge of the domain. The design domain is considered to have an inclined edge. A solid non-design domain is considered, as represented in Figure 4.10. This also can be an initial approximation for a water dam design problem.

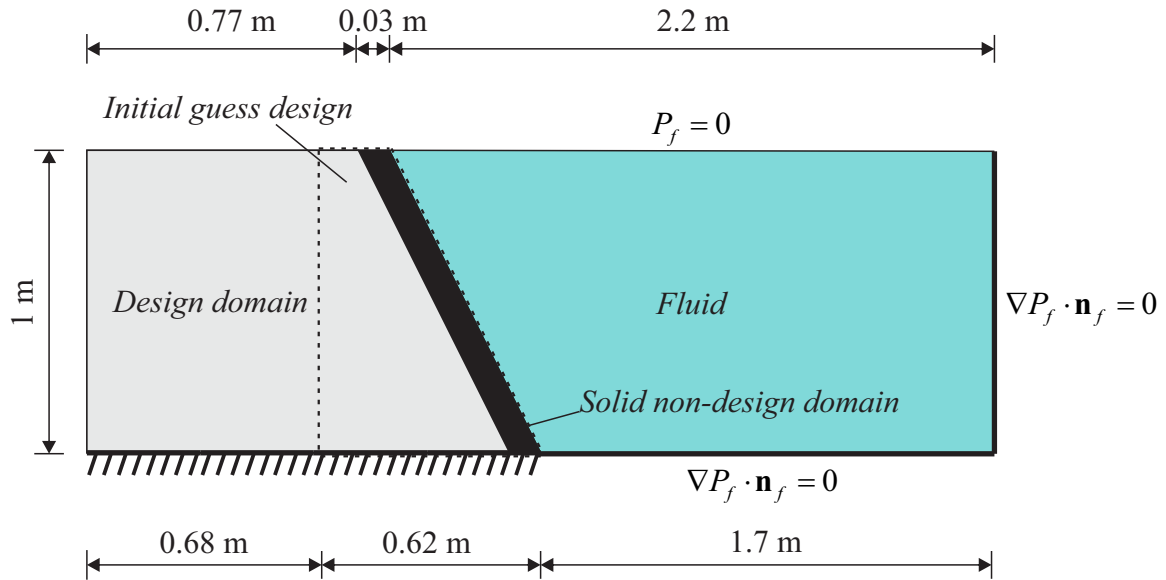


Figure 4.10: Water tank model.

With the initial guess design, BESO started with an evolutionary ratio $ER = 1\%$ until a prescribed volume fraction $V_s = 35\%$. The other BESO parameters are set as $r_{min} = 75$ mm, $AR_{max} = 1\%$, $x_{min} = 0.0001$, $\tau = 0.0001$ and $p = 3$. In this example, multiple frequencies maximization is explored. The model is discretized with 76800 finite elements. The

solid Young's modulus used is 17 GPa, density of 2400 kg/m³ and the Poisson's ratio is taken as 0.3. The fluid domain has density of 1000 kg/m³ and the speed of sound in the medium of 1450 m/s. Figure 4.11 presents the topology solutions for ω_1 maximization and for both $\omega_1 + \omega_2$ maximization, as well as the evolutionary history of the objective function for each case.

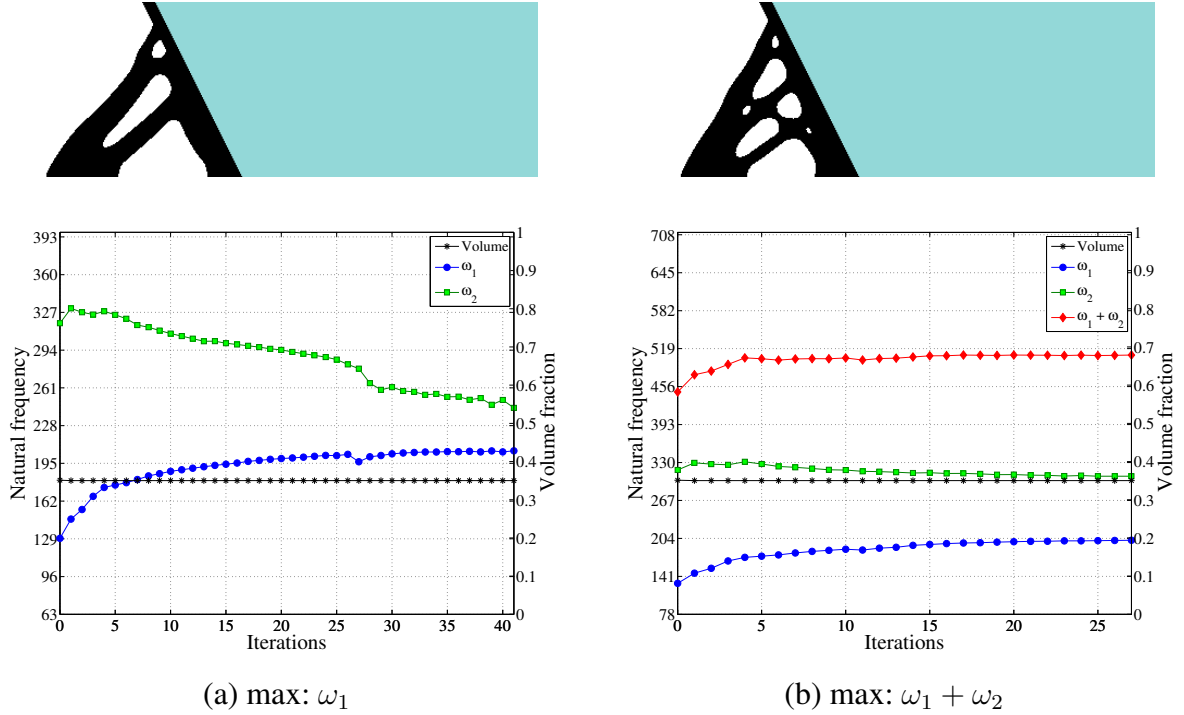


Figure 4.11: Topology and evolutionary history for the solutions of the water tank design problem considering (a) ω_1 maximization and (b) multiple $\omega_1 + \omega_2$ maximization.

Considering only the first natural frequency maximization, the value ω_1 increased from 129.50 Hz to 205.93 Hz, representing an increase of 59%, while the second natural frequency suffered a significant reduction. For the case of multiple frequencies maximization, ω_1 increased from 129.50 Hz to 200.97 Hz, representing an increase of 55%, almost as the only ω_1 maximization. In addition, ω_2 did not suffer the same reduction as in the first case and the objective function $\omega_1 + \omega_2$ increased from 447.07 Hz to 508.29, representing an increase of 14%. For this example, the fluid-structure interfaces do not change their location. Even though, the relation between stiffness and mass summing the coupled contributions of both acoustic and structure fields are changing while structural elements are removed. To illustrate this change, Figure 4.12 presents the first two vibration modes for the acoustic field considering the initial guess design and the topologies after the optimization cases. This characterizes the dependency of the responses (eigenmodes) on the coupled acoustic-structure model also for fixed fluid-structure interfaces.

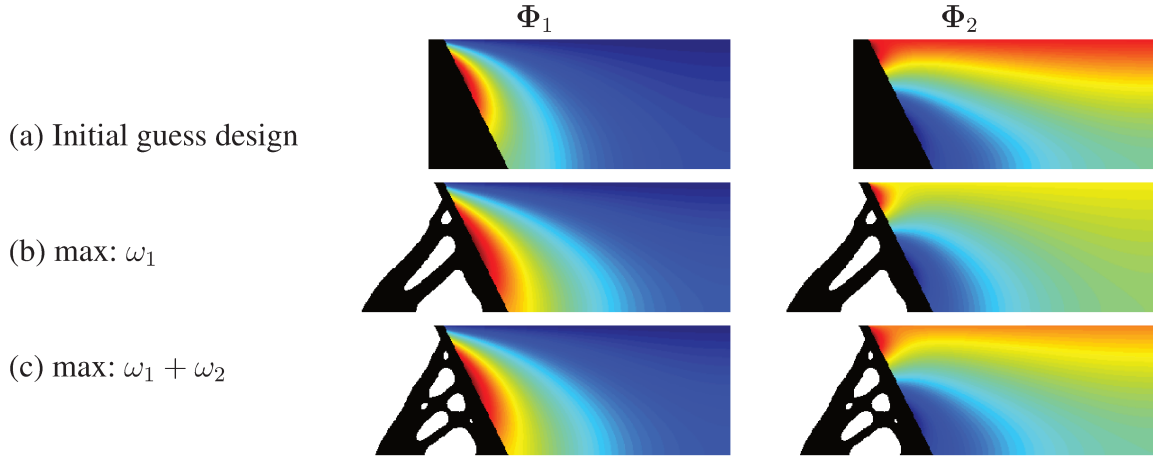


Figure 4.12: Pressure distribution according to the acoustic vibration modes Φ_1 and Φ_2 for (a) the initial guess design, (b) after ω_1 maximization and (c) after $\omega_1 + \omega_2$ maximization.

4.4.4 Water tower example

This example aims to verify the crossing of vibration modes during the optimization procedures, using a water tower model. A structural design domain supports a water tank in its upper edge, as illustrated in Figure 4.13. Similarly to the previous example, a free surface condition is imposed at the upper edge of the fluid domain as $P_f = 0$ and the hard-wall condition, $\nabla P_f \cdot \mathbf{n}_f = 0$, at the left and the right edge of the domain. Thus, as an approximation, surface waves are disregarded here and no sloshing dynamics is taken in account. A solid non-design domain is considered at the left, right and upper edges of the structural design domain, as represented in Figure 4.13. This also implies that the fluid-structure interface is kept fixed in this example.

The system showed in Figure 4.13 is modelled with 20000 structural and 10000 fluid finite elements. The thickness of the model is considered as 0.2 m and plane stress condition is applied. The solid Young's modulus used is 70 GPa, density of 2700 kg/m³ and the Poisson's ratio is taken as 0.3. The fluid domain has density of 1000 kg/m³ and the speed of sound in the medium of 1450 m/s. With the initial full design, BESO started with an evolutionary ratio $ER = 1\%$ until a prescribed volume fraction $V_s = 65\%$. The other BESO parameters are set as $r_{min} = 60$ mm, $AR_{max} = 5\%$, $x_{min} = 0.0001$, $\tau = 0.001$ and $p = 3$. Considering the maximization of the first natural frequency, ω_1 , Figure 4.14 presents the final structural topology obtained with the BESO method (a) as well as the evolutionary history of the objective function (b).

It is possible to observe in Figure 4.14 that, although the final structure presents a quite clear topology, the objective function ω_1 presents multiplicity with ω_2 until final convergence.

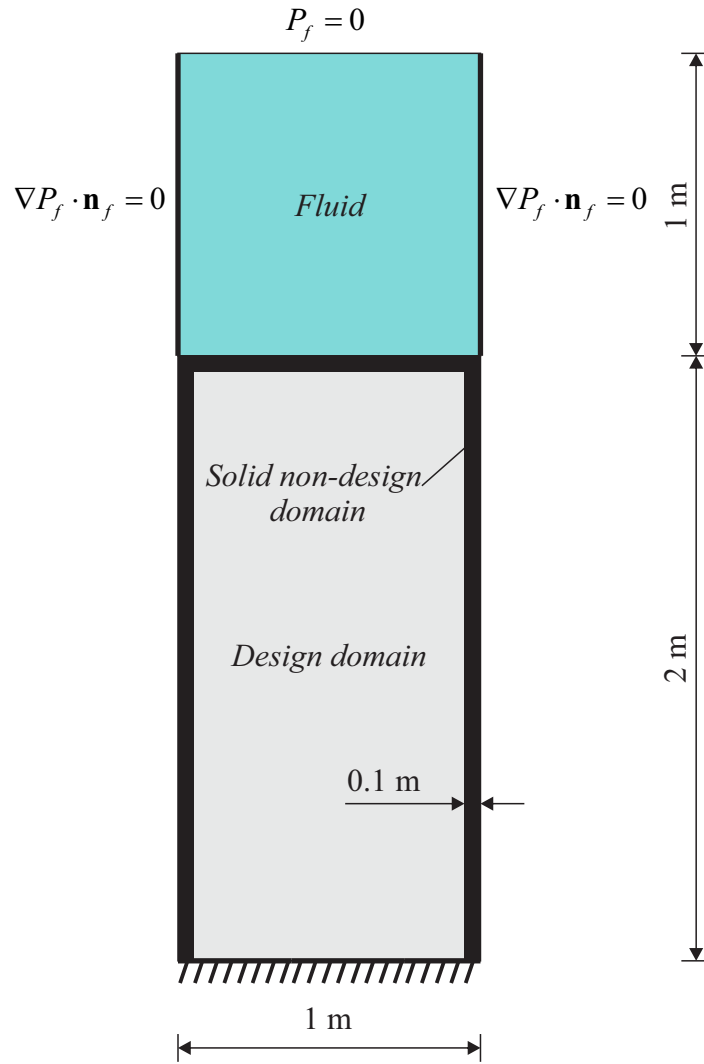


Figure 4.13: Water tower model.

The crossing in these coupled vibration modes may lead to misinformations and the algorithm may not converge. Thus, numerical techniques are needed then to avoid this problem. However, here it is showed that this problem can be avoided by simply averaging both multiple natural frequencies, as shown by Yang *et al.* (1999b) for the evolutionary methods. In this example, considering the maximization of both ω_1 and ω_2 , the vibration modes cross but do not become multiple, as showed in Figure 4.15(b), in the evolutionary history of the objective function. Figure 4.16 presents the first three coupled vibration modes for the initial full design domain and for the structures obtained with ω_1 and with $\omega_1 + \omega_2$ maximization, in which the final crossed modes can be observed. The displacement field is upscaled for better visualization. Similar structures are presented in Bendsoe and Sigmund (2003), considering only structural vibration.

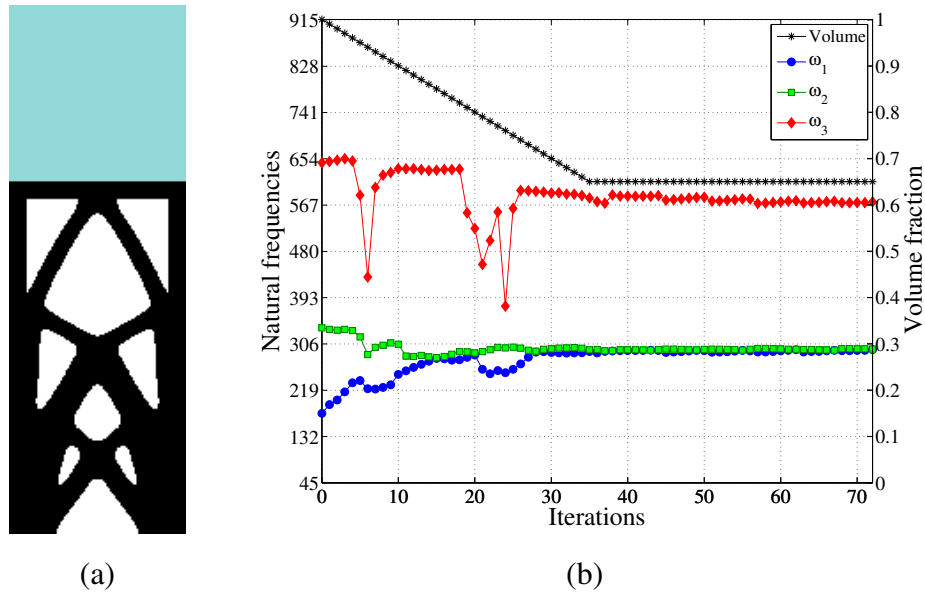


Figure 4.14: Water tower model example: (a) structural topology solution for ω_1 maximization and (b) evolutionary history of the objective function.

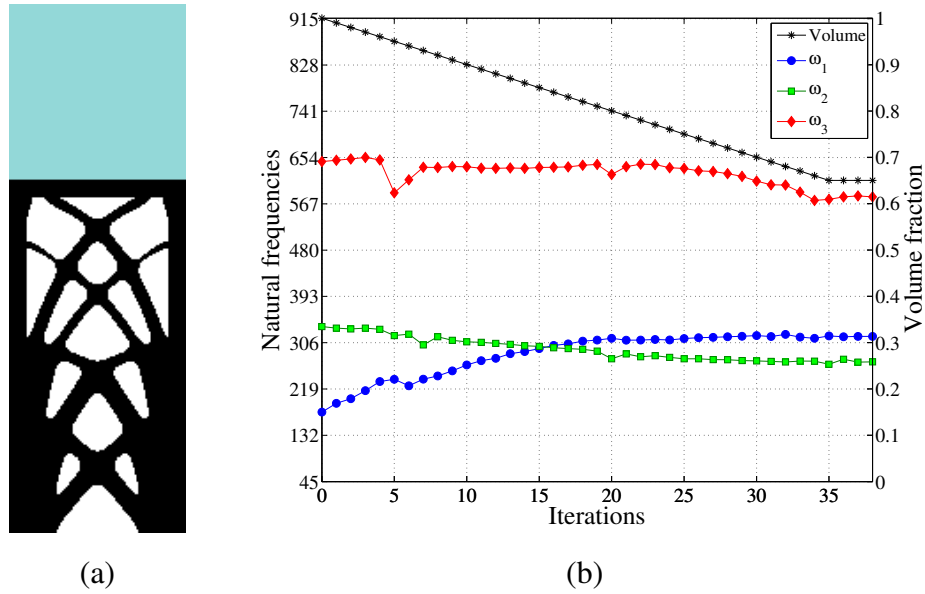


Figure 4.15: Water tower model example: (a) structural topology solution for $\omega_1 + \omega_2$ maximization and (b) evolutionary history of the objective function.

4.5 Conclusions

This work applied the extended fluid-structure BESO method to the maximization of the first natural frequencies of acoustic-structure systems. Coupled models under free vibration were designed considering moving multiphysics interfaces as well as fixed boundaries.

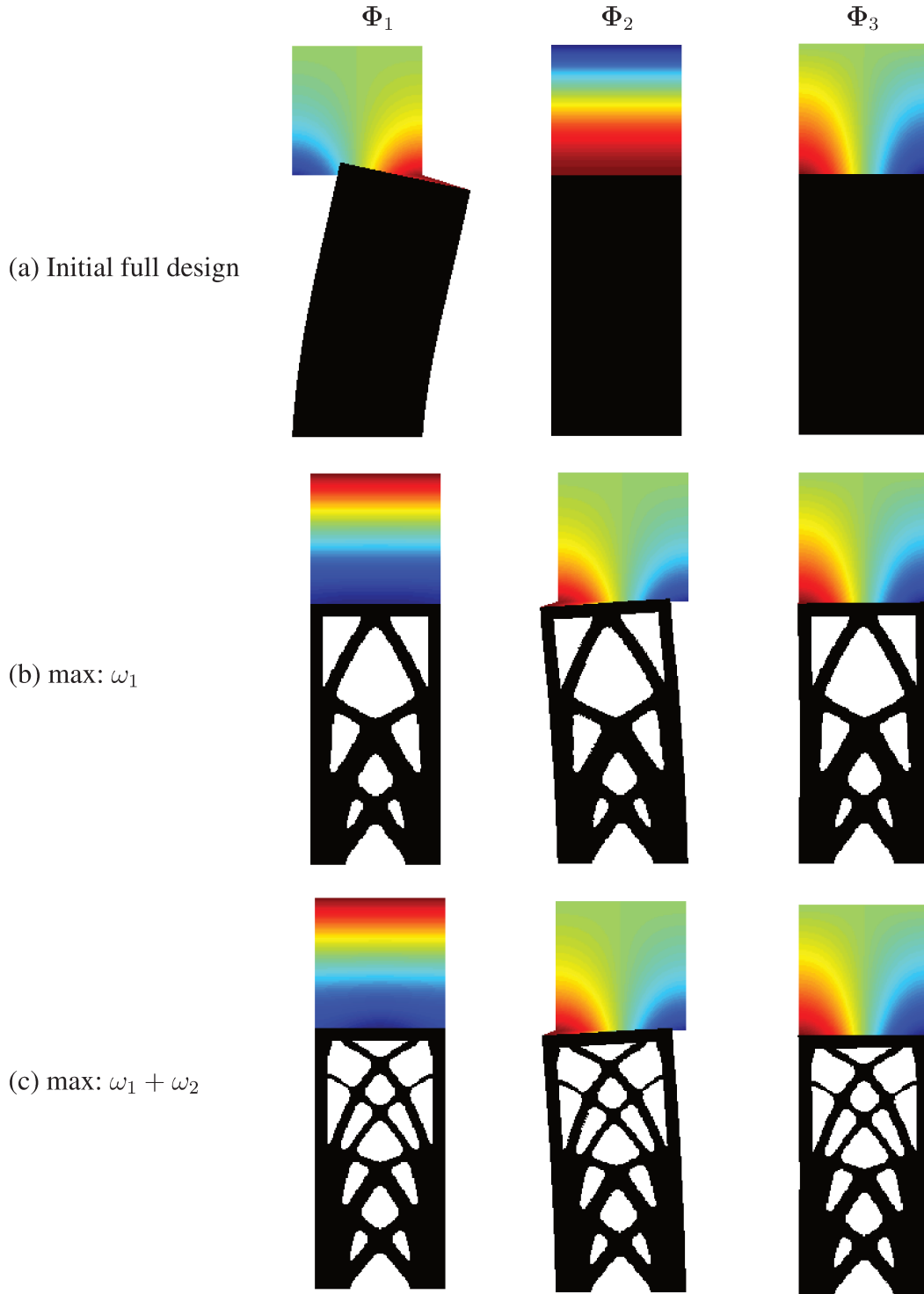


Figure 4.16: Coupled vibration modes for (a) initial full design and for the structures obtained with (b) ω_1 maximization and with (c) $\omega_1 + \omega_2$ maximization.

The first example consisted of a clamped beam vibrating between two acoustic domains. The solution found is in accordance with results in the literature. In the second example, a tunable device was explored. Closed fluid cavities drastically change the resonance frequencies of the coupled systems, dropping at least one vibration mode to zero frequency, i.e., eliminating

it in practical examples. Thus, the coupled modes change. Both open and closed configurations were analyzed considering the first natural frequency maximization. The last example considered a water tank model with fixed solid-fluid boundaries. Even though the interface and the fluid field were kept fixed, it was shown that the pressure modes in the fluid changed from one case to another. This characterizes the coupled dependency of the acoustic-structure model on the vibration modes and, consequently, in the optimization of acoustic-structure free vibration problems.

To the best of the authors' knowledge, the combination of acoustic-structure free vibration problems and the evolutionary optimization methods are considered for the first time in this work. The discrete nature of the BESO method present potential to handle complex multiphysics problems, since the moving interfaces can be explicitly evaluated in each step of the optimization. Thus, with the virtual explosion of the multiphysics optimization problems, the evolutionary methods might be of useful application in science and industrial matters.

5 STRUCTURAL TOPOLOGY OPTIMIZATION CONSIDERING STATIONARY VISCOUS FLUID FLOW LOADS

Context

This work explores the evolutionary topology optimization approach in problems with fluid-structure interaction. First, fluid flow pressure drop minimization has been carried out using Brinkman equations. Later, cases of “dry” and “wet” structural topology optimization have been explored solving Stokes and Navier-Stokes equations (*Fluid 3* mentioned in Chapter 1). In “dry” optimization, fluid-structure interfaces have been kept fixed. For “wet” optimization, the BESO fluid-structure update scheme by Picelli *et al.* (2015b) has been extended to track the changes in the interfaces between the structures and the viscous fluid flow. Part of this contribution considering “wet” topology optimization has been published in the conference proceedings of the 11th World Congress of Structural and Multidisciplinary Optimisation (Picelli *et al.*, 2015c).

5.1 Introduction

In order to improve the mechanical system design in the field of engineering, Structural Topology Optimization (Bendsoe and Sigmund, 2003) has been developed. The idea is to find optimal structural topologies inside predefined design domains concerning objective functions and constraints. Much has been done in industrial applications of structural topology optimization, but some topics are still challenging and open to research, specially concerning the interaction between structures and different other types of phenomena.

This work concerns the interaction between linear structural models and fluid flow models governed by incompressible Navier-Stokes equations. Here, evolutionary topology optimization is applied to pressure drop minimization in viscous fluid flow problems and also structural design in fluid-structure interaction (FSI) problems.

Considering fluid flow problems, topology optimization has been applied first by Borrvall and Petersson (2003) in order to minimize the dissipated power of the fluid flow, aiming to obtain optimal fluid paths considering stationary Stokes flow equations. One year later, the approach was generalized by Evgrafov (2005) to allow optimization of Stokes fluid flow in porous materials, using Navier-Stokes equations (Evgrafov, 2006). Aage *et al.* (2008) showed the application of fluid flow topology optimization in large scale problems. Alternative formulations

were proposed using Darcy-Stokes representation (Guest and Prévost, 2006; Wiker *et al.*, 2007). The full incompressible Navier-Stokes equations were considered for the first time in topology optimization by Gersborg-Hansen *et al.* (2005), in which inertia effects are also relevant to the fluid flow. Unsteady incompressible Navier-Stokes flow was also considered (Deng *et al.*, 2011, 2013). Besides that, other methods were applied to fluid flow topology optimization, such as level-set methods (Challis and Guest, 2009; Kreissl and Maute, 2012). Up to the date of this thesis, the evolutionary methods were not considered in fluid flow topology optimization. At the other hand, the methodologies for fluid flow optimization are well established and have been associated with other physics problems, such as heat transfer (Koga *et al.*, 2013; Alexandersen *et al.*, 2014).

In the scope of fluid-structure interaction, only a few authors have developed methodologies for structural topology optimization in FSI problems. Recently, Jenkins and Maute (2015) adopted the nomenclature used in aeroelasticity (internal “dry” and external “wet” surfaces) to distinguish and classify the topology optimization methods of FSI problems according to the treatment they apply on the fluid-structure boundaries. They classified as dry optimization the cases where only the shape and topology of the internal structure are optimized and wet optimization when the methods are able to manipulate the geometry of the fluid-structure interface, S_{fsi} , as illustrated by Figure 5.1.

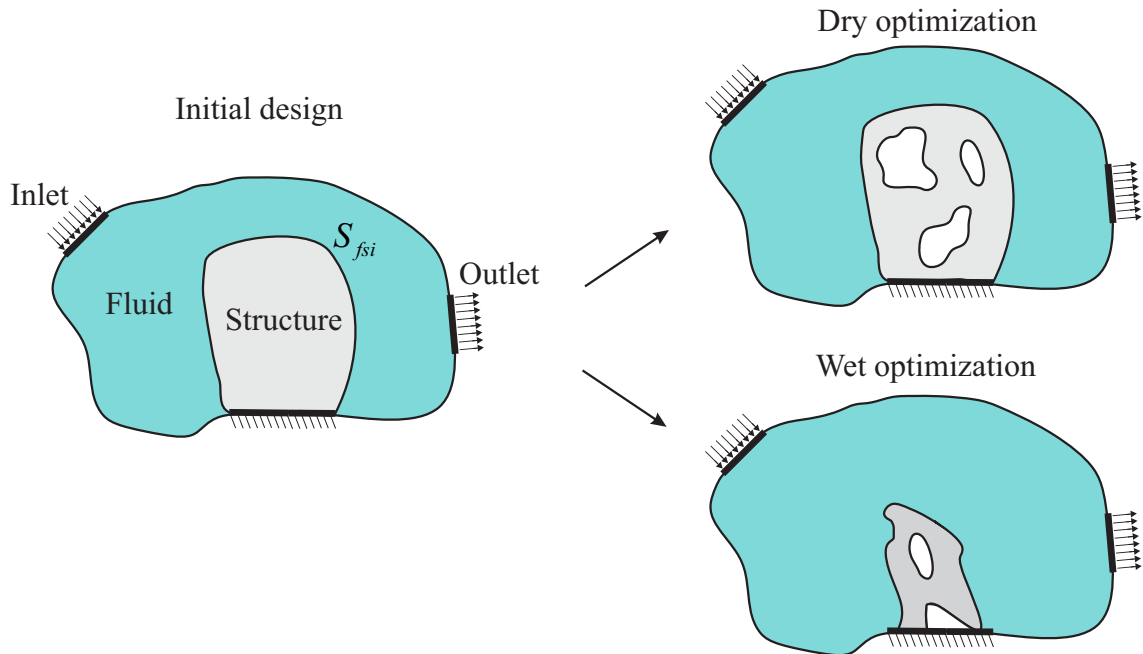


Figure 5.1: Representation of “dry” and “wet” topology optimization approaches in FSI problems, as classified by Jenkins and Maute (2015).

In the case of dry topology optimization, the fluid-structure interfaces are explicitly defined and coupling conditions can be formulated and discretized with standard methods (Allen

and Maute, 2005; Jenkins and Maute, 2015). On the other hand, the classic density-based topology optimization methods become arduous when dealing with the case of wet optimization and specialized computational techniques are needed to track the coupling conditions during optimization. The main challenge is similar to those from design-dependent pressure loads (Sigmund and Clausen, 2007; Picelli *et al.*, 2015b), where fluid-structure interfaces can change when the structural design is changed by the optimizer. Thus, FSI loads may also change their location, direction and magnitude during optimization. Methods with intermediate density elements are not able to identify straightforwardly these interface changes. To circumvent this problem a few techniques have been proposed in the recent years.

Kreissl *et al.* (2010) carried out shape and topology optimization considering fluid-structure interaction, however they did not really consider the changes of the interfaces. In the wet optimization case, Yoon (2010) used a monolithic approach for the FSI model in topology optimization. The methodology was then extended to include an electro-fluid-thermo-compliant multiphysics actuator design (Yoon, 2012) and to stress-based problems (Yoon, 2014). Andreasen and Sigmund (2013) considered FSI in poroelasticity for shock absorbers. These ideas basically used mixed and overlapping physics formulations, similarly as proposed by Sigmund and Clausen (2007), which was also applied to frequency responses minimization in acoustic-structure problems (Yoon *et al.*, 2007). Up to the date of this thesis, no other methods of topology optimization were applied to real “wet” optimization cases in this type of fluid-structure interaction problems.

In this context, the presented work proposes the application of the extended BESO method for FSI system design. The discrete nature of the evolutionary methods imply that no intermediate density elements are allowed during the optimization procedures. Thus, fluid-structure boundaries are always explicitly defined and the coupling boundary conditions evaluation is straightforward.

The following sections formulate the optimization problems, in which potential power minimization (drag or pressure drop reduction) in viscous fluid flow is applied and structural mean compliance minimization is carried out in “dry” and “wet” optimization.

5.2 Fluid-structure models: governing equations and finite element discretizations

This work describes the use of evolutionary topology optimization in viscous flow problems, considering fluid flow microchannels and also fluid-structure interaction. Following, the governing equations and finite element formulations are described for all models used.

5.2.1 Viscous fluids

The motion of a fluid particle in space are given by the Navier-Stokes equations. These equations are the basic governing equations for a viscous, heat conducting fluid in a domain Ω_f . They are expressed by the combination of the momentum and continuity equations, Equations 5.1 and 5.2, respectively, which describe the changes in momentum and acceleration of a fluid flow due to pressure and viscous forces acting on the fluid (Gresho and Sani, 2000). The referred Navier-Stokes equations can be written as:

$$\rho_f \left(\frac{\partial \mathbf{v}_f}{\partial t} + \mathbf{v}_f \cdot \nabla \mathbf{v}_f \right) = -\nabla P_f + \mu \nabla^2 \mathbf{v}_f + \mathbf{f}, \quad (5.1)$$

$$\frac{\partial \rho_f}{\partial t} + \nabla \cdot (\rho_f \mathbf{v}_f) = 0, \quad (5.2)$$

where ρ_f is the fluid density, μ is the fluid dynamic viscosity, \mathbf{v}_f is the fluid velocity field, P_f the fluid pressure and t is time.

The fluid in this work undergoes some assumptions, which simplify the problem: the flow is laminar and at steady-state ($\partial \mathbf{v}_f / \partial t = 0$); the medium is incompressible ($\partial \rho_f / \partial t = 0$ and ρ_f is constant); the medium has a Newtonian character (μ is constant); there are no body forces ($\mathbf{f} = 0$) and the medium properties are temperature and energy independent (no addition of a heat conduction equation).

Under these assumptions, the viscous fluid flow used in this work is governed by the so called *incompressible Navier-Stokes equations*, expressed as:

$$\begin{cases} \rho_f (\mathbf{v}_f \cdot \nabla \mathbf{v}_f) = -\nabla P_f + \mu \nabla^2 \mathbf{v}_f \\ \nabla \cdot (\mathbf{v}_f) = 0 \end{cases} \quad (5.3)$$

The left side of the steady-state incompressible Navier-Stokes equations consists of a convective term $\rho_f (\mathbf{v}_f \cdot \nabla \mathbf{v}_f)$, which depends on \mathbf{v}_f and represents inertia effects. The right side is the divergence of the fluid stress tensor $\boldsymbol{\sigma}_f$, which presents a diffusive term $\mu \nabla^2 \mathbf{v}_f$. The relation between the convective and diffusive terms is an indicative of the flow speed or how the fluid flow is affected by inertia. This relation can also be called *Reynolds number* (Re) and can be used to predict the fluid flow pattern. Higher Reynolds number implies more complex fluid flow patterns, such as turbulent flows.

Although the fluid flow is considered to be laminar in this work, the presence of a convective term in the governing equation still makes the problem nonlinear, requiring more spe-

cialized solvers. In order to solve Equation 5.3, the following boundary conditions are applied (see Figure 5.2:

$$\mathbf{v}_f = \mathbf{v}_0 \quad \text{on } S_{in}, \quad (5.4)$$

$$\mathbf{v}_f = 0 \quad \text{on } S_w, \quad (5.5)$$

$$P_f = 0 \quad \text{on } S_{out}, \quad (5.6)$$

representing the velocity profile given at the inlet (Equation 5.4), no-slip condition at fluid flow walls (Equation 5.5) and outlet constrained pressure value (Equation 5.6).

By imposing the previous boundary conditions and solving Equation 5.3, one can obtain the velocity and pressure profiles of the viscous fluid flow.

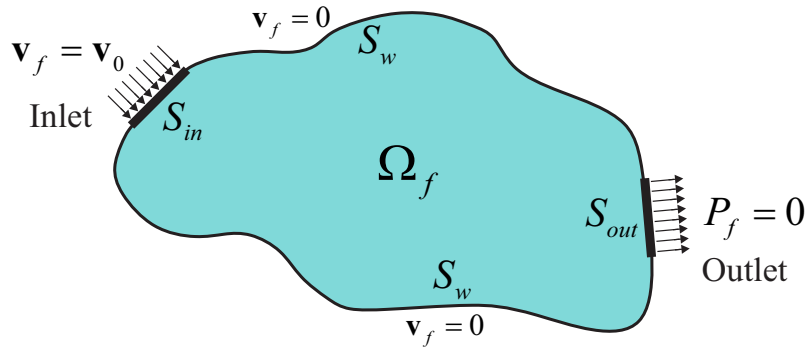


Figure 5.2: The viscous fluid domain Ω_f and boundary conditions. A velocity profile $\mathbf{v}_f = \mathbf{v}_0$ is given at inlet boundary S_{in} , outlet pressure is set as $P_f = 0$ in S_{out} and the no-slip conditions (zero velocities $\mathbf{v}_f = 0$) are imposed at the fluid flow walls S_w .

For very low Reynolds number ($Re \ll 1$), the fluid has very high viscosity or flows with very small velocities. In cases like this, the convective term of the Navier-Stokes equations tends to be negligible if compared with the diffusive term. When this is true, the flow is viscous driven and governed by the so called Stokes flow equations:

$$\begin{cases} \mu \nabla^2 \mathbf{v}_f - \nabla P_f = 0 \\ \nabla \cdot (\mathbf{v}_f) = 0 \end{cases} . \quad (5.7)$$

These equations are a particular case of the incompressible Navier-Stokes equations, which consists in a linear system of equations making the problem much easier to be solved. The same boundary conditions from Equations 5.4, 5.5 and 5.6 and the scheme in Figure 5.2 are used to solve Stokes flow in this work. The simplifying assumptions used for Navier-Stokes equations are also considered here. This type of flow can also be called as *creeping flow*.

In order to minimize pressure drop and find optimal fluid flow channels, Borrvall and Petersson (2003) initiated a research area using topology optimization in fluid mechanics. The authors used a combination of the previously described Stokes flow with Darcy's Law, which describes the flow of a fluid through a porous medium. This combination results in the Brinkman equations. Neglecting body forces, these equations can be expressed as:

$$\begin{cases} \mu \nabla^2 \mathbf{v}_f + \alpha(x_i) \mathbf{v}_f - \nabla P_f = 0 \\ \nabla \cdot (\mathbf{v}_f) = 0 \end{cases} \quad (5.8)$$

where $\alpha(x_i)$ is the inverse permeability of the porous media, added with the aid of Darcy's law, which depends on a design variable x_i .

The inverse permeability is a measure of flow resistance through the fluid medium. In the scope of topology optimization, the fluid elements with higher α are said to be more resistant (low porosity medium) to the flow than the elements set with lower α (high porosity medium). Higher α implies in nearly solid medium (low porosity) and increases the flow resistance, dropping down fluid velocities. In the limit when α tends to zero, the fluid has very high permeability (high porosity) and the flow is governed only by Stokes flow equations. This is very advantageous for topology optimization, since fluid elements can be turned into nearly solid elements by setting a high inverse permeability α and the fluid flow can be solved without any extra Dirichlet boundary conditions. Furthermore, fixed walls or flow obstacles can be inserted with the same approach. Brinkman's equations are solved in the same manner as the previous Stokes and Navier-Stokes equations. The function that defines the inverse permeability used in this work is:

$$\alpha(x_i) = \alpha_U + (\alpha_L - \alpha_U) x_i \frac{1+q}{x_i+q}, \quad (5.9)$$

where q is a penalty parameter considered as 1 in this work, x_i is the design variable in pressure drop minimization problems and $\alpha_U = 2,5\mu/0,01^2$ and $\alpha_L = 2,5\mu/100^2$ are the upper and lower limits of the inverse permeability (Gartling *et al.*, 1996).

5.2.2 Solid domain

Herein it is considered linear elasticity, small displacements and deformations, for a solid domain Ω_s interacting with a viscous fluid flow loads. Neglecting body forces and any acceleration, the linear structural analysis is governed by

$$\nabla \cdot \boldsymbol{\sigma}(\mathbf{u}_s) = -\mathbf{f}^{fsi}, \quad (5.10)$$

where $\nabla \cdot \boldsymbol{\sigma}_s(\mathbf{u})$ is the divergence of the Cauchy stress tensor, \mathbf{u} is the structural displacement field and \mathbf{f}^{fsi} denotes the vector with the loads from the viscous fluid flow calculated at the fluid-structure interface S_{fs} , see Figure 5.3. Then, before solving Equation 5.10, Dirichlet boundary conditions are applied to the solid domain:

$$\mathbf{u} = 0. \quad (5.11)$$

Following, the FSI coupling conditions are presented, from which the tractions \mathbf{f}^{fsi} are obtained. By topology optimizing the structure, a void domain Ω_v can also be present.

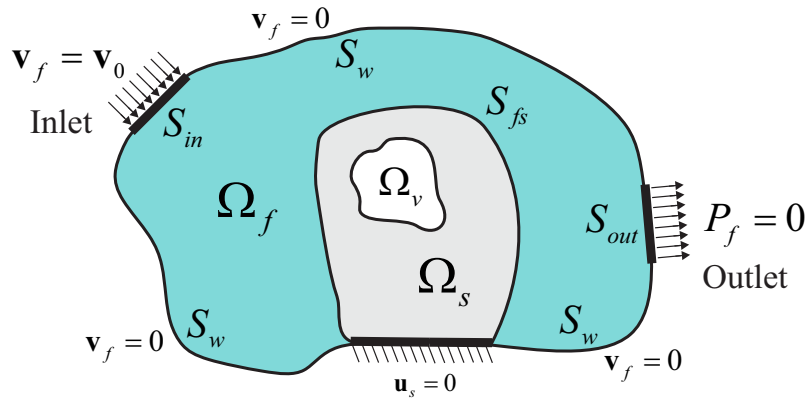


Figure 5.3: The solid (Ω_s), fluid (Ω_f) and void (Ω_v) domains and boundary conditions. With steady-state fluid velocities and pressures profiles, fluid flow reaction forces can be calculated on the fluid-structure interfaces S_{fs} and imposed as loads in the structural analysis.

5.2.3 Fluid-structure interaction model

The existence of both fluid and structure domains with a shared interface in FSI leads to some possibilities in the modelling description. Such possibilities means to model the FSI systems with: *Eulerian/spatial*, *Lagrangian/material* or *Arbitrary Lagrangian Eulerian* (ALE) descriptions.

In this work, the governing equations are derived and used in an Eulerian description for the fluid flow and a Lagrangian description for the structure, which implies the use of two different meshes. To ensure the FSI coupling conditions (Bazilevs *et al.*, 2013; Hou *et al.*, 2012; Bosma, 2013), the following relations must be satisfied:

$$\mathbf{v}_f = \dot{\mathbf{u}} \quad \text{on } S_{fs} \text{ and,} \quad (5.12)$$

$$\boldsymbol{\sigma}_s \mathbf{n}_s = -\boldsymbol{\sigma}_f \mathbf{n}_f \quad \text{on } S_{fs}. \quad (5.13)$$

The first relation (Equation 5.12) states that the fluid follows the structure on S_{fsi} with same velocity, declaring that the fluid does not leave or penetrate the structure. In this work, this is guaranteed when steady-state is considered ($\dot{\mathbf{u}} = 0$) and no-slip conditions for the fluid flow are imposed on the fluid-structure interface,

$$\mathbf{v}_f = 0 \quad \text{on } S_{fs}. \quad (5.14)$$

To obey the second relation, Equation 5.13, the vector of FSI loads \mathbf{f}^{fsi} can be calculated as reactions forces on S_{fs} using the fluid stress tensor $\boldsymbol{\sigma}_f$ and imposed as tractions \mathbf{f}^{fsi} on the structural boundaries in contact with S_{fs} (Hou *et al.*, 2012).

By solving Equation 5.10, the displacement field of the linear elastic structure can be obtained. In fully coupled FSI problems, structural displacements implies deformations in the fluid-structure interfaces S_{fs} . The fluid equations need then to be solved again in order to consider the deformations on S_{fs} . Different staggered and monolithic approaches are used to solve these FSI problems (Yoon, 2010; Bosma, 2013).

This work is limited to small structural displacements and deformations, similarly as considered by Yoon (2010) in topology optimization. This implies a minimum deformation of the interface S_{fsi} and, consequently, it does not effectively alter the fluid responses. Thus, the problems considered here are actually one-way coupled, where the steady-state fluid velocity and pressure profiles are used to calculate the fluid reactions that are used to solve the structural problem. After the structural displacements are obtained, the problem is considered solved. Following, the FSI algorithm used in this work is described in the scope of the finite element discretization.

The finite element modelling of the compressible or incompressible Navier-Stokes equations are a challenge in computational mechanics (Zienkiewicz and Taylor, 2005; Brooks and Hughes, 1982; Oñate *et al.*, 2006). In this work, a finite element code is implemented to solve these equations. Two main difficulties arise in the finite element modelling of the incompressible Navier-Stokes equations: the incompressibility condition and convective-dominated cases (high Reynolds number).

A mixed finite element method is chosen in order to model the incompressible Navier-Stokes equations, in which fluid velocities and pressures are interpolated in the same finite element. With adequate shape functions, these elements are stable and satisfy compatibility conditions, such as the *Ladyzenskaja-Babuska-Brezzi* (LBB) condition for incompressible elements (Gresho and Sani, 2000; Brezzi and Fortin, 1991). Although they can be costly for

large-scale problems, they showed to be effective for the cases explored in this work. Figure 5.4 shows the finite element used here, named as Q2rP1 (Rupp *et al.*, 2015), in which velocities are interpolated with serendipity shape functions and pressures with bilinear shape functions in the isoparametric axes (r, s) .

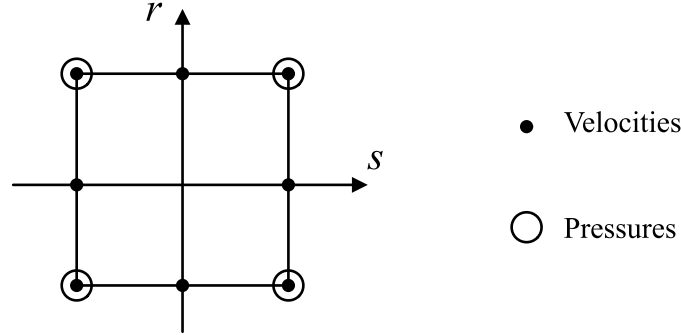


Figure 5.4: Mixed finite element Q2rP1.

In a Cartesian coordinate system (x, y) , the finite element matrices which solve the incompressible Navier-Stokes equations (described in Equation 5.3) are

$$\begin{bmatrix} \mathbf{K}_f + \mathbf{K}_T(\mathbf{v}_f) & -\mathbf{Q} \\ -\mathbf{Q} & \mathbf{0} \end{bmatrix} \begin{Bmatrix} \mathbf{v}_f \\ \mathbf{P}_f \end{Bmatrix} = \begin{Bmatrix} \mathbf{0} \\ \mathbf{0} \end{Bmatrix}, \quad (5.15)$$

where,

$$\mathbf{K}_f = \mu \int_{\Omega_e} \mathbf{B}^T \mathbf{I}_0 \mathbf{B} d\Omega_e, \quad (5.16)$$

$$\mathbf{K}_T(\mathbf{v}_f) = \rho_f \int_{\Omega_e} \mathbf{N}_v^T \mathbf{N}_v (\mathbf{v}_x \nabla \mathbf{N}_v^x + \mathbf{v}_y \nabla \mathbf{N}_v^y) d\Omega_e \text{ and,} \quad (5.17)$$

$$\mathbf{Q} = \int_{\Omega_e} \nabla \mathbf{N}_v^T \mathbf{N}_P d\Omega_e. \quad (5.18)$$

The matrices \mathbf{N} contain the shape functions for velocities and pressures with the correspondent v and P subscripts, respectively (Bathe, 2006). The matrix \mathbf{B} contains the partial derivatives of the shape functions and, for 2D cases,

$$\mathbf{I}_0 = \begin{bmatrix} 2 & 0 & 0 \\ 0 & 1 & 0 \\ 0 & 0 & 1 \end{bmatrix}. \quad (5.19)$$

All matrices are evaluated in the element domain Ω_e . The matrix \mathbf{K}_f includes the dif-

fusive terms, viscosity effects, and $\mathbf{K}_T(\mathbf{v}_f)$ includes the inertia terms, while \mathbf{Q} models the incompressibility condition. For Stokes flow, i.e., very small velocities, $\mathbf{K}_T(\mathbf{v}_f)$ is negligible and the finite element model is

$$\begin{bmatrix} \mathbf{K}_f & -\mathbf{Q} \\ -\mathbf{Q} & \mathbf{0} \end{bmatrix} \begin{Bmatrix} \mathbf{v}_f \\ \mathbf{P}_f \end{Bmatrix} = \begin{Bmatrix} \mathbf{0} \\ \mathbf{0} \end{Bmatrix}. \quad (5.20)$$

By imposing the boundary conditions described in Equations 5.4, 5.5, 5.6 and 5.14 the discretized incompressible Navier-Stokes and Stokes systems (Equations 5.15 and 5.20, respectively) can be solved and the response vectors \mathbf{v}_f and \mathbf{P}_f on the fluid domain can be obtained. When Brinkman equations are considered, a new term is added to the fluid stiffness matrix, which is then expressed as:

$$\mathbf{K}_f = \mu \int_{\Omega_e} \mathbf{B}^T \mathbf{I}_0 \mathbf{B} d\Omega_e + \int_{\Omega_e} \alpha(x_i) \mathbf{N}^T \mathbf{N} d\Omega_e, \quad (5.21)$$

where $\alpha(x_i)$ is the inverse permeability that depends on the design variables x_i used only in pressure drop minimization problems, and not in fluid-structure interaction in this work.

For the structural analysis, the elements are also discretized with serendipity shape functions (S_2 element) in order to match both fluid and solid finite element meshes. With a matching fluid-structure mesh, the evaluation of the fluid loads at the structural boundaries is straightforward and no extra interpolation techniques are needed. The finite element model for the structure is used here as

$$\mathbf{K}_s \mathbf{u}_s = - \{ [\mathbf{K}_f + \mathbf{K}_T(\mathbf{v}_f)] \mathbf{v}_f - \mathbf{Q} \mathbf{P}_f \}^{fsi}, \quad (5.22)$$

where \mathbf{K}_s is the finite element matrix for the structure and \mathbf{u}_s is the displacements vector. The FSI loads $\{ [\mathbf{K}_f + \mathbf{K}_T(\mathbf{v}_f)] \mathbf{v}_f - \mathbf{Q} \mathbf{P}_f \}^{fsi}$ are evaluated as fluid reaction forces at the fluid-structure interfaces S_{fs} .

In order to model the fluid-structure interaction, two assumptions are made: incompressible fluid and structure are at steady state; and small structural displacements and deformations are considered. Thus, the control volumes of the fluid domain before and after structural deformation are identical.

These assumptions leads the fluid-structure interaction problem of this work to be one-way coupled, as mentioned previously. This means that the fluid velocities and pressures imply loads on the structure, but the structural displacements and deformations are considered linear and small and do not alter the fluid flow domain. The following items summarize the fluid-

structure algorithm in the manner it is implemented in this work.

1. Discretize the fluid and the solid domains Ω_f and Ω_s , respectively, with Q2rP1 mixed finite elements for the fluid and eight nodes serendipity quadrilateral elements S_2 for the structure.
2. Apply the boundary conditions from Equations 5.4, 5.5, 5.6 and 5.14 and solve Equation 5.15, if the incompressible Navier-Stokes flow is considered, or Equation 5.20, if Stokes flow is considered.

If Navier-Stokes is considered, use a Newton-Raphson solver with solution step:

$$\mathbf{V}_{NS}^{k+1} = \mathbf{V}_{NS}^k - \frac{f(\mathbf{V}_{NS}^k)}{F'(\mathbf{V}_{NS}^k)}, \quad (5.23)$$

where \mathbf{V}_{NS}^k is the k th approximation of the solution of function f . In FEM context, the function f is the residual and F' the first order derivative of f with respect to the solution \mathbf{V}_{NS} . Here,

$$f(\mathbf{V}_{NS}^k) = \begin{bmatrix} \mathbf{K}_f + \mathbf{K}_T(\mathbf{v}_f) & -\mathbf{Q} \\ -\mathbf{Q} & \mathbf{0} \end{bmatrix} \begin{Bmatrix} \mathbf{v}_f \\ \mathbf{P}_f \end{Bmatrix} - \begin{Bmatrix} \mathbf{f}_{bc} \\ \mathbf{0} \end{Bmatrix}, \quad (5.24)$$

where \mathbf{f}_{bc} is the force vector after applying the Dirichlet boundary condition (Equation 5.4),

$$F'(\mathbf{V}_{NS}^k) = \begin{bmatrix} \mathbf{K}_f + \mathbf{K}_T(\mathbf{v}_f) & -\mathbf{Q} \\ -\mathbf{Q} & \mathbf{0} \end{bmatrix}, \quad (5.25)$$

and

$$\mathbf{V}_{NS}^k = \begin{Bmatrix} \mathbf{v}_f \\ \mathbf{P}_f \end{Bmatrix}. \quad (5.26)$$

3. Calculate the FSI loads \mathbf{f}^{fsi} by evaluating the fluid reaction forces $\{[\mathbf{K}_f + \mathbf{K}_T(\mathbf{v}_f)] \mathbf{v}_f - \mathbf{Q} \mathbf{P}_f\}^{fsi}$ at the fluid-structure interface S_{fs} .
4. Solve linear elasticity from Equation 5.22 to obtain the structural displacements \mathbf{u}_s .

5.3 Topology optimization problems

Here, both fluid flow energy dissipation and structural compliance minimization for FSI problems are formulated. Fluid flow energy dissipation minimization is first carried out. The aim is to obtain optimal fluid paths or channels. These patterns are then discretized as linear structures and dry topology optimization is carried out. Finally, wet optimization cases are explored in order to evidence the features of the extended fluid-structure BESO method.

5.3.1 Pressure drop minimization

Fluid flow drag or pressure drop (energy dissipation) minimization can be carried out by minimizing the potential power of the fluid flow. Here, we consider the potential power of Stokes flows (Evgrafov, 2005). The evolutionary topology optimization problem for this case can be formulated as:

$$\begin{aligned}
 \min_{x_i} \quad & D(x_i) = \frac{1}{2} \mathbf{v}_f^T \mathbf{K}_f \mathbf{v}_f, \\
 \text{subject to:} \quad & \begin{bmatrix} \mathbf{K}_f & -\mathbf{Q} \\ -\mathbf{Q} & \mathbf{0} \end{bmatrix} \begin{Bmatrix} \mathbf{v}_f \\ \mathbf{P}_f \end{Bmatrix} = \begin{Bmatrix} \mathbf{0} \\ \mathbf{0} \end{Bmatrix} \text{ and b.c.,} \\
 & h = V(x_i) / V_0 = V_f, \\
 & x_i = [0, 1],
 \end{aligned} \tag{5.27}$$

where $D(x_i)$ is the fluid potential power function, \mathbf{v}_f and \mathbf{P}_f are the velocity and pressure vectors, respectively, and \mathbf{K}_f and \mathbf{Q} are fluid matrices which discretize Darcy-Stokes equations. The term V_0 is the volume of the full design domain, V_f is the prescribed final fluid volume fraction, nel is the number of elements inside the design domain and x_i represents the discrete design variables, in which 1 is a fluid with low porosity and 0 is a fluid with high porosity (representing a rigid solid element). Thus, in this case, fluids with low porosity allow the viscous fluid to flow and represent the optimal fluid path, while fluids with high porosity are considered as rigid walls in this model.

5.3.2 Sensitivity analysis: Pressure drop minimization

The sensitivity of the potential power can be obtained by direct derivation of $D(x_i)$:

$$\frac{\partial D}{\partial x_i} = \mathbf{v}_f^T \mathbf{K}_f \frac{\partial \mathbf{v}_f}{\partial x_i} + \frac{1}{2} \mathbf{v}_f^T \frac{\partial \mathbf{K}_f}{\partial x_i} \mathbf{v}_f. \tag{5.28}$$

In this model, a velocity profile is given at inlet as a constant boundary condition value $\mathbf{v}_f = \mathbf{v}_0$. In this case,

$$\mathbf{v}_f = \mathbf{v}_0 \Rightarrow \frac{\partial \mathbf{v}_f}{\partial x_i} = 0. \tag{5.29}$$

At the other hand, when Dirichlet boundary conditions are imposed, in this case $\mathbf{v}_f = \mathbf{v}_0$, a load vector \mathbf{f}_f is applied to guarantee the equilibrium of the equation. The derivatives of \mathbf{f}_f are not zero, though. However, they are disregarded here. Returning to Equation 5.28, one can write

the sensitivity of the objective function $D(x_i)$, similarly presented by Bendsoe and Sigmund (2003), as

$$\frac{\partial D}{\partial x_i} = \frac{1}{2} \mathbf{v}_f^T \frac{\partial \mathbf{K}_f}{\partial x_i} \mathbf{v}_f. \quad (5.30)$$

The derivative of matrix \mathbf{K}_f evaluated locally at the element level can be directly expressed as

$$\frac{\partial \mathbf{K}_f}{\partial x_i} = \frac{d\alpha(x_i)}{dx_i} \mathbf{K}_\alpha, \quad (5.31)$$

$$\frac{d\alpha(x_i)}{dx_i} = (\alpha_L - \alpha_U) q \frac{(1+q)}{(x_i + q)^2}, \quad (5.32)$$

where \mathbf{K}_α is the finite element matrix which discretize the Brinkman term in Darcy-Stokes equations and α_L , α_U and q are the related parameters of the model. Then, rewriting Equation 5.30, the sensitivity number for pressure drop minimization in Darcy-Stokes flow can be stated as following:

$$\alpha_i = \frac{1}{2} \frac{\partial D}{\partial x_i} = (\alpha_L - \alpha_U) q \frac{(1+q)}{(x_i + q)^2} \mathbf{v}_i^T \mathbf{K}_\alpha \mathbf{v}_i, \quad (5.33)$$

where the subscript i indicates the values of \mathbf{v}_f at the nodal element level.

Simplifying Equation 5.33, for $x_i = 1$ and $x_1 = 0$, one can rewrite the sensitivity numbers for pressure drop minimization as

$$\alpha_i = \begin{cases} (\alpha_L - \alpha_U) \frac{q}{(1+q)} \mathbf{v}_i^T \mathbf{K}_\alpha \mathbf{v}_i & x_i = 1 \\ (\alpha_L - \alpha_U) \frac{(1+q)}{q} \mathbf{v}_i^T \mathbf{K}_\alpha \mathbf{v}_i & x_i = 0 \end{cases} \quad (5.34)$$

In practice, both sensitivity numbers are very similar, since the parameter value $q = 1$ is used in this work. However, for elements with $x_i = 0$, the flow undergoes a high porosity fluid and the velocity field at those elements are nearly zero, which diminishes the sensitivities at these regions.

5.3.3 Structural compliance minimization under FSI loads

The dry and wet topology optimization cases considered in this work concern structural compliance minimization under viscous fluid flow loads and volume constraints. The fluid model considered is governed by the incompressible Navier-Stokes equations. The evolutionary

topology optimization problem for this case can be formulated as:

$$\begin{aligned}
 \min_{x_i} \quad & C(x_i) = \frac{1}{2} \mathbf{u}_s^T \mathbf{K}_s \mathbf{u}_s \\
 \text{subject to:} \quad & \mathbf{K}_s \mathbf{u}_s = - \{ [\mathbf{K}_f + \mathbf{K}_T(\mathbf{v}_f)] \mathbf{v}_f - \mathbf{Q} \mathbf{P}_f \}^{f si} \\
 & h = V(x_i) / V_0 = V_s \\
 & x_i = [0,1]
 \end{aligned} \tag{5.35}$$

where $C(x_i)$ is the structural mean compliance, \mathbf{K}_s and \mathbf{u}_s are the stiffness matrix and the displacement vector of the structure, respectively. Pressure and viscous loads are imposed as tractions in the linear structural analysis using the Navier-Stokes fluid model by the matrices \mathbf{K}_f , $\mathbf{K}_T(\mathbf{v}_f)$, \mathbf{Q} , \mathbf{v}_f and \mathbf{P}_f . When inertia terms are neglected and only Stokes flow is considered, $\mathbf{K}_T(\mathbf{v}_f) = 0$. The term V_0 is the full design domain volume, V_s is the prescribed final solid volume, nel is the number of elements inside the design domain and x_i represents the discrete design variables, in which 1 is a solid element and 0 is void or an occupying fluid.

5.3.4 Sensitivity analysis: Structural compliance minimization

The sensitivity of the structural compliance due to an element removal can be obtained by its derivative:

$$\frac{\partial C}{\partial x_i} = \mathbf{u}_s^T \mathbf{K}_s \frac{\partial \mathbf{u}_s}{\partial x_i} + \frac{1}{2} \mathbf{u}_s^T \frac{\partial \mathbf{K}_s}{\partial x_i} \mathbf{u}_s. \tag{5.36}$$

The equilibrium equation of the structural system (Equation 5.22) can be derived in order to find the unknown $\partial \mathbf{u}_s / \partial x_i$:

$$\frac{\partial (\mathbf{K}_s \mathbf{u}_s)}{\partial x_i} = - \frac{\partial \{ [\mathbf{K}_f + \mathbf{K}_T(\mathbf{v}_f)] \mathbf{v}_f - \mathbf{Q} \mathbf{P}_f \}}{\partial x_i}. \tag{5.37}$$

Considering that, the change in the pressure \mathbf{P}_f and the velocity \mathbf{v}_f due to a solid element removal is small enough or even inexistent, its derivative is considered to be zero. Applying the chain rule on the left side of the previous equation and deriving the right side, one have

$$\frac{\partial \mathbf{K}_s}{\partial x_i} \mathbf{u}_s + \mathbf{K}_s \frac{\partial \mathbf{u}_s}{\partial x_i} = - \frac{\partial \mathbf{K}_f}{\partial x_i} \mathbf{v}_f - \frac{\partial \mathbf{K}_T(\mathbf{v}_f)}{\partial x_i} \mathbf{v}_f + \frac{\partial \mathbf{Q}}{\partial x_i} \mathbf{P}_f. \tag{5.38}$$

Isolating the derivative of the displacement vector:

$$\frac{\partial \mathbf{u}_s}{\partial x_i} = \mathbf{K}_s^{-1} \left(- \frac{\partial \mathbf{K}_f}{\partial x_i} \mathbf{v}_f - \frac{\partial \mathbf{K}_T(\mathbf{v}_f)}{\partial x_i} \mathbf{v}_f + \frac{\partial \mathbf{Q}}{\partial x_i} \mathbf{P}_f - \frac{\partial \mathbf{K}_s}{\partial x_i} \mathbf{u}_s \right). \tag{5.39}$$

With the substitution of Equation 5.39 in Equation 5.36, one can rewrite the compliance derivative as

$$\frac{\partial C}{\partial x_i} = \mathbf{u}_s^T \mathbf{K}_s \mathbf{K}_s^{-1} \left(-\frac{\partial \mathbf{K}_f}{\partial x_i} \mathbf{v}_f - \frac{\partial \mathbf{K}_T(\mathbf{v}_f)}{\partial x_i} \mathbf{v}_f + \frac{\partial \mathbf{Q}}{\partial x_i} \mathbf{P}_f - \frac{\partial \mathbf{K}_s}{\partial x_i} \mathbf{u}_s \right) + \frac{1}{2} \mathbf{u}_s^T \frac{\partial \mathbf{K}_s}{\partial x_i} \mathbf{u}_s. \quad (5.40)$$

The product $\mathbf{K}_s \mathbf{K}_s^{-1}$ becomes the identity. Then, multiplying and making the summation of the terms, the sensitivity of the objective function is expressed as

$$\frac{\partial C}{\partial x_i} = -\mathbf{u}_s^T \frac{\partial \mathbf{K}_f}{\partial x_i} \mathbf{v}_f - \frac{\partial \mathbf{K}_T(\mathbf{v}_f)}{\partial x_i} \mathbf{v}_f + \mathbf{u}_s^T \frac{\partial \mathbf{Q}}{\partial x_i} \mathbf{P}_f - \frac{1}{2} \mathbf{u}_s^T \frac{\partial \mathbf{K}_s}{\partial x_i} \mathbf{u}_s. \quad (5.41)$$

To evaluate the sensitivity from Equation 5.41 at the elemental level, the variation of the stiffness, $\partial \mathbf{K}_s / \partial x_i$, must be found. Similarly to Chapters 2 and 3 of this thesis, using a hard-kill approach, the material is simply defined by its design variable as

$$E_i = x_i E^0, \quad (5.42)$$

and,

$$\mathbf{K}_s = \sum_{i=1}^{nel} x_i \mathbf{K}_s^i, \quad (5.43)$$

where E^0 denotes the Young's modulus of the solid material and \mathbf{K}_s^i is the i th element stiffness matrix. Thus, the derivative of the structural stiffness matrix with respect to the design variable of the i th element is expressed as

$$\frac{\partial \mathbf{K}_s}{\partial x_i} = \mathbf{K}_s^i, \quad (5.44)$$

when $x_i = 1$. For void/fluid elements, $x_i = 0$, this derivative is null.

The derivatives of the other terms from Equation 5.41 represent the changes in the fluid domain due to the removal of the i th element. These changes occur only in the fluid-structure interface, since the fluid domain is changed only when solid elements at the interface are removed. It is assumed that pressure values are transferred throughout the element when a solid is replaced by a fluid, characterizing a design-dependent load, similarly as presented by Picelli *et al.* (2015b) for pressure loading problems. However, this is not valid for the velocity values, since there are no-slip boundary conditions at the fluid walls. Even though a fluid element replaces a solid one at the interface, the fluid velocities at that element are still zero. Thus, it is assumed the hypothesis that the terms multiplied by \mathbf{v}_f in the sensitivity expressed by Equation 5.41 vanish at the element level. For the third term, multiplied by \mathbf{P}_f , the derivative of the

incompressibility matrix is expressed as

$$\frac{\partial \mathbf{Q}}{\partial x_i} = \mathbf{Q}^i, \quad (5.45)$$

where \mathbf{Q}^i is the fluid elemental incompressibility matrix. It represents an addition of a fluid matrix in the problem, when a solid element at the fluid-structure interface is removed. Thus, the complete sensitivity numbers for stiffness maximization of structures under incompressible viscous fluid flow loads are

$$\alpha_i = -\frac{\partial C}{\partial x_i} = \begin{cases} \frac{1}{2} \mathbf{u}_i^T \mathbf{K}_s^i \mathbf{u}_i - \mathbf{u}_i^T \mathbf{Q}^i \mathbf{P}_i & x_i = 1 \\ 0 & x_i = 0 \end{cases}, \quad (5.46)$$

where the subscript i indicates the values of \mathbf{u}_s and \mathbf{P}_f at the element level.

This analysis is carried out for each element i in the design domain. For structural elements which are not at the fluid-structure interface, the pressure transferred by the occupying fluid is null and the term $\mathbf{u}_i^T \mathbf{Q}^i \mathbf{P}_i$ in Equation 5.46 vanishes, leading to the traditional number $\frac{1}{2} \mathbf{u}_i^T \mathbf{K}_s^i \mathbf{u}_i$, the elemental strain energy. The complete sensitivity number is evaluated then only for the solid elements at the fluid-structure interface. For the case of dry optimization, considering that the interfaces do not change during optimization, the second term of the sensitivities from Equation 5.46 can be disregarded.

5.4 Optimization procedures

For pressure drop minimization and “dry” structural topology optimization cases, the standard BESO approach (Xie and Huang, 2010) can be applied since no design-dependent physics occur in these problems. For “wet” structural topology optimization, the methodology described by Picelli *et al.* (2015b) can be extended for this type of fluid-structure interaction system. Following, these procedures are summarized for the present “wet” optimization case. For further numerical details, see Xie and Huang (2010); Picelli *et al.* (2015b).

5.4.1 The extended BESO method for fluid-structure interaction problems

The following algorithm lists the steps of extended the BESO method for “wet” structural compliance minimization in steady state and small displacements fluid-structure interaction problems.

1. Define design domain, loads and boundary conditions.
2. Define BESO parameters.
3. Discretize the design domain using a FE mesh for the given fluid and structure domains.
4. Apply the fluid boundary conditions and solve fluid flow FE Equations 5.15.
5. Identify the fluid flow loads considering the fluid-structure boundary conditions, apply the solid boundary condition and solve structural FE Equation 5.22.
6. Calculate the sensitivity numbers according to Equation 5.46.
7. Apply a filter scheme. Project the nodal sensitivity numbers on the finite element mesh and smooth the sensitivity numbers for all (fluid, void and solid) elements in the design domain.
8. Average the sensitivity numbers with their previous iteration numbers and save the resulting sensitivity numbers for the next iteration.
9. Determine the target structural volume V_{n+1} for the next iteration.
10. Construct a new fluid-structure design by switching design variables x_i from 1 to 0 and from 0 to 1, tracking the changes of the fluid-structure interfaces. Details of the material update scheme can be found in Xie and Huang (2010); Picelli *et al.* (2015b).
11. Assemble the global matrices according to the change of the current design.
12. Repeat steps 2-12 until the following stop criterion is satisfied:

$$\frac{|\sum_{k=1}^5 C_{n-k+1} - \sum_{k=1}^5 C_{n-5-k+1}|}{\sum_{i=1}^5 C_{n-k+1}} \leq \tau \quad (5.47)$$

where n is the current iteration number, C is the value of the objective function (structural compliance) and τ is a prescribed convergence tolerance.

5.5 Numerical results

In this section, numerical results are presented. Pressure drop minimization problems considering Darcy-Stokes flow are briefly explored with the BESO method. An “aerodynamic” profile obtained with this methodology is used as a structural profile for dry optimization considering both Navier-Stokes and Stokes flow loads. At last, “wet” optimization cases are explored. The focus of this work is on wet optimization, since this is the main contribution of the extended fluid-structure BESO method.

5.5.1 Pressure drop minimization

Benchmark examples

In order to validate the application of the BESO method to fluid flow pressure drop minimization, two benchmark examples are shown. Figure 5.5 presents the examples first proposed by Borrvall and Petersson (2003), pipe bend and double pipe models.

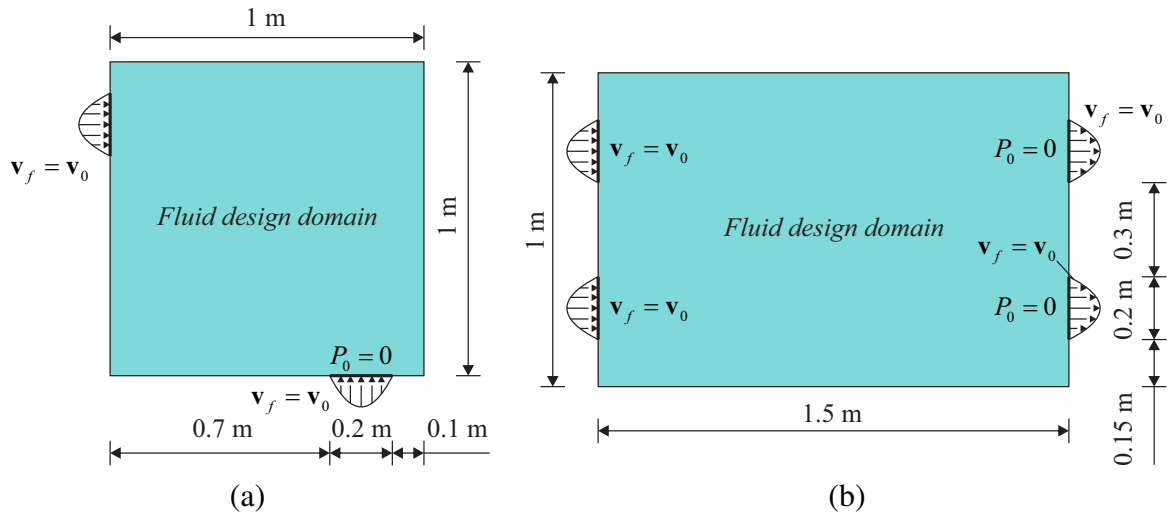


Figure 5.5: Benchmark examples for fluid flow pressure drop minimization: (a) pipe bend and (b) double pipe models.

Discretized Darcy-Stokes flow equations are used to obtain the responses of the fluid flow, velocities and pressures, \mathbf{v}_f and \mathbf{P}_f , respectively, using Q1P0 finite elements, one order lower than the element described in Section 5.2.3. The sensitivity numbers from Equation (5.34) are used to rank the efficiency of the fluid elements relative to the objective function. Starting from the initial full design domain, i.e., all elements begin as $x_i = 1$, BESO method iteratively removes and adds elements in the design domain towards the final prescribed volume fraction V_f . BESO parameters for the pipe bend model are set as $ER = 2\%$, $AR_{max} = 5\%$, $r_{min} = 0.04$ m, $V_f = 25\%$ and $\tau = 0.001$. For the double pipe model, $ER = 2\%$, $AR_{max} = 2\%$, $r_{min} = 0.06$ m, $V_f = 30\%$ and $\tau = 0.001$. Figure 5.6 presents the fluid flow paths obtained with the BESO method for both benchmark examples.

Both solutions are in accord with the literature, (Borrvall and Petersson, 2003; Challis and Guest, 2009). In each iteration, BESO's update scheme declares the next design variables distribution. Elements with $x_i = 0$ are set with a high porosity Brinkman coefficient, which drops down the velocity field in these elements nearly to zero and represent a rigid element in this optimization problem. The fluid flows then basically through the low porosity elements,

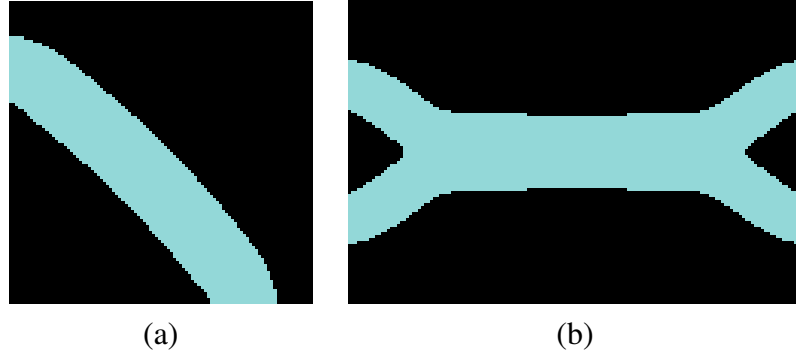


Figure 5.6: Fluid flow paths for (a) pipe bend and (b) double pipe models obtained with the BESO method and Darcy-Stokes equations.

where $x_i = 1$. It is observed that the solution evolves quickly to a topology similar to the final one when the volume constraint is reached. After that, the solution slowly moves towards the final topology taking quite many iterations to converge, as showed in Figure 5.7.

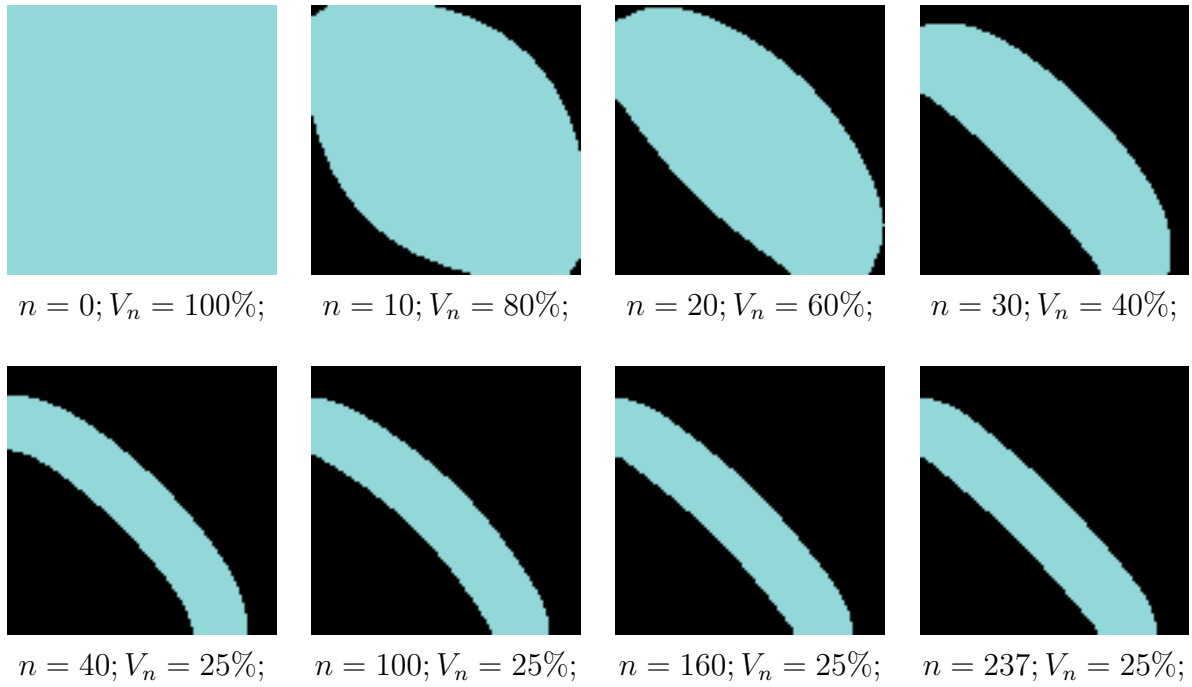


Figure 5.7: Topology evolution of the pipe bend example obtained with BESO method for pressure drop minimization.

Fluid flow with obstacles

This example considers a fluid flow with obstacles. BESO method should find the optimal fluid path which circumvents the obstacles (rigid walls) and present minimum pressure drop

(Koga, 2010). The fluid design domain is shown in Figure 5.8. Inlet and outlet velocity profile are set as $\mathbf{v}_f = \mathbf{v}_0 = 1 \text{ m/s}$. Fluid mass density and dynamic viscosity are $\rho_f = 1000 \text{ kg/m}^3$ and $\mu = 0.001 \text{ kg m}^{-1} \text{ s}^{-1}$, respectively.

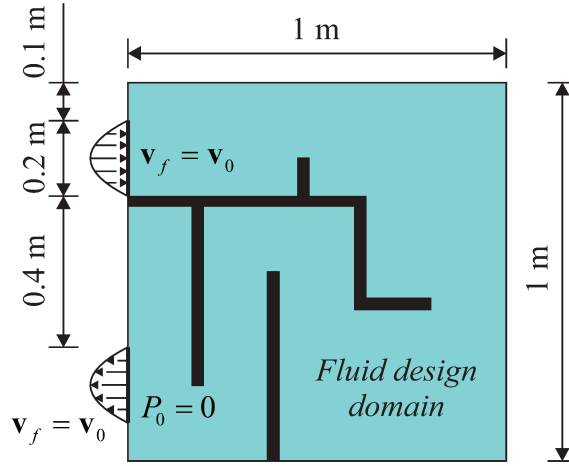


Figure 5.8: Fluid flow with obstacle example for pressure drop minimization.

BESO method started from the initial full design domain with an evolutionary ratio, $ER = 2\%$, towards a final fluid volume fraction, $V_f = 50\%$. The other parameters are set as $AR_{max} = 5\%$, $r_{min} = 0.04 \text{ m}$, $V_f = 50\%$ and $\tau = 0.001$. Figure 5.9 presents the fluid path solution for this example, as well as the velocity and pressure fields. Colourmap indicates response values, red for higher and blue for smaller velocities and pressures. The pressure field in this case is not continuous (see Figure 5.9(c)) due to the discretization by Q1P0 finite elements, which do not attend the *Ladyzenskaja-Babuska-Brezzi* (LBB) condition (Brezzi and Fortin, 1991). Higher order discretization or stabilization techniques are able to model continuous pressure fields, however the final solution do not change much, since the sensitivities are based only on the fluid velocities.

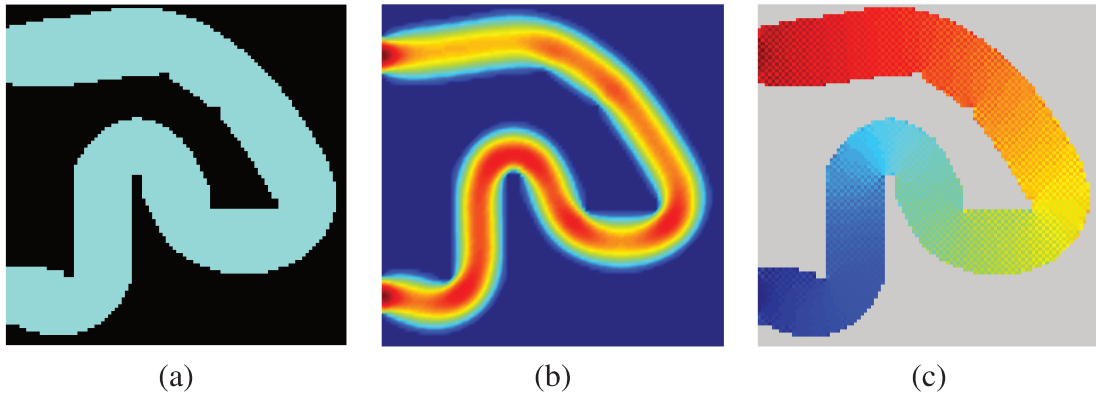


Figure 5.9: Fluid flow with obstacle: (a) final fluid path obtained with BESO method, (b) fluid velocity and (c) pressure fields.

Aerodynamic profile

The model illustrated in Figure 5.10 represents a fluid flowing with constant velocity profile, $\mathbf{v}_f = \mathbf{v}_0$. BESO method must find the fluid profile (with volume constraint) that minimizes pressure drop in the fluid flow. Such profile is expected to be aerodynamic, which is the geometry that tends to imply minimum change in the fluid flow streamlines.

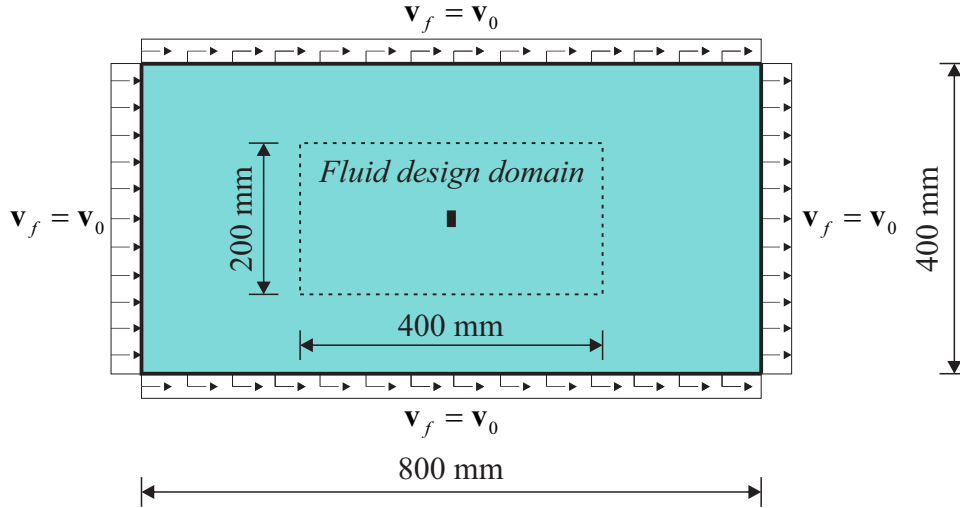


Figure 5.10: Fluid flow in a channel: example for aerodynamic profile.

A fluid design domain of 400×200 mm is centered in the model. A non-design domain, set as rigid elements, is centered in the model with dimension 1×2 mm. Starting with the full design domain, BESO parameters are set as $ER = 1\%$, $AR_{max} = 5\%$, $r_{min} = 0.02$ mm, $V_f = 80\%$ and $\tau = 0.0001$, while fluid mass density and dynamic viscosity are $\rho_f = 1000$ kg/m³ and $\mu = 0.001$ N·s/m², respectively. Figure 5.11 presents the final solution obtained with BESO method and the fluid flow streamlines. The wedge at the front and back of the optimal shape is of angle 90° , which is in accord with the solution presented by Borrvall and Petersson (2003) and also previously obtained by Pironneau (1973) with shape optimization.

5.5.2 Structural compliance minimization: “dry” optimization

The fluid profile of the previous example is used here for structural mean compliance minimization, considering the case of dry optimization. The rigid elements which builds the aerodynamic profile are substituted by linear elastic structural elements. The fluid flow is now governed by the incompressible Navier-Stokes equations and the one-way coupled FSI analysis is applied. This fluid-structure model is illustrated in Figure 5.12. The fluid boundary conditions are the same as in the previous example, except for the outlet, where only P_0 is set and no

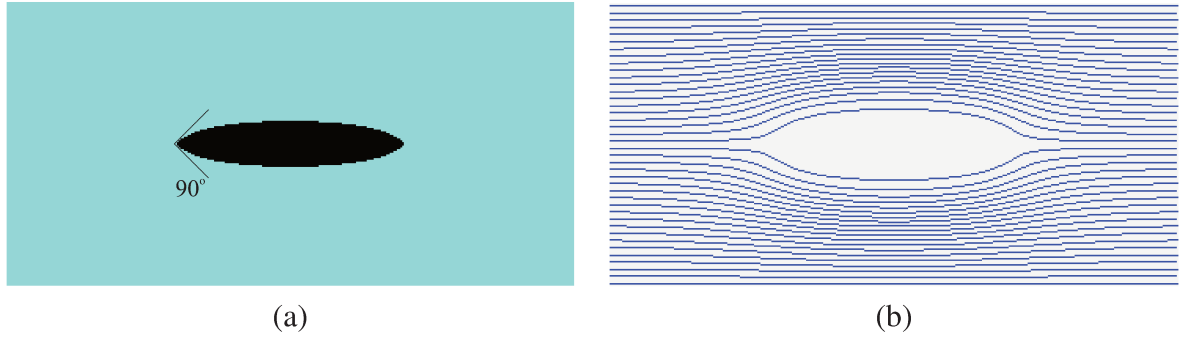


Figure 5.11: Aerodynamic example: (a) solution obtained with BESO method and (b) fluid flow streamlines.

velocity profile is imposed. At the other edges, a fluid velocity profile $\mathbf{v}_0 = 1$ m/s is applied.

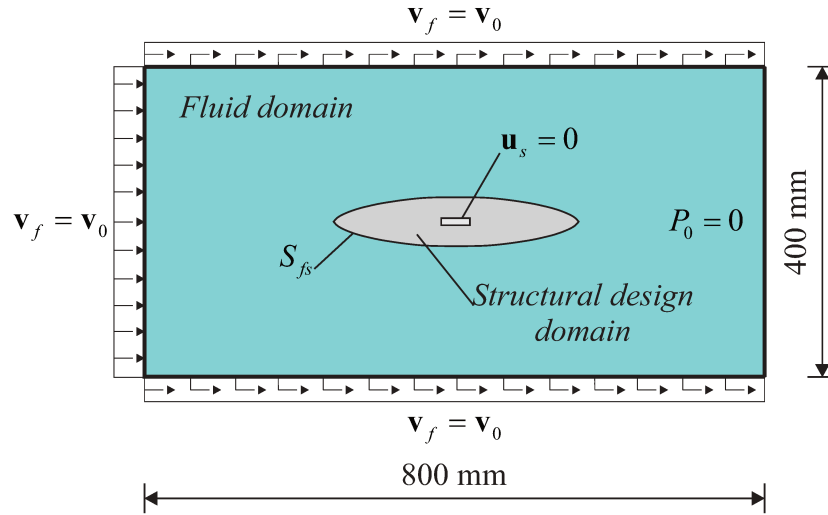


Figure 5.12: Fluid-structure model for “dry” structural topology optimization.

Structural compliance minimization is carried out considering a dry optimization case. The fluid-structure interfaces are not allowed to change during optimization. In this example, design variables are set as $x_i = 1$ for solid elements and $x_i = 0$ for void elements. Structural elements close to the fluid-interface are set as $x_i = 1$ during the whole optimization. The one-way coupled FSI problem turns the problem simpler, since the FSI loads do not change between the iterations. Thus, standard topology optimization procedures could be straightforwardly applied. Here, the BESO method is applied to this type of problems in its standard form and the examples are briefly shown. BESO parameters are set as $ER = 1\%$, $AR_{max} = 5\%$, $r_{min} = 0.0075$ mm, $V_f = 60\%$ and $\tau = 0.001$. The fluid density is chosen to be $\rho_f = 1000$ kg/m³ and its viscosity as $\mu = 0.001$ N·s/m². The Q2P1 finite element is used to discretize the fluid domain and the structure is discretized with standard serendipity S_2 finite elements. Figure 5.13(a) presents the structural topology obtained with BESO method considering Stokes fluid flow loads. Including inertia effects, Figure 5.13(b) presents the structure optimized considering

the full Navier-Stokes fluid flow loads.

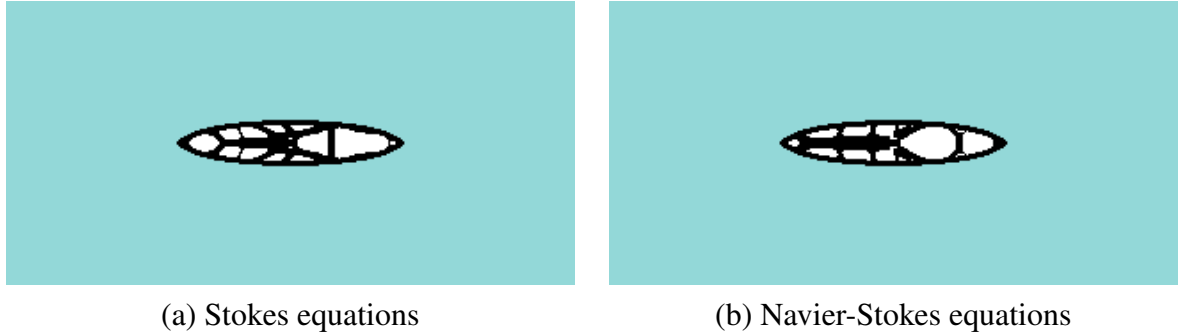


Figure 5.13: Solution for “dry” structural topology optimization of the aerodynamic profile considering: (a) Stokes fluid flow loads and (b) full Navier-Stokes fluid flow loads.

Both solutions showed to be quite different, presenting structural members with different relative inclinations. This is expected when comparing the Stokes flow, which neglects inertia terms, with full Navier-Stokes equations. Figure 5.14 presents the velocity and pressure fields for both type of flows. Stokes flow is a viscous driven flow, in which viscous and pressure loads acts, while in Navier-Stokes flow the loads are mainly pressure dominant. This is reflected in the structural topology, where inclined structural members arise to support the drag forces from the Stokes flow and, considering Navier-Stokes flow, structural members are distributed in order to support the high pressure field at the front of the aerodynamic profile. It indicates the complexity of the fluid-structure problem and how non-intuitive structural design can be in these cases.

5.5.3 Structural compliance minimization: “wet” optimization

The next examples explores the features of the extended BESO method in wet structural topology optimization of FSI problems. Results are presented considering both incompressible Stokes and Navier-Stokes fluid flow equations for the fluid field, discretized with Q2rP1 finite elements. The structure is considered linear elastic and is discretized with serendipity shape functions S_2 elements, in order to match nodes with the fluid domain. Thus, no interpolation schemes are needed in order to transfer the FSI loads through the domains.

Flexible structure immersed in a fluid flow channel

A viscous fluid flows through a microchannel with a flexible structure immersed obstructing the flow. The physical model is shown in Figure 5.15. A constant inlet velocity profile $\mathbf{v}_f = \mathbf{v}_0$ is considered. The pressure boundary condition is imposed at the outlet as $P_0 = 0$ and

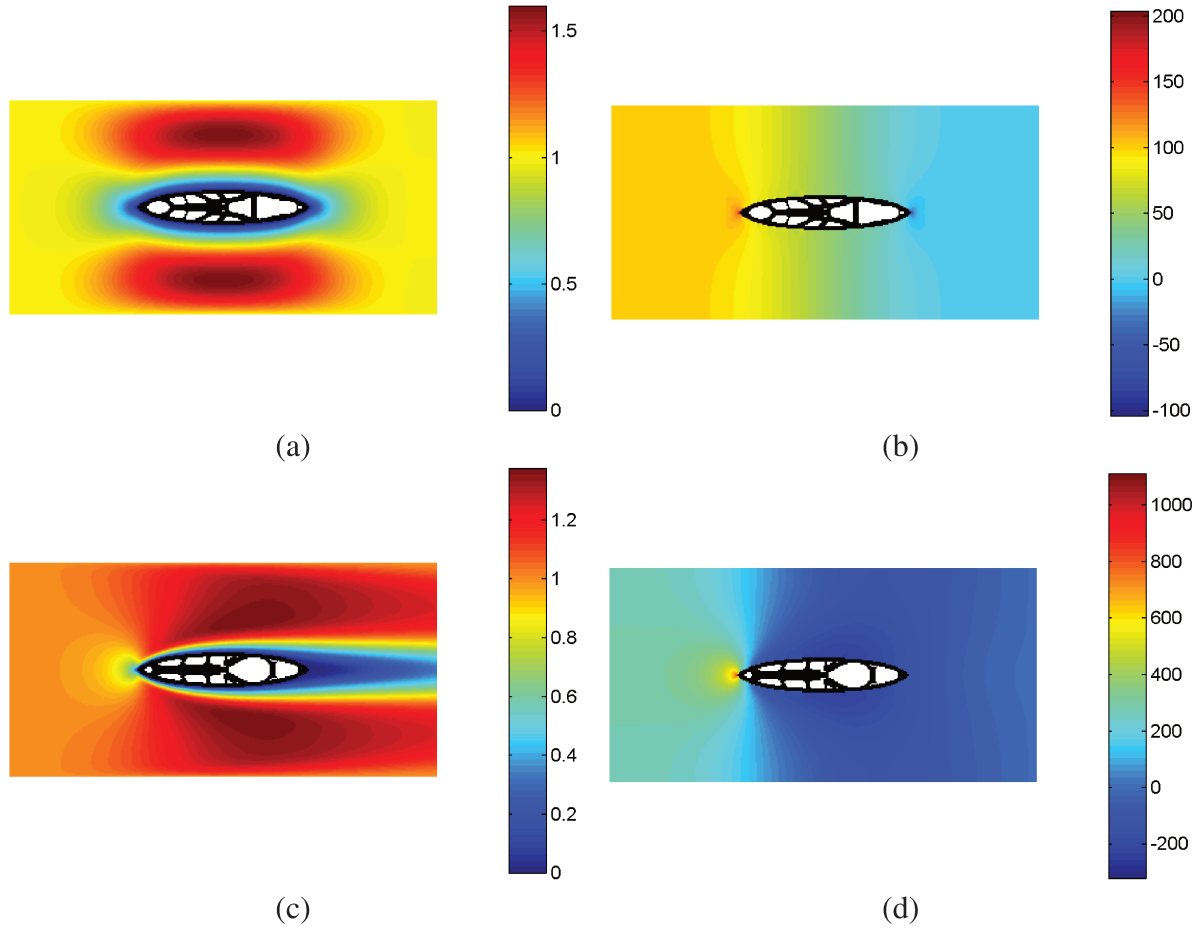


Figure 5.14: Fluid flow responses in the aerodynamic profile example: (a) velocity field and (b) pressure field considering incompressible Stokes flow equations and (c) velocity field and (d) pressure field considering incompressible Navier-Stokes flow equations.

no-slip conditions are imposed at the fluid flow walls. The fluid density is chosen to be $\rho_f = 1000 \text{ kg/m}^3$ and its viscosity as $\mu = 0.001 \text{ N}\cdot\text{s/m}^2$. The structural design domain is represented by a flexible structure of $60 \times 60 \mu\text{m}$, including a rectangular area of $50 \times 10 \mu\text{m}$ considered as a non-design domain in order to avoid trivial solutions. The elasticity modulus of the structure is chosen to be as $E = 3 \times 10^9 \text{ N/m}^2$ and the Poisson's ratio $\nu = 0.3$. This example is similar to the one presented by Yoon (2010) for compliance minimization considering design-dependent fluid flow loads.

The model is discretized with 25600 finite elements in total, being 2304 solid elements and the other 23296 ones modelling the fluid flow. The BESO method started from the initial full design domain with an evolutionary ratio $ER = 1\%$. The final solid volume is taken as $V_s = 30\%$ from the design domain, taking the non-design domain volume in account. The other BESO parameters are chosen to be $AR_{max} = 5\%$, $r_{min} = 7.5 \times 10^{-6} \text{ m}$, $\tau = 0.0001$ and $N = 5$. Figure 5.16 presents the structural topology solutions obtained with the extended BESO method for three different inlet velocity profiles: Case 1 with $v_0 = 0.0001 \text{ m/s}$, Case 2 with $v_0 = 0.1$

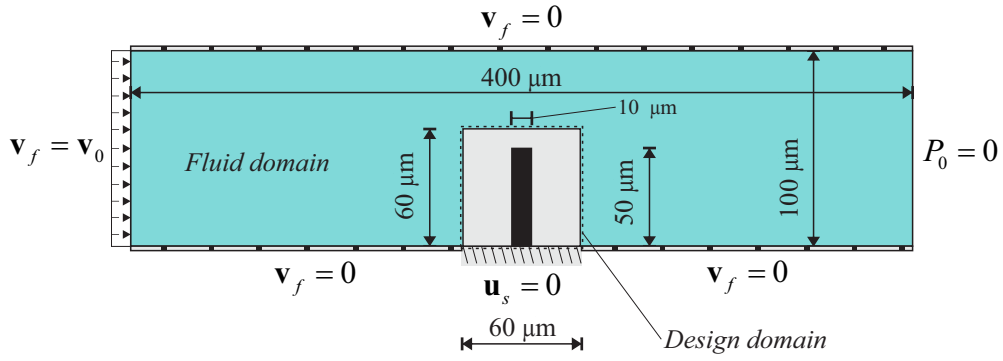


Figure 5.15: Structural design problem for a fluid flow channel.

m/s and Case 3 with $v_0 = 1$ m/s. For the smallest velocity profile (Case 1) considered, Stokes flow equations are used, since the inertia terms of Navier-Stokes equations tend to zero in such small velocity regime. For Cases 2 and 3, full incompressible Navier-Stokes equations are used.

(a) Case 1: $v_0 = 0.0001$ m/s
Stokes equations



(b) Case 2: $v_0 = 0.1$ m/s
Navier-Stokes equations



(c) Case 3: $v_0 = 1$ m/s
Navier-Stokes equations



Figure 5.16: Topology solutions obtained with BESO method for the structural barrier example with inlet velocities: (a) $v_0 = 0.0001$ m/s, (b) $v_0 = 0.1$ m/s and (c) $v_0 = 1$ m/s. The fluid flow in Case 1 is governed by incompressible Stokes flow equations and for Cases 2 and 3 the fluid flows are governed by incompressible Navier-Stokes equations.

The structures obtained with BESO method showed to be different for different fluid velocity regimes. This is expected, since the pressure and viscous loads are different for each case, implying in different structural deformation. Figure 5.17 presents the velocity and pressure responses for Cases 1, 2 and 3.

In each iteration, BESO's update scheme set a new distribution of design variables, x_i . Figure 5.18 presents snapshots of the topology evolution along the n th iterations for Case 1,

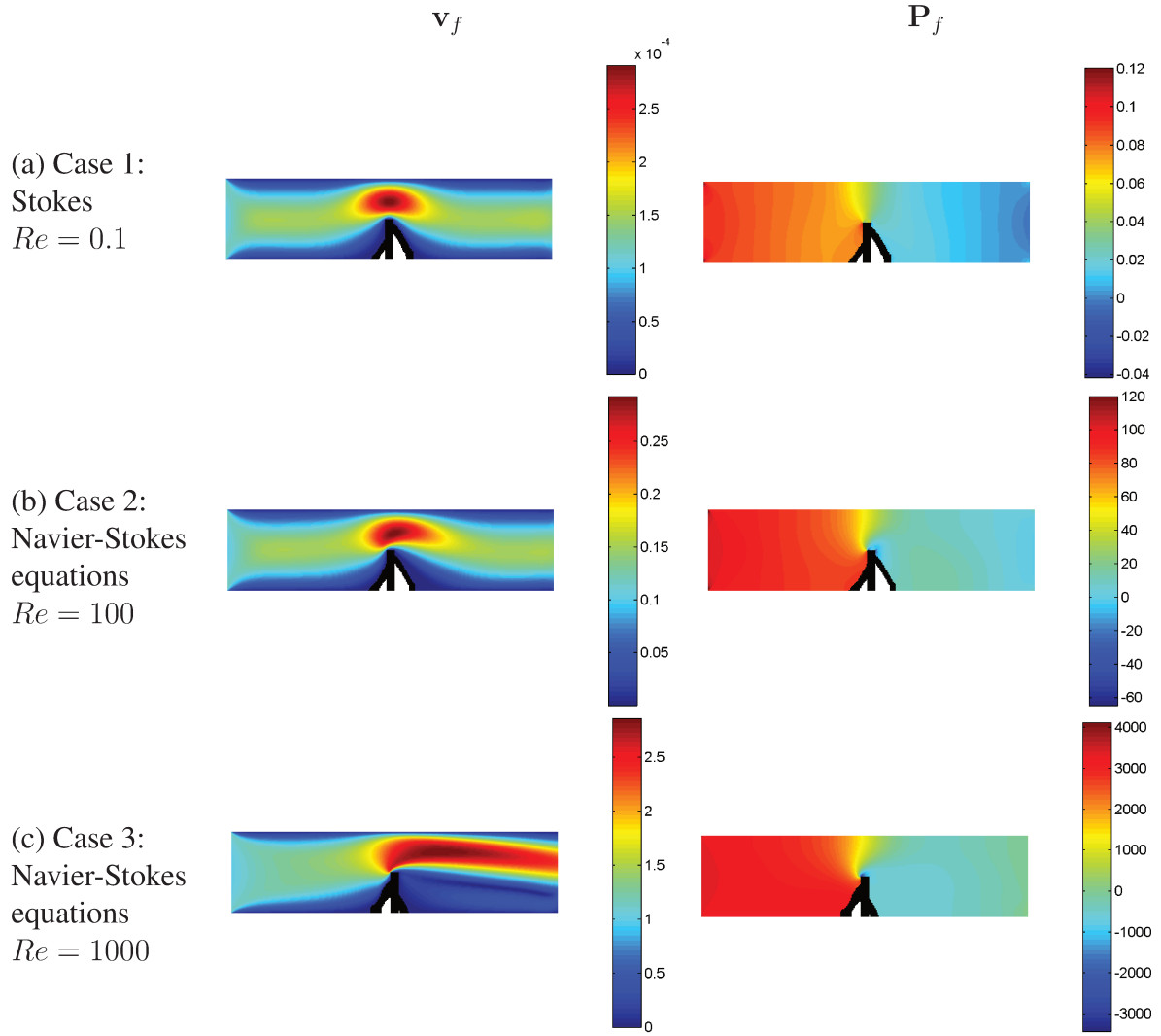


Figure 5.17: Velocity and pressure fields for the fluid flow in Cases 1, 2 and 3.

considering Stokes fluid flow loads.

Each iteration has a set of discrete design variables, $x_i = [0, 1]$. This discrete approach allows fluid elements to be placed inside the structural design domain, when $x_i = 0$. With new fluid elements arising, the fluid flows through a new domain and the fluid flow responses can change from one iteration to another, as illustrated in Figure 5.19 for Case 3. It characterizes the design-dependency of this optimization problem. When the fluid-structure interfaces are modified, loads on the structure (calculated with pressure and velocity responses) change their direction, location and magnitude.

The solution is said to be converged when the volume constraint and the convergence criterion are satisfied. For Case 1, considering small fluid velocities, the solution converged at 110th iteration to an almost constant value, as shown in Figure 5.20(a). For Case 3, with higher

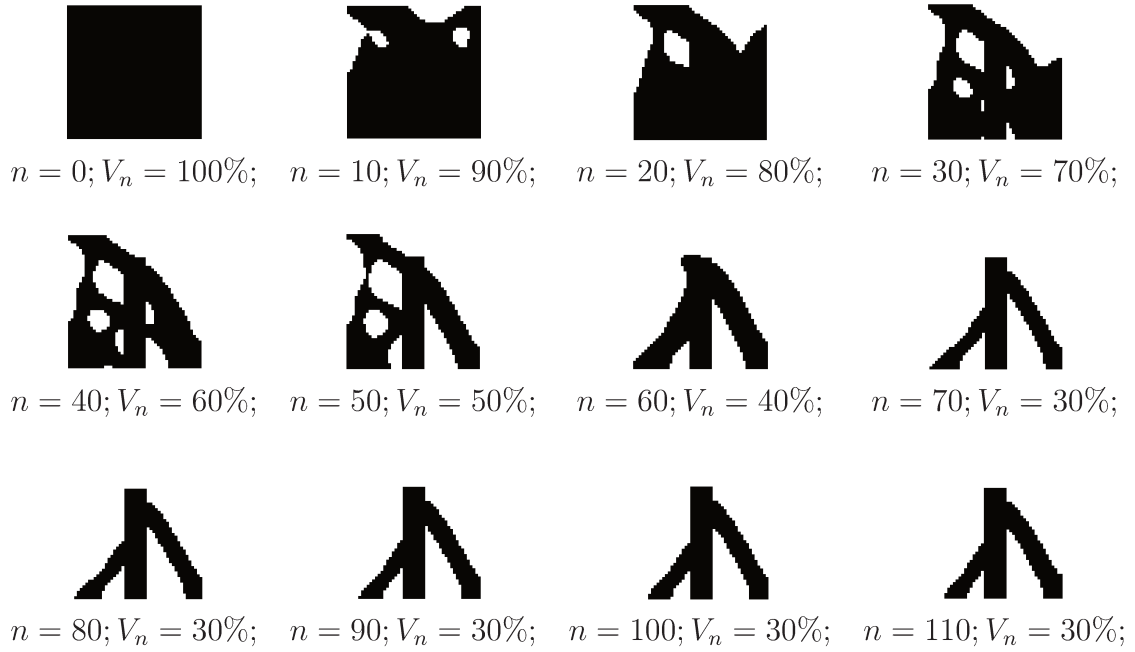


Figure 5.18: Topology evolution of the structural barrier obtained with BESO method in “wet” FSI topology optimization for Case 1.

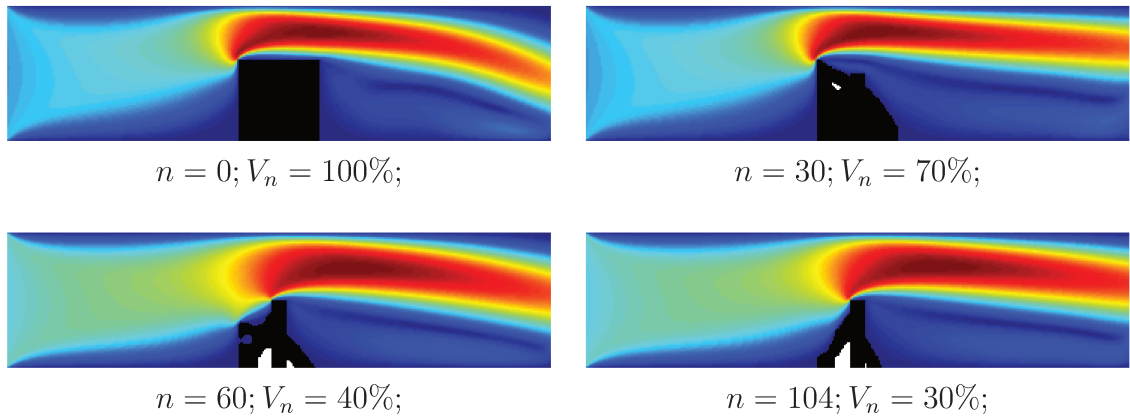


Figure 5.19: Topology and velocity field evolution of the structural barrier example in “wet” FSI topology optimization for Case 3.

fluid velocities, some oscillations in the objective function are observed in the final iterations, as shown in Figure 5.20(b).

Flow chamber design

This example considers a fluid-structure chamber design problem, identical to Example 2.5.3 - *Pressure chamber design* presented in Chapter 2 and similar to other topology opti-

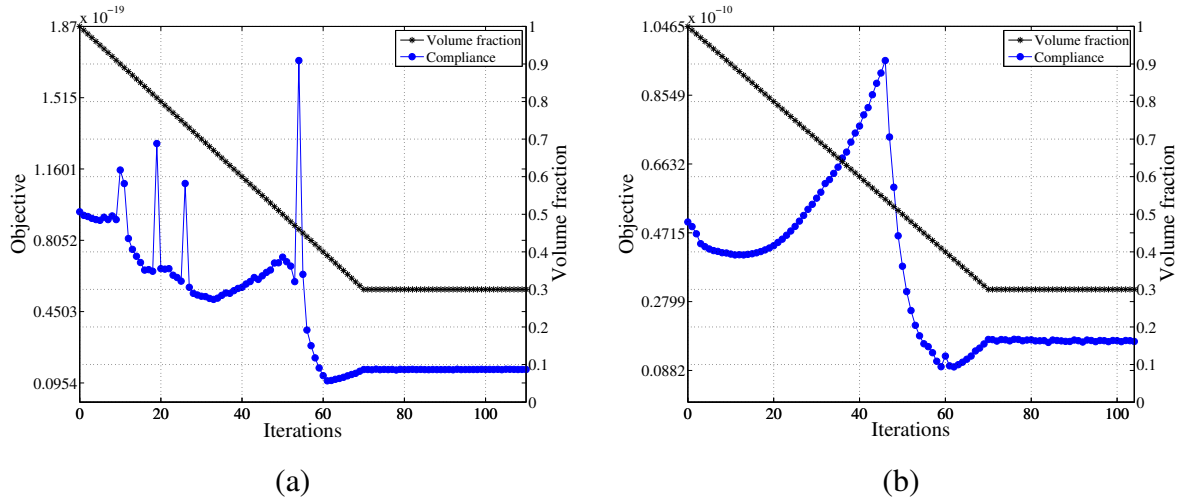


Figure 5.20: Topology and velocity field evolution of the structural barrier example in “wet” FSI topology optimization for: (a) Case 1 and (b) Case 3.

mization papers (Chen and Kikuchi, 2001; Zhang *et al.*, 2008), which consider only nonviscous pressure loads. The presented work explores the proposed design problem including viscous flow loads. The physical model is presented in Figure 5.21. In this example, the fluid is governed by incompressible Stokes flow equations. A linear elastic structure should be designed with volume constraints in order to support the FSI loads. The fluid density is chosen to be $\rho_f = 1000 \text{ kg/m}^3$ and its viscosity as $\mu = 0.001 \text{ N}\cdot\text{s/m}^2$ with inlet velocity $\mathbf{v}_0 = 1 \text{ m/s}$. No-slip boundary conditions are imposed at the fluid flow walls and the fluid-structure interface. Right after the inlet the fluid flows through two structural domains considered as elastic non-design domain. The model was discretized with 9152 finite elements in total, being 7648 solid elements and the other 1504 ones modelling the initial fluid flow. The elasticity modulus of the structure is chosen to be as $E = 7 \times 10^9 \text{ N/m}^2$ and the Poisson’s ratio $\nu = 0.3$.

BESO started from the initial full design domain with an evolutionary ratio $ER = 2\%$ until a prescribed structural volume fraction $V_s = 25\%$. The other BESO parameters are set as $AR_{max} = 5\%$, $r_{min} = 0.015 \text{ m}$, $\tau = 0.001$ and $N = 5$. Figure 5.22 presents the structural topology solution for the flow chamber design problem. Figure 5.23 presents snapshots of the topology solution and the fluid velocity fields during the optimization.

This example evidences the strong design-dependency between the structural topology evolution and the fluid flow in wet topology optimization. The fluid region is updated while structural elements are iteratively removed. Thus, viscous and pressure loads change their location, direction and magnitude during the optimization. Figure 5.24 compares the viscous fluid flow chamber design with the method which considers design-dependent fluid (nonviscous) pressure loads. The same design problem is considered for both cases. However, for the nonvis-

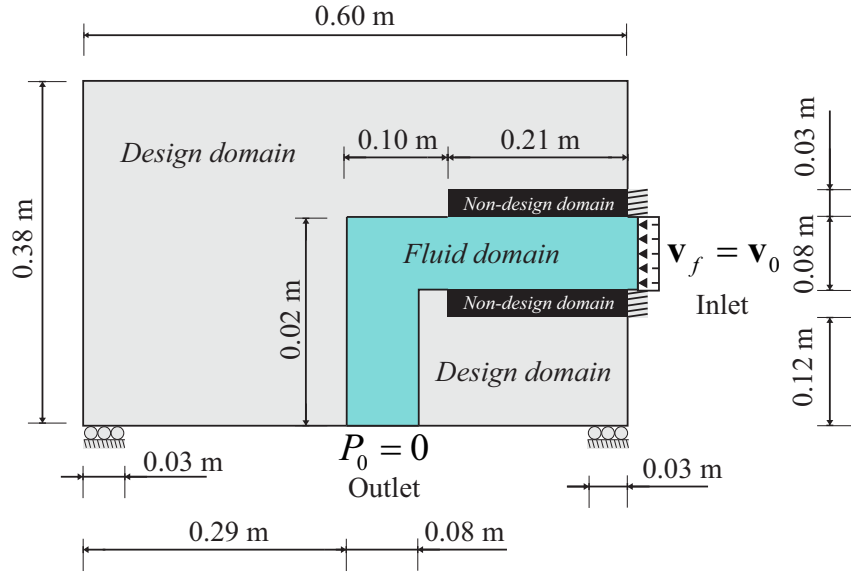


Figure 5.21: Structural design problem for a fluid flow chamber.



Figure 5.22: Structural topology solution for the flow chamber example.

cous case a pressure boundary condition is imposed at the inlet as $P_0 = 500$ Pa (similar value to the obtained with the Stokes flow inlet) and at the outlet as $P_0 = 0$. Although this is not a proper comparison, it indicates the behavior of the viscous flow loads. The minimum compliance solution obtained considering stokes flow loads presents bar-like structures while when considering a nonviscous fluid the obtained structure presents curved shapes.

5.6 Conclusions

The standard BESO method is applied to pressure drop minimization in Stokes flow problems in this work. Darcy-Stokes equations are used to model the fluid flow with Brinkman's porosity term, which facilitates the use of standard topology optimization methods. A profile can be obtained with such procedure. This profile obtained with BESO method is used in struc-

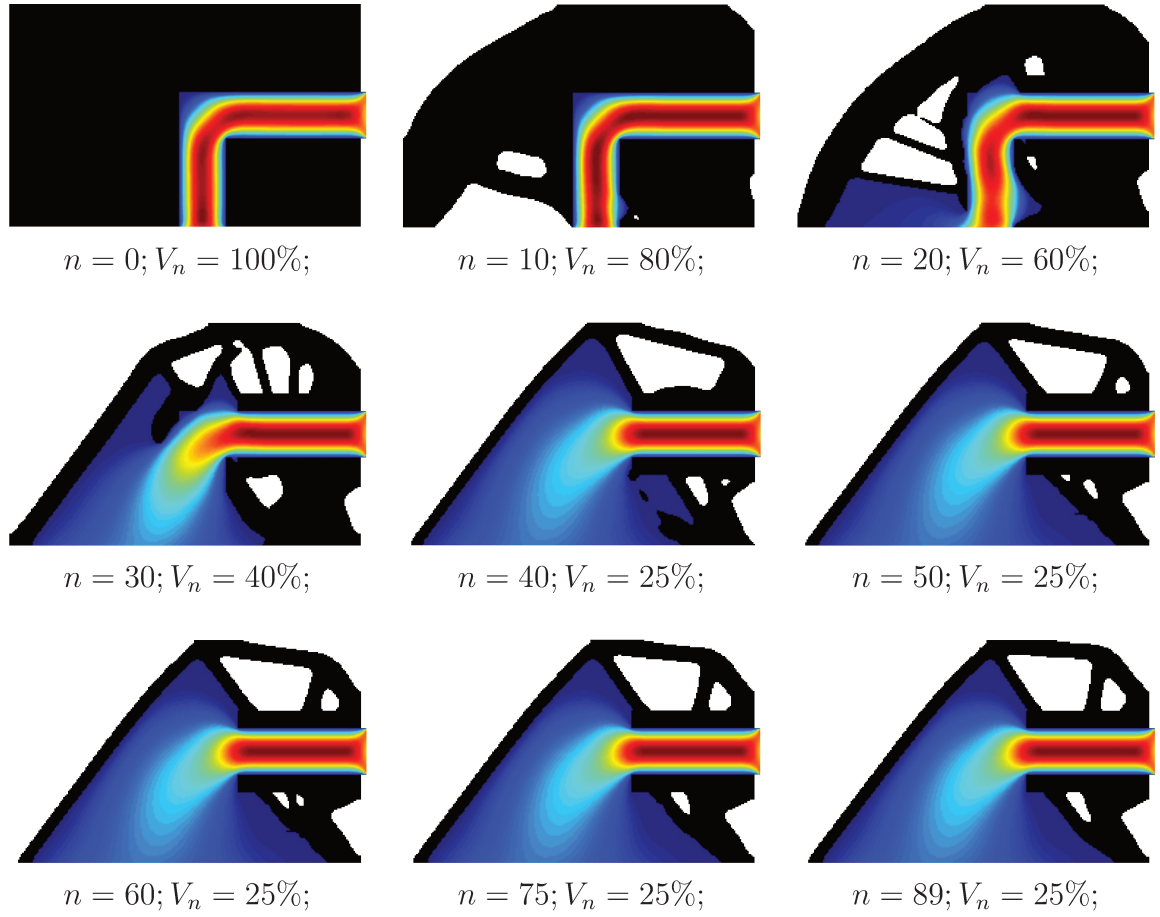


Figure 5.23: Snapshots of the structural topology solution and its velocity fields for the n th iterations.

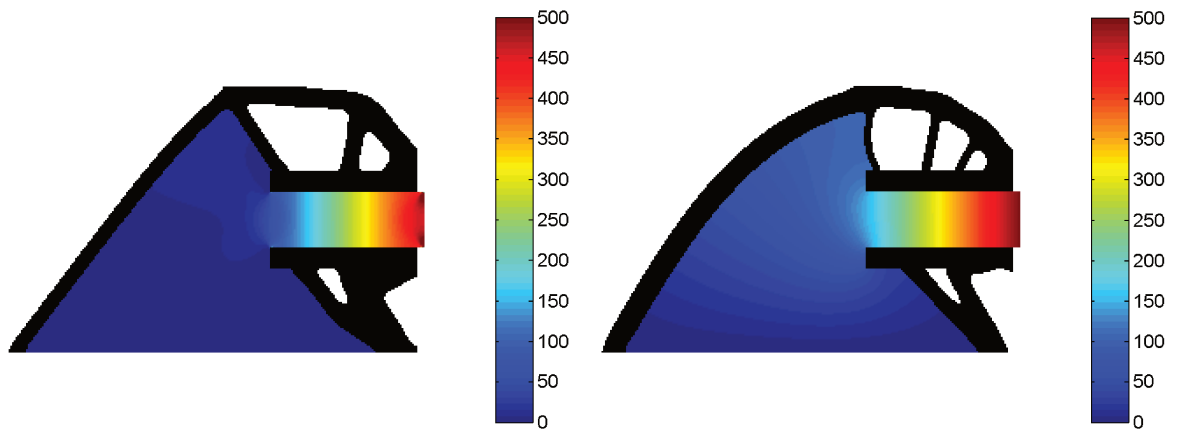


Figure 5.24: Structural topologies and pressure fields obtained considering loads from: (a) viscous fluid flow and (b) nonviscous pressurized fluid.

tural compliance minimization considering one-way coupled steady state FSI with Stokes and Navier-Stokes flow equations. Such procedures are already well established in the scientific literature, however are here first described with the evolutionary methods.

The main contribution in this work is the application of the proposed extended BESO method in “wet” structural topology optimization in FSI problems. The features of the evolutionary methods allow the switch between fluid and solid elements, which address the main challenge of dealing with moving fluid-structure boundaries during the optimization procedures. This represents the potential use in the area of fluid-structure interaction systems design. The results considered a flexible structure in contact with viscous fluid flows governed by incompressible Navier-Stokes equations. The structural topology is designed considering compliance minimization and design-dependent FSI loads. A steady state one-way coupled FSI model is used. This limits the applications of the proposed methodology to small deformation problems. The extension to more complex and robust FSI models are the future of this research. Different fluid discretizations, e.g. meshless methods, and nonlinear elasticity can be considered to improve the extended BESO method described in this thesis.

6 CONCLUDING REMARKS

In this chapter some concluding remarks are presented. General comments on the scientific contributions are outlined. The methodology developed and each topology optimization problem explored are discussed. Finally, some suggestions for future research are pointed out.

6.1 Summary and discussions

This thesis focused on contributing to the methods of *Structural Topology Optimization* in problems with design-dependent physics, one of the open research topics pointed out by the survey from Deaton and Grandhi (2014). Different design-dependent FSI models were used. An extension of the evolutionary optimization methods was developed in order to allow the switch between solid, fluid and void finite elements. The research was divided in four different topology optimization problems, each one introduced, formulated, solved and discussed with numerical results in separate chapters. Following, general conclusions concerning each optimization problem are given:

- Chapter 2: *Bi-directional evolutionary structural optimization for design-dependent fluid pressure loading problems*: This topology optimization problem aimed to design stiffest structures under constant and non constant fluid pressure fields. The main contribution to general topology optimization problems is that the technique developed here allows the handling of design-dependent fluid pressure loads straightforwardly, without any need of boundaries parametrization nor approximated multiphysics mixed models. Hydrostatic fluids and linear structural finite elements could be switched during the optimization procedures for the first time with separate domains by using a discrete optimization technique (BESO method). The use of separate domains allows the implementation of classic governing equations, which can be useful for the association of the present methodology with commercial FEM packages. The BESO method presented crisply defined fluid-structure interfaces, showed to be mesh-independent and solved efficiently the same benchmark examples presented by Hammer and Olhoff (2000); Chen and Kikuchi (2001); Sigmund and Clausen (2007) and others, with less than 70 iterations. The idea of using a coupled fluid-structure formulation can be extended to other multiphysics problems, such as the ones explored in the other chapters of this thesis and the extension to frequency responses by Vicente *et al.* (2015).
- Chapter 3: *Topology optimization for submerged buoyant structures*: This work aimed to apply the extended fluid-structure BESO method to design stiffest buoyant structures for

offshore pipelines support. Constant pressure fields were considered because of the deep-water condition of the buoyancy modules. Design-dependent fluid pressure loads were handled in the same manner as in the previous problem as well as the same governing equations were used. The main contribution to general topology optimization problems is the introduction of an inequality constraint which sets the minimum volume of the buoyant structure, represented by the sum of void and structural elements, at the same time as solving a design-dependent pressure loading problem. This also aims to improve the formulations of the evolutionary methods, since one of the main drawbacks of the ES-O/BESO methods is the difficulty in handling different constraints rather than the standard volume equality ones. With crisply defined and moving fluid-structure interfaces, a stiffer structure could be design in comparisons with a case with fixed interfaces. The methodology was validated with a test case and a subsea buoy design case, presenting bubble-like topologies and convergence with less than 60 iterations.

- Chapter 4: *Evolutionary topology optimization for natural frequency maximization problems considering acoustic-structure interaction*: The idea of switching fluid, structural and void elements was extended to acoustic-structure systems in free vibration problems. Coupled natural frequencies could be maximized as shown by several numerical results. The acoustic-structural physical model also allowed the modelling of open and closed acoustic cavities, which strongly influences the coupled modes. The main contribution to the evolutionary and general topology optimization problems is the handling of coupled free vibration problems, considering the maximization of coupled acoustic-structure natural frequencies in a global manner. Papers such as the one by Yoon *et al.* (2007) developed topology optimization for minimizing local responses. During this PhD research, Vicente *et al.* (2015) applied the idea of the extended BESO method to frequency responses minimization at some points (or areas) of the fluid or structural domains. The method presented crisp solutions with refined meshes and convergence with less than 45 iterations, except the case with crossing modes. This last also indicates a future step of this research, in which an algorithm to control crossing eigenmodes should be tested.
- Chapter 5: *Structural topology optimization considering stationary viscous fluid flow loads*: This topology optimization problem aimed to design stiffest structures under design-dependent viscous flow loads. As suggested by Jenkins and Maute (2015), the terms of “dry” and “wet” topology optimization problems in FSI were discussed. The “dry” optimization approach was explored with the standard BESO method and presented in this work. This characterizes an incremental scientific contribution, since the novelty is only the new application for the evolutionary methods. The main contribution in Chapter 5 to general topology optimization problems is the handling of the “wet” approach by using the idea of the extended fluid-structure BESO method. To the date of this thesis defense, only Yoon (2010) explored a “wet” optimization approach with topology op-

timization using a density-based method. Both works from Yoon (2010) and this thesis considered small displacements and deformations, which turns the fluid-structure interaction problem easier to be solved. A more robust algorithm can be used to consider the fully coupled FSI model in order to achieve more practical design problems. The same features of the presented methodology described in the previous chapters were observed in this FSI design problem, except the number of iterations after convergence, which reached up to 110.

In general, the extended fluid-structure BESO method showed to be efficient in solving topology optimization problems with design-dependent physics. The modelling of both fluid and structural fields with separate governing equations and finite element meshes can indicate other research directions or new possibilities in solving different multiphysics optimization problems.

6.2 Suggestions for further research

Following, some suggestions for further research are given:

- To apply the extended BESO method in different design-dependent physics problems, such as mass and heat transfer, acoustic absorption, eletromagnetics, compliant mechanisms, etc.
- To explore different equality and inequality constraints as well as the deepening of the proposed buoyancy inequality constraint.
- To implement the extended BESO method considering multiscale topology optimization.
- To construct 3D printed prototypes for experimental tests, specially in dynamic problems.
- To include different governing equations, such as acoustic absorption models, in order to develop an extended BESO method capable to optimize systems with four or more different finite elements during the optimization procedures, e.g., fluids, structures, voids and acoustic absorbers.
- To use other discretizations for the FSI models such as meshless methods, e.g., the *Smooth Particle Hydrodynamics* (SPH) method.
- To consider large structural displacements and deformations in the FSI problems with viscous flow loads as well as transient problems.
- To associate the extended BESO method with commercial FEM codes.

References

- AAGE, N.; POULSEN, T.H.; GERSBORG-HANSEN, A. and SIGMUND, O. Topology optimization of large scale Stokes flow problems. **Structural and Multidisciplinary Optimization**, v. 35, 175–180, 2008.
- ALEXANDERSEN, J.; AAGE, N.; ANDREASEN, C.S. and SIGMUND, O. Topology optimization for natural convection problems. **International Journal for Numerical Methods in Fluids**, v. 76, n. 10, 699–721, 2014.
- ALLAIRE, G.; JOUVE, F. and TOADER, A.M. Structural optimization using sensitivity analysis and a level-set method. **Journal of Computational Physics**, v. 194, 363–393, 2004.
- ALLEN, M. and MAUTE, K. Reliability-based shape optimization of structures undergoing fluid-structure interaction phenomena. **Computer Methods in Applied Mechanics and Engineering**, v. 194, 3472–3495, 2005.
- AMSTUTZ, S.; NOVOTNY, A.A. and NETO, E.A.S. Topological derivative-based topology optimization of structures subject to Drucker-Prager stress constraints. **Computer Methods in Applied Mechanics and Engineering**, v. 233-236, 123–136, 2012.
- ANDREASEN, C.S. and SIGMUND, O. Topology optimization of fluid-structure interaction problems in poroelasticity. **Computer Methods in Applied Mechanics and Engineering**, v. 258, 55–62, 2013.
- ANDREASSEN, E.; AAGE, N.; LAZAROV, B.S. and SIGMUND, O. Extremely large-scale topology optimization. In **Proceedings of the 11th World Congress of Structural and Multidisciplinary Optimization (WCSMO-11)**, Sydney, Australia. 2015.
- ANSOLA, R.; CANALES, J. and TÁRRAGO, J.A. An efficient sensitivity computation strategy for the evolutionary structural optimization (ESO) of continuum structures subjected to self-weight loads. **Finite Elements in Analysis and Design**, v. 42, 12220–1230, 2006.

AXISA, F. and ANTUNES, J. **Modelling of Mechanical Systems: Fluid-Structure Interaction**. Butterworth-Heinemann, Oxford, UK, 1st ed., 2007.

BATHE, K.J. **Finite Element Procedures**. Prentice Hall, Pearson Education, Inc., 2006.

BAZILEVS, Y.; TAKIZAWA, K. and TEZDUYAR, T.E. **Computational Fluid-Structure Interaction: Methods and Applications**. Wiley, 2013.

BENDSOE, M.P. Optimal shape design as a material distribution problem. **Structural Optimization**, v. 1, 193–202, 1989.

BENDSOE, M.P. **Optimization of Structural Topology, Shape and Material**. Springer, Berlin, 1995.

BENDSOE, M.P.; DIAZ, A.R. and KIKUCHI, N. **Topology and generalized layout optimization of elastic structures**, in *Topology Design of Structures*, pp. 159–206. Kluwer Academic Publishers, 1993.

BENDSOE, M.P. and KIKUCHI, N. Generating optimal topologies in structural design using a homogenization method. **Computer Methods in Applied Mechanics and Engineering**, v. 71, 197–224, 1988.

BENDSOE, M.P. and SIGMUND, O. **Topology Optimization - Theory, Methods and Applications**. Springer Verlag, Berlin Heidelberg, 2003.

BORRVALL, T. and PETERSON, J. Large-scale topology optimization in 3D using parallel computing. **Computer Methods in Applied Mechanics and Engineering**, v. 190, 6201–6229, 2001.

BORRVALL, T. and PETERSSON, J. Topology optimization of fluids in Stokes flow. **International Journal for Numerical Methods In Fluids**, v. 41, 77–107, 2003.

BOSMA, T. **Levelset Based Fluid-structure Interaction Modeling with the eXtended Finite Element Method**. 2013. Master of sciences thesis. Faculty of Mechanical, Maritime and Materials Engineering (3mE), Delft University of Technology.

BOURDIN, B. and CHAMBOLLE, A. Design-dependent loads in topology optimization. **ESAIM: Control, Optimisation and Calculus of Variations**, v. 9, 19–48, 2003.

BREZZI, F. and FORTIN, M. **Mixed and Hybrid Finite Element Methods**. Springer, Berlin, 1991.

BROOKS, A.N. and HUGHES, T.J.R. Streamline Upwind/Petrov-Galerkin formulations for convection dominated flows with particular emphasis on the incompressible Navier-Stokes equations. **Computer Methods in Applied Mechanics and Engineering**, v. 32, 199–259, 1982.

BRUGGI, M. and CINQUINI, C. An alternative truly-mixed formulation to solve pressure load problems in topology optimization. **Computer Methods in Applied Mechanics and Engineering**, v. 198, 1500–1512, 2009.

BRUNS, T.E. and TORTORELLI, D.A. Topology optimization of non-linear elastic structures and compliant mechanisms. **Computer Methods in Applied Mechanics and Engineering**, v. 190, n. 26-27, 3443–3459, 2001.

BRUYNEEL, M. and DUYSINX, P. Note on topology optimization of continuum structures including self-weight. **Structural and Multidisciplinary Optimization**, v. 29, 245–256, 2005.

BUHL, T.; PEDERSEN, C.B. and SIGMUND, O. Stiffness design of geometrically non-linear structures using topology optimization. **Structural and Multidisciplinary Optimization**, v. 19, n. 2, 93–104, 2000.

CÉA, J.; GARREAU, S.; GUILLAUME, P. and MASMOUDI, M. The shape and topological optimization connection. **Computer Methods in Applied Mechanics and Engineering**, v. 188, 713–725, 2000.

CHALLIS, V.J. and GUEST, J.K. Level set topology optimization of fluids in Stokes flow. **International Journal for Numerical Methods In Engineering**, v. 79, 1284–1308, 2009.

CHANG, C.C. Design and topology optimisation of fractal vasculature. In **Proceedings of the 11th World Congress of Structural and Multidisciplinary Optimization (WCSMO-11)**, Sydney, Australia. 2015.

CHAPMAN, C.D.; SAITOU, K. and JAKIELA, M.J. Genetic algorithms as an approach to configuration and topology design. **Journal of Mechanical Design, Transactions of ASME**, v. 116, 1005–1012, 1994.

CHEN, B.C. and KIKUCHI, N. Topology optimization with design-dependent loads. **Finite Elements in Analysis and Design**, v. 37, 57–70, 2001.

CHENG, G.D. and PEDERSEN, P. On sufficiency conditions for optimal design based on extremum principles of mechanics. **Journal of the Mechanics and Physics of Solids**, v. 45, n. 1, 135–150, 1997.

CHU, D.N.; XIE, Y.M.; HIRA, A. and STEVEN, G.P. Evolutionary structural optimization for problems with stiffness constraints. **Finite Elements in Analysis and Design**, v. 21, 239–251, 1996.

CHU, D.N.; XIE, Y.M.; HIRA, A. and STEVEN, G.P. On various aspects of evolutionary structural optimization for problems with stiffness constraints. **Finite Elements in Analysis and Design**, v. 24, 197–212, 1997.

CLAUSEN, A.; AAGE, N. and SIGMUND, O. Topology optimization with flexible void area. **Structural and Multidisciplinary Optimization**, v. 50, 927–943, 2014.

DE LEON, D.M.; ALEXANDERSEN, J.; FONSECA, J.S.O. and SIGMUND, O. Topology optimization of compliant mechanism design using a constraint on the maximum stress. In **Proceedings of the 11th World Congress of Structural and Multidisciplinary Optimization (WCSMO-11), Sydney, Australia**. 2015.

DEATON, J.D. and GRANDHI, R.V. A survey of structural and multidisciplinary continuum topology optimization: post 2000. **Structural and Multidisciplinary Optimization**, v. 49, 1–38, 2014.

DENG, Y.; LIU, Z. and WU, Y. Topology optimization of steady and unsteady incompressible Navier-Stokes flows driven by body forces. **Structural and Multidisciplinary Optimization**, v. 47, n. 4, 555–570, 2013.

DENG, Y.; LIU, Z.; ZHANG, P.; LIU, Y. and WU, Y. Topology optimization of unsteady

incompressible Navier-Stokes flows. **Journal of Computational Physics**, v. 230, 6688–6708, 2011.

DIAZ, A. and KIKUCHI, N. Solutions to shape and topology eigenvalue optimization problems using a homogenization method. **International Journal for Numerical Methods In Engineering**, v. 35, 1487–1502, 1992.

DIAZ, A. and SIGMUND, O. Checkerboard patterns in layout optimization. **Structural Optimization**, v. 10, 40–45, 1995.

DIAZ, A.R. and BENDSOE, M.P. Shape optimization of structures for multiple loading situations using a homogenization method. **Structural Optimization**, v. 4, 17–22, 1992.

DORN, W.S.; GOMORY, R.E. and GREENBERG, H.J. Automatic design of optimal structures. **Journal de Mecanique**, v. 3, 25–62, 1964.

DU, J. and OLHOFF, N. Topological optimization of continuum structures with design-dependent surface loading. Part I: new computational approach for 2D problems. **Structural and Multidisciplinary Optimization**, v. 27, 151–165, 2004a.

DU, J. and OLHOFF, N. Topological optimization of continuum structures with design-dependent surface loading. Part II: algorithm and examples for 3D problems. **Structural and Multidisciplinary Optimization**, v. 27, 166–177, 2004b.

DU, J. and OLHOFF, N. Minimization of sound radiation from vibrating bi-material structures using topology optimization. **Structural and Multidisciplinary Optimization**, v. 33, 305–321, 2007a.

DU, J. and OLHOFF, N. Topological design of freely vibrating continuum structures for maximum values of simple and multiple eigenfrequencies and frequency gaps. **Structural and Multidisciplinary Optimization**, v. 34, 91–110, 2007b.

DUHRING, M.B.; JENSEN, J.S. and SIGMUND, O. Acoustic design by topology optimization. **Journal of Sound and Vibration**, v. 317, 557–575, 2008.

DUYSINX, P. and BENDSOE, M.P. Topology optimization of continuum structures with local

stress constraints. **International Journal for Numerical Methods In Engineering**, v. 43, n. 8, 1453–1478, 1998.

DUYSINX, P. and SIGMUND, O. New developments in handling stress constraints in optimal material distribution. In **7th Symposium on Multidisciplinary Analysis and Optimization, AIAA/USAF/NASA/ISSMO, AIAA-88-4906, 1501-1509**. 1998.

DUYSINX, P.; VAN MIEGROET, L.; LEMAIRE, E.; BRULS, O. and BRUYNEEL, M. Topology and generalized shape optimisation: why stress constraints are so important? **International Journal for Simulation and Multidisciplinary Design Optimization**, v. 4, 253–258, 2008.

EVGRAFOV, A. The limits of porous materials in the topology optimization of Stokes flow. **Applied Mathematics and Optimization**, v. 52, n. 3, 263–277, 2005.

EVGRAFOV, A. Topology optimization of slightly compressible fluids. **ZAMM - Journal of Applied Mathematics and Mechanics**, v. 86, n. 1, 46–62, 2006.

EVGRAFOV, A. On Chebyshev's method for topology optimization of Stokes flow. **Structural and Multidisciplinary Optimization**, v. 51, n. 4, 801–811, 2015.

GALILEI, G. **Dialogues Concerning Two New Sciences**. English translation by Henry Crew and Alfonso de Salvio, The Macmillan Company, New York, 1933.

GAO, T. and ZHANG, W. Topology optimization involving thermo-elastic stress loads. **Structural and Multidisciplinary Optimization**, v. 42, n. 5, 725–738, 2010.

GAO, T.; ZHANG, W.H.; ZHU, J.H.; XU, Y.J. and BASSIR, D.H. Topology optimization of heat conduction problem involving design-dependent heat load effect. **Finite Elements in Analysis and Design**, v. 44, 805–813, 2008.

GARTLING, D.; HICKOX, C. and GIVLER, R. Simulation of coupled viscous and porous flow problems. **International Journal of Computational Fluid Dynamics**, v. 7, 23–48, 1996.

GERSBORG-HANSEN, A.; BENDSOE, M.P. and SIGMUND, O. Topology optimization of heat conduction problems using the finite volume method. **Structural and Multidisciplinary Optimization**, v. 31, n. 4, 251–259, 2006.

GERSBORG-HANSEN, A.; SIGMUND, O. and HARBER, R.B. Topology optimization of channel flow problems. **Structural and Multidisciplinary Optimization**, v. 30, 181–192, 2005.

GRESHO, P.M. and SANI, R.L. **Incompressible Flow and the Finite Element Method**. Wiley, 2000.

GUEST, J.K.; ASADPOURE, A. and HA, S.H. Eliminating beta-continuation from heaviside projection and density filter algorithms. **Structural and Multidisciplinary Optimization**, v. 44, n. 4, 443–453, 2011.

GUEST, J.K. and PRÉVOST, J.H. Topology optimization of creeping fluid flows using a Darcy-Stokes finite element. **International Journal for Numerical Methods In Engineering**, v. 66, n. 3, 1006–1017, 2006.

GUEST, J.K.; PRÉVOST, J.H. and BELYTSCHKO, T. Achieving minimum length scale in topology optimization using nodal design variables. **International Journal for Numerical Methods In Engineering**, v. 61, n. 2, 238–254, 2004.

HABER, R.B.; JOG, C.S. and BENDSOE, M.P. A new approach to variable topology shape design using a constraint on the perimeter. **Structural Optimization**, v. 11, n. 1, 1–11, 1996.

HAMMER, V.B. and OLHOFF, N. Topology optimization of continuum structures subjected to pressure loading. **Structural and Multidisciplinary Optimization**, v. 19, 85–92, 2000.

HASSANI, B. and HINTON, E. **Homogenization and Structural Topology Optimization**. Springer, 1999.

HEATH, T.L. **The Works of Archimedes**. Mineola, NY: Dover Publications, 2002.

HEMP, W.S. **Optimum Structures**. Clarendon Press, Oxford, 1973.

HERSKOVITS, J.; GOULART, E. and AROZTEGUI, M. **Optimization of Structural and Mechanical Systems**, chapter Optimization of Large Scale Systems, pp. 35–57. World Scientific, 2007.

HOU, G.; WANG, J. and LAYTON, A. Numerical methods for fluid-structure interaction – a review. **Communications in Computational Physics**, v. 12, 337–377, 2012.

HU, W.; CHOI, K.K.; CHO, K.; GAUL, N.J. and ZHUPANSKA, O.I. Reliability-based design optimization of wind turbine blades for fatigue life under wind load uncertainty. In **Proceedings of the 11th World Congress of Structural and Multidisciplinary Optimization (WCSMO-11)**, Sydney, Australia. 2015.

HUANG, X. and XIE, Y. A further review of ESO type methods for topology optimization. **Structural and Multidisciplinary Optimization**, v. 41, 671–683, 2010.

HUANG, X. and XIE, Y.M. Convergent and mesh-independent solutions for the bi-directional evolutionary structural optimization method. **Finite Elements in Analysis and Design**, v. 43, 1039–1049, 2007.

HUANG, X. and XIE, Y.M. A new look at eso and beso optimization methods. **Structural and Multidisciplinary Optimization**, v. 35, n. 1, 89–92, 2008a.

HUANG, X. and XIE, Y.M. Topology optimization of nonlinear structures under displacement loading. **Engineering Structures**, v. 30, 2057–2068, 2008b.

HUANG, X. and XIE, Y.M. Bi-directional evolutionary topology optimization of continuum structures with one or multiple materials. **Computational Mechanics**, v. 43, 393–401, 2009.

HUANG, X. and XIE, Y.M. Evolutionary topology optimization of continuum structures including design-dependent self-weight loads. **Finite Elements in Analysis and Design**, v. 47, 942–948, 2011.

HUANG, X.; ZHOU, S.; SUN, G.; LI, G. and XIE, Y.M. Topology optimization for microstructures of viscoelastic composite materials. **Computer Methods in Applied Mechanics and Engineering**, v. 283, 503–516, 2015.

HUANG, X.; ZUO, Z.H. and XIE, Y.M. Evolutionary topological optimization of vibrating continuum structures for natural frequencies. **Computers and Structures**, v. 88, 357–364, 2010.

JANG, G.W.; JEONG, J.H.; KIM, Y.Y.; SHEEN, D.; PARK, C. and KIM, M.N. Checkerboard-free topology optimization using non-conforming finite elements. **International Journal for Numerical Methods In Engineering**, v. 57, n. 12, 1717–1735, 2003.

JENKINS, N. and MAUTE, K. Level set topology optimization of stationary fluid-structure interaction problems. **Structural and Multidisciplinary Optimization**, v. 52, n. 1, 179–195, 2015.

JENSEN, J.S. and PEDERSEN, N.L. On maximal eigenfrequency separation in two-material structures: the 1D and 2D scalar cases. **Journal of Sound and Vibration**, v. 289, 967–986, 2006.

JOG, C.S. Distributed-parameter optimization and topology design for nonlinear thermoelasticity. **Computer Methods in Applied Mechanics and Engineering**, v. 132, n. 1-2, 117–134, 1996.

JUNG, D. and GEA, H.C. Topology optimization of nonlinear structures. **Finite Elements in Analysis and Design**, v. 40, n. 11, 1417–1427, 2004.

KIM, M.; QUERIN, O.M.; STEVEN, G.P. and XIE, Y.M. Improving efficiency of evolutionary structural optimization by implementing fixed grid mesh. **Structural and Multidisciplinary Optimization**, v. 24, 441–448, 2003.

KIRSCH, U. Optimal topology of structures. **Applied Mechanics Reviews**, v. 42, 223–239, 1989.

KOGA, A.A. **Projeto de Dispositivos de Microcanais Utilizando o Método de Otimização Topológica**. 2010. Master Thesis. Department of Mechatronics and Mechanical Systems Engineering, Polytechnic School of the University of São Paulo.

KOGA, A.A.; LOPES, E.C.C.; NOVA, H.F.V.; LIMA, C.R. and SILVA, E.C.N. Development of heat sink device by using topology optimization. **International Journal of Heat and Mass Transfer**, v. 64, 759–772, 2013.

KREISSL, S. and MAUTE, K. Levelset based fluid topology optimization using the extended finite element method. **Structural and Multidisciplinary Optimization**, v. 46, 311–326, 2012.

KREISSL, S.; PINGEN, G.; EVGRAFOV, A. and MAUTE, K. Topology optimization of flexible micro-fluidic devices. **Structural and Multidisciplinary Optimization**, v. 42, 495–516, 2010.

KROG, L.A. and OLHOFF, N. Optimum topology and reinforcement design of disk and plate structures with multiple stiffness and eigenfrequency objectives. **Computers and Structures**, v. 72, 535–563, 1999.

LAZAROV, B.S. and SIGMUND, O. Filters in topology optimization based on Helmholtz-type differential equations. **International Journal for Numerical Methods In Engineering**, v. 86, n. 6, 765–781, 2011.

LEE, E. and MARTINS, J.R.R.A. Structural topology optimization with design-dependent pressure loads. **Computer Methods in Applied Mechanics and Engineering**, v. 233-236, 40–48, 2012. In press.

LEE, T.H. **Optimization of Structural and Mechanical Systems**, chapter Shape Optimization, pp. 149–159. World Scientific, 2007.

LEON, D.M.; SOUZA, C.E.; FONSECA, J.S.O. and SILVA, R.G.A. Aeroelastic tailoring using fiber orientation and topology optimization. **Structural and Multidisciplinary Optimization**, v. 46, n. 5, 663–677, 2012.

LEWINSKI, T. and ROZVANY, G.I.N. Exact analytical solutions for some popular benchmark problems in topology optimization III: L-shaped domains. **Structural and Multidisciplinary Optimization**, v. 35, 165–174, 2008.

LI, Q.; STEVEN, G.P. and XIE, Y.M. Displacement minimization of thermoelastic structures by evolutionary thickness design. **Computer Methods in Applied Mechanics and Engineering**, v. 179, 361–378, 1999.

LI, Q.; STEVEN, G.P.; XIE, Y.M. and QUERIN, O.M. Evolutionary topology optimization for temperature reduction of heat conducting fields. **International Journal of Heat and Mass Transfer**, v. 47, 5071–5083, 2004.

LIAN, H. and SIGMUND, O. Combined topology and shape optimization with the dsc method

for stokes flow problems. In **Proceedings of the 11th World Congress of Structural and Multidisciplinary Optimization (WCSMO-11)**, Sydney, Australia. 2015.

LOPES, C.G.; DOS SANTOS, R.B. and NOVOTNY, A.A. Topological derivative-based topology optimization of structures subject to multiple load-cases. **Latin American Journal of Solids and Structures**, v. 12, n. 5, 834–860, 2015.

LUENBERGER, D.G. and YE, Y. **Linear and Nonlinear Programming**. Springer, 3rd ed., 2008.

LUO, Z.; ZHANG, N.; JI, J. and WU, T. A meshmesh level-set method for topological shape optimization of compliant multiphysics actuators. **Computer Methods in Applied Mechanics and Engineering**, v. 223-224, 133–152, 2012.

LYU, N. and SAITOU, K. Topology optimization of multicomponent beam structure via decomposition-based assembly synthesis. **Journal of Mechanical Design**, v. 127, 170–183, 2005.

MA, Z.D.; KIKUCHI, N. and CHENG, H.C. Topological design for vibrating structures. **Computer Methods in Applied Mechanics and Engineering**, v. 121, 259–280, 1995.

MARTINEZ, J. A note on the theoretical convergence properties of the simp method. **Structural and Multidisciplinary Optimization**, v. 29, n. 29, 319–332, 2005.

MAUTE, K. and ALLEN, M. Conceptual design of aerolastic structures by topology optimization. **Structural and Multidisciplinary Optimization**, v. 27, 27–42, 2004.

MAUTE, K. and RAMM, E. Adaptive topology optimization of shell structures. **AIAA Journal**, v. 35, n. 11, 1767–1777, 1997.

MAUTE, K.; SCHWARZ, S.T. and RAMM, E. Structural optimization - The interaction between form and mechanics. **ZAMM - Journal of Applied Mathematics and Mechanics**, v. 79, n. 10, 651–673, 1999.

MAXWELL, J.C. On reciprocal figures and diagrams of forces. **Philosophical Magazine**, v. 26, 250–261, 1864.

MICHELL, A.G.M. The limits of economy of material in frame structures. **Philosophical Magazine**, v. 8, n. 6, 589–597, 1904.

MIN, S.J. and KIKUCHI, N. Optimal reinforcement design of structures under the buckling load using the homogenization design method. **Structural Engineering and Mechanics**, v. 5, 565–576, 1997.

MORAND, H.J.P. and OHAYON, R. **Fluid Structure Interaction - Applied Numerical Methods**. John Wiley & Sons, Inc., Masson, Paris, 1st ed., 1995.

NEVES, M.M.; SIGMUND, O. and BENDSOE, M.P. Topology optimization of periodic microstructures with a penalization of highly localized buckling modes. **International Journal for Numerical Methods In Engineering**, v. 54, n. 6, 809–834, 2002.

NEWTON, I. **The Principia: mathematical principles of natural philosophy / Isaac Newton; a new translation by U. Bernard Cohen and Anne Whitman**. University of California Press, 1999.

NORATO, J.A.; BENDSOE, M.P.; HABER, R.B. and TORTORELLI, D.A. A topological derivative method for topology optimization. **Structural and Multidisciplinary Optimization**, v. 33, 375–386, 2007.

NORGAARD, S.; LAZAROV, B. and SIGMUND, O. Topology optimization of unsteady fluid flow patterns using the lattice Boltzmann method. In **Proceedings of the 11th World Congress of Structural and Multidisciplinary Optimization (WCSMO-11)**, Sydney, Australia. 2015.

NOVOTNY, A.A. **Análise de sensibilidade topológica**. 2003. PhD Thesis. LNCC/MCT, Petrópolis, Brasil.

NOVOTNY, A.A. and SOKOLOWSKIXIE, J. **Topological derivatives in shape optimization**. Springer, 2003.

OÑATE, E.; GARCÍA, J.; IDELSOHN, S.R. and PIN, F.D. Finite calculus formulations for finite element analysis of incompressible flows. Eulerian, ALE and Lagrangian approaches. **Computer Methods in Applied Mechanics and Engineering**, v. 195, 3001–3037, 2006.

OLHOFF, N.; LUND, E. and RASMUSSEN, J. **Concurrent Engineering: tools and technologies for mechanical system design**, pp. 523–586. Springer-Verlag, 1993.

PAPALAMBROS, P.Y. and WILDE, D.J. **Principles of Optimal Design: modeling and computation**. Cambridge University Press, Cambridge, 2000.

PEDERSEN, N.L. Maximization of eigenvalues using topology optimization. **Structural and Multidisciplinary Optimization**, v. 20, 2–11, 2000.

PEREIRA, J.T.; FANCELLO, E.A. and BARCELLOS, C.S. Topology optimization of continuum structures with material failure constraints. **Structural and Multidisciplinary Optimization**, v. 26, n. 1, 50–66, 2004.

PETERSSON, J. and SIGMUND, O. Slope constrained topology optimization. **International Journal for Numerical Methods In Engineering**, v. 41, n. 8, 1417–1434, 1998.

PICELLI, R.; VAN DIJK, R.; VICENTE, W.M.; PAVANELLO, R.; LANGELAAR, M. and VAN KEULEN, F. Topology optimization including buoyancy inequality constraints. In **Proceedings of the 11th World Congress on Computational Mechanics - WCCM XI, Barcelona, Spain**. 2014.

PICELLI, R.; VAN DIJK, R.; VICENTE, W.M.; PAVANELLO, R.; LANGELAAR, M. and VAN KEULEN, F. Topology optimization for submerged buoyant structures (submitted - 06 july 2015). **Engineering Optimization**, v. x, n. x, x–x, 2015a.

PICELLI, R.; VICENTE, W.M. and PAVANELLO, R. Evolutionary topology optimization for fluid-structure interaction problems and natural frequency maximization. In **Proceedings of the 10th World Congress on Computational Mechanics - WCCM X, Sao Paulo, Brazil**. 2012.

PICELLI, R.; VICENTE, W.M. and PAVANELLO, R. Topology optimization considering design-dependent loads. In (Abstract only) **Proceedings of the V International Conference on Coupled Problems in Science and Engineering - COUPLED PROBLEMS 13, Ibiza, Spain**. 2013.

PICELLI, R.; VICENTE, W.M. and PAVANELLO, R. Bi-directional evolutionary structural optimization for design-dependent fluid pressure loading problems. **Engineering Optimization**,

v. 47, n. 10, 1324–1342, 2015b.

PICELLI, R.; VICENTE, W.M.; PAVANELLO, R. and VAN KEULEN, F. Topology optimization considering design-dependent Stokes flow loads. In **Proceedings of the 11th World Congress of Structural and Multidisciplinary Optimization (WCSMO-11)**, Sydney, Australia. 2015c.

PICELLI, R.; VICENTE, W.M.; PAVANELLO, R. and XIE, Y.M. Evolutionary topology optimization for natural frequency maximization problems considering acoustic-structure interaction. **Finite Elements in Analysis and Design**, v. 106, 56–64, 2015d.

PINGEN, G.; WAIDMANN, M.; EVGRAFOV, A. and MAUTE, K. A parametric level-set approach for topology optimization of flow domains. **Structural and Multidisciplinary Optimization**, v. 41, 117–131, 2010.

PIRONNEAU, O. On optimal profiles in Stokes flow. **Journal of Fluid Mechanics**, v. 59, 117–128, 1973.

POULSEN, T.A. A new schem for imposing a minimum length scale in topology optimization. Technical report, Danish Center for Applied Mathematics and Mechanics, **DCAMM Report No. 663**, 2001.

POULSEN, T.A. A simple scheme to prevent checkerboard patterns and one-node connected hinges in topology optimization. **Structural and Multidisciplinary Optimization**, v. 24, n. 5, 396–399, 2002.

POULSEN, T.A. A new schem for imposing a minimum length scale in topology optimization. **International Journal for Numerical Methods In Engineering**, v. 57, n. 6, 741–760, 2003.

PRAGER, W. and ROZVANY, G.I.N. **Optimization of Structural Geometry**, chapter In: Bednarek, A. R.; Cesari, L. (eds.): Dynamical systems., pp. 265–293. Academic Press, New York, 1977.

QIU, G.Y. and LI, X.S. A note on the derivation of global stress constraints. **Structural and Multidisciplinary Optimization**, v. 40, 625–628, 2010.

QUERIN, O.M. and STEVEN, G.P. Evolutionary structural optimisation using a bidirectional algorithm. **Engineering Computations**, v. 15, 1031–1048, 1998.

QUERIN, O.M.; YOUNG, V.; STEVEN, G.P. and XIE, Y.M. Computational efficiency and validation of bi-directional evolutionary structural optimization. **Computer Methods in Applied Mechanics and Engineering**, v. 189, 559–573, 2000.

ROSSOW, M.P. and TAYLOR, J.E. A finite element method for the optimal design of variable thickness sheets. **AIAA Journal**, v. 11, 1566–1569, 1973.

ROZVANY, G.I.N.; BENDSOE, M.P. and KIRSCH, U. Layout optimization of structures. **Applied Mechanics Reviews**, v. 48, n. 2, 41–119, 1995.

ROZVANY, G.I.N. and QUERIN, O. Combining ESO with rigorous optimality criteria. **International Journal of Vehicle Design**, v. 28, 294–299, 2002.

ROZVANY, G.I.N.; ZHOU, M. and BIRKER, T. Generalized shape optimization without homogenization. **Structural Optimization**, v. 4, 250–254, 1992.

ROZVANY, G.I.N.; ZHOU, M. and SIGMUND, O. **Topology optimization in structural design**, chapter 10, pp. 340–399. Chapman and Hall, London, 1994.

RUPP, C.; HOWARD, M. and WEICKUM, G. Incompressible mixed (u/p) elements for the CAS FEM code, 2015. Online, Centre for Aerospace Structures, Department of Aerospace Engineering Sciences, University of Colorado at Boulder, Boulder, CO 80309, USA.

SETHIAN, J.A. **Level Set Methods and Fast Marching Methods: evolving interfaces in computational geometry, fluid mechanics, computer vision, and materials science**. Cambridge University Press, Cambridge, 1999.

SHU, L.; WANG, M.Y.; FANG, Z.; MA, Z. and WEI, P. Level set based structural topology optimization for minimizing frequency response. **Journal of Sound and Vibration**, v. 330, 5820–5834, 2011.

SHU, L.; WANG, M.Y. and MA, Z. Level set based topology optimization of vibrating structures for coupled acoustic-structural dynamics. **Computers and Structures**, v. 132, 34–42,

2014.

SIGMUND, O. **Design of material structures using topology optimization.** 1994. PhD Thesis. Department of Solid Mechanics, Technical University of Denmark.

SIGMUND, O. Tailoring materials with prescribed elastic properties. **Mechanics of Materials**, v. 20, 351–368, 1995.

SIGMUND, O. On the design of compliant mechanisms using topology optimization. **Mechanics of Structures and Machines**, v. 25, n. 4, 495–526, 1997.

SIGMUND, O. A 99 line topology optimization code written in matlab. **Structural and Multidisciplinary Optimization**, v. 21, 120–127, 2001a.

SIGMUND, O. Design of multiphysics actuators using topology optimization - Part I: One material structures. **Computer Methods in Applied Mechanics and Engineering**, v. 190, 6577–6604, 2001b.

SIGMUND, O. Morphology-based black and white filters for topology optimization. **Structural and Multidisciplinary Optimization**, v. 33, n. 4-5, 401–424, 2007.

SIGMUND, O. and CLAUSEN, P.M. Topology optimization using a mixed formulation: An alternative way to solve pressure load problems. **Computer Methods in Applied Mechanics and Engineering**, v. 196, 1874–1889, 2007.

SIGMUND, O. and MAUTE, K. Sensitivity filtering from a continuum mechanics perspective. **Structural and Multidisciplinary Optimization**, v. 46, n. 6, 471–475, 2012.

SIGMUND, O. and MAUTE, K. Topology optimization approaches: A comparative review. **Structural and Multidisciplinary Optimization**, v. 48, 1031–1055, 2013.

SIGMUND, O. and PETERSON, J. Numerical instabilities in topology optimization: A survey on procedures dealing with checkerboards, mesh-dependencies and local minima. **Structural Optimization**, v. 16, 68–75, 1998.

SIGMUND, O. and TORQUATO, S. Composites with extremal thermal expansion coefficients. **Applied Physics Letters**, v. 69, n. 21, 3203–3205, 1996.

SILVA, E.C.N.; FONSECA, J.S.O. and KIKUCHI, N. Optimal design of piezoelectric microstructures. **Computational Mechanics**, v. 19, n. 5, 397–410, 1997.

SILVA, F.I. and PAVANELLO, R. Synthesis of porous-acoustic absorbing systems by an evolutionary optimization method. **Engineering Optimization**, v. 42, n. 10, 887–905, 2010.

SMITH, C.; GILBERT, M. and TODD, I. Layout optimization of components suitable for additive manufacture. In **Proceedings of the 11th World Congress of Structural and Multidisciplinary Optimization (WCSMO-11)**, Sydney, Australia. 2015.

SOKÓL, T. and ROZVANY, G.I.N. On the adaptive ground structure approach for multi-load truss topology optimization. In **Proceedings of 10th World Congress on Structural and Multidisciplinary Optimization**, Orlando, Florida, USA. 2013.

SOKÓL, T. and ROZVANY, G.I.N. On the numerical optimization of multi-load spatial Michell trusses using a new adaptive ground structure approach. In **Proceedings of 11th World Congress on Structural and Multidisciplinary Optimization**, Sydney, Australia. 2015.

SOKOŁOWSKI, J. and ZOCHOWSKI, A. On the topological derivative in shape optimization. **SIAM Journal on Control and Optimization**, v. 37, 1251–1272, 1999.

STEVEN, G.P.; LI, Q. and XIE, Y.M. Evolutionary topology and shape design for general physical field problems. **Computational Mechanics**, v. 26, 129–139, 2000.

STOLPE, M. and SVANBERG, K. An alternative interpolation scheme for minimum compliance topology optimization. **Structural and Multidisciplinary Optimization**, v. 22, 116–124, 2001.

SUTRADHAR, A.; PAULINO, G.H.; MILLER, M.J. and NGUYEN, T.H. Topological optimization for designing patient-specific large craniofacial segmental bone replacements. **Proceedings of the National Academy of Sciences**, v. 107, n. 30, 13222–13227, 2010.

SVANBERG, K. The method of moving asymptotes - a new method for structural optimization.

International Journal for Numerical Methods In Engineering, v. 24, 359–373, 1987.

SVANBERG, K. Global convergence of the stress ratio method for truss sizing. **Structural Optimization**, v. 8, 60–68, 1994.

TANGARAMWONG, S. and TIN-LOI, F. Structural optimization under complementarity constraints. In **Proceedings of 11th World Congress on Structural and Multidisciplinary Optimization**, Sydney, Australia. 2015.

TERADA, K. and KIKUCHI, N. Microstructural design of composites using the homogenization method and digital images. **Materials Science Research International**, v. 2, 65–72, 1996.

TIMOSHENKO, S.P. **History of Strength of Materials**. Dover Publications, Inc., New York, 1953.

VAN DIJK, N. **Pushing the Boundaries: level-set methods and geometrical nonlinearities in structural topology optimization**. 2012. PhD Thesis. Faculty of Mechanical, Maritime and Materials Engineering (3mE), Delft University of Technology.

VAN DIJK, N.P.; LANGELAAR, M. and VAN KEULEN, F. Explicit level-set-based topology optimization using an exact heaviside function and consistent sensitivity analysis. **International Journal for Numerical Methods In Engineering**, v. 91, 67–97, 2012.

VAN DIJK, N.P.; MAUTE, K.; LANGELAAR, M. and VAN KEULEN, F. Level-set methods for structural topology optimization: a review. **Structural and Multidisciplinary Optimization**, v. 48, n. 3, 437–472, 2013.

VAN DIJK, N.P.; YOON, G.H.; VAN KEULEN, F. and LANGELAAR, M. A level-set based topology optimization using the element connectivity parameterization method. **Structural and Multidisciplinary Optimization**, v. 42, 269–282, 2010.

VICENTE, W.M.; PICELLI, R.; PAVANELLO, R. and XIE, Y.M. Topology optimization of frequency responses of fluid-structure interaction systems. **Finite Elements in Analysis and Design**, v. 98, 1–13, 2015.

WADBRO, E. and BERGGREN, M. Topology optimization of an acoustic horn. **Computer**

Methods in Applied Mechanics and Engineering, v. 196, n. 1-3, 420–436, 2006.

WANG, F.; LAZAROV, B.S. and SIGMUND, O. On projection methods, convergence and robust formulations in topology optimization. **Structural and Multidisciplinary Optimization**, v. 43, n. 6, 767–784, 2011.

WANG, M.Y.; WANG, X. and GUO, D. A level set method for structural topology optimization. **Computer Methods in Applied Mechanics and Engineering**, v. 192, n. 1-2, 227–246, 2003.

WELLS, M. **Engineers: A History of Engineering and Structural Design**. Routledge, Taylor & Francis group, 2010.

WIKER, N.; KLARBING, A. and BORRVALL, T. Topology optimization of regions of Darcy and Stokes flow. **International Journal for Numerical Methods In Engineering**, v. 69, n. 7, 1374–1404, 2007.

XIA, L. and BREITKOPF, P. Concurrent topology optimization design of material and structure within FE^2 nonlinear multiscale analysis framework. **Computer Methods in Applied Mechanics and Engineering**, v. 278, 524–542, 2014.

XIA, L. and BREITKOPF, P. Multiscale structural topology optimization with an approximate constitutive model for local material microstructure. **Computer Methods in Applied Mechanics and Engineering**, v. 286, 147–167, 2015.

XIA, Q.; WANG, M.Y. and SHI, T. Topology optimization with pressure load through a level set method. **Computer Methods in Applied Mechanics and Engineering**, v. 283, 177–195, 2015.

XIE, Y.M. and HUANG, X. **Evolutionary Topology Optimization of Continuum Structures: Methods and Applications**. John Wiley & Sons, Ltd, West Sussex, 1st ed., 2010.

XIE, Y.M. and STEVEN, G.P. A simple evolutionary procedure for structural optimization. **Computer and Structures**, v. 49, 885–896, 1993.

XIE, Y.M. and STEVEN, G.P. Evolutionary structural optimization for dynamic problems. **Computer and Structures**, v. 58, 1067–1073, 1996.

XIE, Y.M. and STEVEN, G.P. **Evolutionary Structural Optimization**. London: Springer, London, 1997.

XIE, Y.M.; ZUO, Z.H.; HUANG, X. and RONG, J.H. Convergence of topological patterns of optimal periodic structures under multiple scales. **Structural and Multidisciplinary Optimization**, v. 46, 41–50, 2012.

YANG, R.J. and CHUANG, C.H. Optimal topology design using linear programming. **Computers and Structures**, v. 52, n. 2, 265–276, 1994.

YANG, X.Y.; XIE, Y.M.; LIU, G.T. and CLARKSON, P.J. Bidirectional evolutionary method for stiffness optimization. **AIAA Journal**, v. 37, 1483–8, 1999a.

YANG, X.Y.; XIE, Y.M. and STEVEN, G.P. Evolutionary methods for topology optimisation of continuous structures with design dependent loads. **Computers and Structures**, v. 83, 956–963, 2005.

YANG, X.Y.; XIE, Y.M.; STEVEN, G.P. and QUERIN, O.M. Topology optimization for frequencies using an evolutionary method. **Journal of Structural Engineering-ASCE**, v. 125, 1432–1438, 1999b.

YI, Y.; PARK, S. and YOUN, S.K. Design of microstructures of viscoelastic composites for optimal damping characteristics. **International Journal for Numerical Methods In Engineering**, v. 37, 4791–4810, 2000.

YOON, G.H. Topology optimization for stationary fluid-structure interaction problems using a new monolithic formulation. **International Journal for Numerical Methods In Engineering**, v. 82, 591–616, 2010.

YOON, G.H. Topological layout design of electro-fluid-thermal-compliant actuator. **Computer Methods in Applied Mechanics and Engineering**, v. 209, 28–44, 2012.

YOON, G.H. Acoustic topology optimization of fibrous material with Delany-Bazley empirical material formulation. **Journal of Sound and Vibration**, v. 332, 1172–1187, 2013.

YOON, G.H. Stress-based topology optimization method for steady-state fluid-structure in-

teraction problems. **Computer Methods in Applied Mechanics and Engineering**, v. 278, 499–523, 2014.

YOON, G.H.; JENSEN, J.S. and SIGMUND, O. Topology optimization of acoustic-structure problems using a mixed finite element formulation. **International Journal for Numerical Methods In Engineering**, v. 70, 1049–1075, 2007.

YOON, G.H. and KIM, Y.Y. The element connectivity parameterization formulation for the topology design optimization of multiphysics systems. **International Journal for Numerical Methods In Engineering**, v. 64, 1649–1677, 2005.

YOON, G.H. and KIM, Y.Y. Topology optimization of material-nonlinear structures by the element connectivity parametrization. **International Journal for Numerical Methods In Engineering**, v. 69, n. 10, 2196–2218, 2007.

YOON, G.H. and SIGMUND, O. A monolithic approach for topology optimization of electrostatically actuated devices. **Computer Methods in Applied Mechanics and Engineering**, v. 197, 4062–4075, 2008.

ZEGARD, T. and PAULINO, G.H. GRAND - ground structure based topology optimization for arbitrary 2D domains using MATLAB. **Structural and Multidisciplinary Optimization**, v. 50, 861–882, 2014.

ZHANG, H.; LIU, S. and ZHANG, X. Topology optimization of 3D structures with design-dependent loads. **Acta Mechanica Sinica**, v. 26, 767–775, 2010.

ZHANG, H.; ZHANG, X. and LIU, S. A new boundary search scheme for topology optimization of continuum structures with design-dependent loads. **Structural and Multidisciplinary Optimization**, v. 37, 121–129, 2008.

ZHENG, B.; CHANG, C. and GEA, H.C. Topology optimization with design-dependent pressure loading. **Structural and Multidisciplinary Optimization**, v. 38, 535–543, 2009.

ZHONG, W.; SU, R.; GUI, L. and FAN, Z. Topology and sizing optimisation of integral bus chassis with the use of a cooperative coevolutionary genetic algorithm with independent ground structures. In **Proceedings of 11th World Congress on Structural and Multidisciplinary**

Optimization, Sydney, Australia. 2015.

ZHOU, M. and ROZVANY, G.I.N. On the validity of ESO type methods in topology optimization. **Structural and Multidisciplinary Optimization**, v. 21, 80–83, 2001.

ZIENKIEWICZ, O.C. and BETTESS, P. Fluid-structure dynamic interaction and wave forces. an introduction to numerical treatment. **International Journal for Numerical Methods In Engineering**, v. 13, 1–16, 1978.

ZIENKIEWICZ, O.C. and TAYLOR, R.L. **The Finite Element Method (Vol. 1-3)**. Elsevier Butterworth Heinemann, Oxford, 6 ed., 2005.

ZUO, Z.H.; HUANG, X.; RONG, J.H. and XIE, Y.M. Multi-scale design of composite materials and structures for maximum natural frequencies. **Materials Design**, v. 51, 1023–1034, 2013.

ZUO, Z.H. and XIE, Y.M. Maximizing the effective stiffness of laminated composite materials. **Computational Materials Science**, v. 83, 57–63, 2014.

ZUO, Z.H.; XIE, Y.M. and HUANG, X. An improved bi-directional evolutionary topology optimization method for frequencies. **International Journal of Structural Stability and Dynamics**, v. 10, 55–75, 2010.

A IMPLEMENTATION DETAILS

This appendix aims to expose the implementation details of the basic methodology presented in this work. They are described by aspects of preprocessing, processing, postprocessing and specific functions needed to reproduce the results of this thesis.

The development of computational routines was carried out using the commercial softwares ANSYS in APDL programming, for preprocessing, and MATLAB, for processing and postprocessing. A computer with a 64-bit Intel Core i7-4770 processor at 3.40 Ghz and 16.0 GB of RAM was available for this work. Figure A.1 illustrates the computational tasks distribution for the developed methodologies.

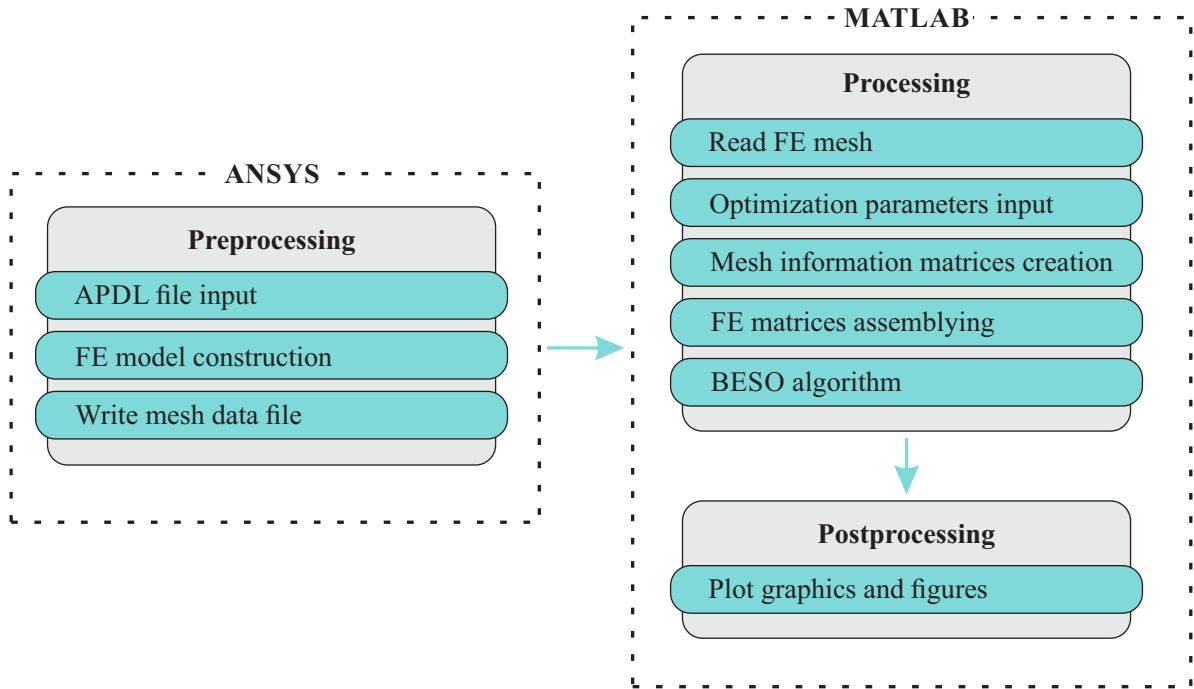


Figure A.1: Computational tasks distribution for the presented methodology.

A.1 Preprocessing

The ANSYS was chosen as a finite element mesh generator for the presented thesis using its Parametric Design Language (APDL). Thus, complex geometries can be easily parametrized by programming APDL codes. The computational routine includes two APDL files, one for creating parametrically designed meshes and another for writing the mesh data file.

A.2 Processing

The processing initiates with a MATLAB code for reading the finite element mesh data file in a standard manner chosen for this work, such as

$$\text{coordinates} = \begin{bmatrix} x & y \\ \vdots & \vdots \end{bmatrix}, \quad (\text{A.1})$$

defining the node in each row number and its coordinates in each column,

$$\text{incidence} = \begin{bmatrix} \text{type} & \text{node1} & \text{node2} & \text{node3} & \text{node4} \\ \vdots & \vdots & \vdots & \vdots & \vdots \end{bmatrix}, \quad (\text{A.2})$$

which declares the incidence of the finite elements, defining the element type (mat = [void = 0, solid = 1, fluid = 2]) and its nodes,

$$\text{b.c.} = \begin{bmatrix} \text{node} & \text{DOF} & \text{value} \\ \vdots & \vdots & \vdots \end{bmatrix}, \quad (\text{A.3})$$

with boundary conditions and, if external loads are imposed,

$$\text{loads} = \begin{bmatrix} \text{node} & \text{DOF} & \text{value} \\ \vdots & \vdots & \vdots \end{bmatrix}. \quad (\text{A.4})$$

A Matlab file is written with material properties and optimization parameters input. Before the finite element analysis, some matrices are created containing some mesh informations, e.g., nodal connectivity, element centroids and element neighbours. For example, the information with neighbour elements are stored in a matrix such as

$$\text{neighbor} = \begin{bmatrix} \text{number} & \text{ele1} & \text{ele2} & \text{ele3} & \text{ele4} \\ \vdots & \vdots & \vdots & \vdots & \vdots \end{bmatrix}, \quad (\text{A.5})$$

with the element number and all its neighboring element numbers in a regular quadrilateral mesh. These matrices are useful for identifying the fluid-structure interfaces in the presented methodology. With the information of element neighbors and shared nodes, the coupling matrices can be calculated and assembled directly and structural elements at the fluid-structure interface can be identified, i.e., structural elements with fluid neighbors.

For the finite element analysis, a degree of freedom (DOF) identification matrix, **ID**, is

created. This ID matrix depends on the problem and can have the form,

$$\text{ID} = \begin{bmatrix} (v_{fx})^{\text{node1}} & (v_{fx})^{\text{node2}} & \dots \\ (v_{fy})^{\text{node1}} & (v_{fy})^{\text{node2}} & \dots \\ (P_f)^{\text{node1}} & (P_f)^{\text{node2}} & \dots \\ (u_{sx})^{\text{node1}} & (u_{sx})^{\text{node2}} & \dots \\ (u_{sy})^{\text{node1}} & (u_{sy})^{\text{node2}} & \dots \end{bmatrix} \quad (\text{A.6})$$

indicating a number for each DOF in each node. Not all the problems considered in this work need all these DOF's, e.g., in nonviscous fluids no velocities are present. Thus, the number 0 is included in $(v_{fx})^{\text{node1}}$, $(v_{fx})^{\text{node2}}$, etc. and represents inexistent DOF's. With the aid of the ID matrix the following function can be used for assembling the global finite element matrices:

```

1 function [K] = KassembleFSIpress(inci, ID, Kef, Ke, mat, nelsol, nelflu)
2 % Fluid elements DOF's
3 loc = [ID(3, inci(find(mat == 2), 2));
4         ID(3, inci(find(mat == 2), 3));
5         ID(3, inci(find(mat == 2), 4));
6         ID(3, inci(find(mat == 2), 5))];
7 % Index vectors
8 If = reshape(repmat(loc, 4, 1), nelflu*16, 1);
9 Jf = kron(loc(:), ones(4, 1));
10 Kf = repmat(Kef(:), nelflu, 1);
11 % Solid elements DOF's
12 loc = [ID(4, inci(find(mat == 1), 2));
13         ID(5, inci(find(mat == 1), 2));
14         ID(4, inci(find(mat == 1), 3));
15         ID(5, inci(find(mat == 1), 3));
16         ID(4, inci(find(mat == 1), 4));
17         ID(5, inci(find(mat == 1), 4));
18         ID(4, inci(find(mat == 1), 5));
19         ID(5, inci(find(mat == 1), 5))];
20 % Index vectors
21 Is = reshape(repmat(loc, 8, 1), nelsol*64, 1);
22 Js = kron(loc(:), ones(8, 1));
23 Ks = repmat(Ke(:), nelsol, 1);
24 % Global index vectors
25 I = [If; Is];
26 J = [Jf; Js];
27 Kg = [Kf; Ks];
28 % Assembly
29 K = sparse(I, J, Kg);
30 end

```

This function is used to assemble the uncoupled fluid-structure matrix in the design-dependent pressure loading problems from Chapters 2 and 3. It makes use of some predefined Matlab functions to organize the matrix values and their degrees of freedom in order to use the *sparse* function to finally assemble the global matrix. The inputs Ke and Kef indicate the structural and fluid stiffness matrices, respectively, while $nelsol$ and $nelflu$ are the numbers of solid and fluid elements present in the model.

In the nonviscous static and dynamic models from Chapters 2, 3 and 4, the fluid-structure matrices must coupled calculating the matrix L_{fs} (expressed in Equation 2.8) for each interface segment, connecting fluid pressure and structural displacements. In stationary viscous flow problems, Chapter 5, the fluid and structural matrices can be assembled in a single uncoupled matrix. However, each domain is solved separately, provided the traction balance is carried out.

The global finite element matrix is assembled considering that all DOF's can exist in some iteration during the optimization. This allows the switch between solid, fluid and void elements. In each iteration the active DOF's must be identified in order to solve the global matrix. For example, in a hard-kill approach, a node which eventually is connected to only void elements should be considered to have only non active DOF's. Thus, a sub-matrix which includes only the active DOF's can be extracted from the global finite element matrix. This step does not represent a significant computational cost for the whole calculation time and can be carried out, for example, with the following programming lines:

```

1  disp(['          Identifying active DOFs!'])
2  dof_n = [1:neq]';
3  for i = 1:nnos
4      % Types of elements connected to the node i
5      ele_type = inci(nonzeros(noconnect(i,2:5)),1);
6      % Identifying and blocking DOF's
7      if (isempty(find(ele_type == 1))) && (isempty(find(ele_type == 2)))
8          % Only void elements connected to the node i
9          dof_n(ID(3,i)) = 0;
10         dof_n(ID(4,i)) = 0;
11         dof_n(ID(5,i)) = 0;
12     end
13     if (isempty(find(ele_type == 1)))
14         % Only fluid elements connected to the node i
15         dof_n(ID(4,i)) = 0;
16         dof_n(ID(5,i)) = 0;
17     elseif (isempty(find(ele_type == 2)))
18         % Only solid elements connected to the node i
19         dof_n(ID(3,i)) = 0;
20     end

```

```

21 end
22 % Blocking DOF's with boundary conditions
23 for i = 1:ncont
24     if (cont(i,1) ≠ 0) && (cont(i,2) ≠ 4) && (cont(i,3) == 0)
25         dof(ID(cont(i,2)+3,cont(i,1))) = 0;
26     elseif (cont(i,1) ≠ 0) && (cont(i,2) == 4) && (cont(i,3) == 0)
27         dof(ID(3,cont(i,1))) = 0;
28     end
29 end
30 % DOF's ativos
31 dofa = nonzeros(dofn);

```

The variable *neq* indicates the total number of available DOF's. Imposed DOF's of zero values are also included here. This procedure allows the switch between different types of elements without the need of changing the numeration of DOF's and finite element equations.

After solving the global finite element matrix a response vector **U** is obtained. The sensitivities can be then calculated. A matrix **H** is evaluated containing all the filtering weight factors $w(r_{ij})$ as described in previous chapters. This is a similar procedure as the one proposed by Sigmund and Peterson (1998) and it is well known in the field of structural topology optimization. The matrix **H** with the weight factors is the same for whenever filtering is needed and it can be built only once before the BESO algorithm starts. To filter the sensitivities, averaged nodal sensitivity numbers are calculated and multiplied by the matrix **H**. The sensitivities and filtering are only evaluated for the design domain.

Before the BESO update scheme, the sensitivities are sorted, the target volume is calculated and the sensitivities thresholds are defined. The standard BESO update scheme verifies the sensitivities thresholds and switches solid and void elements, obtaining a discrete void/solid design, as described in the previous chapters. Then, the proposed BESO fluid region update scheme is carried out. This scheme introduces fluid elements through neighboring elements layer by layer until the fluid region is completely in contact with the structure, as illustrated in Figure A.2. Some programming loops are needed to verify whether void elements inside the design domain have fluid neighbors. This iterative procedure is repeated until no more void elements have fluid neighbor ones. This step also does not represent a significant computational cost for the whole calculation time.

The following function is used as the extended fluid-structure BESO update scheme, including the standard BESO scheme and the proposed fluid region update.

```

1 function [mat,inci] = ...

```

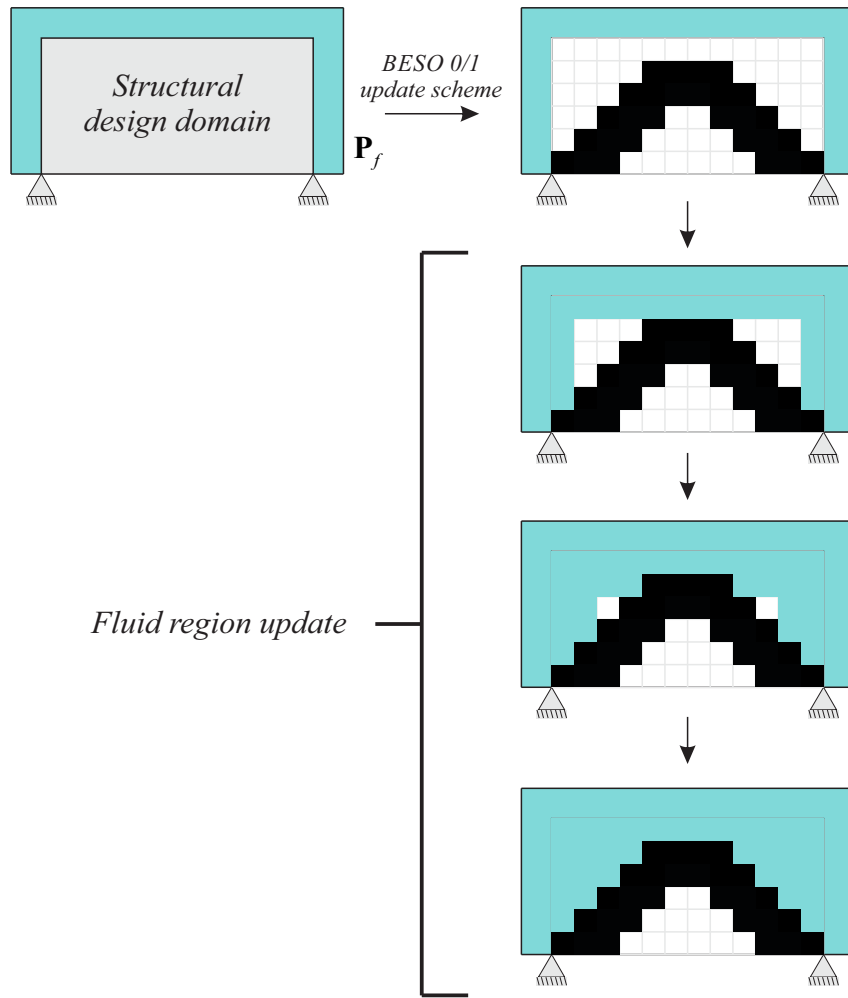


Figure A.2: BESO fluid region update scheme illustration.

```

    updatematBESO (ARi,ARmax,In,mat,inci,designD,nath,I,V,elside,fixedfluid)
2  % Removing/adding elements considering first only 0 and 1
3  if (ARi ≤ ARmax)      % If AR is lesser or equal maximum AR
4      % Removing/adding elements in mat vector
5      mat(In(1:nath)) = 1;
6      mat(In((nath+1):end)) = 0;
7  else                  % If AR is greater than maximum AR
8      % Material vector sorted according to In
9      In_mat = mat(In);
10     % Numbers of elements to be added
11     nadd_ath = round(ARmax*length(designD));
12     % Adjusting nath for even amount of removed elements
13     nadd_ath = round(nadd_ath/2)*2;
14     % Searching i index in In_mat corresponding to ath_add
15     % Counting amount of 0's in In_mat until the value of nadd_nath
16     aux_In_mat = 0;
17     for i = 1:length(In_mat)

```

```

18         if (In_mat(i) == 0) || (In_mat(i) == 2)
19             aux_In_mat = aux_In_mat+1;
20             if aux_In_mat == nadd_ath
21                 In_add = i;
22                 break
23             end
24         end
25     end
26     % Number of elements to be removed
27     nret_ath_aux = round((V(I+1)-V(I))*length(designD));
28     % Adjusting nath for even amount of removed elements
29     nret_ath_aux = round(nret_ath_aux/2)*2;
30     nret_ath = nadd_ath-nret_ath_aux;
31     % Searching i index in In_mat corresponding to ath_del
32     % Counting amount of 1's in In_mat until the value of nret_nath
33     aux_In_mat = 0;
34     for i = length(In_mat):-1:1
35         if In_mat(i) == 1
36             aux_In_mat = aux_In_mat+1;
37             if aux_In_mat == nret_ath
38                 In_ret = i;
39                 break
40             end
41         end
42     end
43     % Removing/adding elements in mat vector
44     mat(In(1:In_add)) = 1;
45     mat(In((In_ret):end)) = 0;
46 end
47 %-----%
48 % Extended BESO fluid region update scheme
49 % Returning fixed fluids to mat
50 mat(fixedfluid) = 2;
51 % Setting auxiliary counter
52 aux = 1;
53 % While fluid region still advances
54 while (aux ≠ 0)
55     % Resetting auxiliary counter
56     aux = 0;
57     % Updating fluid region
58     for i = 1:length(mat)
59         % For fluid elements
60         if (mat(i) == 2)
61             % Identifying type of neighbour elements
62             for j = 2:5
63                 % If neighbour element exists
64                 if (elside(i,j) ≠ 0)

```



```

65         % If neighbour element is void
66         if mat(elside(i,j),1) == 0
67             % Neighbour element becomes fluid
68             mat(elside(i,j),1) = 2;
69             % Auxiliary counter
70             aux = aux+1;
71         end
72     end
73 end
74 end
75 end
76 end
77 % Updating type of elements
78 inci(:,1) = mat;
79 end

```

The original uncoupled fluid-structure matrix must be then updated by removing and/or adding element matrices or re-assembling the whole matrix considering the new fluid-structure configuration. A new finite element analysis should be carried out and the BESO algorithm iterated until the convergence criterion and the volume constraints are satisfied. During the BESO iterations the computational cost is concentrated in solving the finite element equations, i.e., coupling matrices calculation, filtering, design variables update and others do not represent costly procedures.

A.3 Postprocessing

The postprocessing is carried out in Matlab by using predefined functions such as *imagesc*, *colormap*, *fill* and graphic edition.